Scaffold repurposing:

Towards parasite selective inhibitors

Erik de Heuvel

VRIJE UNIVERSITEIT

SCAFFOLD REPURPOSING: TOWARDS PARASITE SELECTIVE INHIBITORS

ACADEMISCH PROEFSCHRIFT

ter verkrijging van de graad Doctor aan
de Vrije Universiteit Amsterdam,
op gezag van de rector magnificus
prof.dr. C.M. van Praag,
in het openbaar te verdedigen
ten overstaan van de promotiecommissie
van de Faculteit der Bètawetenschappen
op woensdag 16 februari 2022 om 13.45 uur
in een bijeenkomst van de universiteit,
De Boelelaan 1105

door

Erik de Heuvel

geboren te Bemmel

"You cannot pick the destination, only the path." – Brandon Sanderson

Table of Contents

Chapter 1

Introduction

1.   Neglected tropical diseases

The neglected tropical diseases (NTDs) are a subset of infectious diseases caused by various pathogens including protozoa, bacteria and helminths.[1] These diseases are characterized by two features: they predominate in the tropics and have been neglected to some extend by the pharmaceutical industry.[1-3] However, since the establishment of a neglected tropical disease department within the world health organization (WHO), the interest in transmission control and (preventive) chemotherapy for NTDs has increased.[2, 3] In 2018, the WHO listed 19 different NTDs that have a significant effect on the health of more than 1 billion people.[4, 5]

1.1.   Human African trypanosomiasis

Human African trypanosomiasis (HAT), also known as African sleeping sickness, has been designated as one of the NTDs and is caused by two subspecies of the parasitic protozoan *Trypanosoma brucei* (*T.b.*).[6, 7] *T.b. rhodesiense* is endemic in eastern and southern Africa while *T.b. gambiense* is found in western and central Africa (Figure 1A), but both forms are vector-borne diseases and are transmitted by the bite of blood-sucking tsetse fly.[8] The vast majority of cases of HAT is caused by *T.b. gambiense* (98%), while an infection with *T.b. rhodesiense* is responsible for only 2% of the cases (Figure 1B).[9, 10] Several epidemics occurred during the 20th century, which were probably triggered by ecological disruptions and colonialism.[8, 11] Coordinated efforts to gain disease control were initialized after the last alarming outbreak of HAT in the late 1990s, resulting in a 90% reduction of reported HAT cases to the WHO.[8, 12] With 992 reported cases to the WHO in 2019 the disease is close to eradication, but under-detection and a potential re-emergence of the disease in areas of civil unrest should be taken into account.[6, 8]
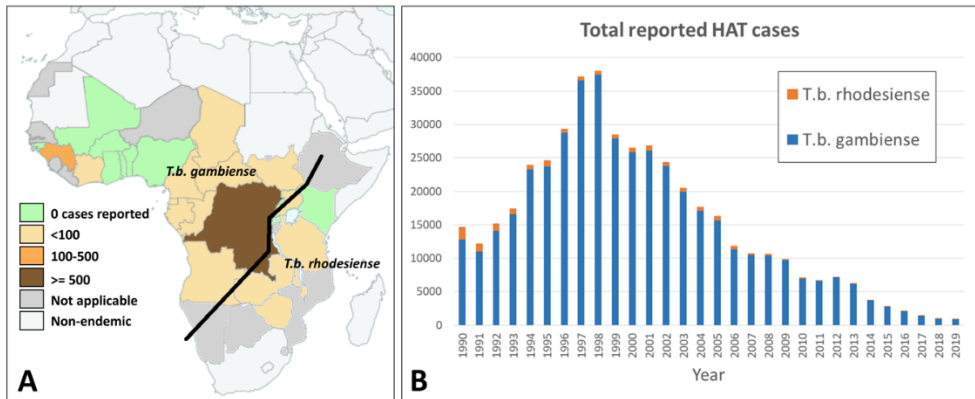
Figure 1: A) Geographical distribution of HAT caused by T.b. gambiense and T.b. rhodesiense in 2019. Figure adapted from WHO.[10] B) Number of reported cases of HAT by the WHO over the last decades.[10, 13]

The spread of the disease is limited to the habitat of the tsetse fly as the life cycle of the *T.b. gambiense* and *T.b. rhodesiense* consists of a tsetse fly stage in addition to a mammalian stage (Figure 2). The mammalian part of the life cycle can be started when an infected tsetse fly has a blood meal and thereby transfers metacyclic trypomastigotes into a mammalian host .[14] The parasites transform into bloodstream trypomastigotes that spread through the bloodstream and lymph. A transformation into a slender form allows the trypomastigotes to reach other fluids such as the cerebral-spinal fluid where they multiply by binary fission. The bloodstream form trypomastigotes can be transferred back to the tsetse fly by another blood meal and can undergo two more stages to reform the epimastigotes which can infect a new mammalian host[15]. Although there are several parasite reservoirs in Africa besides humans (e.g. domestic and wild animals), only a relatively small portion of the adult flies (<5%) is able to successfully transmit the parasite.[16] Several factors have been identified to contribute to the tsetse fly natural refractory system, such as fly age,[16, 17] antimicrobial peptides[18-20] and parasite inhibitory peptidoglycan recognition protein LB amongst others.[16, 20] Development of effective and cheap methods to target vector viability or parasite transmission is, next to drug and diagnostic assay development, one of the strategies to control this disease.[20] However, empirical models suggest that vector control and treatment of the disease play also an important role in complete eradication of the disease. [21, 22]

In the mammalian host each of the stages of the life cycle of the parasite are essential for proliferation.[23] Biological changes that occur during these transformations include the expression of variant surface glycoproteins (VSGs) that allow the parasite to avoid the host immune system in the bloodstream form.[14]
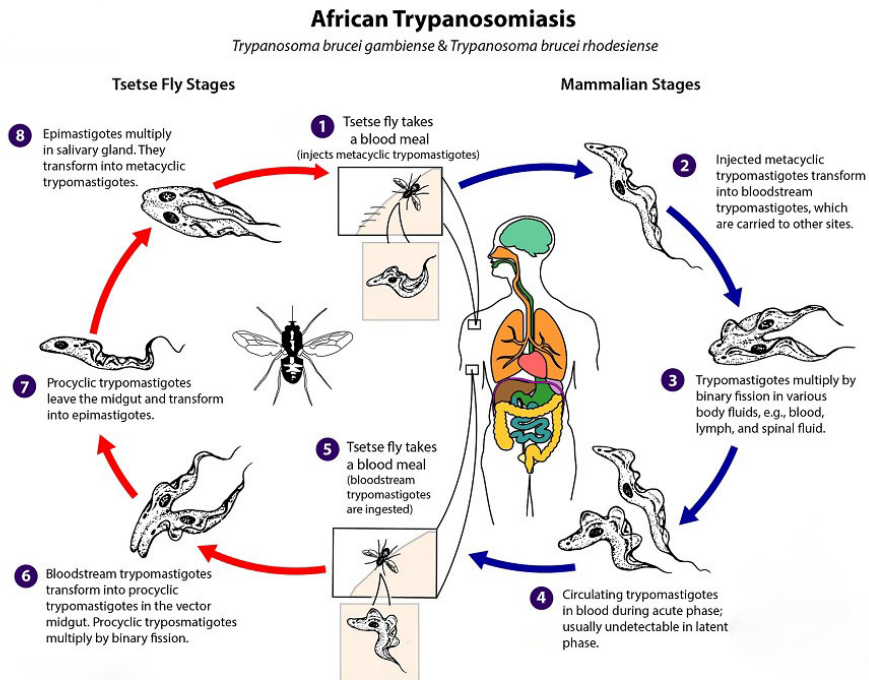
Figure 2: Life cycle of *T.b. Gambiense* and *T.b. rhodesiense*. Figure taken from CDC with minor revisions.[30]

The mammalian stage of the life cycle can be subdivided in two stages based on the disease progression and the subsequent observed symptoms. The first stage, the heamolymphatic stage, is characterized by several mild symptoms (e.g. headache and fever).[11] The second stage, the meningoencephalitic stage, consists of more severe symptoms due to invasion of the CNS by the parasite and includes neurological decline, distortion of the circadian rhythm and coma.[1, 6] Although the time for disease progression differs between the two parasites, both forms of the disease are almost invariably fatal if left untreated.[9] Diagnosis and treatment of HAT is made difficult by the fact that most patients live in remote rural areas and current diagnostic tests lack sensitivity or specificity.[1, 2, 9, 24, 25] Furthermore, current treatments for HAT have major disadvantages including subspecies selectivity, disease stage selectivity, complex administration and toxicity.[26-29]

1.2. Current medications

Over the years, several medicines have been registered for treating HAT, including atoxyl (**1,** Figure 3), nifurtimox (**2**), pentamidine (**3**), eflornithine (**4**), melarsoprol (**5**), suramin (**6**) and fexinidazole (**7**).[24, 31-35] The curative properties of arsenic for Nagana (animal trypanosomiasis) have been known since mid-19th century,[36] and led to the discovery of atoxyl in the early 1900's.[31] However, the extensive use of atoxyl revealed severe toxicity issues and further development was needed.[31] Currently, treatment regimens for HAT depend on the causative subspecies and the stage of the disease (Table 1). Until recently pentamidine was recommended for a first stage infection with *T.b. gambiense*, but has been replaced by treatment with fexinidazole in 2019.[37] Early stage infections of *T.b. rhodesiense*, however, are still treated with suramin.[24, 26, 38] For a second stage infection, eflornithine, nifurtimox and melarsoprol are used.[26]

1
Atoxyl
T.b. rhodesiense EC$_{50}$ = 1.09 μM

2
Nifurtimox
T.b. rhodesiense EC$_{50}$ = 1.09 μM

3
Pentamidine
T.b rhodesiense EC$_{50}$ = 0.002 μM

4
Eflornithine
T.b. rhodesiense EC$_{50}$ = 8.58 μM

5
Melarsoprol
T.b. rhodesiense EC$_{50}$ = 0.011 μM

6
Suramin
T.b. rhodesiense EC$_{50}$ = 0.046 μM

7
Fexinidazole
T.b. rhodesiense EC$_{50}$ = 2.17 μM
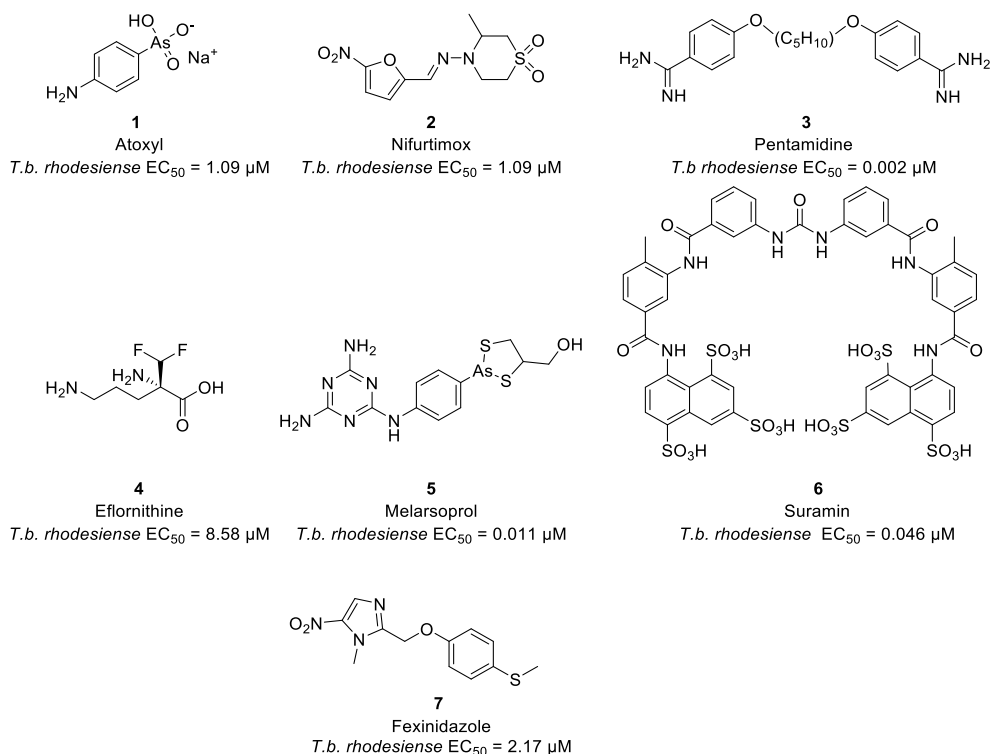
Figure 3: Structures of the current and past medications against HAT and their EC$_{50}$ values against T.b. rhodesiense. [26, 29, 35, 39, 41]

Most treatments show a broad range of undesirable side effects and/or suffer from challenging treatment regimens. For example, the use of melarsoprol is associated with a mortality rate of 5-10% and eflornithine requires *i.v.* administration during a 14-day period.[26, 29] Nifurtimox and eflornithine are commonly used as combination therapy (NECT) to reduce the dosing regimen to a 10 days treatment with nifurtimox and 7 days dosing with eflornithine.[39] However, this new combination treatment is only used for *T.b. gambiense* infections.[39] However, an slight improvement in efficacy (96% vs. 94%) and a reduction in adverse side effects (10% vs. 26%) was observed when nifurtimox and eflornithine were used as combination therapy (NECT) compared to a normal eflornithine treatment.[39] Currently NECT is recommended as first in line treatment for late stage trypanosomiasis and is applied as a 10 days nifurtimox dosing regime and a 7 days eflornithine dosing regimen.[39] In the last 30 years only one new treatment (fexinidazole) against HAT has passed the clinical stage. As it is, the very limited chemotherapy options in combination with an increasing drug resistance by the parasite poses a considerable threat to mammalian health.[26, 31, 40]

Table 1: Overview of the current drugs against both forms of HAT and their dosing regimen.

Drug	Subspecies	Dosing regime (*Adm.*)	Year of first use
Pentamidine	*T.b. gambiense (Stage I)*	4 mg/kg/day for 7-10 days (*I.M.*)	1940
Fexinidazole	*T.b. gambiense (Stage I)*	1.8 g/day on day 1-4 + 1.2 g/day for 6 days (*P.O.*)	2019
Nifurtimox*	*T.b. gambiense + rhodesiense (Stage II)*	8-20 mg/kg/day for >90 days (*P.O.*)	1977
Eflornithine*	*T.b. gambiense (Stage II)*	400 mg/kg/day for 14 days (*I.V.*)	1981
Suramin	*T.b. gambiense + rhodesiense (Stage I)*	1 g/day on day 1, 3, 7, 14 and 21 (*I.V.*)	1922
Melarsoprol	*T.b. gambiense + rhodesiense (Stage II)*	2.2 mg/kg/day for 10 days (*I.V.*)	1949

Nifurtimox and Eflornithine are commonly used as combination therapy (NECT) with a 10 days nifurtimox dosing regime and a 7 days eflornithine dosing regimen

1

1.3.   Latest research development

Research groups in different areas are now unraveling the parasites genome and proteome,[12, 38, 42, 43] improving the sensitivity of diagnosis methods[11, 25, 44, 45] and designing new chemotherapeutics for the treatment of HAT.[27, 28, 40] Two compounds, Fexinidazole (**7**) and Acoziborole (**8**) (Figure 4), are currently finalizing clinical phase III and are both promising candidates as monotherapy for HAT.[46]

Fexinidazole, **7**
T.b. rhodesiense EC$_{50}$ = 2.17 µM
T.b. gambiense EC$_{50}$ = 1.84 µM

SCYX-7158, **8**
T.b. rhodesiense EC$_{50}$ = 0.8 µM
T.b. gambiense EC$_{50}$ = 0.6 µM
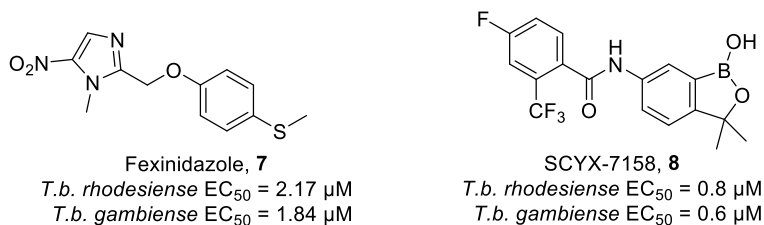
Figure 4: Structures of fexinidazole and acoziborole (SCYX-7158) currently in clinical phase 3 for treatment against HAT with their EC$_{50}$ value against *T. brucei* parasites.[35, 47]

Fexinidazole, a nitroimidazole, has been in preclinical studies as a broad spectrum antimicrobial in the 1970's and was also identified as being a potent compound against *T.b. brucei* and *T.b. cruzi* (Chagas disease) in 1983.[48-50] However, further development of fexinidazole was never pursued.[48, 51] The compound was "rediscovered" in a project by the Drugs for Neglected Diseases *initiative* (DNDi) following a systematic review of more than 700 nitroheterocyclic compounds.[52] Fexinidazole, a DNA synthesis inhibitor,[53] was found to be well tolerated with no specific warnings for toxicity or adverse effects and entered clinical phase II/III mid-2012.[52] Remarkably, fexinidazole is less efficacious than the nifurtimox/eflornithine combination treatment, but this is more than compensated for by an increased access to treatment resulting from the possibility of an oral monotherapy against both stages of *gambiense*-HAT (*g*-HAT).[46] In 2019 the European Medicines Agency (EMA) gave a positive opinion about the treatment of *g*-HAT using fexinidazole for both stages of the disease.[53, 54] However, the NECT-treatment is still preferred as late stage treatment, because of the 11.8% less favorable outcome of fexinidazole against 2nd stage *g*-HAT with respect to NECT (86.9% vs 98.7%, respectively).[54] Unfortunately, hospitalization or presence of trained staff is still needed for administration of fexinidazole because of the possible nausea and vomiting caused by fexinidazole administration. Since drug absorption is dependent on food ingestion, trained health staff should make sure that the patient is in fed condition

when treated.[54] It should also be noted that more neuropsychiatric adverse events (e.g. headache, insomnia or anxiety) were observed in patients treated with fexinidazole.[46, 53] Furthermore, patients should be informed about possible relapses after fexinidazole treatment and should be monitored 12 and 24 months after treatment for suggestive symptoms of *g-HAT*.[54] Beside its effect on *Trypanosoma brucei* parasites fexinidazole was also shown to be effective against *Trypanosoma cruzi* (Chagas disease) and *Leishmania* spp.[53, 55, 56]

Acoziborole, also known as SCYX-7158, was discovered by Anacor Pharmaceuticals in a screening campaign of a focused library of anti-infective benzoxaboroles.[47, 57] These boron containing compounds are relatively unknown in the medicinal chemistry field, but were shown to be effective against various infectious diseases, including malaria and Chagas disease.[58] The initial hits underwent several rounds of SAR exploration ultimately resulting in the discovery of acoziborole.[47, 58, 59] The compound successfully completed clinical study phase I in 2015 and phase II/III was started by the end of 2016.[60] Once approved, acoziborole will be the first one-day, one-dose treatment and thereby have a much less complex administration regimen than the current treatments against HAT. However, the long-term effects and toxicity of boron containing compounds is not yet fully known and will be answered in the next few years.[59]

Fexinidazole as well as Acoziborole do not show subspecies specificity and show a similar phenotypic activity against *T.b. gambiense* and *T.b. rhodesiense*.[35, 47] However, both are currently in clinical phase II/III as potential treatment for *T.b. gambiense* HAT only.[46, 47, 60] A study against *T.b. rhodesiense* for both compounds is required to be able to replace the highly toxic drug melarsoprol, which remains the only drug to treat the second stage of *T.b. rhodesiense* HAT.[46] Considering the potential cross resistance for fexinidazole with nifurtimox and the observed resistance for melarsoprol, development of new trypanosidals with different modes of action is still needed.[31, 61]

Target repurposing is one of the approaches used in the design of new chemotherapeutics, where a pathogen target is matched with a homologues human target that have been pursued for drug discovery.[62, 63] Several proteins have been identified as potential targets to treat HAT, including *N*-myristoyltransferase, leucyl-tRNA synthetase, glycogen synthase kinase-3 and phosphodiesterase B1/2.[62,

[64-67] The work presented here is focused on phosphodiesterase, more precisely *Trypanosoma brucei* phosphodiesterase B1 (TbrPDEB1).

2. Human and parasitic phosphodiesterases (PDE)

2.1. Human PDEs

The human genome encodes 21 genes organized in 11 structurally related PDE families (PDE1-11), which all together generate approximately 100 PDE isozymes by alternative mRNA splicing or transcriptional processing.[68, 69] These proteins play an important role in the cellular cyclic nucleotide signaling system (Box 1), wherein PDEs are responsible for the hydrolysis of the 3',5'-phosphodiester bond of cAMP or cGMP to yield 5'-AMP or 5'-GMP, respectively.[68] PDEs regulate their intracellular concentrations and, consequently, regulate various cellular functions, such as cell differentiation and proliferation.[70] The 11 human PDE families can be divided in three groups based on their substrate specificity (Figure 5).[68-70] Several human PDE families (hPDE1-3, 10 and 11) do not display a specific substrate selectivity and can catalyze the conversion of both cAMP and cGMP.[70] The remaining six PDE families are substrate specific for cGMP (hPDE5, 6 and 9) or cAMP (hPDE4, 7 and 8).
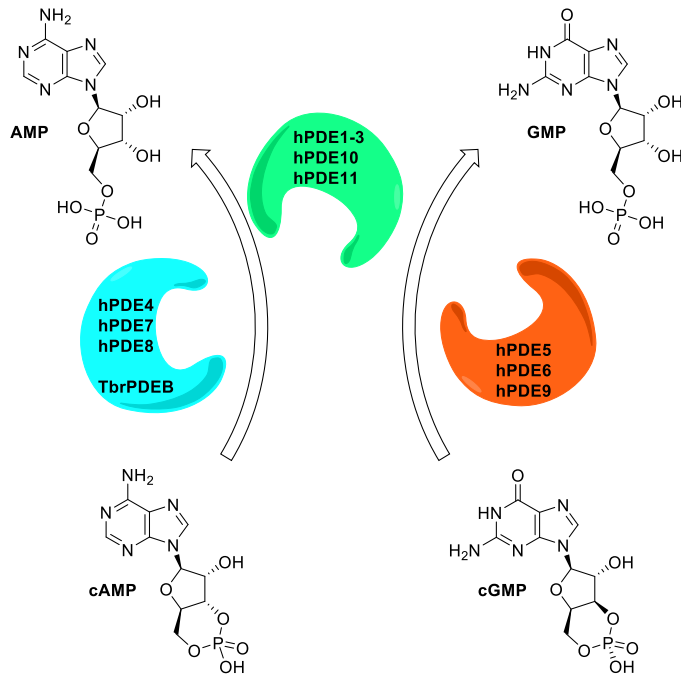
Figure 5: Division of hPDEs by substrate specificity.

Box 1: cAMP cell signalling in eukaryotic cells

The communication between eukaryotic cells and their environment consists of complex transduction pathways involving many (surface) receptors and chemical substances (Figure 6). Many of the extracellular substances (first messengers) cannot penetrate the cell surface, but transfer signals via surface receptors towards second messengers like adenosine 3',5'-cyclic monophosphate (cAMP) and cyclic guanosine monophosphate (cGMP).[78] Binding of ligands (e.g. hormones, neurotransmitters and growth factors) to GPCRs activates transmembrane adenylate cyclase (AC), which convert ATP into cAMP. The formed cAMP then activates one of the three main effector proteins, consisting of protein kinase A (PKA),[79] guanine-nucleotide exchange proteins activated by cAMP (EPAC)[80] and cyclic-nucleotide-gated ion channels (CNG).[81, 82] The activation of intracellular second messengers gives rise to a variety of biochemical reactions that result in several physiological effects, which oppose each other in some cases (e.g. cell proliferation and cell death).[78, 82] Since various first messengers make use of the cAMP signalling pathway, it became clear that the original linear view of the pathway – where external stimuli result in increase of cellular cAMP – was too simplistic. The ability of the cell to respond to multiple simultaneous stimuli led to the hypothesis of compartmentalized cAMP signal cascades in so-called 'signalosomes'.[82-85] Signal termination by hydrolysis of cAMP and cGMP is regulated by phosphodiesterase (PDE) protein family.[79] PDE inhibitors have been demonstrated to significantly increase the cAMP levels in cells resulting in various beneficial effects like reduction of inflammation, immunosuppression and treatment of depression and asthma. However, lack of isoform specificity of some of these inhibitors resulted in a broad spectrum of unwanted side effects.[78]

Figure 6: Overview of the cAMP signaling pathway. Illustration taken from Cusabio with minor revisions.[86]

2.2. Trypanosoma PDEs

Characterization of the *T. brucei* genome revealed 4 well-conserved parasite PDE families (TbrPDEA-D) which have a substrate selectivity or high preference for cAMP.[71] TbrPDEA shows no catalytic activity towards cGMP, but has a remarkably high K_m fo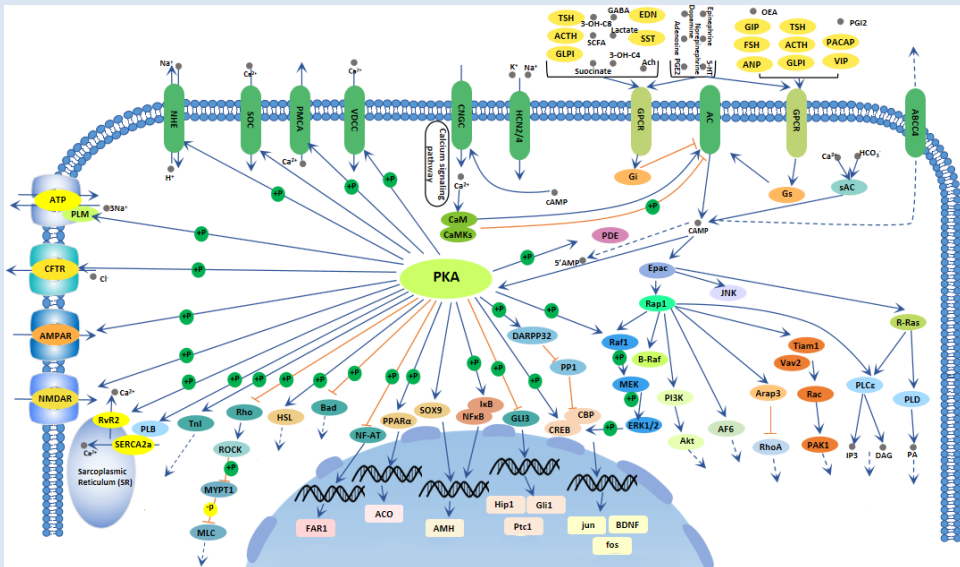r cAMP ($K_m > 600$ µM) and appears to be an enzyme which is nonessential for proliferation in *T. brucei*.[72, 73] The TbrPDEB family consists of two isoforms (TbrPDEB1 and B2) that are both cAMP specific with K_m values in the range of 5 µM.[74-76] Studies with genetic TbrPDEB knock-out strains using RNAi have shown that both enzymes are essential for the proliferation of the parasite.[76, 77] Later studies validated that TbrPDEB can be used as druggable targets for HAT.[87, 88] The two isoforms show a high sequence identity (88%) of the catalytic domain and it is expected that TbrPDEB inhibitors show similar potencies against both isoforms.[89] The sequence conservation between TbrPDEB1 and most mammalian PDEs is about 30%,[76] but when considering substrate specificity, TbrPDEB is mostly related to hPDE4, 7 and 8. Several drug repurposing studies have been performed to find new hits as potential new starting points for further drug development, revealing a preference for hPDE4 inhibitors (*vide infra*).[87] Due to mutations during evolution, PDEC became an inactive enzyme in several trypanosomes including *T. brucei*, while it remained active in several other kinetoplastids.[90] The genome of *Trypanosoma cruzi* (causative agent of Chagas disease) also encodes one PDEC family and was shown to be the only enzyme capable of hydrolyzing cGMP ($K_m \sim 80$ µM), although it shows a preference for cAMP ($K_m \sim 30$ µM).[71] TbrPDED is relatively underexplored and there is not much known about its function and localization.[75]

2.3. Phosphodiesterases in T. brucei cell signaling

Although PDEs have the same function in kinetoplastids as eukaryotic cells, i.e., the conversion of cAMP to AMP, their importance in the cell signaling cascade is slightly different given the small size of kinetoplastids (2-20 µm for trypanosomes *versus* a diameter of 10-100 µm for eukaryotic cells).[91] Strict control over cAMP concentrations in the trypanosome cell is important to prevent diffusion of cAMP throughout the whole cell and thereby disrupting the homeostasis.[92] Control over the cAMP concentration is also largely dependent on precise localization of the PDEs in the cell. TbrPDEB1 is localized in the paraflagellar rod structure of the flagellum, while TbrPDEB2 is mostly found in the cytoplasm of the flagellum.[77]

In the cell signaling pathway, cAMP is formed by activation of one of the adenylyl cyclases (ACs) located in the plasma membrane of the flagellum (Figure 7).[91, 93] These ACs are structurally different from mammalian ACs being only one single trans-membrane helix with an extracellular N-terminus.[91, 94] With the lack of G-protein coupled receptors in trypanosomes, this N-terminal extracellular domain is suggested to function as a receptor for signaling.[73, 91] Unfortunately, it is still unknown what ligands activate the receptor since no endogenous ligand has been identified yet. Nevertheless, extracts from *T. brucei* insect vectors were shown to activate ACs, probably caused by a low-molecular weight molecule named stumpy induction factor (SIF), which results in the differentiation of long slender bloodstream *T. brucei* in non-replicating stumpy form. Furthermore, the ACs are involved in the parasites interaction with the host by modulation of tumor necrosis factor alpha (TNF-α).[73, 95, 96] In contrast to mammalian cells, where cAMP-dependent protein kinase A (PKA) is one of the major effectors of cAMP, no evidence has been reported of a similar effector protein in *T. brucei*. Instead, four cAMP responsive proteins (CARPs) were identified as being downstream effectors of cAMP in *T. brucei*, but their exact role in cellular processes is yet unknown.[73, 96]
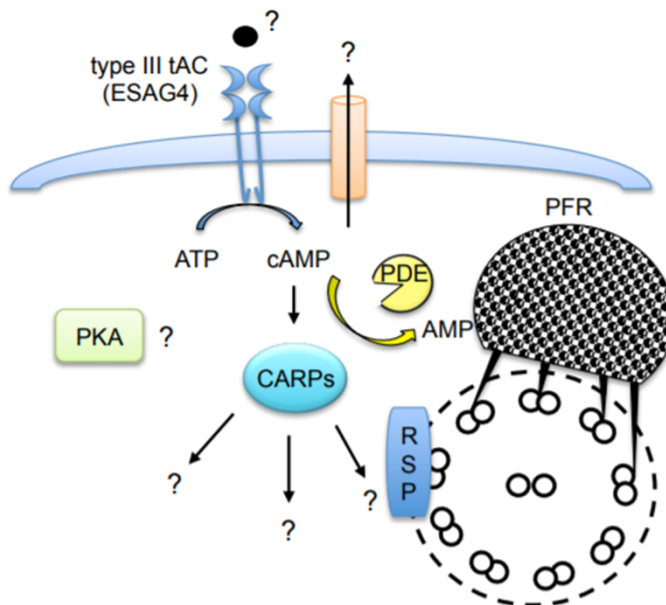
Figure 7: Schematic overview of cAMP cell signaling pathway in trypanosomes. Illustration taken from Salmon *et al*.[96]

2.4. PDE as druggable targets

The crucial role of mammalian PDEs in different biological processes have made them interesting targets for many different diseases, including COPD, inflammation, heart failure and cancer.[68-70] Over the years, several hPDE4 inhibitors were discovered and developed as treatment for various diseases (Figure 8, for more information about hPDE4, see Box 2).[70] Rolipram was discovered as one of the first human PDE4 inhibitors and further developed as a potential antidepressant or treatment for multiple sclerosis.[97, 98] However, further development was terminated due to its limited clinical use caused by side effects or lack of efficacy, but it has often been used as a valuable reference compound.[99, 100] Further research on Rolipram led to the discovery of Piclamilast, which failed in clinical phase 2 due to undesirable side effects and poor pharmacokinetics.[101, 102] Further development of Piclamilast resulted in the discovery of Roflumilast (Daxas®; Daliresp®), which was the first hPDE4 inhibitor to be approved for the treatment of severe COPD.[103] Cilomilast was developed as a potential oral treatment for COPD as well, but was abandoned by GSK before final approval by de FDA.[68, 104] Apremilast (Otezla®) was approved as a treatment for psoriatic arthritis and psoriasis by de FDA in 2014.[105, 106]

Rolipram, **9**
hPDE4 IC_{50} = 132 nM

Piclamilast, **10**
hPDE4 IC_{50} = 0.4 nM

Roflumilast, **11**
hPDE4 IC_{50} = 0.2 nM

Cilomilast, **12**
hPDE4 IC_{50} = 120 nM

Apremilast, **13**
hPDE4 IC_{50} = 220 nM

Crisaborole, **14**
hPDE4 IC_{50} = 860 nM

GSK256066, **15**
hPDE4 IC_{50} = 0.003 nM

16
hPDE4 IC_{50} = 0.07 nM
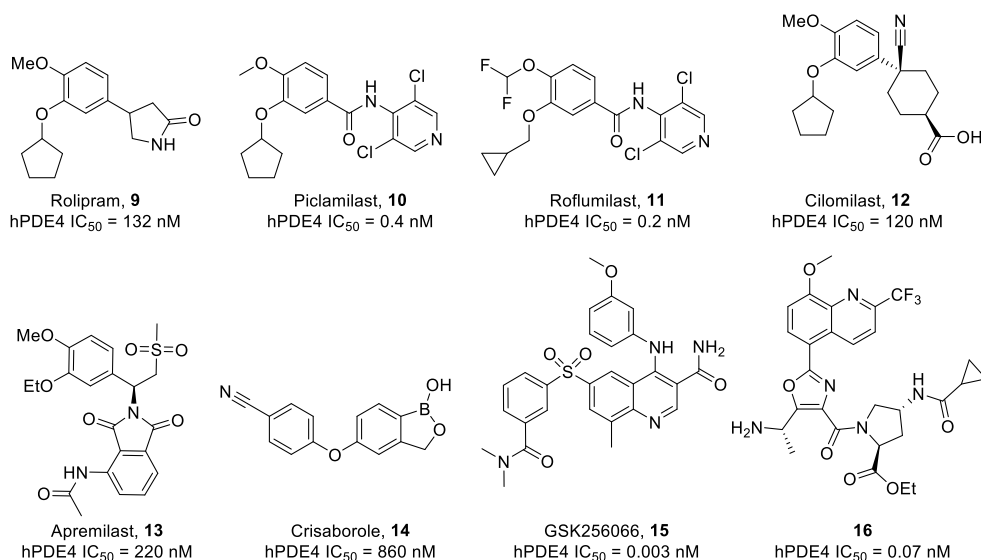
Figure 8: Structures of hPDE4 inhibitors[104, 108-113]

More recently, Crisaborole (Eucrisa®) was accepted as a treatment for patients with mild to moderate atopic dermatitis.[107] GSK256066 (**15**) and **16** are currently in development as oral (GSK256066) or inhaled (**16**) treatment for COPD by GSK and Merck, respectively.[108, 109]

Several compounds have been co-crystallized in hPDE4 and show a conserved binding mode of substrates in the active site of hPDE4 (Figure 9).[114-118] The crystal structure of cAMP bound to the catalytic domain hPDE4 shows that 3 amino acids play an important role in binding of the substrate to the protein.[116] The adenine of cAMP is situated in a hydrophobic clamp between Phe372 and Ile336 and makes a hydrogen bond with Gln369. Rolipram and Piclamilast show a very similar binding mode where the catechol moiety is positioned in the hydrophobic clamp and forming hydrogen bonds with the two ether functionalities.[115, 117]
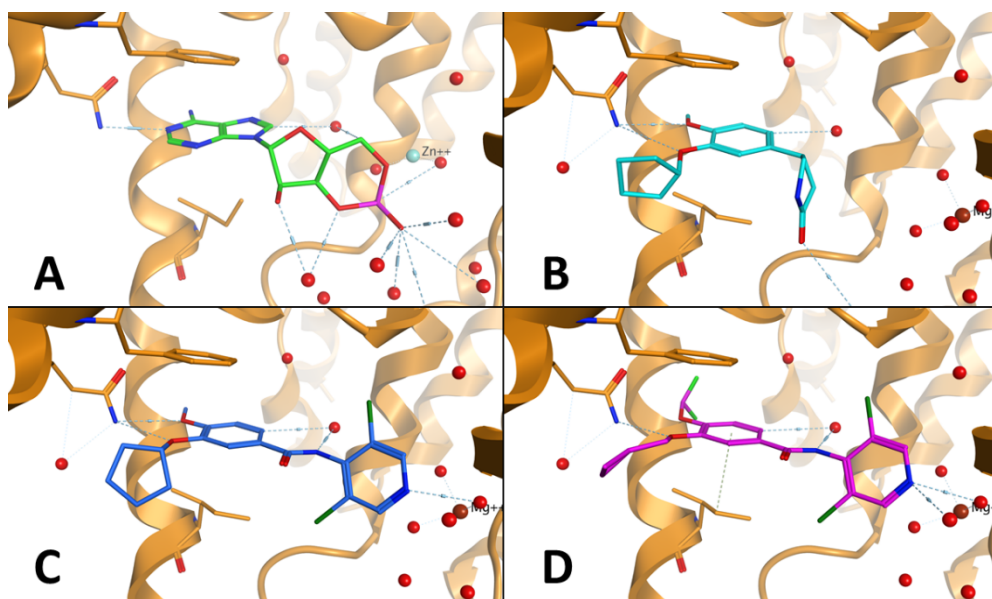
Figure 9: A) cAMP (PDB: 2PW3) and hPDE4 inhibitors B) Rolipram (PDB: 1TBB), C) Piclamilast (PDB: 1XON) and D) Roflumilast (PDB: 1XOQ) co-crystallized in hPDE4D. Residues responsible for binding (Gln369, Phe372 and Ile336), water and metal ions are shown for clarity.

Box 2: PDE4 in humans

The eight human cAMP-catalysing PDE families are thought to be the basis for compartmentalized cAMP signalling in cells, since they are the only enzymes capable of degrading cAMP.[119, 120] The hPDE4 family is one of the most extensively investigated group of enzymes.[84] hPDE4 plays a pivotal role in many different cell types and tissues, including leukocytes, airway and smooth muscle cells, vascular endothelium and brain tissue.[84, 85, 121-124] The four hPDE4 genes (hPDE4A-D) encode for over 16 isoforms and each has a unique N-terminal domain. The unique N-terminal domain in combination with upstream conserved regions (UCRs) have an important role in cellular localization and their catalytic activity.[119] The small variations in UCRs allow different isoforms to be phosphorylated by ERK or PKA, but also allows isoforms to interact with other proteins like scaffold protein myomegalin, cardiac L-type Ca^{2+} channel, the immunophilin XAP2 and phosphatidic acid.[119] The influence of hPDE4 on the function of these other proteins explains the broad applicability as drug target. hPDE4 inhibitors have been shown to have an important effect in many inflammatory based diseases like COPD, severe asthma's, Crohn's disease or psoriasis.[124] In these diseases PDE-mediated increase of cAMP leads to reduced formation of tumor necrosis factor-α (TNF-α), interleukin-10 (IL-10) or superoxide anions.[84, 125] hPDE4 is also thought to play a central role in the mechanism of action of many different antidepressants.[126] Furthermore, is has been shown that the downstream influence of PDE-inhibitors on PKA activity has a positive effect on memory and dopamine uptake.[121] These findings make hPDE4 inhibitors interesting for many CNS related diseases, such as multiple sclerosis, OCD, depression, addictions or stroke.[121, 126-132]

Structural comparison of TbrPDEB1 with hPDE4 shows a highly conserved active site with the same amino acids providing bonding of the substrate (Figure 10).[133] However, an additional pocket is visible in the TbrPDEB1 crystal structure which is located near the active site.[133] This parasite specific pocket (P-pocket) has been recognized as a potential target for obtaining selectivity over human PDEs, especially hPDE4.[133] Selectivity of new TbrPDEB1 inhibitors over human PDEs is essential since lack of selectivity can result in a broad spectrum of side effects. For instance, a strong inhibitory effect on hPDE4 often results in side effects like emesis,

nausea, diarrhea and suppression of the immune system.[84, 124, 134, 135] Although the side effects are not life threatening on their own, they can cause severe problems for patients with HAT. The emerging structural information as represented in Figure 10 gives opportunities for structure-based design, i.e., by exploiting the apparent differences in the enzyme structures.
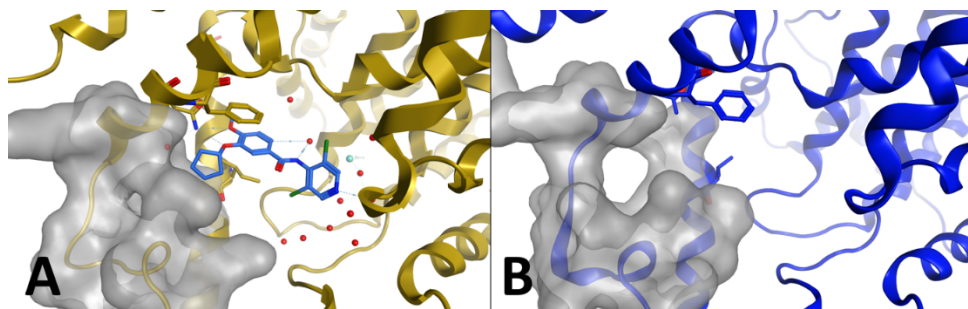
Figure 10: Comparison catalytic domain hPDE4 and TbrPDEB1 A) Crystal structure of Piclamilast in hPDE4 with the molecular surface of the M-loop region visualized in grey. B) Crystal structure of unliganded TbrPDEB1 with the molecular surface of the M-loop region visualized in grey.

In order to find new leads against TbrPDEs, several studies have been performed to develop selective TbrPDEB inhibitors. A set of known hPDE inhibitors has been screened by Bland *et al.* for activity against TbrPDEB1, showing a preference in hPDE4 inhibitors.[87] Piclamilast (**10**, TbrPDEB1 IC_{50} = 4.7 µM) was deemed suitable as starting point for further structure activity relationship (SAR) studies. Although a divers set of Piclamilast analogues were tested for their TbrPDEB1 inhibitory activity, none of the synthesized compounds showed an improved potency (<50% inhibition at 10 µM).[87, 136] Amata *et al.* used a similar approach starting from Cilomilast (**12**) and replacing the cyclopentyl by a long flexible tail towards the P-pocket (**17**, Figure 11).[112] Although an improvement in TbrPDEB1 inhibition was observed (IC_{50} = 0.98 µM), the potency for hPDE4 was still about 25-fold higher (IC_{50} = 0.038 µM).[112] Furthermore, only a weak effect on the growth of *T. brucei* parasites was observed (EC_{50} = 26 µM).[112]

A fragment growing approach starting from Rolipram and a hPDE3 inhibitor reported by Orrling *et al.* resulted in the finding of a very active pyrazolone based compound (**18**, IC_{50} = 0.049 µM).[89] The *in vitro* trypanocidal effect was validated by measuring the intracellular cAMP levels of *T. brucei* parasites after administration of the compound. The accumulation of cAMP in the cells was dose dependent and the parasites showed a typical phenotype with multiple nuclei and kinetoplasts, as

1

previously reported in genetic and chemical interference studies.[77, 88, 89]. However, the potency of **18** for hPDE4 (IC$_{50}$ = 0.0046 µM) is a 10-fold higher than the potency for TbrPDEB1 stressing the difficulty to obtain selectivity over the human homologues.

A more potent, but structurally similar TbrPDEB1 inhibitor (NPD-001, **19**) has been identified by de Koning *et al.* using high-throughput screening of 400,000 compounds against recombinant TbrPDEB1.[88] This compound was developed as a hPDE4 inhibitor by Van der Mey *et al.* and contains the often observed catechol moiety in human PDE4 inhibitors.[137, 138] Although NPD-001 shows a very high potency for TbrPDEB1 (IC$_{50}$ = 4.0 nM), the potency for hPDE4 is even higher (hPDE4 IC$_{50}$ = 0.6 nM).[139] This undesirable high activity was one the focus points for a follow-up SAR study, where NPD-001 was modified at three different positions.[139] Unfortunately, this did not lead to any improvement in activity or selectivity and NPD-001 remains the most active TbrPDEB1 inhibitor reported at this moment.[139]

17
TbrPDEB1 IC$_{50}$ = 0.95 µM
hPDE4B IC$_{50}$ = 0.038 µM
T. brucei EC$_{50}$ = 26 µM

18
TbrPDEB1 IC$_{50}$ = 0.049 µM
hPDE4B IC$_{50}$ = 0.0046 µM
T. brucei EC$_{50}$ = 0.52 µM

NPD-001, **19**
TbrPDEB1 IC$_{50}$ = 0.004 µM
hPDE4 IC$_{50}$ = 0.0006 µM
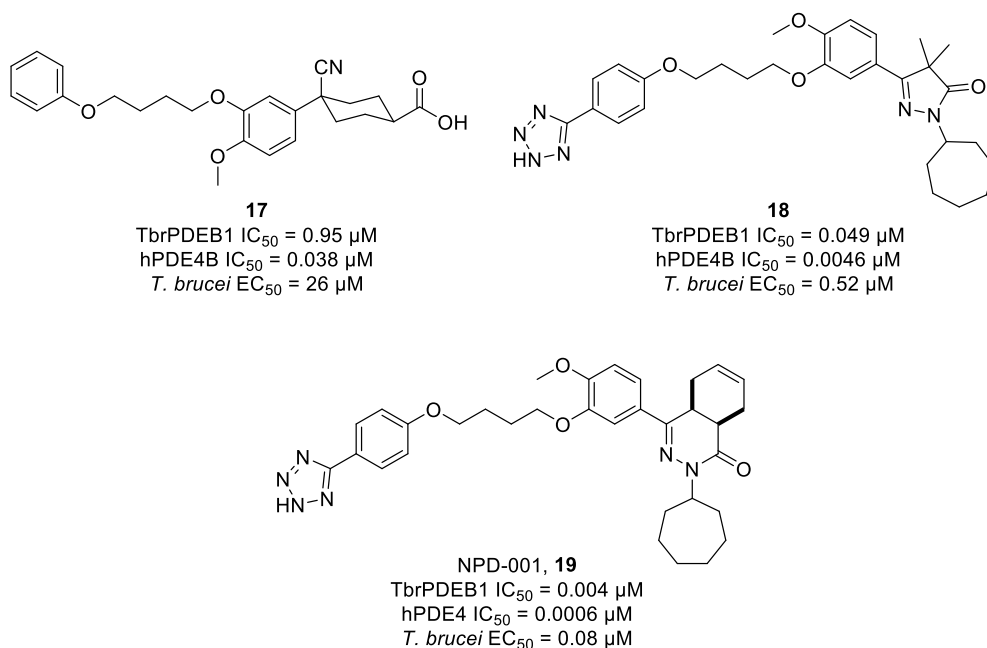*T. brucei* EC$_{50}$ = 0.08 µM

Figure 11: Structures of TbrPDEB1 inhibitors originating from hPDE4 inhibitors with their activity against TbrPDEB1, hPDE4 and *T. brucei* parasites.

3. Aim and outline of this thesis

Active screening and monitoring of human African trypanosomiasis have brought the disease close to eradication. However, ineffective screening of especially the rural and politically unstable regions of Africa result in underreporting of the disease.[140] New and easily available drugs can have a major effect on the process toward complete eradication of this fatal disease. Over the last decades, several biological targets have gained interest for small molecule drug discovery, of which one is the trypanosome PDEB1/2. Tetrahydrophthalazinone-based TbrPDEB1 inhibitors show great potential as new treatment for human African trypanosomiasis. However, the enzyme selectivity profile for this class of compounds is still undesirably in favor for hPDE4, instead of TbrPDEB1. The aim of this thesis was the structure-based drug development of TbrPDEB1 selective compounds using tetrahydrophthalazinones as core scaffold and exploiting the small parasite specific pocket in TbrPDEB1 as handle to obtain selectivity over hPDE4.

Chapter 2 describes the development of the first selective TbrPDEB1 inhibitors by introducing a rigid phenyl linker to activity probe the parasitic P-pocket. Several crystal structures of selective inhibitors in TbrPDEB1 prove the successful targeting of the P-pocket and form the basis of further exploration of selective TbrPDEB1 inhibitors (**Chapter 3** to **5**). **Chapter 3** concentrates on development of diaryl tetrahydrophthalazinones to restore the lost cellular activity of the selective biphenyl class. The typical catechol character of the phthalazinones was reestablished and new linkers were designed based on the crystal structures of selective TbrPDEB1 inhibitors. New linker analogues of the biphenyl tetrahydrophthalazinones are discussed in **Chapter 4** to determine the best vector for P-pocket targeting and find alternatives for the lipophilic phenyl moiety. Various linkers with different sizes, aromaticity and vector angles were tested. The combination of good cellular activity and a promising vector for P-pocket targeting in a TbrPDEB1 crystal structure pushed the alkynamide class forward for further development (**Chapter 5** and **6**). A structure-guided development of new alkynamides is described in **Chapter 5**. Computational techniques were used to predict new alkynamide modifications to probe the P-pocket to obtain a better TbrPDEB1 selectivity while retaining the cellular activity and cytotoxicity profile. Here we prove that selectivity for TbrPDEB1 over hPDE4 can be obtained for

alkynamide phthalazinones, despite their lack of interaction with the P-pocket in the crystal structure. **Chapter 6** extends the applicability of the alkynamide tetrahydrophthalazinones as possible new treatments for taxonomically related parasites *Trypanosoma cruzi, Leishmania major* and *Plasmodium falciparum*. Furthermore, the compound set is increased by several alkynamide isosteres to investigate the Michael accepting properties of the alkynamide functionality, which is indicated as one of the potential pitfalls. Finally, in **Chapter 7** I will end with some concluding remarks and future prospects.

4. References

1. N. Feasey, M. Wansbrough-Jones, D.C. Mabey, *et al.*, Neglected tropical diseases, British Medical Bulletin, 93 (2010) 179-200.

2. J. Utzinger, S.L. Becker, S. Knopp, *et al.*, Neglected tropical diseases: diagnosis, clinical management, treatment and control, Swiss Med Wkly, 142 (2012) w13727.

3. G. Yamey, P. Hotez, Neglected tropical diseases, BMJ, 335 (2007) 269-270.

4. S.L. Reed, J.H. McKerrow, Why Funding for Neglected Tropical Diseases Should be a Global Priority, Clinical Infectious Diseases, (2018) ciy349-ciy349.

5. WHO, WHO Neglected Diseases, http://www.who.int/neglected_diseases/diseases/summary/en/; 2020, Accessed on 30-04-2020

6. P.G.E. Kennedy, Human African trypanosomiasis of the CNS: current issues and challenges, Journal of Clinical Investigation, 113 (2004) 496-504.

7. C. Klausen, F. Kaiser, B. Stuven, *et al.*, Elucidating cyclic AMP signaling in subcellular domains with optogenetic tools and fluorescent biosensors, Biochem Soc Trans, 47 (2019) 1733-1747.

8. P. Büscher, G. Cecchi, V. Jamonneau, *et al.*, Human African trypanosomiasis, The Lancet, 390 (2017) 2397-2409.

9. A. Buguet, G. Mpanzou, M. Bentivoglio, Human African Trypanosomiasis: A Highly Neglected Neurological Disease, (2014) 165-181.

10. WHO, Global Health Observatory data repository Human African Trypanosmiasis, http://apps.who.int/gho/data/node.main.A1635?lang=en; 2020, Accessed on 22-12-2020

11. R. Brun, J. Blum, F. Chappuis, *et al.*, Human african trypanosomiasis, The Lancet, 375 (2010) 148-159.

12. S. Aksoy, G. Attardo, M. Berriman, *et al.*, Human African Trypanosomiasis Research Gets a Boost: Unraveling the Tsetse Genome, PLoS Neglected Tropical Diseases, 8 (2014) e2624.

13. D. Al-Sajee, X. Yin, G.M. Gauvreau, An evaluation of roflumilast and PDE4 inhibitors with a focus on the treatment of asthma, Expert Opin Pharmacother, 20 (2019) 609-620.

14. J.C.F. Rodrigues, J.L.P. Godinho, W. de Souza, Biology of Human Pathogenic Trypanosomatids: Epidemiology, Lifecycle and Ultrastructure, in: A.L.S. Santos, M.H. Branquinha, C.M. d'Avila-Levy, L.F. Kneipp, C.L. Sodré (Eds.) Proteins and Proteomics of Leishmania and Trypanosoma, Springer Netherlands, Dordrecht, 2014, pp. 1-42.

15. M.D. Urbaniak, M.L.S. Guther, M.A.J. Ferguson, Comparative SILAC Proteomic Analysis of Trypanosoma brucei Bloodstream and Procyclic Lifecycle Stages, PLOS ONE, 7 (2012) e36619.

16. B.L. Weiss, J. Wang, M.A. Maltz, *et al.*, Trypanosome Infection Establishment in the Tsetse Fly Gut Is Influenced by Microbiome-Regulated Host Immune Barriers, PLOS Pathogens, 9 (2013) e1003318.

17. D.P. Walshe, M.J. Lehane, L.R. Haines, Post Eclosion Age Predicts the Prevalence of Midgut Trypanosome Infections in Glossina, PLOS ONE, 6 (2011) e26984.

18. C. Hu, S. Aksoy, Innate immune responses regulate trypanosome parasite infection of the tsetse fly Glossina morsitans morsitans, Mol Microbiol, 60 (2006) 1194-1204.

19. Y. Hu, S. Aksoy, An antimicrobial peptide with trypanocidal activity characterized from Glossina morsitans morsitans, Insect Biochemistry and Molecular Biology, 35 (2005) 105-115.

20. S. Aksoy, Tsetse peritrophic matrix influences for trypanosome transmission, Journal of Insect Physiology, 118 (2019) 103919.

21. S. Davis, S. Aksoy, A. Galvani, A global sensitivity analysis for African sleeping sickness, Parasitology, 138 (2010) 516-526.

22. K.S. Rock, S.J. Torr, C. Lumbala, *et al.*, Quantitative evaluation of the strategy to eliminate human African trypanosomiasis in the Democratic Republic of Congo, Parasites & Vectors, 8 (2015) 532.

23. M.D. Urbaniak, D.M.A. Martin, M.A.J. Ferguson, Global Quantitative SILAC Phosphoproteomics Reveals Differential Phosphorylation Is Widespread between the Procyclic and Bloodstream Form Lifecycle Stages of Trypanosoma brucei, Journal of Proteome Research, 12 (2013) 2233-2244.

24. M. Njoroge, N.M. Njuguna, P. Mutai, *et al.*, Recent Approaches to Chemical Discovery and Development Against Malaria and the Neglected Tropical Diseases Human African Trypanosomiasis and Schistosomiasis, Chem Rev, (2014).

25. C.M. Mugasa, D. Katiti, A. Boobo, *et al.*, Comparison of nucleic acid sequence-based amplification and loop-mediated isothermal amplification for diagnosis of human African trypanosomiasis, Diagnostic Microbiology and Infectious Disease, 78 (2014) 144-148.

26. D. Legros, G. Ollivier, M. Gastellu-Etchegorry, *et al.*, Treatment of human African trypanosomiasis—present situation and needs for research and development, The Lancet Infectious Diseases, 2 (2002) 437-440.

27. A.J. Jones, V.M. Avery, Future treatment options for human African trypanosomiasis, Expert Rev Anti Infect Ther, (2015) 1-4.

28. P. Babokhov, A.O. Sanyaolu, W.A. Oyibo*, et al.*, A current analysis of chemotherapy strategies for the treatment of human African trypanosomiasis, Pathogens and Global Health, 107 (2013) 242-252.

29. A.H. Fairlamb, Chemotherapy of human African trypanosomiasis: current and future prospects, Trends Parasitol, 19 (2003) 488-494.

30. Centers for Disease Control and Prevention, https://www.cdc.gov/parasites/sleepingsickness/biology.html; 2019, Accessed on 25-08-2019

31. A.H. Fairlamb, D. Horn, Melarsoprol Resistance in African Trypanosomiasis, Trends Parasitol, (2018).

32. R.F.R.S. Boyce, The treatment of sleeping sickness and other trypanosomiases by the atoxyl and mercury method, British Medical Journal, 2 (1907) 624-625.

33. C. Burri, R. Brun, Eflornithine for the treatment of human African trypanosomiasis, Parasitol Res, 90 (2003) S49-52.

34. S. Riethmiller, From Atoxyl to Salvarsan: searching for the magic bullet, Chemotherapy, 51 (2005) 234-242.

35. M. Kaiser, M.A. Bray, M. Cal*, et al.*, Antitrypanosomal activity of fexinidazole, a new oral nitroimidazole drug candidate for treatment of sleeping sickness, Antimicrob Agents Chemother, 55 (2011) 5602-5608.

36. D. Livingstone, Arsenic as a Remedy for the Tsetse Bite, British Medical Journal, s4-1 (1858) 360.

37. A.K. Lindner, V. Lejon, F. Chappuis*, et al.*, New WHO guidelines for treatment of gambiense human African trypanosomiasis including fexinidazole: substantial changes for clinical practice, Lancet Infect Dis, 20 (2020) e38-e46.

38. C.H. Baker, S.C. Welburn, The Long Wait for a New Drug for Human African Trypanosomiasis, Trends Parasitol, (2018).

39. G. Priotto, S. Kasparian, D. Ngouama*, et al.*, Nifurtimox-Eflornithine Combination Therapy for Second-Stage Trypanosoma brucei gambiense Sleeping Sickness: A Randomized Clinical Trial in Congo, Clinical Infectious Diseases, 45 (2007) 1435-1442.

40. J. Keiser, A. Stich, C. Burri, New drugs for the treatment of human African trypanosomiasis research and development, Trends Parasitol, 17 (2001) 42-49.

41. WHO, Application for revision of antitrypanosomal medicines in WHO model list of essential medicines, WHO, 2006.

42. E.A. Saada, Z.P. Kabututu, M. Lopez*, et al.*, Insect Stage-Specific Receptor Adenylate Cyclases Are Localized to Distinct Subdomains of the Trypanosoma brucei Flagellar Membrane, Eukaryotic Cell, 13 (2014) 1064-1076.

43. G. Langousis, K.L. Hill, Motility and more: the flagellum of Trypanosoma brucei, Nature Reviews Microbiology, 12 (2014) 505-518.

44. F. Chappuis, L. Loutan, P. Simarro*, et al.*, Options for field diagnosis of human African trypanosomiasis, Clinical Microbiology Reviews, 18 (2005) 133-146.

45. E. Hasker, J. Kwete, R. Inocencio da Luz*, et al.*, Innovative digital technologies for quality assurance of diagnosis of human African trypanosomiasis, PLOS Neglected Tropical Diseases, 12 (2018) e0006664.

46. F. Chappuis, Oral fexinidazole for human African trypanosomiasis, The Lancet, 391 (2018) 100-102.

47. R.T. Jacobs, B. Nare, S.A. Wring*, et al.*, SCYX-7158, an orally-active benzoxaborole for the treatment of stage 2 human African trypanosomiasis, PLoS Negl Trop Dis, 5 (2011) e1151.

48. E. Torreele, B. Bourdin Trunz, D. Tweats*, et al.*, Fexinidazole--a new oral nitroimidazole drug candidate entering clinical development for the treatment of sleeping sickness, PLoS Negl Trop Dis, 4 (2010) e923.

49. F. Jennings, G. Urquhart, The use of the 2 substituted 5-nitroimidazole, fexinidazole (Hoe 239) in the treatment of chronicT. brucei infections in mice, Zeitschrift für Parasitenkunde, 69 (1983) 577-581.

50. W. Raether, H. Seidenath, The activity of fexinidazole (HOE 239) against experimental infections with Trypanosoma cruzi, trichomonads and Entamoeba histolytica, Annals of tropical medicine and parasitology, 77 (1983) 13-26.

51. A.Y. Sokolova, S. Wyllie, S. Patterson*, et al.*, Cross-resistance to nitro drugs and implications for treatment of human African trypanosomiasis, Antimicrobial agents and chemotherapy, 54 (2010) 2893-2900.

52. M.T. Bahia, I.M. de Andrade, T.A. Martins*, et al.*, Fexinidazole: a potential new drug candidate for Chagas disease, PLoS Negl Trop Dis, 6 (2012) e1870.

53. E.D. Deeks, Fexinidazole: First Global Approval, Drugs, 79 (2019) 215-220.

54. E. Pelfrene, M. Harvey Allchurch, N. Ntamabyaliro*, et al.*, The European Medicines Agency's scientific opinion on oral fexinidazole for human African trypanosomiasis, PLOS Neglected Tropical Diseases, 13 (2019) e0007381.

55. J.A. Watson, N. Strub-Wourgraft, A. Tarral*, et al.*, Pharmacokinetic-Pharmacodynamic Assessment of the Hepatic and Bone Marrow Toxicities of the New Trypanoside Fexinidazole, Antimicrobial Agents and Chemotherapy, 63 (2019) e02515-02518.

56. E. de Morais-Teixeira, A. Rabello, M.M.G. Aguiar, In vitro activity and in vivo efficacy of fexinidazole against New World Leishmania species, Journal of Antimicrobial Chemotherapy, 74 (2019) 2318-2325.

57. D. Ding, Y. Zhao, Q. Meng, *et al.*, Discovery of novel benzoxaborole-based potent antitrypanosomal agents, ACS Med Chem Lett, 1 (2010) 165-169.
58. R.T. Jacobs, J.J. Plattner, M. Keenan, Boron-based drugs as antiprotozoals, Curr Opin Infect Dis, 24 (2011) 586-592.
59. R.T. Jacobs, J.J. Plattner, B. Nare, *et al.*, Benzoxaboroles: a new class of potential drugs for human African trypanosomiasis, Future Medicinal Chemistry, 3 (2011) 1259-1278.
60. DNDi Acoziborole, https://www.dndi.org/diseases-projects/portfolio/scyx-7158/; Accessed on 01-05-2018
61. S. Patterson, S. Wyllie, Nitro drugs for the treatment of trypanosomatid diseases: past, present, and future prospects, Trends Parasitol, 30 (2014) 289-298.
62. D.M. Klug, M.H. Gelb, M.P. Pollastri, Repurposing strategies for tropical disease drug discovery, Bioorganic & medicinal chemistry letters, 26 (2016) 2569-2576.
63. M.P. Pollastri, R.K. Campbell, Target repurposing for neglected diseases, Future medicinal chemistry, 3 (2011) 1307-1315.
64. B.D. Galvin, Z. Li, E. Villemaine, *et al.*, A Target Repurposing Approach Identifies N-myristoyltransferase as a New Candidate Drug Target in Filarial Nematodes, PLOS Neglected Tropical Diseases, 8 (2014) e3145.
65. D. Ding, Q. Meng, G. Gao, *et al.*, Design, synthesis, and structure-activity relationship of Trypanosoma brucei leucyl-tRNA synthetase inhibitors as antitrypanosomal agents, J Med Chem, 54 (2011) 1276-1287.
66. R.O. Oduor, K.K. Ojo, G.P. Williams, *et al.*, Trypanosoma brucei glycogen synthase kinase-3, a target for anti-trypanosomal drug development: a public-private partnership to identify novel leads, PLoS Negl Trop Dis, 5 (2011) e1017.
67. D. Steverding, D.W. Sexton, X. Wang, *et al.*, Trypanosoma brucei: Chemical evidence that cathepsin L is essential for survival and a relevant drug target, International journal for parasitology, 42 (2012) 481-488.
68. D.H. Maurice, H. Ke, F. Ahmad, *et al.*, Advances in targeting cyclic nucleotide phosphodiesterases, Nature Reviews Drug Discovery, 13 (2014) 290.
69. S.H. Francis, M.A. Blount, J.D. Corbin, Mammalian Cyclic Nucleotide Phosphodiesterases: Molecular Mechanisms and Physiological Functions, Physiological Reviews, 91 (2011) 651-690.
70. T. Peng, J. Gong, Y. Jin, *et al.*, Inhibitors of phosphodiesterase as cancer therapeutics, European Journal of Medicinal Chemistry, 150 (2018) 742-756.
71. S. Laxman, J.A. Beavo, Cyclic Nucleotide Signaling Mechanisms in Trypanosomes: Possible Targets for Therapeutic Agents, Molecular Interventions, 7 (2007) 203-215.
72. S. Kunz, T. Kloeckner, L.-O. Essen, *et al.*, TbPDE1, a novel class I phosphodiesterase of Trypanosoma brucei, European Journal of Biochemistry, 271 (2004) 637-647.
73. D.N. Tagoe, T.D. Kalejaiye, H.P. de Koning, The ever unfolding story of cAMP signaling in trypanosomatids: vive la difference!, Front Pharmacol, 6 (2015) 185.
74. A. Rascón, S.H. Soderling, J.B. Schaefer, *et al.*, Cloning and characterization of a cAMP-specific phosphodiesterase (TbPDE2B) from Trypanosoma brucei, Proceedings of the National Academy of Sciences, 99 (2002) 4714.
75. Y. Shakur, H.P. de Koning, H. Ke, *et al.*, Therapeutic Potential of Phosphodiesterase Inhibitors in Parasitic Diseases, in: S.H. Francis, M. Conti, M.D. Houslay (Eds.) Phosphodiesterases as Drug Targets, Springer Berlin Heidelberg, Berlin, Heidelberg, 2011, pp. 487-510.
76. R. Zoraghi, T. Seebeck, The cAMP-specific phosphodiesterase TbPDE2C is an essential enzyme in bloodstream form Trypanosoma brucei, Proceedings of the National Academy of Sciences, 99 (2002) 4343-4348.
77. M. Oberholzer, G. Marti, M. Baresic, *et al.*, The Trypanosoma brucei cAMP phosphodiesterases TbrPDEB1 and TbrPDEB2: flagellar enzymes that are essential for parasite virulence, The FASEB Journal, 21 (2007) 720-731.
78. K. Yan, L.N. Gao, Y.L. Cui, *et al.*, The cyclic AMP signaling pathway: Exploring targets for successful drug discovery (Review), Mol Med Rep, 13 (2016) 3715-3723.
79. P.B. Daniel, W.H. Walker, J.F. Habener, Cyclic AMP signaling and gene regulation, Annu Rev Nutr, 18 (1998) 353-383.
80. M. Gloerich, J.L. Bos, Epac: defining a new mechanism for cAMP action, Annu Rev Pharmacol Toxicol, 50 (2010) 355-375.
81. K. Matulef, W.N. Zagotta, Cyclic nucleotide-gated ion channels, Annu Rev Cell Dev Biol, 19 (2003) 23-44.
82. K. Lefkimmiatis, M. Zaccolo, cAMP signaling in subcellular compartments, Pharmacol Ther, 143 (2014) 295-304.
83. A. Stangherlin, M. Zaccolo, Phosphodiesterases and subcellular compartmentalized cAMP signaling in the cardiovascular system, Am J Physiol Heart Circ Physiol, 302 (2012) H379-390.
84. M.D. Houslay, P. Schafer, K.Y.J. Zhang, Keynote review: Phosphodiesterase-4 as a therapeutic target, Drug Discovery Today, 10 (2005) 1503-1519.
85. H. Huang, M. Xie, L. Gao, *et al.*, Rolipram, a PDE4 Inhibitor, Enhances the Inotropic Effect of Rat Heart by Activating SERCA2a, Front Pharmacol, 10 (2019) 221.

86. Cusabio, cAMP signaling pathway, https://www.cusabio.com/pathway/cAMP-signaling-pathway.html; 2020, Accessed on 17-05-2021

87. N.D. Bland, C. Wang, C. Tallman*, et al.*, Pharmacological validation of Trypanosoma brucei phosphodiesterases B1 and B2 as druggable targets for African sleeping sickness, J Med Chem, 54 (2011) 8188-8194.

88. H.P. de Koning, M.K. Gould, G.J. Sterk*, et al.*, Pharmacological validation of Trypanosoma brucei phosphodiesterases as novel drug targets, Journal of Infectious Diseases, 206 (2012) 229-237.

89. K.M. Orrling, C. Jansen, X.L. Vu*, et al.*, Catechol pyrazolinones as trypanocidals: fragment-based design, synthesis, and pharmacological evaluation of nanomolar inhibitors of trypanosomal phosphodiesterase B1, Journal of Medicinal Chemistry, 55 (2012) 8745-8756.

90. H. Wang, S. Kunz, G. Chen*, et al.*, Biological and structural characterization of Trypanosoma cruzi phosphodiesterase C and Implications for design of parasite selective inhibitors, J Biol Chem, 287 (2012) 11788-11797.

91. T. Seebeck, K. Gong, S. Kunz*, et al.*, cAMP signalling in Trypanosoma brucei, Int J Parasitol, 31 (2001) 491-498.

92. M. Oberholzer, E.A. Saada, K.L. Hill, Cyclic AMP Regulates Social Behavior in African Trypanosomes, mBio, 6 (2015) e01954-01914.

93. S. Shaw, S.F. DeMarco, R. Rehmann*, et al.*, Flagellar cAMP signaling controls trypanosome progression through host tissues, Nat Commun, 10 (2019) 803.

94. C. Naula, T. Seebeck, Cyclic AMP signaling in trypanosomatids, Parasitol Today, 16 (2000) 35-38.

95. D. Salmon, G. Vanwalleghem, Y. Morias*, et al.*, Adenylate cyclases of Trypanosoma brucei inhibit the innate immune response of the host, Science, 337 (2012) 463-466.

96. D. Salmon, Adenylate Cyclases of Trypanosoma brucei, Environmental Sensors and Controllers of Host Innate Immune Response, Pathogens, 7 (2018).

97. N. Sommer, P.A. Löschmann, G.H. Northoff*, et al.*, The antidepressant rolipram suppresses cytokine production and prevents autoimmune encephalomyelitis, Nature Medicine, 1 (1995) 244.

98. H. Wachtel, Potential antidepressant activity of rolipram and other selective cyclic adenosine 3',5'-monophosphate phosphodiesterase inhibitors, Neuropharmacology, 22 (1983) 267-272.

99. B. Bielekova, N. Richert, T. Howard*, et al.*, Treatment with the phosphodiesterase type-4 inhibitor rolipram fails to inhibit blood—brain barrier disruption in multiple sclerosis, Multiple Sclerosis Journal, 15 (2009) 1206-1214.

100. J. Zhu, E. Mix, B. Winblad, The Antidepressant and Antiinflammatory Effects of Rolipram in the Central Nervous System, CNS Drug Reviews, 7 (2006) 387-398.

101. A.K. Chakraborti, B. Gopalakrishnan, M.E. Sobhia*, et al.*, 3D-QSAR studies of indole derivatives as phosphodiesterase IV inhibitors, European Journal of Medicinal Chemistry, 38 (2003) 975-982.

102. M.J. Ashton, D.C. Cook, G. Fenton*, et al.*, Selective Type IV Phosphodiesterase Inhibitors as Antiasthmatic Agents. The Syntheses and Biological Activities of 3-(Cyclopentyloxy)-4-methoxybenzamides and Analogs, Journal of Medicinal Chemistry, 37 (1994) 1696-1703.

103. M.A. Giembycz, S.K. Field, Roflumilast: first phosphodiesterase 4 inhibitor approved for treatment of COPD, Drug Design, Development and Therapy, 4 (2010) 147-158.

104. D.W. Baeumer, P.I. Szelenyi, P.M. Kietzmann, Cilomilast, an orally active phosphodiesterase 4 inhibitor for the treatment of COPD, Expert Review of Clinical Immunology, 1 (2005) 27-36.

105. H.-W. Man, P. Schafer, L.M. Wong*, et al.*, Discovery of (S)-N-{2-[1-(3-Ethoxy-4-methoxyphenyl)-2-methanesulfonylethyl]-1,3-dioxo-2,3-dihydro-1H-isoindol-4-yl}acetamide (Apremilast), a Potent and Orally Active Phosphodiesterase 4 and Tumor Necrosis Factor-α Inhibitor, Journal of Medicinal Chemistry, 52 (2009) 1522-1524.

106. L. Fala, Otezla (Apremilast), an Oral PDE-4 Inhibitor, Receives FDA Approval for the Treatment of Patients with Active Psoriatic Arthritis and Plaque Psoriasis, American Health & Drug Benefits, 8 (2015) 105-110.

107. D.M. Paton, Crisaborole: Phosphodiesterase inhibitor for treatment of atopic dermatitis, Drugs Today, 53 (2017) 239-246.

108. P.C. Ting, J.F. Lee, R. Kuang*, et al.*, Discovery of oral and inhaled PDE4 inhibitors, Bioorganic & Medicinal Chemistry Letters, 23 (2013) 5528-5532.

109. C.J. Tralau-Stewart, R.A. Williamson, A.T. Nials*, et al.*, GSK256066, an Exceptionally High-Affinity and Selective Inhibitor of Phosphodiesterase 4 Suitable for Administration by Inhalation: In Vitro, Kinetic, and In Vivo Characterization, Journal of Pharmacology and Experimental Therapeutics, 337 (2011) 145.

110. A. Hatzelmann, C. Schudt, Anti-Inflammatory and Immunomodulatory Potential of the Novel PDE4 Inhibitor Roflumilast in Vitro, Journal of Pharmacology and Experimental Therapeutics, 297 (2001) 267-279.

111. S.J. MacKenzie, M.D. Houslay, Action of rolipram on specific PDE4 cAMP phosphodiesterase isoforms and on the phosphorylation of cAMP-response-element-binding protein (CREB) and p38 mitogen-activated protein (MAP) kinase in U937 monocytic cells, The Biochemical journal, 347 (2000) 571-578.

112. E. Amata, N.D. Bland, C.T. Hoyt*, et al.*, Repurposing human PDE4 inhibitors for neglected tropical diseases: Design, synthesis and evaluation of cilomilast analogues as Trypanosoma brucei PDEB1 inhibitors, Bioorganic & Medicinal Chemistry Letters, 24 (2014) 4084-4089.

113. K. Jarnagin, S. Chanda, D. Coronado*, et al.*, Crisaborole Topical Ointment, 2%: A Nonsteroidal, Topical, Anti-Inflammatory Phosphodiesterase 4 Inhibitor in Clinical Development for the Treatment of Atopic Dermatitis, J Drugs Dermatol, 15 (2016) 390-396.

114. A.R. Blaazer, A.K. Singh, E. de Heuvel*, et al.*, Targeting a subpocket in Trypanosoma brucei phosphodiesterase B1 (TbrPDEB1) enables the structure-based discovery of selective inhibitors with trypanocidal activity, Journal of Medicinal Chemistry, 61 (2018) 3870-3888.

115. R.X. Xu, W.J. Rocque, M.H. Lambert*, et al.*, Crystal Structures of the Catalytic Domain of Phosphodiesterase 4B Complexed with AMP, 8-Br-AMP, and Rolipram, Journal of Molecular Biology, 337 (2004) 355-365.

116. H. Wang, H. Robinson, H. Ke, The Molecular Basis for Different Recognition of Substrates by Phosphodiesterase Families 4 and 10, Journal of Molecular Biology, 371 (2007) 302-307.

117. G.L. Card, B.P. England, Y. Suzuki*, et al.*, Structural Basis for the Activity of Drugs that Inhibit Phosphodiesterases, Structure, 12 (2004) 2233-2247.

118. K.Y.J. Zhang, G.L. Card, Y. Suzuki*, et al.*, A Glutamine Switch Mechanism for Nucleotide Selectivity by Phosphodiesterases, Molecular Cell, 15 (2004) 279-286.

119. M.D. Houslay, D.R. Adams, PDE4 cAMP phosphodiesterases: modular enzymes that orchestrate signalling cross-talk, desensitization and compartmentalization, Biochem J, 370 (2003) 1-18.

120. G.S. Baillie, J.D. Scott, M.D. Houslay, Compartmentalisation of phosphodiesterases and protein kinase A: opposites attract, FEBS Lett, 579 (2005) 3264-3270.

121. A. Blokland, P. Heckman, T. Vanmierlo*, et al.*, Phosphodiesterase Type 4 Inhibition in CNS Diseases, Trends Pharmacol Sci, 40 (2019) 971-985.

122. R. Schreiber, R. Hollands, A. Blokland, A Mechanistic Rationale for PDE-4 Inhibitors to Treat Residual Cognitive Deficits in Acquired Brain Injury, Curr Neuropharmacol, 18 (2020) 188-201.

123. A. Castro, M.J. Jerez, C. Gil*, et al.*, Cyclic nucleotide phosphodiesterases and their role in immunomodulatory responses: advances in the development of specific phosphodiesterase inhibitors, Med Res Rev, 25 (2005) 229-244.

124. L. Pages, A. Gavalda, M.D. Lehner, PDE4 inhibitors: a review of current developments (2005 - 2009), Expert Opin Ther Pat, 19 (2009) 1501-1519.

125. L.I. Sakkas, A. Mavropoulos, D.P. Bogdanos, Phosphodiesterase 4 Inhibitors in Immune-mediated Diseases: Mode of Action, Clinical Applications, Current and Future Perspectives, Curr Med Chem, 24 (2017) 3054-3067.

126. J.M. O'Donnell, H.T. Zhang, Antidepressant effects of inhibitors of cAMP phosphodiesterase (PDE4), Trends Pharmacol Sci, 25 (2004) 158-163.

127. H. Wang, U. Gaur, J. Xiao*, et al.*, Targeting phosphodiesterase 4 as a potential therapeutic strategy for enhancing neuroplasticity following ischemic stroke, Int J Biol Sci, 14 (2018) 1745-1754.

128. S. Peng, H. Sun, X. Zhang*, et al.*, Effects of selective phosphodiesterases-4 inhibitors on learning and memory: a review of recent research, Cell Biochem Biophys, 70 (2014) 83-85.

129. A. Aldrich, M.E. Bosch, R. Fallet*, et al.*, Efficacy of phosphodiesterase-4 inhibitors in juvenile Batten disease (CLN3), Ann Neurol, 80 (2016) 909-923.

130. G.B. Bolger, The PDE4 cAMP-Specific Phosphodiesterases: Targets for Drugs with Antidepressant and Memory-Enhancing Action, Adv Neurobiol, 17 (2017) 63-102.

131. A. Blokland, M.A. Van Duinen, A. Sambeth*, et al.*, Acute treatment with the PDE4 inhibitor roflumilast improves verbal word memory in healthy old individuals: a double-blind placebo-controlled study, Neurobiol Aging, 77 (2019) 37-43.

132. C.M. Olsen, Q.S. Liu, Phosphodiesterase 4 inhibitors and drugs of abuse: current knowledge and therapeutic opportunities, Front Biol (Beijing), 11 (2016) 376-386.

133. C. Jansen, H. Wang, A.J. Kooistra*, et al.*, Discovery of NovelTrypanosoma bruceiPhosphodiesterase B1 Inhibitors by Virtual Screening against the Unliganded TbrPDEB1 Crystal Structure, Journal of Medicinal Chemistry, 56 (2013) 2087-2096.

134. N.J. Press, K.H. Banner, PDE4 inhibitors - a review of the current field, Prog Med Chem, 47 (2009) 37-74.

135. P.M. Seldon, P.J. Barnes, K. Meja*, et al.*, Suppression of lipopolysaccharide-induced tumor necrosis factor-alpha generation from human peripheral blood monocytes by inhibitors of phosphodiesterase 4: interaction with stimulants of adenylyl cyclase., Molecular Pharmacology, 48 (1995) 747-757.

136. J.L. Woodring, N.D. Bland, S.O. Ochiana*, et al.*, Synthesis and assessment of catechol diether compounds as inhibitors of trypanosomal phosphodiesterase B1 (TbrPDEB1), Bioorganic & Medicinal Chemistry Letters, 23 (2013) 5971-5974.

1

137. M. Van der Mey, A. Hatzelmann, I.J. Van der Laan, *et al.*, Novel Selective PDE4 Inhibitors. 1. Synthesis, Structure-Activity Relationships, and Molecular Modeling of 4-(3, 4-Dimethoxyphenyl)-2 H-phthalazin-1-ones and Analogues, Journal of Medicinal Chemistry, 44 (2001) 2511-2522.

138. M. Van der Mey, A. Hatzelmann, G.P.M. Van Klink, *et al.*, Novel Selective PDE4 Inhibitors. 2. Synthesis and structure-activity relationships of 4-aryl-substituted cis-tetra- and cis-hexahydrophthalazinones, Journal of Medicinal Chemistry, 44 (2001) 2523-2535.

139. J. Veerman, T. van den Bergh, K.M. Orrling, *et al.*, Synthesis and evaluation of analogs of the phenylpyridazinone NPD-001 as potent trypanosomal TbrPDEB1 phosphodiesterase inhibitors and in vitro trypanocidals, Bioorganic & Medicinal Chemistry, 24 (2016) 1573-1581.

140. R. Ettari, S. Previti, S. Maiorana, *et al.*, Optimization Strategy of Novel Peptide-Based Michael Acceptors for the Treatment of Human African Trypanosomiasis, J Med Chem, 62 (2019) 10617-10629.
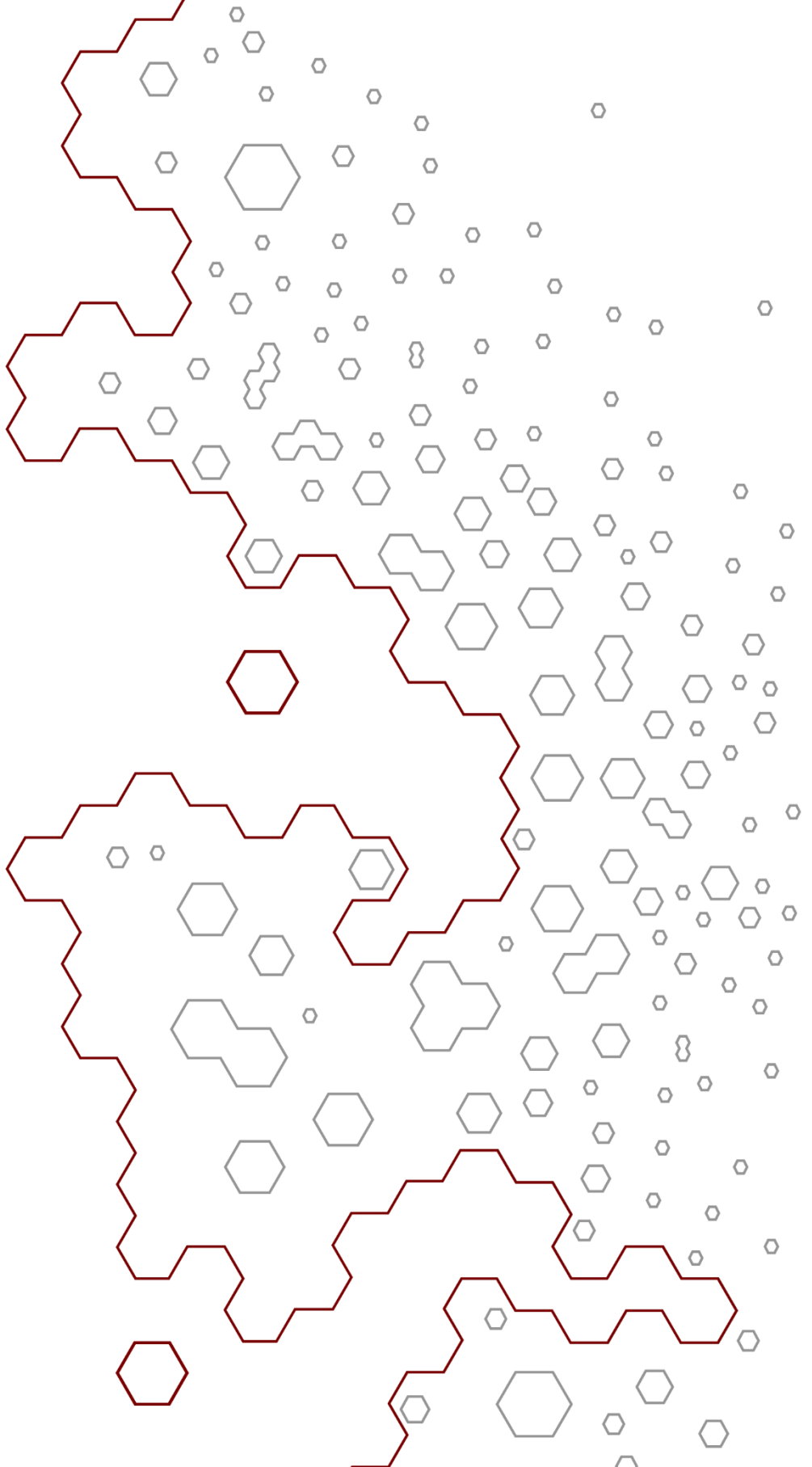
Chapter 2

Targeting a subpocket in *Trypanosoma brucei* phosphodiesterase B1 enables the structure-based discovery of selective inhibitors with trypanocidal activity

Erik de Heuvel, Antoni R. Blaazer, Abhimanyu K. Singh, Ewald Edink, Kristina M. Orrling, Johan Veerman, Toine van den Bergh, Chimed Jansen, Erin Balasubramaniam, Maikel Wijtmans, Hans Custers, Maarten Sijm, Daniel N.A. Tagoe, Jane C. Munday, Hermann Tenor, An Matheeussen, Marco Siderius, Chris de Graaf, Louis Maes, Harry P. de Koning, Geert Jan Sterk, David Bailey, Iwan J.P. de Esch, David G. Brown, Rob Leurs

Abstract

Trypanosoma brucei PDE B1 (TbrPDEB1) is considered to be a viable drug target for the treatment of human African trypanosomiasis. One of the challenges in drug discovery is obtaining selectivity over structurally similar proteins. For the development of new TbrPDEB1 inhibitors selectivity over the human PDEs is desired to reduce unwanted side effects. Here we explore the possibilities of rigidified tetrahydrophthalazinones TbrPDEB1 inhibitors to target the parasite specific P-pocket and the effect on binding and selectivity. Iterative cycles of design, synthesis and pharmacological evaluation resulted in the development of the first series of selective TbrPDEB1 inhibitors. Elucidation of structures of inhibitor-bound TbrPDEB1 and hPDE4B/4D complexes gave additional insight in the binding mode of these biphenyl-based inhibitor class. Two compounds, **8** (NPD-008) and **9** (NPD-039) showed good potency (K_i = 100 nM) against TbrPDEB1 and showed antitrypanosomal effects (IC$_{50}$ = 5.5 and 6.7 µM, respectively). Treatment of trypanosomes with **8** resulted in an increase of cellular cAMP and severe disruption of the cellular organization, which validated the PDE-mediated mode of action.

2

1.   Introduction

Human African trypanosomiasis has been listed by the WHO as one of the neglected tropical diseases (NTDs) since 2012.[1] It is caused by two protozoan parasites (*Trypanosoma brucei rhodesiense* and *T.b. gambiense*) that are endemic in sub-Saharan Africa. Active screening and control initiated by the WHO pushed the disease close to eradication, but the current options for reliable and safe drugs to completely eradicate the disease are still limited.[2]

3',5'-cyclic nucleotide phosphodiesterases (PDEs) have been identified as viable targets for a new therapy for these kinetoplastid protozoans.[3-6] It has been demonstrated by Seebeck and coworkers that simultaneous inhibition of *Trypanosoma brucei* PDEB1 (TbrPDEB1) and TbrPDEB2 by inducible siRNA blocks parasite proliferation and can eliminate parasitemia from infected mice.[7] The viability of TbrPDEB1/2 as drug targets was further explored by various efforts to identify TbrPDEB1 inhibitors.[8-10] Repurposing ligands that were originally developed as human PDE4 (hPDE4) inhibitors resulted in valuable hits for further development (Figure 1).[8-10] Unfortunately, none of the analogues were more potent on TbrPDEB1 than on hPDE4, resulting in an undesirable selectivity profile for the human homologues.[10] The most potent TbrPDEB1 inhibitor reported to date is NPD-001 (TbrPDEB1 IC_{50} = 4 nM), but the compound has a 10 fold higher potency for hPDE4 (hPDE4 IC_{50} = 0.4 nM).[10] Despite the high similarity between the active sites of TbrPDEB1 and hPDE4, there is evidence that selectivity between the two enzymes can be established since hPDE4 inhibitors such as Rolipram and etazolate do not show any activity on TbrPDEB1, or *T. brucei* cell activity, and do not kill the parasite.[8, 9]
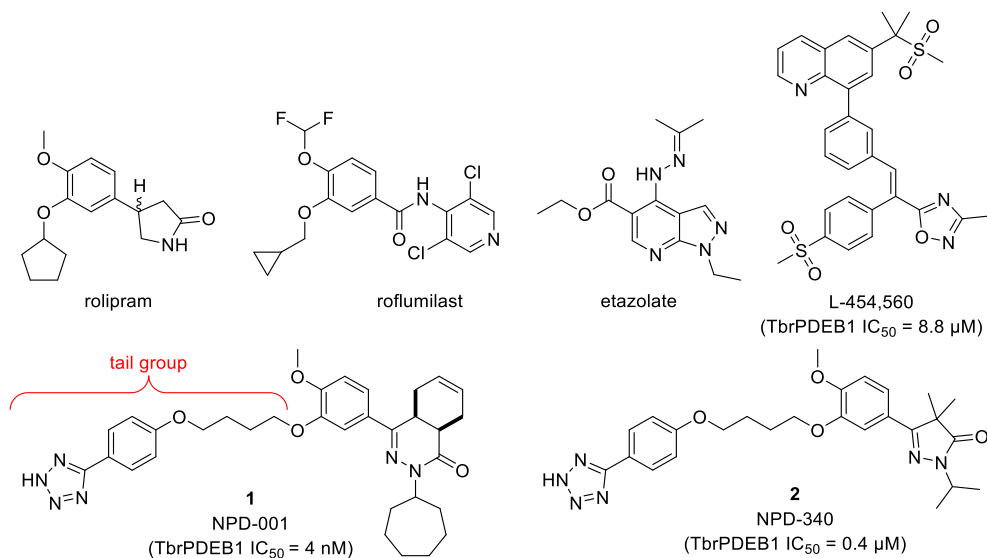
Figure 1: Representative hPDE4 inhibitors and reported TbrPDEB1 inhibitors.[11-13] Figure copied from paper by Blaazer et al.[14]

A structure-based virtual screening on the apo-TbrPDEB1 catalytic domain performed by Jansen *et al*. gave additional insight in methods to design selective TbrPDEB1 inhibitors.[15] An open cavity between helix 14 (H14), helix 15 (H15) and the M-loop was revealed in the high-resolution structure of the TbrPDEB1 catalytic domain (Figure 2). This cavity is also present in PDEs of taxonomically related parasites including *Leishmania major* PDEB1 (LmjPDEB1) and *Trypanosoma cruzi* PDEC (TcrPDEC), while it is not present in any of the 11 human PDEs.[15-17] This so-called parasite specific P-pocket has been considered a promising feature for the design of selective TbrPDEB1 inhibitors.[15] Molecular docking of **1** and **2** in TbrPDEB1 suggested that the phenyltetrazole-containing tail group can interact with the residues inside the P-pocket.[10, 18] However, both molecules display a higher potency for hPDE4 over TbrPDEB1, and therefore the possibility to achieve selectivity by P-pocket targeting remains to be demonstrated.
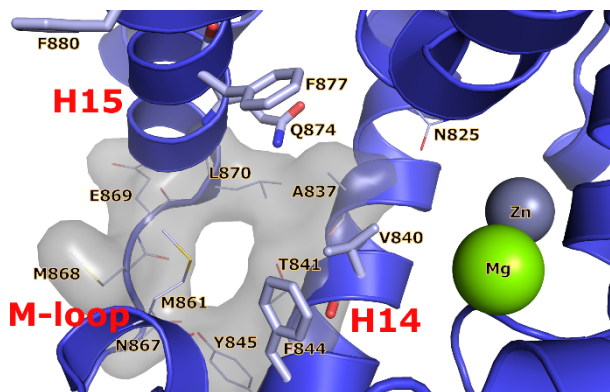
Figure 2: Crystal structure of apo-TbrPDEB1 (PDB: 4I15) active site highlighting the parasite P-pocket. Helix 14 (H14), helix 15 (H15) and the M-loop are labeled in red, the main binding site features are labeled in black, water molecules have been omitted for clarity. The conserved Gln874, the hydrophobic clamp residues Val840 and Phe877, and the distal aromatic residues Phe844 and Phe880 are shown as sticks. P-pocket residues Ala837, Thr841, Tyr845, Asn867, Met868, Glu869 and Leu870 are shown as lines.[19] Figure copied from paper by Blaazer *et al*.[14]

Here, we describe the usefulness of P-pocket targeting to obtain the first class of TbrPDEB1 inhibitors with selectivity over hPDE4. Crystal structures of **1** and **2** clearly explain the lack of selectivity of these previously reported inhibitors and guided the design of novel P-pocket targeting inhibitors. Furthermore, we show that these novel compounds retain their trypanocidal activity via cAMP accumulation in *T. brucei* and thereby validating a PDE-mediated mode of action.

2. Results and Discussion

Although tetrahydrophthalazinone NPD-001 (**1**) is the most potent TbrPDEB1 inhibitor (TbrPDEB1 pIC_{50} = 8.4) reported to date, it also shows subnanomolar inhibition of hPDE4 subtypes (pIC_{50} > 9). Similarly, the structurally related pyrazolone analogs, such as NPD-340 (**2**), also show a preference for hPDE4 over TbrPDEB1. In previously reported molecular docking studies both molecules show a commonly observed binding mode in the active site of TbrPDEB1. The catechol moiety of **1** and **2** is positioned in the hydrophobic clamp of TbrPDEB1 and forms a hydrogen bond with the PDE-family-wide conserved Gln874. The flexible tail-group is then directed towards the P-pocket, where the tetrazole can form additional interactions with the P-pocket residues.[10, 18] Although the high potency for **1** and **2** are in agreement with this theory, the selectivity profile is inconsistent with theory of successful P-pocket targeting as a means of obtaining selectivity.

We obtained a high resolution crystal structure (1.73 Å) of **1** in the catalytic domain of TbrPDEB1 (PDB: 5G57) to gain a better understanding of the lack of selectivity of these compounds (Figure 3A). The binding mode of the phenyl tetrahydrophthalazinone core of **1** was in agreement with the observed docking pose. The main interactions between the ligand and protein were formed by the catechol by means of a hydrogen bond with Gln874 while occupying the hydrophobic clamp. Only the (4a*S*,8a*R*)-enantiomer of **1** was obtained in the crystal structure, but no significant additional interactions were observed between the tetrahydrophthalazinone and the protein, suggesting a favorable steric fit for this isomer. Despite the correct prediction of the core in computation studies the tail group is oriented away from the P-pocket and forms a π- π stacking interaction with Phe880. A crystal structure of **2** in complex with the catalytic domain of TbrPDEB1 (Figure 3B, PDB: 5L9H) shows a highly similar binding mode for this structurally related compound. The same key interactions of the catechol with the protein were observed and the tail group was oriented away from the P-pocket as well.

To get a better understanding of the possible binding mode difference between TbrPDEB and hPDE4 we determined the crystal structure of **1** ligated in hPDE4B (Figure 3C, PDB: 5LAQ) and hPDE4D (Figure 3D, PDB: 5LBO). In both structures only the (4a*S*,8a*R*)-isomer was observed which showed an identical binding mode between hPDE4B and hPDE4D. As expected for a high potency hPDE4 inhibitor, the compound was observed in the cAMP-binding site where the catechol moiety situated in the hydrophobic clamp while having a double hydrogen bond interaction with Gln615. In addition, the tail-group tetrazole is well-positioned for a stacking interaction with Tyr621. The high similarity between the binding modes of **1** and **2** in the four crystal structures clearly show that the phenyltetrazole is not targeting the P-pocket and could potentially explain the lack of selectivity of the compounds for TbrPDEB1 over hPDE4. As observed in the three crystal structures of **1**, the tail group is of sufficient length and flexibility to successfully interact with an aromatic residue in the hydrophobic region outside of the cAMP-binding site, being Phe880 in TbrPDEB1 and Tyr621 in hPDE4B. It was conceived that reducing the flexibility of this linker by installing a more rigid functionality could be beneficial for the selectivity for TbrPDEB over hPDE4. For the design of such ligands PhosphoDiEsterase Structure and Ligand Interaction Annotated (PDEStrIAn) was used.[16] One of the observations was that some co-crystallized ligands contained an

additional (hetero)aromatic group next to the central aromatic moiety which was bound to the hydrophobic clamp. This second aromatic functionality was in some cases (for example, PDB codes 3IAD and 4AEL) directed along the vector towards the P-pocket in TbrPDEB1. It was hypothesized that substitution of the flexible linker with functionalized phenyl groups could result in a series of compounds with a more favorable length, rigidity and directionality to successfully target the P-pocket.
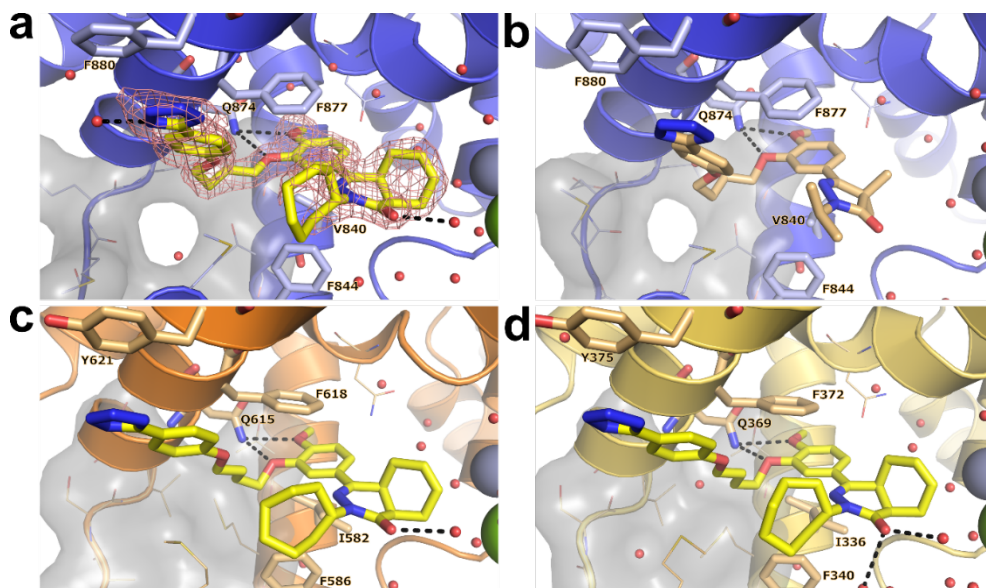

Figure 3: Crystal structures of non-selective inhibitors with TbrPDEB1, hPDE4B and hPDE4D. (a) TbrPDEB1 in complex with **1** (PDB: 5G57), including $|Fo\text{-}Fc|_{\alpha calc}$ electron density map contoured at 2.5 σ (b) TbrPDEB1 in complex with **2** (PDB: 5L9H). (c) hPDE4B in complex with **1** (PDB: 5LAQ). (d) hPDE4D in complex with **1** (PDB: 5LBO). In all panels: key binding site amino acid residues are shown as sticks, minor amino acid residues are shown as lines. The P-pocket is shown as a gray surface with P-pocket residues represented as lines, and key polar interactions are depicted with black dashed lines. Water molecules are displayed as red spheres, zinc cations as metallic blue spheres, and magnesium cations as green spheres. Figure copied from paper by Blaazer *et al*.[14]

As a first series of biphenyl analogs we synthesized **3**-**6** with small carboxylic acid, amide or nitrile substituents on the 3'- and 4'-position of the second phenyl group to quickly screen the possibilities of obtaining selectivity (Table 1). Fortunately, the introduction of the benzoic acid groups of **3** and **4** resulted in some selectivity for TbrPDEB1 over hPDE4 (2-fold and 5-fold, respectively). The activity on TbrPDEB1 and hPDE4B1 was greatly reduced for both carboxylic acids, but was partially recovered by introducing a carboxamide on the *para*-position (**5**). The equipotency

for both TbrPDEB1 and hPDE4B1 of carboxamide **5** further confirmed the possibility to adapt the selectivity profile in favor of TbrPDEB1.

Table 1: Introduction of the biphenyl linker[a]
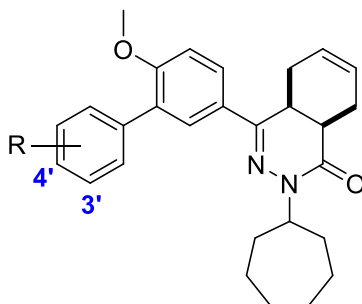
#	Position	R	TbrPDEB1 pK_i	hPDE4B1 pK_i	Selectivity[b]
roflumilast	-	-	5.5	9.4	0.0001
1 (NPD-001)	-	-	8.4	9.2	0.16
3 (NPD-740)	3'	-COOH	5.1	4.9	2
4 (NPD-733)	4'	-COOH	5.8	5.1	5
5 (NPD-584)	4'	-CONH$_2$	6.8	6.8	1
6 (NPD-744)	4'	-CN	6.3	7.5	0.1

[a]pK_i values are averages (n ≥ 2, with s.e.m. ± < 0.2 for all). [b]Selectivity is calculated as hPDE4B1 (K_i)/TbrPDEB1 (K_i).

In order to validate that the introduced rigid linker has no effect on the potency for other human PDEs, **5** was tested against a panel of human PDEs (Table 2). Benzamide **5** showed a highly similar potency for all hPDE4 isoforms and a good selectivity over the other human PDE subtypes. Some activity was observed for the non-specific hPDE2 and hPDE3, while no activity was observed for other cAMP-specific hPDE7 and hPDE8.

Based on these findings we hypothesized that improvements in potency and selectivity could be obtained by extending the 4'-substituted carboxamides with more flexible head groups (Table 3). The extension of the carbamate with a methoxyethyl substituent (**7**) led to a 7-fold increase in selectivity, while the potency for TbrPDEB1 is comparable to its parent compound (**5**). Introduction of a glycinamide group (**8**) resulted in an even more potent TbrPDEB1 inhibitor (K_i = 100 nM) and an increased selectivity profile over hPDE4B1. *N*-Methylation or *N,N*-dimethylation of the glycinamide tail (**9-11**) resulted in decrease in activity and selectivity, which could indicate that these amide protons are involved in

interaction with the protein or water network. Introduction of a more lipophilic isopropyl group at the terminal nitrogen (**12**) resulted in further reduction of the activity and selectivity. Elongating the chain with one carbon (**13**) decreased selectivity to a 2-fold, mainly caused by increase in hPDE4B1 activity. Inversion of the amide bond (**14**) also restored some of the selectivity to a 5-fold, but did not result in a more potent compound than **8**.

Table 2: Potency of **5** against a panel of hPDEs.

| PDE-subtype	pIC_{50}[a]	PDE-subtype	pIC_{50}[a]
hPDE1B1	< 5	hPDE5A1	< 5
hPDE2A3	5.4	hPDE7A1	< 5
hPDE3A1	5.1	hPDE8A1	< 5
hPDE4A1	6.6	hPDE9A3	< 5
hPDE4B1	6.8	hPDE10A	< 5
hPDE4C1	6.3	hPDE11A	5.2
hPDE4D3	6.9		

[a]pIC_{50} values are averages (n ≥ 2) determined by Nycomed GmbH using the standard scintillation proximity assay (SPA) as reported, at a cAMP or cGMP substrate concentration of 0.5 µM.[10]

Finally, extension of the glycinamide of **8** with more hydrophilic substituents hydroxyethyl (**15**) or methoxyethyl (**16**) was tolerated and resulted in ~8 fold selective TbrPDEB1 inhibitors. However, both modifications resulted in a slight reduction of activity, highlighting the sensitivity of the pocket towards small modifications in the tail group.

Since only one stereoisomer was observed in the three crystal structures of **1**, it was decided to investigate the difference in binding affinity of the two isomers of **8** (Table 4). Both isomers (**17** and **18**) are selective TbrPDEB1 inhibitors, but the activity of racemic **8** was mostly explained by the activity of **18**, which is a 100-fold higher than the other optical isomer **17**. Furthermore, with an eye on lipophilicity of the molecule, we synthesized an *N*-isopropyl analogue (**19**) as present in **2**. Fortunately, the less lipophilic analogue showed an increased selectivity for TbrPDEB1 over hPDE4B1, caused by a decrease in affinity for hPDE4.

Table 3: Exploration of SAR in the P-pocket[a]
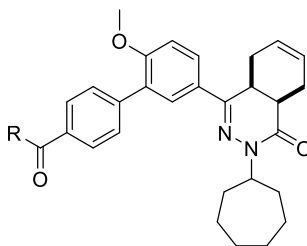
#	R	TbrPDEB1 pK_i	hPDE4B1 pK_i	Selectivity[b]
7 (NPD-734)		6.5	5.7	7
8 (NPD-008)		7.0	6.0	10
9 (NPD-935)		6.4	5.6	7
10 (NPD-936)		6.4	5.6	6
11 (NPD-939)		6.1	5.5	4
12 (NPD-942)		5.7	5.2	4
13 (NPD-800)		6.3	6.0	2
14 (NPD-801)		6.1	5.4	5
15 (NPD-937)		6.4	5.5	7
16 (NPD-878)		6.3	5.4	8

[a]pK_i values are averages (n ≥ 2, with s.e.m. ± < 0.2 for all). [b]Selectivity is calculated as hPDE4B1 (K_i)/TbrPDEB1 (K_i).

In order to confirm that the observed selectivity of these compounds originates from the P-pocket targeting approach, we obtained the crystal structure of **8** (Figure 4A, PDB: 5G2B), **19** (Figure 4B, PDB: 5L8C) and **15** (Figure 4C, PDB: 5L8Y). In

all three crystal structures only the (4a*R*,8a*S*)-isomer was found which is in agreement with previously obtained crystal structures of **1**. With the assumption that the highest affinity isomer will be most abundant in the crystal structure, we propose the 100-fold more potent enantiomer **18** to be the (4a*R*,8a*S*)-isomer.

Table 4: Exploration of SAR in the P-pocket[a]
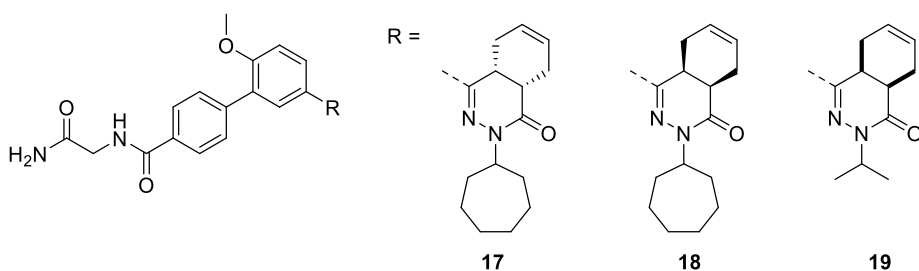
#	TbrPDEB1 pK_i	hPDE4B1 pK_i	Selectivity[b]
17 (NPD-949)	5.4	4.3	13
18 (NPD-1373)	7.4	6.2	16
19 (NPD-039)	7.0	5.7	19

[a]pK_i values are averages (n ≥ 2, with s.e.m. ± < 0.2 for all). [b]Selectivity is calculated as hPDE4B1 (K_i)/TbrPDEB1 (K_i).

The overall binding mode of the three biphenyl compounds is highly comparable with reference compounds **1** and **2** (Figure 3a and 3b, respectively). The anisole moiety occupies the hydrophobic clamp while making a hydrogen bond interaction with key residue Gln874 via the ether functionality. The rigid phenyl linker directs the glycinamide of **8** and **19** towards the P-pocket. The glycinamide tail of **8** successfully targets the P-pocket where it forms a hydrogen bond with residue Tyr845. Furthermore, both amides form multiple hydrogen bonds with the water network surrounding the P-pocket. The glycinamide tail of **19** adopts a slightly different conformation in which it can form an additional interaction with Glu869 next to Tyr845. Based on the weaker electron density and the higher average temperature factor (B-factor) of the P-pocket region when compared to the rest of the crystal structure, it can be stated that the protein and the ligand have a greater flexibility in the P-pocket region.

The crystal structure of the catalytic domain of TbrPDEB1 with **15** shows that an elongated tail has little effect on the conformation of the glycinamide (Figure 4C).

The overall binding mode of **15** is highly similar to **8** and **19**, but the extended glycinamide tail fully occupies the P-pocket. However, this increased occupancy of the P-pocket is not accompanied by an increase in TbrPDEB1 activity nor selectivity.
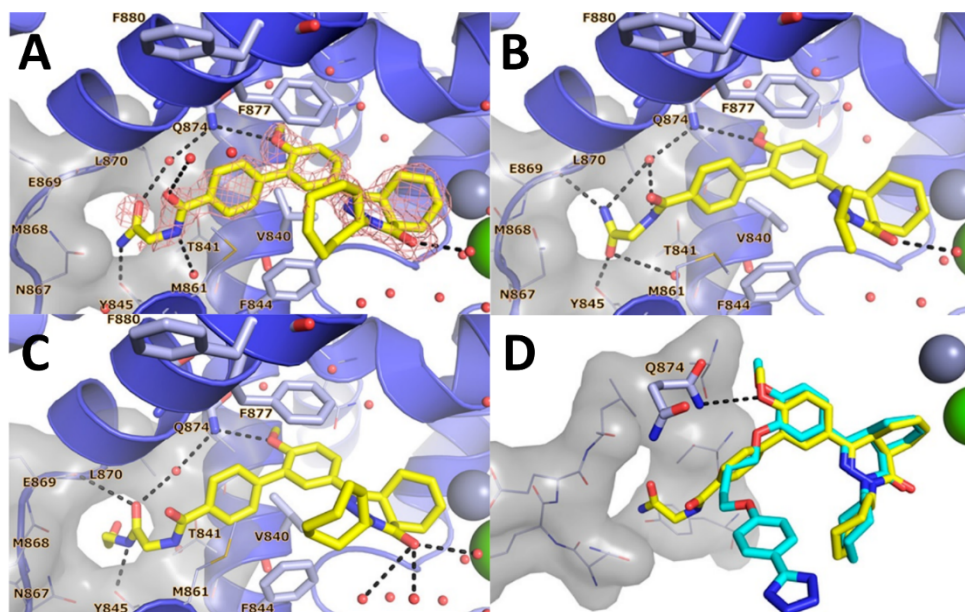

Figure 4: TbrPDEB1 crystal structures of selective inhibitors. (A) TbrPDEB1 in complex with **8**, (PDB: 5G2B), including |Fo-Fc|$_{\alpha calc}$ electron density map contoured at 2.5 σ. (B) TbrPDEB1 in complex with **19** (PDB: 5L8C). (C) X-ray crystal structure of TbrPDEB1 in complex with **15** (PDB: 5L8Y). (D) Alignment of the TbrPDEB1 crystal structures of **1** (cyan) and **8** (yellow). Coordinates of Gln874, P-pocket residues and metal cations were derived from TbrPDEB1–**8** and are shown for clarity. Figure copied from paper by Blaazer *et al*.[14]

Direct comparison of the crystal structure of **8** with the crystal structure of **1** (Figure 4D) clearly shows the effect of adding rigidity to direct the linker towards the P-pocket. The immediate positive effect on the selectivity of the compounds prompted us to continue our design with more rigid aliphatic heterocyclic tail groups to further accommodate the tail group into the P-pocket region (Table 5). Although the glycinamide tail is involved in several hydrogen bonds, most of the interactions are with the water molecules that can be displaced.

The first constrained glycinamides synthesized were imidazolinone **20** and its *N*-methylated analogue **21**. It was conceived that the cyclization between glycinamide nitrogen would have the smallest impact on the overall fold and thus activity of the

compounds. However, both compounds showed a decreased potency for TbrPDEB1 while retaining most of the activity for hPDE4B1, resulting in less potent compounds with a decreased selectivity. As observed for the non-cyclized glycinamides **9**-**11**, *N*-methylation led to a further reduction in potency.

Table 5: SAR of aliphatic heterocycles in the P-pocket[a]
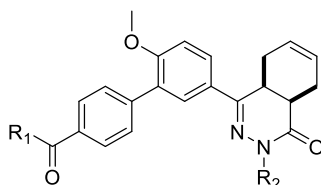
	R₁	R₂	TbrPDEB1 pKᵢ	hPDE4B1 pKᵢ	Selectivity[b]
20 (NPD-060)		*c*-heptyl	6.2	6.2	1
21 (NPD-062)		*c*-heptyl	5.8	5.6	1.4
22 (NPD-887)		*c*-heptyl	6.0	5.5	3
23 (NPD-746)		*c*-heptyl	6.6	5.7	9
24 (NPD-802)		*c*-heptyl	6.3	5.2	13
25 (NPD-038)		*i*-propyl	6.7	5.5	15
26 (NPD-885)		*i*-propyl	6.2	5.0	18

[a]pKᵢ values are averages (n ≥ 2, with s.e.m. ± < 0.2 for all). [b]Selectivity is calculated as hPDE4B1 (Kᵢ)/TbrPDEB1 (Kᵢ).

The importance of the amide carbonyl and amine was further investigated in pyrrolidinone **22** and (*R*)-pyrrolidinol **23**. The removal of the terminal amide

functionality resulted in a comparable potency for TbrPDEB1 and slightly lower potency for hPDE4B1. Reduction of the carbonyl group to an alcohol resulted in an increased activity on TbrPDEB1 and increased the selectivity over hPDE4 to a 9-fold. Substitution of the glycinamide by a D-prolinamide (**24**) resulted in an overall lower potency, but slightly better selectivity profile. The isopropyl analogues with the pyrrolidinol (**25**) and D-prolinamide (**26**) showed slightly more desirable activities against both proteins resulting in an improved selectivity profile for both compounds.

To investigate how these more rigid heterocycles interact with the P-pocket in TbrPDEB1 we determined the crystal structure of TbrPDEB1 ligated with selective compound **25** (Figure 5, PDB: 5G5V). The overall binding mode of the ligand is highly comparable to the other TbrPDEB1 inhibitors in this series, but small differences are observed in the P-pocket region. The pyrrolidinol hydroxyl group makes a direct interaction with the backbone carbonyl of residue Met861 and to the side chain of Asn867. The overall conformation of the cyclized tail group is slightly pointed away from the P-pocket entrance and the number of (indirect) interactions with P-pocket residues is lower than observed in the crystal structure of glycinamide **8**. However, it should be noted that in the crystal structure of **25** in TbrPDEB1 the ligand is only present at the chain with a symmetry-related molecule close to the ligand binding site, which might influence the binding mode of the ligand.
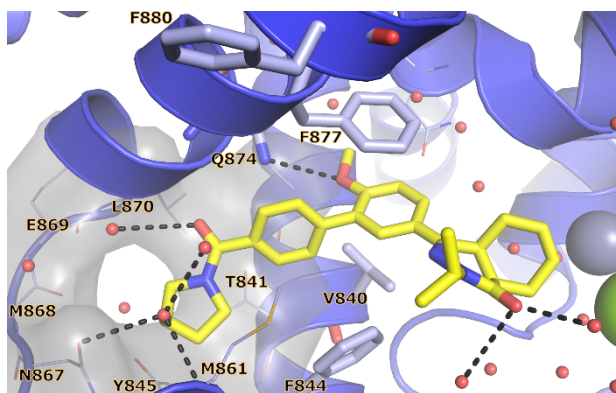

Figure 5: X-ray crystal structure of TbrPDEB1 in complex with **25**. Figure copied from paper by Blaazer *et al.*[14]

It has previously been demonstrated that the inhibition of TbrPDEB1 and TbrPDEB2 by **1** led to a rapid and dose-dependent increase in intracellular cAMP in *T.b. brucei*

parasites.[9, 10, 20] To pharmacologically validate the PDE mode of action of the biphenyl series bloodstream form trypanosomes were incubated with different concentrations of **8**. As shown in Figure 6, incubation with glycinamide **8** results in a dose-dependent increase of intracellular cAMP in these parasites. At the lowest measured incubation concentration of 100 nM compound **8** showed a small but significant effect (P <0.05). A stronger effect was observed at a concentration of 10 µM of compound **8** ($P < 0.001$), which was comparable to the effect observed by incubation of 0.3 µM of **1** as positive control. The negative control, antitrypanosomal compound pentamidine, did not show a statistically different effect from the non-treated control.
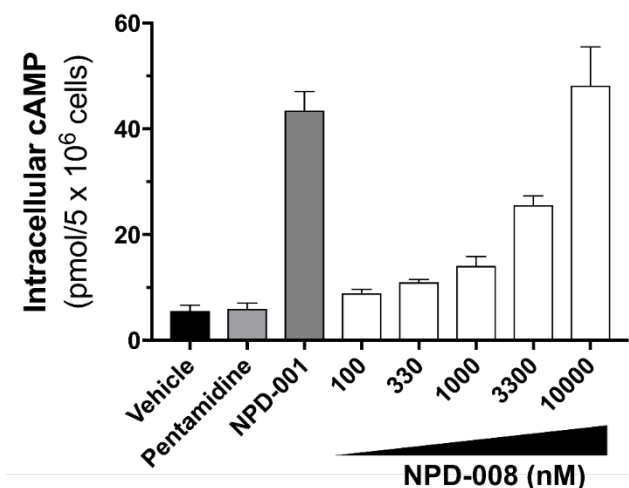

Figure 6: Intracellular cAMP levels in *T. brucei* after treatment with **8** (NPD-008), with 0.3 µM of compound **1** (NPD-001) used as a positive control, and pentamidine as a negative control. Figure copied from paper by Blaazer *et al*.[14]

Incubation of trypanosomes (Figure 7A) with 10 µM of compound **8** for 6 hours (which is roughly equivalent to one doubling time under standard conditions) results in cells having multiple nuclei and kinetoplasts (Figure 7B), indicating a defect in cytokinesis. This result is in line with previously reported studies using siRNA or **1** to validate TbrPDEB as an essential enzyme for the parasites cytokinesis.[4, 6, 9] After 12 hours the cells were severely misshapen with multiple flagella and at least 4 nuclei (Figure 7C). At 24 hours only a few live cells could be observed which all showed signs of an impaired cell division (Figure 7D). These results are in agreement with the observed cellular activity of **8** (*T. brucei* pEC$_{50}$ =

5.3 ± 0.2). The isopropyl analogue **19** showed a similar anti-*T. brucei* effects (pEC$_{50}$ = 5.1 ± 0.1) and both compounds show a comparable cytotoxic effect against human MRC-5 cells (CC$_{50}$ = 4.4 and 4.5 µM, respectively). Unfortunately, the antitrypanosomal and cytotoxicity profile of these compounds do not meet the published criteria of drug candidates for the treatment of human African trypanosomiasis, and require further phenotypic optimization.[21]
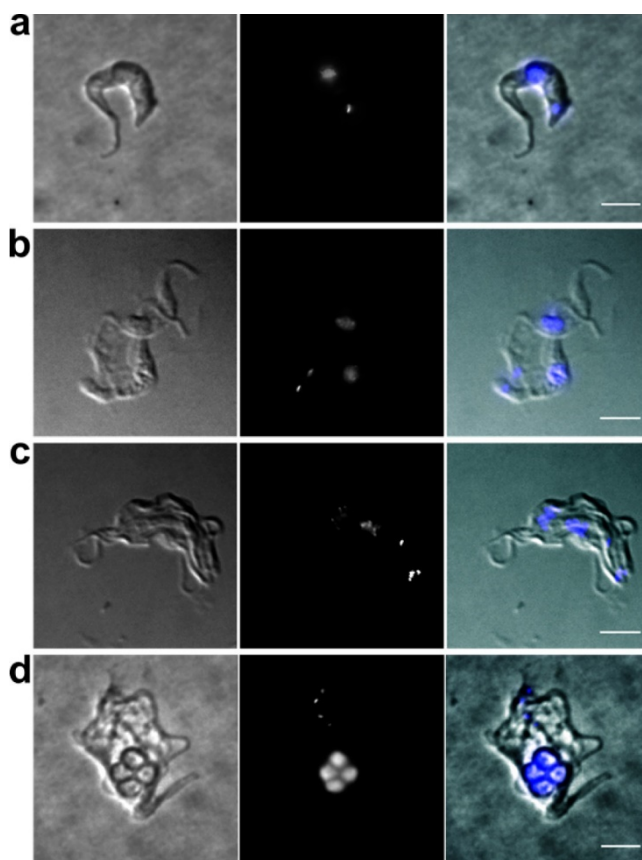
Figure 7: Fluorescence microscopy of wild-type *T. brucei* incubated with **8** (10 µM) for the following periods: (a) 0 h (control); (b) 6 h; (c) 12 h; (d) 24 h. Left panels are brightfield images, middle panels are fluorescence images after DAPI staining, and the right-hand panels are the merged images. Scale bars, 5 µm. Figure copied from paper by Blaazer *et al*.[14]

3. Chemistry

The chemical synthesis of compounds **3**–**6** and intermediate **30** proceeded as shown in Scheme 1. The key 4a,5,8,8a-tetrahydrophthalazin-1(2*H*)-one building

block (**27**)[22-24] was *N*-alkylated with the appropriate alkylhalides, and a Suzuki cross-coupling reaction afforded the biaryl systems.
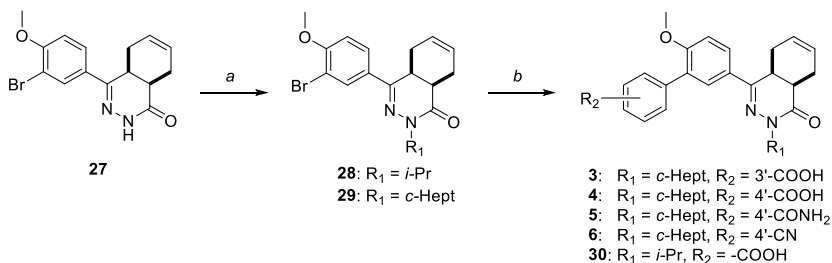
Scheme 1: Reagents and conditions: *a*) alkyl halide, NaH, DMF, RT, 4 h, 65–85%; *b*) arylboronic acid, Pd(dppf)Cl$_2$·CH$_2$Cl$_2$, Na$_2$CO$_3$, DME, H$_2$O, 100 °C, 16 h, 48–81%.

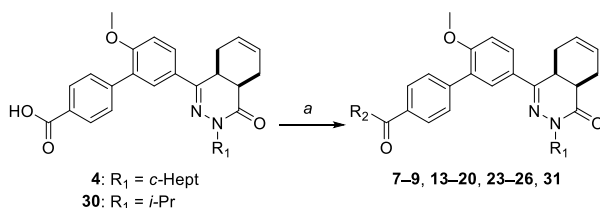Compounds **7**–**9**, **13**–**20**, and **23**–**26** were prepared using carbodiimide-mediated amide coupling methods using **4** or **30** as starting material (Scheme 2). Amide coupling was performed without the addition of DIPEA in the synthesis of **14**, **23**, **24**, and **26**, or without Et$_3$N in the case of analog **25**.

Scheme 2: Reagents and conditions: *a*) amine, EDC·HCl, HOAt, DIPEA, CH$_2$Cl$_2$, RT, 3 h, 38–88% (compounds **7**, **9**, **13**, **14**, **16**, **20**, **23**, **25**, **26**, **31**); or amine, EDC·HCl, HOBt hydrate, Et$_3$N, CH$_2$Cl$_2$, RT, 18 h, 54–65% (compounds **8**, **19**, **15**, **25**); or separation of the enantiomers of **4** by preparative chiral HPLC, then 2-aminoacetamide·HCl, EDC·HCl, HOAt, DIPEA, CH$_2$Cl$_2$, RT, 24 h, 50–55% (**17**, **18**).

To enable access to the enantiomers of **8**, racemic **4** was separated into its enantiomers using preparative chiral HPLC. Each of the enantiomers of **4** was reacted with 2-aminoacetamide, as depicted in Scheme 2. The first eluting enantiomer **17** was obtained with 99.6% e.e., while its optical isomer **18** was obtained with 96.6% e.e. The X-ray crystal structures indicate that TbrPDEB1 exhibits chiral discrimination, allowing the arbitrary assignment of the absolute configuration of (4a*R*,8a*S*) to **18**, as this enantiomer possesses a 100-fold higher potency than **17**.

The synthesis of **10**–**12** is outlined in Scheme 3. Methyl ester **31** was treated with aqueous base to give intermediate **32**, and subsequent carbodiimide-mediated

amide coupling yielded **10–12**. Compound **12** was prepared without the addition of DIPEA.
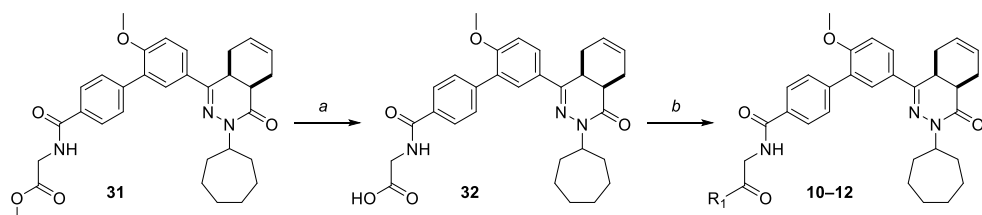
Scheme 3: Reagents and conditions: *a*) NaOH, EtOH, RT, 2 h, 89%; *b*) amine, EDC·HCl, HOAt, DIPEA, CH$_2$Cl$_2$, RT, 36 h, 29–54%.

Scheme 4 depicts the synthesis of **21** and **22**. Analog **21** was prepared by the *N*-alkylation of **20** using iodomethane. Finally, compound **22** was obtained by the oxidation of **23** using Dess-Martin periodinane.
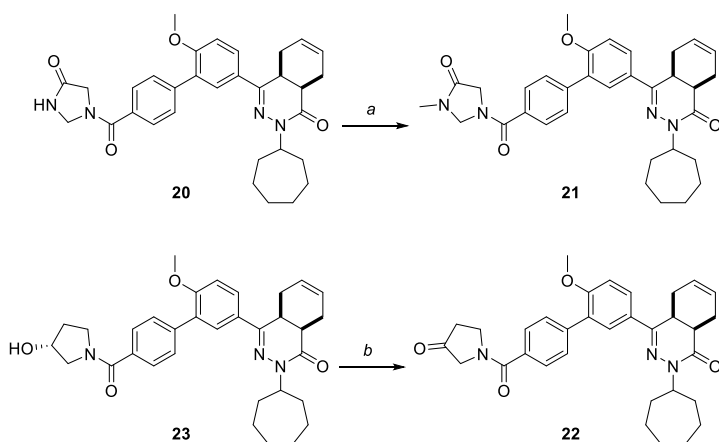
Scheme 4: Reagents and conditions: *a*) iodomethane, NaH, DMF, RT, 1.5 h, 54%; *b*) Dess-Martin periodinane, CH$_2$Cl$_2$, RT, 4 h, 58%.

4. Conclusion

To conclude, we have identified the first series of selective TbrPDEB1 inhibitors by use of iterative cycles of structure based drug design. Our approach to obtain selectivity by rigidifying the flexible tail of **1** by implementing a second phenyl ring has proven fruitful. A series of biphenyl tetrahydrophthalazinones with polar substituents was obtained which successfully target the parasite specific P-pocket. It was shown that incubation of healthy trypanosomes with glycinamide **8** can kill the parasite via a PDE-mediated mode of action. The undesirable cytotoxicity

profile of **8** highlights the importance for further optimization of these rigid tetrahydrophthalazinones. The presence of a similar P-pocket in *L. major* and *T. cruzi* indicates the possibilities to extend this work to other diseases in the field of neglected tropical diseases.[15, 17]

5.   Experimental

5.1.   Chemistry.

All reagents and solvents were obtained from commercial suppliers and were used as received. All reactions were magnetically stirred and carried out under an inert atmosphere. Reaction progress was monitored using thin-layer chromatography (TLC) and LC-MS analysis. Silica gel column chromatography was carried out manually or with automatic purification systems using the indicated eluent. Nuclear magnetic resonance (NMR) spectra were recorded on Bruker Avance 500 (500 MHz for ^{1}H and 126 MHz for ^{13}C) or Bruker Avance 600 (600 MHz for ^{1}H and 151 MHz for ^{13}C) instruments equipped with a Bruker CryoPlatform, or a Bruker DMX300 (300 MHz). Chemical shifts (δ in ppm) and coupling constants (*J* in Hz) are reported with residual solvent as internal standard (δ ^{1}H NMR: CDCl$_3$ 7.26; DMSO-*d$_6$* 2.50; δ ^{13}C NMR: CDCl$_3$ 77.16; DMSO-*d$_6$* 39.52). Various compounds exhibited rotamers leading to more complicated ^{1}H NMR spectra and less accurate integrations. LC-MS analysis was performed on a Shimadzu LC-20AD liquid chromatograph pump system, equipped with an Xbridge (C18) 5 μm column (50 mm, 4.6 mm), connected to a Shimadzu SPD-M20A diode array detector, and MS detection using a Shimadzu LC-MS-2010EV mass spectrometer. The LC-MS conditions were as follows: solvent B (acetonitrile with 0.1% formic acid) and solvent A (water with 0.1% formic acid), flow rate of 1.0 mL/min, start 5% B, linear gradient to 90% B in 4.5 min, then 1.5 min at 90% B, then linear gradient to 5% B in 0.5 min, then 1.5 min at 5% B; total run time of 8 min. Exact mass measurement (HRMS) was performed on a Bruker micrOTOF-Q instrument with electrospray ionization (ESI) in positive ion mode and a capillary potential of 4,500 V. Systematic names for molecules were generated with ChemBioDraw Ultra 14.0.0.117 (PerkinElmer, Inc.). The reported yields refer to isolated pure products; yields were not optimized. The purity, reported as the peak area % at 254 nm, of all final compounds was ≥95% based on LC-MS.

5.2.   Synthetic procedures.

Building block **27**,[22-24] NPD-001 (**1**),[25] and NPD-340 (**2**),[13] were prepared as described elsewhere. All other compounds were prepared as described below.

5.2.1.   *cis*-4-(3-Bromo-4-methoxyphenyl)-2-isopropyl-4a,5,8,8a-tetrahydrophthalazin-1(2*H*)-one (**28**).

To a solution of **27** (50.0 g, 149 mmol) in DMF (500 mL) was added NaH (60% dispersion in mineral oil, 14.9 g, 373 mmol) at RT, the resulting mixture was stirred for 30 min and 2-bromopropane (21.0 mL, 224 mmol) was added. After stirring the reaction mixture for 4 h, 0.5 M aqueous HCl (1.5 L) was added, and the resulting suspension was filtered. The residue was dissolved in a mixture of MeOH and CH$_2$Cl$_2$, dried over Na$_2$SO$_4$, filtered and concentrated under reduced pressure. The light brown solid was triturated with Et$_2$O to give **28** as a white solid in 80% yield. ^{1}H NMR (500 MHz, CDCl$_3$) δ 8.04 (d, *J* = 2.1 Hz, 1H), 7.74 (dd, *J* = 8.7, 2.2 Hz, 1H), 6.93 (d, *J* = 8.7 Hz, 1H), 5.85–5.62 (m, 2H), 5.05 (hept, *J* = 6.7 Hz, 1H), 3.95 (s, 3H), 3.32–3.21 (m, 1H), 3.07–2.95 (m, 1H), 2.74 (t, *J* = 6.0 Hz, 1H), 2.28–2.11 (m, 2H), 2.09–1.95 (m, 1H), 1.33 (d, *J* = 6.6 Hz, 3H), 1.21 (d, *J* = 6.7 Hz, 3H). ^{13}C NMR (126 MHz, CDCl$_3$) δ 166.4, 156.8, 152.3, 130.8, 129.1, 126.2, 126.0, 123.8, 112.2, 111.5, 56.4, 46.8, 34.7, 31.0, 23.0, 22.3, 20.6, 20.2. LC-MS (ESI) *m/z* 377/379 [M + H]$^+$.

5.2.2.   *cis*-4-(3-Bromo-4-methoxyphenyl)-2-cycloheptyl-4a,5,8,8a-tetrahydrophthalazin-1(2*H*)-one (**29**).

 Prepared from building block **27** and bromocycloheptane as described for **28**. The title compound was prepared in 65% yield. ^{1}H NMR (500 MHz, CDCl$_3$) δ 7.98 (d, *J* = 2.2 Hz, 1H), 7.71 (dd, *J* = 8.7, 2.2 Hz, 1H), 6.91 (d, *J* = 8.6 Hz, 1H), 5.83–5.55 (m, 2H), 4.85–4.71 (m, 1H), 3.92 (s, 3H), 3.30–3.16 (m, 1H),

57

2

3.06–2.89 (m, 1H), 2.69 (t, *J* = 6.0 Hz, 1H), 2.27–2.06 (m, 2H), 2.06–1.92 (m, 2H), 1.92–1.81 (m, 1H), 1.81–1.67 (m, 4H), 1.67–1.38 (m, 6H). ^{13}C NMR (126 MHz, CDCl$_3$) δ 165.8, 156.8, 152.2, 130.7, 129.1, 126.2, 126.0, 123.8, 112.1, 111.6, 56.4, 56.3, 34.6, 33.2, 33.0, 31.0, 28.34, 28.27, 25.1, 25.0, 23.0, 22.3. LC-MS (ESI) *m/z* 431/433 [M + H]$^+$.

5.2.3.   5'-(*cis*-3-Isopropyl-4-oxo-3,4,4a,5,8,8a-hexahydrophthalazin-1-yl)-2'-methoxy-[1,1'-biphenyl]-4-carboxylic acid (**30**).

To a degassed solution of **28** (1.00 g, 2.65 mmol) in DME (15 mL), 4-boronobenzoic acid (0.66 g, 4.0 mmol), Pd(dppf)Cl$_2$·CH$_2$Cl$_2$ (0.13 g, 0.16 mmol) and 2 M aqueous Na$_2$CO$_3$ (5.2 mL) was added. The mixture was stirred at 100 °C for 16 h, then diluted with saturated aqueous NH$_4$Cl solution (50 mL) and water (250 mL), and extracted with CH$_2$Cl$_2$ (150 mL). The organic phase was washed with water (150 mL) and brine (100 mL), dried over Na$_2$SO$_4$, filtered and concentrated. The residue was purified on a silica gel column eluting with CH$_2$Cl$_2$/MeOH (gradient, 99:1 to 97:3) to afford **30** in 55% yield. ^{1}H NMR (500 MHz, CDCl$_3$) δ 8.19 (d, *J* = 8.2 Hz, 2H), 7.85 (dd, *J* = 8.7, 2.3 Hz, 1H), 7.80 (d, *J* = 2.2 Hz, 1H), 7.66 (d, *J* = 8.3 Hz, 2H), 7.05 (d, *J* = 8.6 Hz, 1H), 5.86–5.63 (m, 2H), 5.06 (hept, *J* = 6.6 Hz, 1H), 3.89 (s, 3H), 3.40–3.29 (m, 1H), 3.10–2.96 (m, 1H), 2.77 (t, *J* = 6.0 Hz, 1H), 2.28–2.14 (m, 2H), 2.12–1.99 (m, 1H), 1.33 (d, *J* = 6.6 Hz, 3H), 1.21 (d, *J* = 6.7 Hz, 3H). ^{13}C NMR (126 MHz, CDCl$_3$) δ 171.4, 166.5, 157.7, 153.5, 143.7, 130.1, 129.8, 129.7, 128.3, 128.1, 128.0, 127.2, 126.1, 124.0, 111.3, 55.9, 46.8, 34.8, 31.1, 23.2, 22.4, 20.6, 20.2. LC-MS (ESI) *m/z* 419 [M + H]$^+$.

5.2.4.   5'-(*cis*-3-Cycloheptyl-4-oxo-3,4,4a,5,8,8a-hexahydrophthalazin-1-yl)-2'-methoxy-[1,1'-biphenyl]-3-carboxylic acid (**3**, NPD-740).

Prepared from **29** (0.5 g, 1.2 mmol) and 3-boronobenzoic acid (0.25 g, 1.5 mmol) as described for **30**. The title compound was obtained in 65% yield. ^{1}H NMR (500 MHz, DMSO-*d$_6$*) δ 13.09 (s, 1H), 8.05 (s, 1H), 7.92 (d, *J* = 7.7 Hz, 1H), 7.88 (dd, *J* = 8.7, 2.3 Hz, 1H), 7.80–7.71 (m, 2H), 7.56 (t, *J* = 7.7 Hz, 1H), 7.23 (d, *J* = 8.7 Hz, 1H), 5.73–5.56 (m, 2H), 4.74–4.62 (m, 1H), 3.83 (s, 3H), 3.53–3.44 (m, 1H), 2.79 (t, *J* = 6.1 Hz, 1H), 2.76–2.67 (m, 1H), 2.21–2.05 (m, 2H), 1.96–1.63 (m, 7H), 1.62–1.36 (m, 6H). ^{13}C NMR (126 MHz, DMSO-*d$_6$*) δ 167.8, 166.0, 157.7, 154.0, 138.4, 134.1, 131.3, 130.5, 129.5, 128.9, 128.5, 128.3, 128.0, 127.6, 126.4, 124.5, 112.5, 56.3, 55.3, 34.2, 33.3, 33.0, 30.3, 28.7, 28.7, 24.9, 24.8, 23.0, 22.4. LC-MS (ESI): *t$_R$* = 5.44 min, area: >98%, *m/z* 473 [M + H]$^+$. HRMS (ESI) *m/z*: [M + H]$^+$ calcd. for C$_{29}$H$_{33}$N$_2$O$_4$ 473.2435, found 473.2414.

5.2.5.   5'-(*cis*-3-Cycloheptyl-4-oxo-3,4,4a,5,8,8a-hexahydrophthalazin-1-yl)-2'-methoxy-[1,1'-biphenyl]-4-carboxylic acid (**4**, NPD-733).

Prepared from **29** (1.00 g, 2.32 mmol) and 4-boronobenzoic acid (0.66 g, 4.0 mmol) as described for **30**. The title compound was obtained in 66% yield. ^{1}H NMR (500 MHz, CDCl$_3$) δ 8.19 (d, *J* = 8.5 Hz, 2H), 7.84 (dd, *J* = 8.7, 2.4 Hz, 1H), 7.77 (d, *J* = 2.3 Hz, 1H), 7.66 (d, *J* = 8.4 Hz, 2H), 7.05 (d, *J* = 8.7 Hz, 1H), 5.85–5.61 (m, 2H), 4.88–4.74 (m, 1H), 3.88 (s, 3H), 3.38–3.27 (m, 1H), 3.09–2.95 (m, 1H), 2.76 (t, *J* = 5.9 Hz, 1H), 2.27–2.14 (m, 3H), 2.12–1.96 (m, 2H), 1.96–1.85 (m, 1H), 1.85–1.70 (m, 4H), 1.69–1.43 (m, 5H), 1.34–1.18 (m, 1H). ^{13}C NMR (126 MHz, CDCl$_3$) δ 177.1, 166.0, 157.6, 153.5, 143.8, 130.0, 129.7, 129.7, 128.3, 128.1, 128.0, 127.2, 126.1, 123.9, 111.3, 56.3, 55.8, 34.7, 33.2, 33.0, 31.9, 29.0, 28.4, 28.4, 25.1, 25.0, 22.7, 22.4. LC-MS (ESI): *t$_R$* = 5.41 min, area: 98%, *m/z* 473 [M + H]$^+$. HRMS (ESI) *m/z*: [M + H]$^+$ calcd. for C$_{29}$H$_{33}$N$_2$O$_4$ 473.2435, found 473.2432.

5.2.6.   5'-(*cis*-3-Cycloheptyl-4-oxo-3,4,4a,5,8,8a-hexahydrophthalazin-1-yl)-2'-methoxy-[1,1'-biphenyl]-4-carboxamide (**5**, NPD-584).

Prepared from **29** (200 mg, 0.464 mmol) and (4-carbamoylphenyl)boronic acid (116 mg, 0.703 mmol) as described for **30**. The title compound was isolated in 48% yield. ^{1}H NMR (500 MHz, CDCl$_3$) δ 7.90

(d, *J* = 8.3 Hz, 2H), 7.84 (dd, *J* = 8.7, 2.3 Hz, 1H), 7.78 (d, *J* = 2.4 Hz, 1H), 7.65 (d, *J* = 8.3 Hz, 2H), 7.06 (d, *J* = 8.7 Hz, 1H), 6.13 (s, 1H), 5.84–5.66 (m, 2H), 5.62 (s, 1H), 4.87–4.77 (m, 1H), 3.89 (s, 3H), 3.38–3.27 (m, 1H), 3.06–2.97 (m, 1H), 2.76 (t, *J* = 6.0 Hz, 1H), 2.26–1.70 (m, 8H), 1.69–1.60 (m, 4H), 1.57–1.42 (m, 3H). ^{13}C NMR (126 MHz, CDCl$_3$) δ 168.9, 165.9, 157.6, 153.3, 142.0, 131.9, 129.8, 129.7, 128.2, 128.1, 127.2, 127.1, 126.1, 123.9, 111.3, 56.2, 55.8, 34.7, 33.2, 33.0, 31.1, 28.43, 28.36, 25.04, 24.98, 23.1, 22.4. LC-MS (ESI): t_R = 5.34 min, area: 96%, *m/z* 472 [M + H]$^+$. HRMS (ESI) *m/z*: [M + H]$^+$ calcd. for C$_{29}$H$_{34}$N$_3$O$_3$ 472.2595, found 472.2593.

5.2.7.   5'-(*cis*-3-Cycloheptyl-4-oxo-3,4,4a,5,8,8a-hexahydrophthalazin-1-yl)-2'-methoxy-[1,1'-biphenyl]-4-carbonitrile (**6**, NPD-744).

Prepared from **29** (1.0 g, 2.3 mmol) and 4-cyanophenylboronic acid (0.51 g, 3.5 mmol) as described for **30**. The title compound was obtained in 81% yield. ^{1}H NMR (500 MHz, DMSO-*d$_6$*) δ 7.92 (dd, *J* = 8.7, 2.3 Hz, 1H), 7.89 (d, *J* = 8.0 Hz, 2H), 7.75 (d, *J* = 2.3 Hz, 1H), 7.71 (d, *J* = 8.0 Hz, 2H), 7.24 (d, *J* = 8.8 Hz, 1H), 5.73–5.55 (m, 2H), 4.72–4.62 (m, 1H), 3.83 (s, 3H), 3.54–3.44 (m, 1H), 2.80–2.68 (m, 2H), 2.20–2.07 (m, 2H), 1.96–1.61 (m, 7H), 1.61–1.35 (m, 6H). ^{13}C NMR (126 MHz, DMSO-*d$_6$*) δ 170.7, 162.4, 158.6, 147.8, 137.2, 135.5, 133.3, 133.1, 132.9, 132.9, 131.1, 129.2, 124.1, 117.4, 115.0, 61.1, 60.2, 39.0, 38.0, 37.8, 35.0, 33.3, 33.3, 29.7, 29.6, 27.7, 27.2. LC-MS (ESI): t_R = 5.93 min, area: >98%, *m/z* 454 [M + H]$^+$. HRMS (ESI) *m/z*: [M + H]$^+$ calcd. for C$_{29}$H$_{32}$N$_3$O$_2$ 454.2489, found 454.2477.

5.2.8.   5'-(*cis*-3-Cycloheptyl-4-oxo-3,4,4a,5,8,8a-hexahydrophthalazin-1-yl)-2'-methoxy-*N*-(2-methoxyethyl)-[1,1'-biphenyl]-4-carboxamide (**7**, NPD-734).

EDC·HCl (49 mg, 0.26 mmol) was added to a solution of **4** (0.10 g, 0.21 mmol), HOAt (29 mg, 0.21 mmol), 2-methoxyethanamine (0.024 g, 0.32 mmol) and DIPEA (0.11 mL, 0.64 mmol) in CH$_2$Cl$_2$ (5 mL). The mixture was stirred at RT for 3 h, diluted with CH$_2$Cl$_2$ (100 mL), and washed with water (2 × 50 mL) and brine (50 mL). The organic phase was dried over Na$_2$SO$_4$, filtered, concentrated and purified using a reverse phase C18-silica gel column eluting with water/MeCN + 0.1% HCOOH (gradient, 95:5 to 5:95), to afford **7** in 79% yield. ^{1}H NMR (500 MHz, DMSO-*d$_6$*) δ 8.57 (t, *J* = 5.1 Hz, 1H), 7.90 (d, *J* = 8.0 Hz, 2H), 7.87 (dd, *J* = 8.7, 2.3 Hz, 1H), 7.76 (d, *J* = 2.3 Hz, 1H), 7.58 (d, *J* = 8.0 Hz, 2H), 7.22 (d, *J* = 8.7 Hz, 1H), 5.74–5.55 (m, 2H), 4.74–4.59 (m, 1H), 3.82 (s, 3H), 3.54–3.40 (m, 5H), 3.28 (s, 3H), 2.83–2.66 (m, 2H), 2.22–2.06 (m, 2H), 1.96–1.62 (m, 7H), 1.62–1.34 (m, 6H). ^{13}C NMR (126 MHz, DMSO-*d$_6$*) δ 165.0, 164.6, 156.3, 152.5, 139.5, 132.0, 128.2, 126.8, 126.5, 126.2, 126.0, 124.9, 123.1, 111.0, 69.5, 57.0, 54.9, 54.0, 38.0, 32.8, 31.9, 31.6, 28.9, 27.2, 27.2, 23.5, 23.5, 21.6, 21.0. LC-MS (ESI): t_R = 5.30 min, area: >98%, *m/z* 530 [M + H]$^+$. HRMS (ESI) *m/z*: [M + H]$^+$ calcd. for C$_{32}$H$_{40}$N$_3$O$_4$ 530.3013, found 530.3005.

5.2.9.   *N*-(2-Amino-2-oxoethyl)-5'-(*cis*-3-cycloheptyl-4-oxo-3,4,4a,5,8,8a-hexahydrophthalazin-1-yl)-2'-methoxy-[1,1'-biphenyl]-4-carboxamide (**8**, NPD-008).

EDC·HCl (183 mg, 0.952 mmol) was added to a solution of **4** (300 mg, 0.635 mmol), HOBt hydrate (97 mg, 0.63 mmol), 2-aminoacetamide·HCl (105 mg, 0.952 mmol) and Et$_3$N (0.265 mL, 1.90 mmol) in CH$_2$Cl$_2$ (6 mL). The reaction mixture was stirred at RT for 18 h. EtOAc (100 mL) was added, and the resulting solution was washed with water (2 × 50 mL) and brine (50 mL). The organic phase was dried over Na$_2$SO$_4$, filtered and concentrated to obtain the crude product as a light brown oil. The crude oil was purified on a silica gel column eluting with CH$_2$Cl$_2$/MeOH (gradient, 100:0 to 95:5), to give **8** as a white solid in 65% yield. ^{1}H NMR (500 MHz, CDCl$_3$) δ 7.91 (d, *J* = 8.0 Hz, 2H), 7.81 (dd, *J* = 8.7, 2.3 Hz, 1H), 7.75 (d, *J* = 2.4 Hz, 1H), 7.62 (d, *J* = 8.1 Hz, 2H), 7.29–7.24 (m, 1H), 7.03 (d, *J* = 8.7 Hz, 1H), 6.54 (s, 1H), 5.82–5.61 (m, 3H), 4.85–4.74 (m, 1H), 4.23 (d, *J* = 4.7 Hz, 2H), 3.85 (s, 3H), 3.35–3.27 (m, 1H), 3.04–2.94 (m, 1H), 2.73 (t, *J* = 6.0 Hz, 1H), 2.24–2.12 (m, 2H), 2.10–1.94 (m, 2H), 1.93–1.83 (m, 1H), 1.82–1.68 (m, 4H), 1.67–1.42 (m, 6H). ^{13}C NMR (126 MHz, CDCl$_3$) δ 171.2, 167.6, 165.9, 157.6, 153.4, 141.9, 132.0, 129.8, 129.7, 128.2, 128.1, 127.1, 127.0, 126.1, 123.9, 111.3, 56.3, 55.8, 43.3, 34.7, 33.2,

33.0, 31.9, 31.1, 28.43, 28.36, 25.1, 25.0, 23.1, 22.4. LC-MS (ESI): t_R = 4.69 min, area: >98%, *m/z* 529 [M + H]$^+$. HRMS (ESI) *m/z*: [M + H]$^+$ calcd. for $C_{31}H_{37}N_4O_4$ 529.2809, found 529.2811.

5.2.10. *N*-(2-Amino-2-oxoethyl)-5'-(*cis*-3-cycloheptyl-4-oxo-3,4,4a,5,8,8a-hexahydrophthalazin-1-yl)-2'-methoxy-*N*-methyl-[1,1'-biphenyl]-4-carboxamide (**9**, NPD-935).

Prepared from **4** (0.20 mg, 0.42 mmol) and 2-(methylamino)acetamide·HCl (63 mg, 0.51 mmol) as described for **7**. The title compound was obtained in 38% yield. ^{1}H NMR (500 MHz, DMSO-d_6) δ 7.88 (dd, *J* = 8.8, 2.3 Hz, 1H), 7.79–7.70 (m, 1H), 7.62–7.38 (m, 5H), 7.26–7.08 (m, 2H), 5.73–5.56 (m, 2H), 4.67 (tt, *J* = 8.9, 4.7 Hz, 1H), 4.04 (s, 1H), 3.89–3.78 (m, 4H), 3.49 (dt, *J* = 11.4, 5.7 Hz, 1H), 3.01–2.91 (m, 3H), 2.81–2.68 (m, 2H), 2.21–2.07 (m, 2H), 1.96–1.65 (m, 7H), 1.60–1.40 (m, 6H). ^{13}C NMR (126 MHz, DMSO-d_6) δ 171.3, 170.3, 166.0, 157.7, 154.0, 139.2, 135.5, 129.6, 129.5, 128.3, 128.0, 127.5, 127.4, 126.9, 126.3, 124.5, 112.5, 56.3, 55.4, 54.0, 39.0, 34.3, 34.3, 33.3, 33.0, 30.3, 28.6, 28.6, 25.0, 24.9, 23.0, 22.4. LC-MS (ESI): t_R = 4.77 min, area: >95%, *m/z* 543 [M + H]$^+$. HRMS (ESI) *m/z*: [M + H]$^+$ calcd. for $C_{32}H_{39}N_4O_4$ 543.2966, found 543.2969.

5.2.11. *N*-(2-Amino-2-oxoethyl)-5'-((4a*S*,8a*R*)-3-cycloheptyl-4-oxo-3,4,4a,5,8,8a-hexahydrophthalazin-1-yl)-2'-methoxy-[1,1'-biphenyl]-4-carboxamide   and   *N*-(2-Amino-2-oxoethyl)-5'-((4a*R*,8a*S*)-3-cycloheptyl-4-oxo-3,4,4a,5,8,8a-hexahydrophthalazin-1-yl)-2'-methoxy-[1,1'-biphenyl]-4-carboxamide (**17** and **18**).

The enantiomers of racemic **4** were separated using preparative chiral chromatography, the title compounds were synthesized from separate solutions of enantiomerically pure **4** (124 mg, 0.262 mmol) and 2-aminoacetamide HCl (34.8 mg, 0.315 mmol) as described for **7**, and were isolated in 52% yield. The chiral purity of the samples was analyzed by analytical chiral HPLC (Chiralpak AD-H column (250 × 4.6 mm, 5 μm); flow, 1 mL/min; column temperature, 35 °C; detection, 270 nm; eluent, heptane/isopropanol 9:1; runtime, 30 min.), and indicated **17** (first eluting isomer) and **18** (second eluting isomer) to have the same retention times as their respective counterparts in racemic mixture **8**. Absolute configuration was arbitrarily assigned to enantiomer **18**. Compound **17**, Chiralpak AD-H: t_R = 15.93 min, 99.6% e.e.; compound **18**, Chiralpak AD-H: t_R = 19.71 min, 96.9% e.e.

5.2.12. *N*-(2-Amino-2-oxoethyl)-5'-(*cis*-3-isopropyl-4-oxo-3,4,4a,5,8,8a-hexahydrophthalazin-1-yl)-2'-methoxy-[1,1'-biphenyl]-4-carboxamide (**19**, NPD-039).

Prepared from **30** (300 mg, 0.717 mmol) as described for **8**. The title compound was isolated in 59% yield. ^{1}H NMR (500 MHz, CDCl$_3$) δ 7.91 (d, *J* = 8.1 Hz, 2H), 7.84 (dd, *J* = 8.7, 2.3 Hz, 1H), 7.80 (d, *J* = 2.3 Hz, 1H), 7.65 (d, *J* = 8.3 Hz, 2H), 7.05 (d, *J* = 8.7 Hz, 1H), 6.99–6.93 (m, 1H), 5.99 (s, 1H), 5.85–5.64 (m, 2H), 5.48 (s, 1H), 5.06 (hept, *J* = 6.8 Hz, 1H), 4.22 (d, *J* = 4.8 Hz, 2H), 3.89 (s, 3H), 3.39–3.30 (m, 1H), 3.08–2.97 (m, 1H), 2.78 (t, *J* = 6.0 Hz, 1H), 2.24–2.18 (m, 2H), 2.13–2.00 (m, 1H), 1.34 (d, *J* = 6.5 Hz, 3H), 1.22 (d, J = 6.7 Hz, 3H). ^{13}C NMR (126 MHz, CDCl$_3$) δ 170.7, 167.4, 166.4, 157.6, 153.4, 141.9, 132.0, 129.84, 129.76, 128.2, 128.0, 127.0, 126.9, 126.0, 123.9, 111.2, 55.8, 46.7, 43.3, 34.8, 31.1, 23.2, 22.4, 20.6, 20.2. LC-MS (ESI): t_R = 4.13 min, area: >95%, *m/z* 475 [M + H]$^+$. HRMS (ESI) *m/z*: [M + H]$^+$ calcd. for $C_{27}H_{31}N_4O_4$ 475.2340, found 475.2344.

5.2.13. Methyl   (5'-(*cis*-3-cycloheptyl-4-oxo-3,4,4a,5,8,8a-hexahydrophthalazin-1-yl)-2'-methoxy-[1,1'-biphenyl]-4-carbonyl)glycinate (**31**).

Prepared from **4** (1.0 g, 2.1 mmol) and glycine methyl ester·HCl (0.32 g, 2.5 mmol) as described for **7**. The title compound was obtained in 58% yield. ^{1}H NMR (300 MHz, DMSO-d_6) δ 9.00 (t, *J* = 8.2 Hz, 1H), 7.94 (d, *J* = 8.5 Hz, 2H), 7.90 (dd, *J* = 8.8, *J* = 2.3 Hz, 1H) 7.78 (d, *J* = 2.3 Hz, 1H), 7.63 (d, *J* = 8.5 Hz, 2H), 7.25 (d, *J* = 8.8 Hz, 1H), 5.71–5.60 (m, 2H), 4.73–4.64 (m, 1H), 4.05 (d, *J* = 5.8 Hz, 2H), 3.83 (s, 3H), 3.67 (s, 3H), 3.51-3.46 (m, 1H), 2.81–2.72 (m, 2H), 2.20–2.11 (m, 2H), 2.00–1.36 (m, 13H).

5.2.14. (5'-(*cis*-3-Cycloheptyl-4-oxo-3,4,4a,5,8,8a-hexahydrophthalazin-1-yl)-2'-methoxy-[1,1'-biphenyl]-4-carbonyl)glycine (**32**).

Aqueous sodium hydroxide (6.2 mL, 25 mmol) was added to a suspension of **31** (0.84 g, 1.5 mmol) in EtOH (25 mL) and stirred at RT for 2 h. The reaction mixture was acidified with HCl (2 M) and extracted with EtOAc (2 × 30 mL). The combined organic phases were washed with water, dried over Na_2SO_4, filtered and concentrated to give the title compound as a brown solid in 89% yield. ^{1}H NMR (300 MHz, DMSO-d_6) δ 8.87 (t, *J* = 5.8 Hz, 1H), 7.95 (d, *J* = 8.5, 2H), 7.91 (dd, *J* = 8.9, *J* = 2.2 Hz, 1H) 7.79 (d, *J* = 2.3 Hz, 1H), 7.64 (d, *J* = 8.5 Hz, 2H), 7.26 (d, *J* = 8.8 Hz, 1H), 5.73–5.61 (m, 2H), 4.74–4.65 (m, 1H), 3.97 (d, *J* = 5.8 Hz, 2H), 3.85 (s, 3H), 3.55-3.47 (m, 1H), 2.81–2.72 (m, 2H), 2.20–2.11 (m, 2H), 2.00–1.36 (m, 13H). LC-MS (ESI): t_R = 4.93 min, *m/z* 530 [M + H]$^+$

5.2.15. 5'-(*cis*-3-Cycloheptyl-4-oxo-3,4,4a,5,8,8a-hexahydrophthalazin-1-yl)-2'-methoxy-*N*-(2-(methylamino)-2-oxoethyl)-[1,1'-biphenyl]-4-carboxamide (**10**, NPD-936).

EDC·HCl (43 mg, 0.22 mmol) was added to a solution of **32** (0.10 g, 0.19 mmol), HOAt (26 mg, 0.19 mmol), methyl amine·HCl (28 mg, 0.42 mmol) and DIPEA (0.066 mL, 0.38 mmol) in CH_2Cl_2 (4 mL). The reaction mixture was stirred at RT for 36 h, CH_2Cl_2 (100 mL) was added, and the resulting solution was washed with water (2 × 50 mL) and brine (50 mL). The organic phase was dried over Na_2SO_4, filtered and concentrated. The product was purified on a silica gel column eluting with EtOAc, to give **10** as a white solid in 29% yield. ^{1}H NMR (500 MHz, DMSO-d_6) δ 8.86 (t, *J* = 6.0 Hz, 1H), 8.04–7.97 (m, 2H), 7.96–7.88 (m, 2H), 7.83 (d, *J* = 2.4 Hz, 1H), 7.70–7.63 (m, 2H), 7.28 (d, *J* = 8.8 Hz, 1H), 5.80–5.63 (m, 2H), 4.73 (td, *J* = 8.8, 4.5 Hz, 1H), 3.91 (d, *J* = 5.9 Hz, 2H), 3.89 (s, 3H), 3.55 (dt, *J* = 11.6, 5.7 Hz, 1H), 2.88–2.75 (m, 2H), 2.67 (d, *J* = 4.6 Hz, 3H), 2.27–2.13 (m, 2H), 2.02–1.72 (m, 7H), 1.67–1.45 (m, 6H). ^{13}C NMR (126 MHz, DMSO-d_6) δ 169.8, 166.6, 166.0, 157.7, 153.9, 141.1, 133.1, 129.6, 129.6, 128.2, 128.0, 127.7, 127.6, 126.3, 124.5, 112.5, 56.3, 55.4, 43.2, 34.2, 33.3, 33.1, 30.3, 28.6, 28.6, 26.0, 24.9, 24.9, 23.0, 22.4. LC-MS (ESI): t_R = 4.86 min, area: >98%, *m/z* 543 [M + H]$^+$. HRMS (ESI) *m/z*: [M + H]$^+$ calcd. for $C_{32}H_{39}N_4O_4$ 543.2966, found 543.2963.

5.2.16. 5'-(*cis*-3-Cycloheptyl-4-oxo-3,4,4a,5,8,8a-hexahydrophthalazin-1-yl)-*N*-(2-(dimethylamino)-2-oxoethyl)-2'-methoxy-[1,1'-biphenyl]-4-carboxamide (**11**, NPD-939).

Prepared from **32** (25 mg, 0.048 mmol) and dimethylamine·HCl (8.5 mg, 0.11 mmol) as described for **10**. The title compound was obtained in 54% yield. ^{1}H NMR (500 MHz, DMSO-d_6) δ 8.64 (t, *J* = 5.7 Hz, 1H), 7.99 (d, *J* = 8.4 Hz, 2H), 7.95 (dd, *J* = 8.7, 2.3 Hz, 1H), 7.84 (d, *J* = 2.3 Hz, 1H), 7.71–7.63 (m, 2H), 7.29 (d, *J* = 8.8 Hz, 1H), 5.80–5.64 (m, 2H), 4.74 (tt, *J* = 8.6, 4.8 Hz, 1H), 4.19 (d, *J* = 5.6 Hz, 2H), 3.89 (s, 3H), 3.56 (dt, *J* = 11.5, 5.7 Hz, 1H), 3.09 (s, 3H), 2.92 (s, 3H), 2.88–2.76 (m, 2H), 2.27–2.12 (m, 2H), 2.03–1.73 (m, 7H), 1.67–1.45 (m, 6H). ^{13}C NMR (126 MHz, DMSO-d_6) δ 168.7, 166.5, 166.0, 157.7, 154.0, 141.1, 133.2, 129.7, 129.6, 128.3, 128.0, 127.6, 127.5, 126.3, 124.5, 112.5, 56.3, 55.4, 41.4, 36.2, 35.6, 34.2, 33.3, 33.1, 30.3, 28.6, 28.6, 25.0, 24.9, 23.0, 22.4. LC-MS (ESI): t_R = 5.01 min, area: >95%, *m/z* 557 [M + H]$^+$. HRMS (ESI) *m/z*: [M + H]$^+$ calcd. for $C_{33}H_{41}N_4O_4$ 557.3122, found 557.3114.

5.2.17. 5'-(*cis*-3-Cycloheptyl-4-oxo-3,4,4a,5,8,8a-hexahydrophthalazin-1-yl)-*N*-(2-(isopropylamino)-2-oxoethyl)-2'-methoxy-[1,1'-biphenyl]-4-carboxamide (**12**, NPD-942).

Prepared from **32** (0.10 g, 0.19 mmol) and isopropyl amine (0.034 mL, 0.42 mmol) as described for **10**, but excluding DIPEA. The title compound was obtained in 38% yield. ^{1}H NMR (500 MHz, DMSO-d_6) δ 8.69 (t, *J* = 5.9 Hz, 1H), 7.93 (d, *J* = 8.4 Hz, 2H), 7.88 (dd, *J* = 8.7, 2.3 Hz, 1H), 7.82–7.73 (m, 2H), 7.65–7.54 (m, 2H), 7.22 (d, *J* = 8.8 Hz, 1H), 5.77–5.56 (m, 2H), 4.74–4.62 (m, 1H), 3.91–3.83 (m, 3H), 3.83 (s, 3H), 3.49 (dt, *J* = 11.6, 5.8 Hz, 1H), 2.81–2.69 (m, 2H), 2.20–2.08 (m, 2H), 1.95–1.65 (m, 7H), 1.61–1.36 (m, 6H), 1.07 (d, *J* = 6.6 Hz, 6H). ^{13}C NMR (126 MHz, DMSO-d_6) δ 168.2, 166.5, 166.0, 157.7, 154.0, 141.1, 133.2, 129.6, 129.6, 128.2, 128.0, 127.6, 127.6, 126.3, 124.5, 112.5, 56.3, 55.4, 43.0, 40.9, 33.3,

33.1, 30.3, 28.6, 28.6, 24.9, 24.9, 23.0, 22.9, 22.4. LC-MS (ESI): t_R = 5.17 min, area: >98%, *m/z* 571 [M + H]$^+$. HRMS (ESI) *m/z*: [M + H]$^+$ calcd. for $C_{34}H_{43}N_4O_4$ 571.3279, found 571.3262.

5.2.18. *N*-(3-Amino-3-oxopropyl)-5'-(*cis*-3-cycloheptyl-4-oxo-3,4,4a,5,8,8a-hexahydrophthalazin-1-yl)-2'-methoxy-[1,1'-biphenyl]-4-carboxamide (**13**, NPD-800).

Prepared from **4** (80 mg, 0.17 mmol) and 3-aminopropanamide·HCl (42 mg, 0.34 mmol) as described for **7**. The title compound was obtained in 64% yield. ^{1}H NMR (500 MHz, DMSO-d_6) δ 8.55 (t, *J* = 5.6 Hz, 1H), 7.87 (dd, *J* = 8.7, 2.5 Hz, 3H), 7.76 (d, *J* = 2.3 Hz, 1H), 7.62–7.54 (m, 2H), 7.43–7.35 (m, 1H), 7.22 (d, *J* = 8.8 Hz, 1H), 6.86 (s, 1H), 5.73–5.58 (m, 2H), 4.73–4.62 (m, 1H), 3.82 (s, 3H), 3.54–3.41 (m, 3H), 2.81–2.68 (m, 2H), 2.36 (t, *J* = 7.2 Hz, 2H), 2.22–2.08 (m, 2H), 1.97–1.63 (m, 8H), 1.63–1.39 (m, 6H). ^{13}C NMR (126 MHz, DMSO-d_6) δ 173.0, 166.4, 166.0, 157.7, 154.0, 140.9, 133.6, 129.6, 128.2, 128.0, 127.6, 127.4, 126.3, 124.5, 112.5, 56.3, 55.4, 36.5, 35.5, 34.2, 33.3, 33.1, 30.3, 28.7, 28.6, 28.6, 25.0, 24.9, 23.0, 22.4. LC-MS (ESI): t_R = 4.72 min, area: >95%, *m/z* 543 [M + H]$^+$. HRMS (ESI) *m/z*: [M + H]$^+$ calcd. for $C_{32}H_{39}N_4O_4$ 543.2966, found 543.2966.

5.2.19. *N*-(2-Acetamidoethyl)-5'-(*cis*-3-cycloheptyl-4-oxo-3,4,4a,5,8,8a-hexahydrophthalazin-1-yl)-2'-methoxy-[1,1'-biphenyl]-4-carboxamide (**14**, NPD-801).

Prepared from **4** (80 mg, 0.17 mmol) and *N*-(2-aminoethyl)acetamide (35 mg, 0.34 mmol) as described for **7**, but excluding DIPEA. The title compound was obtained in 78% yield. ^{1}H NMR (500 MHz, DMSO-d_6) δ 8.55 (t, *J* = 5.6 Hz, 1H), 8.00 (t, *J* = 5.8 Hz, 1H), 7.91–7.84 (m, 3H), 7.76 (d, *J* = 2.3 Hz, 1H), 7.62–7.55 (m, 2H), 7.22 (d, *J* = 8.9 Hz, 1H), 5.74–5.56 (m, 2H), 4.67 (tt, *J* = 8.5, 4.9 Hz, 1H), 3.82 (s, 3H), 3.49 (dt, *J* = 11.4, 5.7 Hz, 1H), 3.31 (q, *J* = 6.1 Hz, 2H), 3.21 (q, *J* = 6.3 Hz, 2H), 2.81–2.68 (m, 2H), 2.21–2.07 (m, 2H), 1.93–1.66 (m, 11H), 1.60–1.40 (m, 6H). ^{13}C NMR (126 MHz, DMSO-d_6) δ 170.0, 166.5, 166.0, 157.7, 154.0, 141.0, 133.6, 129.6, 129.6, 128.2, 128.0, 127.6, 127.4, 126.3, 124.5, 112.5, 56.3, 55.4, 39.7, 38.7, 34.2, 33.3, 33.1, 30.3, 28.6, 28.6, 25.0, 24.9, 23.1, 23.0, 22.4. LC-MS (ESI): t_R = 4.84 min, area: >95%, *m/z* 557 [M + H]$^+$. HRMS (ESI) *m/z*: [M + H]$^+$ calcd. for $C_{33}H_{41}N_4O_4$ 557.3122, found 557.3128.

5.2.20. 5'-(*cis*-3-Cycloheptyl-4-oxo-3,4,4a,5,8,8a-hexahydrophthalazin-1-yl)-*N*-(2-((2-hydroxyethyl)amino)-2-oxoethyl)-2'-methoxy-[1,1'-biphenyl]-4-carboxamide (**15**, NPD-937).

Prepared from **4** (200 mg, 0.423 mmol) and 2-amino-*N*-(2-hydroxyethyl)acetamide·HCl (65 mg, 0.42 mmol) as described for **8**. The title compound was obtained in 54% yield. ^{1}H NMR (500 MHz, CDCl$_3$) δ 7.84 (d, *J* = 8.1 Hz, 2H), 7.75 (dd, *J* = 8.7, 2.3 Hz, 1H), 7.69 (d, *J* = 2.2 Hz, 1H), 7.57 (d, *J* = 8.0 Hz, 2H), 7.14 (t, *J* = 5.2 Hz, 1H), 6.97 (d, *J* = 8.7 Hz, 1H), 6.77 (t, *J* = 4.7 Hz, 1H), 5.75–5.56 (m, 2H), 4.79–4.68 (m, 1H), 4.14 (d, *J* = 4.9 Hz, 2H), 3.79 (s, 3H), 3.70 (t, *J* = 4.9 Hz, 2H), 3.43 (q, *J* = 5.2 Hz, 2H), 3.28–3.21 (m, 1H), 2.99–2.88 (m, 1H), 2.67 (t, *J* = 6.0 Hz, 1H), 2.19–2.05 (m, 2H), 2.04–1.73 (m, 8H), 1.66–1.36 (m, 7H). ^{13}C NMR (126 MHz, CDCl$_3$) δ 169.7, 167.8, 165.9, 157.6, 153.3, 142.1, 131.9, 129.9, 129.7, 128.2, 128.1, 127.1, 127.0, 126.1, 123.9, 111.3, 61.9, 56.2, 55.8, 43.8, 42.5, 34.7, 33.2, 33.0, 31.1, 28.43, 28.37, 25.1, 25.0, 23.1, 22.4. LC-MS (ESI): t_R = 4.63 min, area: >98%, *m/z* 573 [M + H]$^+$. HRMS (ESI) *m/z*: [M + H]$^+$ calcd. for $C_{33}H_{41}N_4O_5$ 573.3071, found 573.3057.

5.2.21. 5'-(*cis*-3-Cycloheptyl-4-oxo-3,4,4a,5,8,8a-hexahydrophthalazin-1-yl)-2'-methoxy-*N*-(2-((2-methoxyethyl)amino)-2-oxoethyl)-[1,1'-biphenyl]-4-carboxamide (**16**, NPD-878).

Prepared from **4** (0.15 g, 0.32 mmol) and 2-amino-*N*-(2-methoxyethyl)acetamide (50 mg, 0.38 mmol) as described for **7**. The title compound was obtained in 32% yield. ^{1}H NMR (500 MHz, DMSO-d_6) δ 8.77 (t, *J* = 6.0 Hz, 1H), 8.00 (t, *J* = 5.7 Hz, 1H), 7.94 (d, *J* = 8.4 Hz, 2H), 7.88 (dd, *J* = 8.7, 2.3 Hz, 1H), 7.78 (d, *J* = 2.4 Hz, 1H), 7.65–7.55 (m, 2H), 7.22 (d, *J* = 8.8 Hz, 1H), 5.74–5.57 (m, 2H), 4.73–4.62 (m, 1H), 3.88 (d, *J* = 5.9 Hz, 2H), 3.83 (s, 3H), 3.49 (dt, *J* = 11.5, 5.7 Hz, 1H), 3.40–3.31 (m, 2H), 3.25 (d, *J* = 5.0 Hz, 5H),

2.82–2.68 (m, 2H), 2.22–2.07 (m, 2H), 1.97–1.64 (m, 7H), 1.61–1.37 (m, 6H). ^{13}C NMR (126 MHz, DMSO-d_6) δ 169.1, 166.2, 165.6, 157.3, 153.5, 140.7, 132.7, 129.2, 129.2, 127.8, 127.6, 127.2, 125.9, 124.1, 112.0, 70.6, 58.0, 55.9, 55.0, 42.6, 38.4, 33.8, 32.9, 32.6, 29.9, 28.2, 28.2, 24.5, 24.5, 22.6, 22.0. LC-MS (ESI): t_R = 4.92 min, area: >98%, *m/z* 587 [M + H]$^+$. HRMS (ESI) *m/z*: [M + H]$^+$ calcd. for $C_{34}H_{43}N_4O_5$ 587.3228, found 587.3220.

5.2.22. *cis*-2-Cycloheptyl-4-(6-methoxy-4'-(4-oxoimidazolidine-1-carbonyl)-[1,1'-biphenyl]-3-yl)-4a,5,8,8a-tetrahydrophthalazin-1(*2H*)-one (**20**, NPD-060).

Prepared from **4** (0.20 g, 0.42 mmol) and imidazolidin-4-one·HCl (70 mg, 0.57 mmol) as described for **7**. The title compound was obtained in 88% yield. Note: less accurate integrations due to rotamers/diastereomers. ^{1}H NMR (600 MHz, DMSO-d_6) δ 8.71 (s, 0.6H), 8.61 (s, 0.4H), 7.90 (dd, *J* = 8.7, 2.4 Hz, 1H), 7.77 (d, *J* = 2.3 Hz, 1H), 7.69 (d, *J* = 7.9 Hz, 1H), 7.61 (m, 3H), 7.25 (d, *J* = 8.8 Hz, 1H), 5.73–5.60 (m, 2H), 4.90 (m, 2H), 4.69 (tt, *J* = 9.0, 4.8 Hz, 1H), 4.08 (s, 0.6H), 3.98 (s, 0.4H), 3.85 (s, 3H), 3.50 (m, 1H), 2.82–2.70 (m, 2H), 2.20-2.10 (m, 2H), 1.97–1.89 (m, 1H), 1.88–1.68 (m, 6H), 1.62–1.41 (m, 6H). LC-MS (ESI): t_R = 4.81 min, area: >95%, *m/z* 541 [M + H]$^+$. HRMS (ESI) *m/z*: [M + H]$^+$ calcd. for $C_{32}H_{37}N_4O_4$ 541.2809, found 541.2792.

5.2.23. *cis*-2-Cycloheptyl-4-(6-methoxy-4'-(3-methyl-4-oxoimidazolidine-1-carbonyl)-[1,1'-biphenyl]-3-yl)-4a,5,8,8a-tetrahydrophthalazin-1(*2H*)-one (**21**, NPD-062).

To an ice-cooled solution of **20** (0.10 g, 0.19 mmol) in DMF (4 mL), sodium hydride (60% dispersion in mineral oil, 9.3 mg, 0.21 mmol) was added. The temperature of the mixture was allowed to increase to RT, after 30 min iodomethane (27 mg, 0.19 mmol, 12 μL) was added. This mixture was stirred for 1.5 h, diluted with water (25 mL) and extracted with CH_2Cl_2 (3 × 45 mL). The combined organic phases were washed with brine (15 mL), dried over Na_2SO_4, filtered, concentrated and purified on a silica gel column eluting with CH_2Cl_2/MeOH (gradient, 100:0 to 96:4). The product was freeze-dried to obtain **21** in 54% yield. ^{1}H NMR (500 MHz, DMSO-d_6) δ 7.89 (dd, *J* = 8.7, 2.2 Hz, 1H), 7.76 (t, *J* = 2.8 Hz, 1H), 7.69 (d, *J* = 8.0 Hz, 1H), 7.65–7.57 (m, 3H), 7.24 (d, *J* = 8.7 Hz, 1H), 5.73–5.57 (m, 2H), 4.99–4.90 (m, 2H), 4.68 (tt, *J* = 8.8, 4.8 Hz, 1H), 4.17 (s, 1H), 4.07 (s, 1H), 3.84 (s, 3H), 3.49 (dt, *J* = 11.6, 5.8 Hz, 1H), 2.86 (s, 2H), 2.81–2.69 (m, 3H), 2.21–2.07 (m, 2H), 1.97–1.65 (m, 7H), 1.62–1.38 (m, 6H). ^{13}C NMR (126 MHz, DMSO-d_6) δ 168.1, 167.4, 166.0, 157.7, 153.9, 140.4, 133.8, 129.8, 129.7, 129.3, 128.3, 128.0, 127.7, 127.6, 127.4, 126.3, 124.4, 112.5, 64.4, 56.3, 55.4, 50.5, 34.2, 33.2, 33.0, 30.3, 28.6, 28.5, 27.4, 24.9, 24.8, 23.0, 22.4. LC-MS (ESI): t_R = 3.85 min, area: >95%, *m/z* 555 [M + H]$^+$. HRMS (ESI) *m/z*: [M + H]$^+$ calcd. for $C_{33}H_{39}N_4O_4$ 555.2966, found 555.2957.

5.2.24. *cis*-2-Cycloheptyl-4-(6-methoxy-4'-(3-oxopyrrolidine-1-carbonyl)-[1,1'-biphenyl]-3-yl)-4a,5,8,8a-tetrahydrophthalazin-1(*2H*)-one (**22**, NPD-887).

To a solution of **23** (0.58 g, 1.1 mmol) in CH_2Cl_2 (3 mL), Dess-Martin periodinane (0.11 g, 2.7 mmol) was added, and the reaction mixture was stirred at RT for 4 h. Water (0.019 mL, 1.1 mmol) was added and the mixture was stirred for an additional 30 min. A mixture of aqueous 10% sodium metabisulfite and saturated aqueous sodium bicarbonate (1:1 ratio, 2 mL total volume) was added, the resulting mixture was extracted with CH_2Cl_2 (20 mL) and washed with sodium bicarbonate (2 × 10 mL). The organic phase was concentrated, and the product was purified on a silica gel column eluting with EtOAc/heptane (gradient, 6:4 to 9:1), to afford **22** as a white solid in 58% yield. ^{1}H NMR (500 MHz, DMSO-d_6) δ 7.95 (dd, *J* = 8.7, 2.4 Hz, 1H), 7.82 (d, *J* = 2.3 Hz, 1H), 7.71–7.59 (m, 4H), 7.30 (d, *J* = 8.8 Hz, 1H), 5.81–5.60 (m, 2H), 4.74 (tt, *J* = 8.9, 4.8 Hz, 1H), 4.09–3.94 (m, 4H), 3.90 (s, 3H), 3.56 (dt, *J* = 11.5, 5.8 Hz, 1H), 2.87–2.75 (m, 2H), 2.67 (t, *J* = 7.8 Hz, 2H), 2.26–2.15 (m, 2H), 2.02–1.73 (m, 7H), 1.66–1.47 (m, 6H). ^{13}C NMR (126 MHz, DMSO-d_6) δ 169.1, 166.0, 157.7, 154.0, 139.9, 129.7, 129.5, 128.3, 128.0, 127.5, 126.3, 124.5, 112.5, 56.3, 55.6, 55.4, 52.7, 46.4, 42.8, 37.9, 36.1, 34.2, 33.3, 33.1, 30.3, 28.6,

28.6, 25.0, 24.9, 23.0, 22.4. LC-MS (ESI): t_R = 5.19 min, area: >95%, *m/z* 540 [M + H]$^+$. HRMS (ESI) *m/z*: [M + H]$^+$ calcd. for $C_{33}H_{38}N_3O_4$ 540.2857, found 540.2880.

5.2.25. *cis*-2-Cycloheptyl-4-(4'-((*R*)-3-hydroxy-pyrrolidine-1-carbonyl)-6-methoxy-[1,1'-biphenyl]-3-yl)-4a,5,8,8a-tetrahydrophthalazin-1(*2H*)-one (**23**, NPD-746).

Prepared from **4** (0.83 g, 1.8 mmol) and (*R*)-pyrrolidin-3-ol (0.18 g, 2.1 mmol) as described for **7**, but excluding DIPEA. The title compound was obtained in 75% yield. ^{1}H NMR (500 MHz, DMSO-*d$_6$*) δ 7.89 (dd, *J* = 8.7, 2.3 Hz, 1H), 7.76 (d, *J* = 2.2 Hz, 1H), 7.62–7.55 (m, 4H), 7.24 (d, *J* = 8.8 Hz, 1H), 5.75–5.57 (m, 2H), 5.05 (d, *J* = 3.5 Hz, 0H), 4.96 (d, *J* = 3.1 Hz, 1H), 4.74–4.63 (m, 1H), 4.35 (s, 1H), 4.26 (s, 1H), 3.84 (s, 3H), 3.68–3.45 (m, 4H), 3.42–3.38 (m, 1H), 3.30–3.25 (m, 1H), 2.83–2.70 (m, 2H), 2.21–2.09 (m, 2H), 1.98–1.65 (m, 9H), 1.63–1.39 (m, 6H). ^{13}C NMR (126 MHz, DMSO) δ 168.7, 166.0, 157.7, 154.0, 139.6, 136.1, 129.6, 129.5, 128.3, 128.0, 127.5, 127.4, 126.4, 124.5, 112.5, 69.8, 68.5, 57.6, 56.3, 55.4, 54.9, 47.4, 44.6, 34.9, 34.3, 33.3, 33.1, 32.6, 30.3, 28.6, 28.6, 25.0, 24.9, 23.0, 22.4. LC-MS (ESI): t_R = 4.91 min, area: >98%, *m/z* 542 [M + H]$^+$. HRMS (ESI) *m/z*: [M + H]$^+$ calcd. for $C_{33}H_{40}N_3O_4$ 542.3013, found 542.3013.

5.2.26. (*R*)-1-(5'-(*cis*-3-Cycloheptyl-4-oxo-3,4,4a,5,8,8a-hexahydrophthalazin-1-yl)-2'-methoxy-[1,1'-biphenyl]-4-carbonyl)pyrrolidine-2-carboxamide (**24**, NPD-802).

Prepared from **4** (80 mg, 0.17 mmol) and (*R*)-pyrrolidine-2-carboxamide (38 mg, 0.34 mmol) as described for **7**, but excluding DIPEA. The title compound was obtained in 78% yield. Note: less accurate integrations due to rotamers/diastereomers. ^{1}H NMR (500 MHz, DMSO-*d$_6$*) δ 7.88 (dd, *J* = 8.8, 2.3 Hz, 1H), 7.76 (d, *J* = 2.3 Hz, 0.7H), 7.72 (d, *J* = 2.3 Hz, 0.3H), 7.64 (d, *J* = 8.1 Hz, 1.7H), 7.57 (d, *J* = 8.1 Hz, 1.7H), 7.53 (d, *J* = 7.9 Hz, 0.6H), 7.46–7.39 (m, 1.6H), 7.23 (d, *J* = 8.7 Hz, 1H), 7.05 (d, *J* = 3.2 Hz, 0.3H), 6.98 (s, 0.8H), 5.74–5.56 (m, 2H), 4.75–4.63 (m, 1H), 4.38 (dd, *J* = 8.2, 5.6 Hz, 0.8H), 4.25 (d, *J* = 8.0 Hz, 0.3H), 3.83 (s, 3H), 3.70–3.54 (m, 1.3H), 3.54–3.44 (m, 1.8H), 2.83–2.68 (m, 2H), 2.27–2.07 (m, 3H), 1.94–1.66 (m, 10H), 1.62–1.37 (m, 6H). ^{13}C NMR (126 MHz, DMSO-*d$_6$*) δ 173.7, 168.3, 165.6, 157.3, 153.6, 139.3, 135.4, 129.2, 129.0, 127.9, 127.6, 127.2, 127.1, 126.5, 125.9, 124.1, 112.1, 60.2, 55.9, 55.0, 49.9, 33.8, 32.9, 32.6, 29.9, 29.7, 28.2, 28.2, 25.1, 24.6, 24.5, 22.6, 22.0. LC-MS (ESI): t_R = 4.89 min, area: >96%, *m/z* 569 [M + H]$^+$. HRMS (ESI) *m/z*: [M + H]$^+$ calcd. for $C_{34}H_{41}N_4O_4$ 569.3122, found 569.3143.

5.2.27. *cis*-4-(4'-((*R*)-3-Hydroxypyrrolidine-1-carbonyl)-6-methoxy-[1,1'-biphenyl]-3-yl)-2-isopropyl-4a,5,8,8a-tetrahydrophthalazin-1(*2H*)-one (**25**, NPD-038).

Prepared from **30** (300 mg, 0.717 mmol) and (*R*)-pyrrolidin-3-ol (62 mg, 0.72 mmol) analogous to the method described for **8** but excluding Et$_3$N. The title compound was isolated in 64% yield. ^{1}H NMR (500 MHz, CDCl$_3$) δ 7.81 (dd, *J* = 8.7, 2.3 Hz, 1H), 7.77 (d, *J* = 2.4 Hz, 1H), 7.67–7.53 (m, 4H), 7.02 (d, *J* = 8.7 Hz, 1H), 5.82–5.64 (m, 2H), 5.04 (hept, *J* = 6.6 Hz, 1H), 4.69–4.41 (m, 1H), 3.86 (s, 3H), 3.88–3.47 (m, 5H), 3.39–3.26 (m, 1H), 3.06–2.93 (m, 1H), 2.75 (t, *J* = 6.0 Hz, 1H), 2.29–1.96 (m, 5H), 1.32 (d, *J* = 6.6 Hz, 3H), 1.20 (d, *J* = 6.7 Hz, 3H). ^{13}C NMR (126 MHz, CDCl$_3$) δ 169.9, 166.4, 157.7, 153.5, 139.9, 135.3, 130.1, 129.4, 128.3, 128.0, 127.1, 126.8, 126.0, 124.0, 111.2, 71.0, 69.8, 57.4, 55.8, 55.0, 47.4, 46.7, 34.8, 31.1, 23.2, 22.4, 20.6, 20.2. LC-MS (ESI): t_R = 4.31 min, area: >98%, *m/z* 488 [M + H]$^+$. HRMS (ESI) *m/z*: [M + H]$^+$ calcd. for $C_{29}H_{34}N_3O_4$ 488.2544, found 488.2534.

5.2.28. (*R*)-1-(5'-(*cis*-3-Isopropyl-4-oxo-3,4,4a,5,8,8a-hexahydrophthalazin-1-yl)-2'-methoxy-[1,1'-biphenyl]-4-carbonyl)pyrrolidine-2-carboxamide (**26**, NPD-885).

Prepared from **30** (0.10 g, 0.21 mmol) and (*R*)-pyrrolidine-2-carboxamide (43 mg, 0.38 mmol) as described for **7**, but excluding DIPEA. The title compound was obtained in 56% yield. ^{1}H NMR (500 MHz, DMSO-*d$_6$*) δ 7.83 (dd, *J* = 8.8, 2.4 Hz, 1H), 7.72 (d, *J* = 2.3 Hz, 1H), 7.58 (d, *J* = 8.1 Hz, 1H), 7.51 (d,

J = 8.0 Hz, 2H), 7.47 (d, *J* = 7.9 Hz, 1H), 7.36 (d, *J* = 13.1 Hz, 1H), 7.15 (dd, *J* = 8.9, 2.6 Hz, 1H), 6.92 (s, 1H), 5.67–5.51 (m, 2H), 4.81 (hept, *J* = 6.7 Hz, 1H), 4.32 (dd, *J* = 8.3, 5.6 Hz, 1H), 3.77 (d, *J* = 3.1 Hz, 3H), 3.61–3.49 (m, 1H), 3.43 (dt, *J* = 11.1, 5.7 Hz, 2H), 2.76–2.63 (m, 2H), 2.18–2.03 (m, 3H), 1.89–1.65 (m, 4H), 1.17 (d, *J* = 6.6 Hz, 3H), 1.07 (d, *J* = 6.7 Hz, 3H). ^{13}C NMR (126 MHz, DMSO-d_6) δ 174.2, 168.7, 166.5, 157.8, 154.0, 139.7, 135.8, 129.7, 129.4, 128.2, 128.0, 127.7, 127.6, 126.9, 126.3, 124.5, 112.4, 60.6, 56.3, 50.4, 46.2, 34.3, 30.4, 30.2, 25.5, 23.0, 22.4, 20.9, 20.6. LC-MS (ESI): t_R = 4.22 min, area: >95%, *m/z* 515 [M + H]$^+$. HRMS (ESI) *m/z*: [M + H]$^+$ calcd. for $C_{30}H_{35}N_4O_4$ 515.2653, found 515.2652.

5.3.   Interference compounds.

All final compounds have been examined for the presence of substructures classified as Pan Assay Interference Compounds (PAINS) using a KNIME workflow.[26]

5.4.   Phosphodiesterase activity assays.

To determine the effect of test compounds on the enzymatic activity of full length TbrPDEB1 (K_m = 7.97 ± 2.32 µM) and full length recombinant hPDE4B1 (K_m = 2.0 ± 0.7 µM) the standard scintillation proximity assay (SPA) was used, as reported previously.[11, 13] In these assays, the cAMP substrate concentration was 0.5 µM, and enzyme concentrations were adjusted so that < 20% of substrate was consumed. The K_i values are represented as the mean of at least two independent experiments with the associated standard error of the mean (s.e.m.) as indicated.

5.5.   Gene constructs for structural studies.

5.5.1.   TbrPDEB1 catalytic domain.

A gene segment coding for TbrPDEB1 catalytic domain residues 565–918 (Uniprot entry Q8WQX9) was PCR amplified with flanking *Nde*I and *EcoR*I restriction sites and cloned into a pET28a(+) expression vector (Novagen) previously digested with the same set of restriction enzymes. An N-terminal, thrombin cleavable 6xHis tag was kept in-frame with the gene to facilitate subsequent purification of the expressed protein by metal affinity chromatography. The resultant recombinant vector was named pET28a(+)-TbrPDEB1_CD.

5.5.2.   hPDE4B regulatory domain (UCR2+catalytic domain).

Coding sequence for hPDE4B UCR2 and catalytic domain residues 241–659 (Uniprot entry Q07343) was synthesized and cloned into a pMA vector (GeneArt, Invitrogen, Life Technologies). This vector was then used as a PCR template for sub-cloning of the gene segment into a pFastBacHTA insect cell expression vector (Invitrogen, Life Technologies) with a C-terminal 6xHis purification tag.

5.5.3.   hPDE4D2 catalytic domain.

A gene segment coding for residues 381–740 of hPDE4D2 (Uniprot entry Q08499) was PCR amplified using a forward primer including a *Nde*I restriction site and a reverse primer including a *Xho*I restriction site. The PCR product was cloned into a pET15b *E. coli* expression vector (Novagen) previously digested with the same set of enzymes. The primer design was such so as to keep an N-terminal 6xHis tag from the vector in frame with the target gene. The resultant recombinant vector was named pET15b-hPDE4D_CD.

5.6.   Protein expression and purification for structural studies.

5.6.1.   TbrPDEB1 catalytic domain.

Escherichia coli BL21 (DE3) cells were transformed with pET28a(+)-TbrPDEB1_CD and allowed to grow in 2 L 2xYT medium at 37 °C until the optical density at 600 nm reached 0.6–0.8. At this stage the

culture was cooled down, induced with 1 mM isopropyl -D-1-thiogalactopyranoside (IPTG) and further grown overnight at 16 °C. Cells were collected by centrifugation, resuspended in a buffer containing 20 mM Tris-HCl pH 7.5, 200 mM NaCl, 10 mM imidazole, 5% glycerol, 2 mM -mercaptoethanol (BME), protease inhibitor cocktail tablet (Roche) and lysed by passing through a cell disruptor (20 kpsi / 1 pass). Cleared cell lysate was loaded onto a 5 mL HisTrap HP nickel affinity column (GE Healthcare Biosciences) and bound protein was eluted with a linear gradient of 0–1 M imidazole. Fractions containing the target protein, as assessed by SDS gel electrophoresis, were pooled and desalted to remove imidazole. Removal of N-terminal 6xHis tag was performed by overnight incubation at 4 °C of the sample with human thrombin (Abcam) at 5 NIH units/mL of the pooled sample followed by a second nickel affinity purification step to remove any remaining tagged fraction. The protein was then dialyzed against ion exchange buffer (20 mM Tris-HCl pH 7.5, 100 mM NaCl, 5% glycerol, 2 mM BME), loaded onto a HiTrap Q HP column (GE Healthcare Biosciences) and eluted with a linear gradient of 0–1 M NaCl. A final size exclusion chromatography step was performed on the collected sample using a Superdex 200 increase 10/300 GL column (GE Healthcare Biosciences) pre-equilibrated with 20 mM Tris-HCl pH 7.5, 50 mM NaCl, 5% glycerol, 2 mM BME after which the protein was concentrated using Amicon Ultra concentrators (Millipore) to 7 mg/mL and stored at −80 °C prior to use. For crystallization trials NaCl was removed from the buffer while keeping other components intact.

5.6.2.   hPDE4B regulatory domain (UCR2+catalytic domain).

hPDE4B regulatory domain expression and purification was performed according to the method described.[27] Recombinant baculovirus generation, insect cell (Sf21) culture and infection were carried out following manufacturer's instructions (Bac-to-Bac expression system; Invitrogen, Life technologies). Infected cells were grown for 48 h at 28 °C and harvested by centrifugation at 500 *g* for 15 min. Lysis was performed by resuspending the cells in a hypotonic buffer of 10 mM HEPES pH 7.5, 50 mM NaCl, 1 mM Tris(2-carboxyethyl) phosphine (TCEP) followed by centrifugation to remove cell debris. The obtained cleared lysate was loaded onto a 5 mL HisTrap HP nickel affinity column (GE Healthcare Biosciences) pre-equilibrated with 100 mM HEPES 7.5, 150 mM NaCl, 50 mM arginine, 10 mM imidazole, 1 mM TCEP and eluted with a linear gradient of 0–1 M imidazole. Eluted protein was then dialyzed against ion-exchange buffer (100 mM HEPES, 50 mM NaCl, 1 mM dithiothreitol (DTT)) and loaded onto a HiTrap Q HP ion exchange column (GE Healthcare Biosciences). A linear gradient elution of 20–250 mM NaCl was performed followed by dialysis of the collected sample into size exclusion buffer (10 mM HEPES 7.5, 100 mM NaCl, 1 mM DTT). Protein was then passed through a Superdex 200 increase 10/300 GL size exclusion column (GE Healthcare Biosciences). The collected sample was concentrated to 10 mg/mL and stored at −80 °C prior to use in crystallization.

5.6.3.   hPDE4D2 catalytic domain.

BL21 (DE3) Codon Plus cells were transformed with pET15b-hPDE4D_CD and allowed to grow in 1 L 2xYT medium at 37 °C until the optical density at 600 nm reached 0.6–0.8. At this stage culture temperature was lowered down and expression was induced by addition of 0.5 mM IPTG followed by further overnight growth at 22 °C. The same cell disruption and protein purification procedures were followed as performed in the case of TbrPDEB1 catalytic domain protein with the following changes in the buffers used: cell resuspension and nickel affinity chromatography buffer (50 mM Tris-HCl pH 8, 150 mM NaCl, 5 mM BME, 20 mM imidazole), ion exchange chromatography buffer (50 mM Tris-HCl pH 8, 50 mM NaCl, 5 mM DTT) and size exclusion chromatography buffer (50 mM Bis-tris pH 6.8, 100 mM NaCl, 5 mM DTT). Purified protein was concentrated to 9 mg/mL and stored at −80 °C prior to use in crystallization.

5.7. Protein crystallization, ligand soaking and data collection.

All crystallization trials were performed by vapor diffusion hanging drop technique, typically with 500 μL reservoir volume and 2 μL droplets with a protein to crystallization solution ratio of 1:1. Crystals of the TbrPDEB1 catalytic domain were grown in 20% PEG 3350, 400 mM sodium formate, 300 mM guanidine and 100 mM MES, pH 6.5 at 4 °C. Soaking of these crystals with various compounds was performed maintaining a final compound concentration of 5–15 mM and for varying duration of overnight to 48 h. Soaked crystals were then briefly dipped in growth solution supplemented with 20% (*v/v*) glycerol or ethylene glycol and were mounted using CryoLoop (Hampton Research) or LithoLoops (Molecular Dimensions) and vitrified in liquid nitrogen for data collection. In case of hPDE4D2, thick plate-like crystals appeared within 5–6 days in a condition containing 24% PEG 3350, 30% ethylene glycol and 100 mM HEPES, pH 7.5 at 19 °C. For hPDE4B, a condition containing 20% PEG 400, 50 mM calcium acetate, and 100 mM sodium acetate, pH 4.6 resulted in well-diffracting crystals. Compound soaking and crystal harvesting were performed in the same way as for TbrPDEB1 crystals except that in case of hPDE4D2 no cryo-preservative was added prior to vitrification. X-ray diffraction data sets were collected at Diamond Light Source (DLS; Didcot, Oxfordshire, UK) beamlines I03 and I04 at 100 K. The data sets were processed by xia2[28] or autoPROC,[29] which incorporates XDS[30] and AIMLESS,[31] or were integrated using iMOSFLM[32] and reduced using POINTLESS, SCALA and TRUNCATE,[33] all of which are part of CCP4.[34]

5.8. X-ray crystal structure determination, refinement and analysis.

The crystal structure of TbrPDEB1 bound to NPD-008 (**8**) was solved by molecular replacement (MR) using PHASER,[35] taking the apo structure (PDB code 4I15) as search model. Reflections for calculating R_{free} were selected randomly and the same set was used in all other ligand-bound TbrPDEB1 data sets except for NPD-038 (**25**) where the crystal was non-isomorphous. All isomorphous crystal forms were solved by Fourier synthesis using the partially refined, ligand-free **8** model, whereas MR was applied for the **25** data set. hPDE4B and hPDE4D2 structures with NPD-001 (**1**) were solved by MR using their respective apo models (PDB codes 3G45 and 3SL3, respectively). Ligand descriptions were generated by ACEDRG available within the CCP4 package[34] or with the Grade Web Server (http://grade.globalphasing.org/). Adjustment of the models and ligand fitting were performed with COOT[36] and refinement with REFMAC5.[37] The final structures had good geometry and could be refined to low *R*-factors (Tables S1 and S3). All refined models were validated with MOLPROBITY.[38] Root-mean-square (r.m.s.) deviation values were calculated from a sequence alignment, structural superposition and refinement cycle on Cα carbons with the align function as implemented in PyMOL 1.7.4.4 (The PyMOL Molecular Graphics System, Schrödinger, LLC). All binding site residues have been named according to the PDEStrIAn nomenclature system (http://pdestrian.vu-compmedchem.nl/).[19] Structural figures were prepared with PyMOL 1.7.4.4. For clarity, selected residues from the helix capping the substrate binding pocket (i.e., D784, M785, A786, K787, H788, G789, S790, A791, L792, E793 in TbrPDEB1; D518, M519, S520, K521, H522, M523, S524, L525 in hPDE4B; D272, M273, S274, K275, H276, M277, N278, L279 in hPDE4D) have been omitted in the rendering of the figures. Coordinates of the structures have been deposited to the RCSB Protein Data Bank with following accession codes: 5G57 (TbrPDEB1–NPD-001); 5LAQ (hPDE4B–NPD-001); 5LBO (hPDE4D–NPD-001); 5L9H (TbrPDEB1–NPD-340); 5G2B (TbrPDEB1–NPD-008); 5L8C (TbrPDEB1–NPD-039); 5G5V (TbrPDEB1–NPD-038); 5L8Y (TbrPDEB1–NPD-937).

5.9. Parasite culturing for cAMP measurements and microscopy.

Bloodstream forms of *T. b. brucei* Lister 427 were cultured in Hirumi-9 (HMI-9) medium (Invitrogen), supplemented with 10% Heat Inactivated Fetal Bovine Serum (FBS; Gibco) in vented culture flasks (Corning), at 37 °C, in a 5% CO_2 atmosphere, as described previously.[45]

2

5.9.1. Intracellular cAMP measurements.

Intracellular cAMP was measured as described previously,[11] with minor changes. Briefly, log-phase bloodstream form trypanosomes were inoculated into HMI-9/FBS media and incubated at 37 °C overnight. The cells were counted and suspended in HMI-9/FBS at 2×10^6 cells/mL, which was divided into 8 subcultures of 6 mL each. To each culture flask a small volume of HMI-9 medium, containing either NPD-001 (**1**) (positive control; final concentration 0.3 μM), pentamidine (a known trypanocide not acting on cAMP signaling; final concentration 0.025 μM), NPD-008 (**8**) (at 0.1, 0.33, 1, 3.3, and 10 μM), or no drug (negative control) was added. The cultures were incubated under standard conditions (37 °C, 5% CO_2) for 5 h, after which cell densities were determined in each culture using a haemocytometer, 5×10^6 cells were transferred into new tubes and collected by centrifugation at 1,500 *g* for 10 min at 4 °C. Cell pellets were resuspended in 100 μL of 0.1 M HCl and left on ice for 20 min to complete cell lysis. The samples were centrifuged in a microfuge at 12,000 *g* for 10 min at 4 °C, and the supernatants (cell extracts) were stored at −80 °C for the determination of intracellular cAMP. Each cAMP determination was performed in duplicate, data are represented as the mean of four independent cAMP determinations ± s.e.m., and were analyzed with Student's *t*-test, differences were considered significant at *P* < 0.05, with *P* values as indicated.

5.10. Microscopy and DAPI staining.

For the monitoring of the cell cycle (division of nucleus, kinetoplast and cells) and cellular morphology, trypanosomes were stained with 4',6-diamidino-2-phenylindole (DAPI) and observed by fluorescence microscopy as described.[46] Briefly, a culture of *T. b. brucei* bloodstream forms was inoculated at 2×10^5 cell/mL, in the presence of 10 μM NPD-008 (**8**). Samples for microscopy were taken at 0, 6, 12 and 24 h. Cells were fixed in 2% formaldehyde for 15 min, washed with phosphate-buffered saline (PBS) pH 7.4, re-suspended in 20 μL PBS and spread on a microscope slide. These were left to air-dry after which the samples were mounted in VectaShield (Vector Laboratories Inc., USA) mounting medium with DAPI. Samples were imaged on an Axioskop II microscope (Zeiss, Inc) and a DeltaVision Core (AppliedPrecision).

5.11. Phenotypic cellular assays.

For the cellular assays, the following reference drugs were used as positive controls: suramin (Sigma-Aldrich, Germany) for *T. brucei* (pIC_{50} = 7.4 ± 0.2, *n* = 5), and tamoxifen (Sigma-Aldrich, Germany) for MRC-5 cells (pIC_{50} = 5.0 ± 0.1, *n* = 5). All compounds were tested at five concentrations (64, 16, 4, 1 and 0.25 μM) to establish a full dose-titration and determination of the IC_{50} and CC_{50}, data are represented as the mean of triplicate experiments ± s.e.m. The final concentration of DMSO did not exceed 0.5% in the assays.

5.12. Antitrypanosomal cellular assay. T. brucei

Squib-427 strain (suramin-sensitive) was cultured at 37 °C and 5% CO_2 in HMI-9 medium, supplemented with 10% fetal calf serum (FCS). About 1.5×10^4 trypomastigotes were added to each well and parasite growth was assessed after 72 h at 37 °C by adding resazurin. The color reaction was read at 540 nm after 4 h, and absorbance values were expressed as a percentage of the blank controls.

5.13. MRC-5 cytotoxicity cellular assay.

MRC-5 SV2 cells, originally from a human diploid lung cell line, were cultivated in MEM, supplemented with L-glutamine (20 mM), 16.5 mM sodium hydrogen carbonate and 5% FCS. For the assay, 10^4 MRC-5 cells/well were seeded onto the test plates containing the pre-diluted sample and incubated at 37 °C and 5% CO_2 for 72 h. Cell viability was assessed fluorimetrically 4 h after the of addition of resazurin.

Fluorescence was measured (excitation 550 nm, emission 590 nm) and the results were expressed as percentage reduction in cell viability compared to control.

5.14.   Statistical analysis.

Details of the applied statistical analyses are provided with each experiment. No statistical methods were used to predetermine the size of samples. The experiments were not randomized and the investigators were not blinded to allocation during experiments and/or outcome assessment.

5.15.   Author contributions

E.d.H., A.R.B., E.E., K.M.O., J.V., T.v.d.B., H.C., M.S., G.J.S. and I.J.P.d.E. were involved in compound design, synthesis and analysis. A.K.S., E.B. and D.G.B. were involved in protein production, crystallization, data collection and refinement for structural studies. A.R.B., A.K.S., C.J., E.B. and D.G.B. were involved in crystal structure analysis. H.T. was involved in the PDE activity assays. D.N.A.T., J.C.M. and H.P.d.K. were involved in the intracellular cAMP assays and microscopy experiments. A.M. and L.M. were involved in the phenotypic cellular assays. E.E., K.M.O., M.W., M.S., C.d.G., L.M., H.P.d.K., G.J.S., I.J.P.d.E., D.G.B. and R.L. supervised the experiments and conceived the project. E.d.H rewrote the manuscript that was written by A.R.B. and A.K.S.

6.   References

1. M.P. Barrett, The elimination of human African trypanosomiasis is in sight: Report from the third WHO stakeholders meeting on elimination of gambiense human African trypanosomiasis, PLoS Negl Trop Dis, 12 (2018) e0006925.

2. G. Bilbe, Infectious diseases. Overcoming neglect of kinetoplastid diseases, Science, 348 (2015) 974-976.

3. S. Kunz, T. Kloeckner, L.-O. Essen*, et al.*, TbPDE1, a novel class   I phosphodiesterase of Trypanosoma brucei, European Journal of Biochemistry, 271 (2004) 637-647.

4. M. Oberholzer, G. Marti, M. Baresic*, et al.*, The Trypanosoma brucei cAMP phosphodiesterases TbrPDEB1 and TbrPDEB2: flagellar enzymes that are essential for parasite virulence, The FASEB Journal, 21 (2007) 720-731.

5. Y. Shakur, H.P. de Koning, H. Ke*, et al.*, Therapeutic Potential of Phosphodiesterase Inhibitors in Parasitic Diseases, in: S.H. Francis, M. Conti, M.D. Houslay (Eds.) Phosphodiesterases as Drug Targets, Springer Berlin Heidelberg, Berlin, Heidelberg, 2011, pp. 487-510.

6. R. Zoraghi, T. Seebeck, The cAMP-specific phosphodiesterase TbPDE2C is an essential enzyme in bloodstream form Trypanosoma brucei, Proceedings of the National Academy of Sciences, 99 (2002) 4343-4348.

7. T. Seebeck, G.J. Sterk, H. Ke, Phosphodiesterase inhibitors as a new generation of antiprotozoan drugs: exploiting the benefit of enzymes that are highly conserved between host and parasite, Future Medicinal Chemistry, 3 (2011) 1289-1306.

8. N.D. Bland, C. Wang, C. Tallman*, et al.*, Pharmacological validation of Trypanosoma brucei phosphodiesterases B1 and B2 as druggable targets for African sleeping sickness, J Med Chem, 54 (2011) 8188-8194.

9. H.P. de Koning, M.K. Gould, G.J. Sterk*, et al.*, Pharmacological validation of Trypanosoma brucei phosphodiesterases as novel drug targets, Journal of Infectious Diseases, 206 (2012) 229-237.

10. J. Veerman, T. van den Bergh, K.M. Orrling*, et al.*, Synthesis and evaluation of analogs of the phenylpyridazinone NPD-001 as potent trypanosomal TbrPDEB1 phosphodiesterase inhibitors and in vitro trypanocidals, Bioorganic & Medicinal Chemistry, 24 (2016) 1573-1581.

11. H.P. de Koning, M.K. Gould, G.J. Sterk*, et al.*, Pharmacological validation of *Trypanosoma brucei* phosphodiesterases as novel drug targets, J. Infect. Dis., 206 (2012) 229-237.

12. N.D. Bland, C. Wang, C. Tallman*, et al.*, Pharmacological validation of *Trypanosoma brucei* phosphodiesterases B1 and B2 as druggable targets for African sleeping sickness, J. Med. Chem., 54 (2011) 8188-8194.

13. K.M. Orrling, C. Jansen, X.L. Vu*, et al.*, Catechol pyrazolinones as trypanocidals: fragment-based design, synthesis, and pharmacological evaluation of nanomolar inhibitors of trypanosomal phosphodiesterase B1, J. Med. Chem., 55 (2012) 8745-8756.

14. A.R. Blaazer, A.K. Singh, E. de Heuvel*, et al.*, Targeting a subpocket in Trypanosoma brucei phosphodiesterase B1 (TbrPDEB1) enables the structure-based discovery of selective inhibitors with trypanocidal activity, Journal of Medicinal Chemistry, 61 (2018) 3870-3888.

15. C. Jansen, H. Wang, A.J. Kooistra*, et al.*, Discovery of NovelTrypanosoma bruceiPhosphodiesterase B1 Inhibitors by Virtual Screening against the Unliganded TbrPDEB1 Crystal Structure, Journal of Medicinal Chemistry, 56 (2013) 2087-2096.

16. C. Jansen, A.J. Kooistra, G.K. Kanev*, et al.*, PDEStrIAn: A Phosphodiesterase Structure and Ligand Interaction Annotated Database As a Tool for Structure-Based Drug Design, Journal of Medicinal Chemistry, 59 (2016) 7029-7065.

17. H. Wang, Z. Yan, J. Geng*, et al.*, Crystal structure of the Leishmania major phosphodiesterase LmjPDEB1 and insight into the design of the parasite-selective inhibitors, Mol Microbiol, 66 (2007) 1029-1038.

18. K.M. Orrling, C. Jansen, X.L. Vu*, et al.*, Catechol pyrazolinones as trypanocidals: fragment-based design, synthesis, and pharmacological evaluation of nanomolar inhibitors of trypanosomal phosphodiesterase B1, Journal of Medicinal Chemistry, 55 (2012) 8745-8756.

19. C. Jansen, A.J. Kooistra, G.K. Kanev*, et al.*, PDEStrIAn: a phosphodiesterase structure and ligand interaction annotated database as a tool for structure-based drug design, J. Med. Chem., 59 (2016) 7029-7065.

20. M.K. Gould, S. Bachmaier, J.A.M. Ali*, et al.*, Cyclic AMP Effectors in African Trypanosomes Revealed by Genome-Scale RNA Interference Library Screening for Resistance to the Phosphodiesterase Inhibitor CpdA, Antimicrobial Agents and Chemotherapy, 57 (2013) 4882-4893.

21. S. Nwaka, A. Hudson, Innovative lead discovery strategies for tropical diseases, Nat Rev Drug Discov, 5 (2006) 941-955.

22. A. Hatzelmann, D. Marx, W. Steinhilber*, et al.*, (Altana Pharma AG). Novel Phthalazinones. WO 2002085906, 2002.

23. A. Hatzelmann, H. Boss, D. Häfner*, et al.*, (Byk Gulden Lomberg Chemische Fabrik GmbH). Phthalazinone PDE III/IV Inhibitors. WO 199947505, 1999.

24. M. van der Mey, A. Hatzelmann, G.P. Van Klink*, et al.*, Novel selective PDE4 inhibitors. 2. Synthesis and structure-activity relationships of 4-aryl-substituted *cis*-tetra- and *cis*-hexahydrophthalazinones, J. Med. Chem., 44 (2001) 2523-2535.

25. J. Veerman, T. van den Bergh, K.M. Orrling*, et al.*, Synthesis and evaluation of analogs of the phenylpyridazinone NPD-001 as potent trypanosomal TbrPDEB1 phosphodiesterase inhibitors and in vitro trypanocidals, Bioorg. Med. Chem., 24 (2016) 1573-1581.

26. S. Saubern, R. Guha, J.B. Baell, KNIME workflow to assess PAINS filters in SMARTS format. Comparison of RDKit and Indigo cheminformatics libraries, Mol. Inform., 30 (2011) 847-850.

27. A.B. Burgin, O.T. Magnusson, J. Singh*, et al.*, Design of phosphodiesterase 4D (PDE4D) allosteric modulators for enhancing cognition with improved safety, Nat. Biotechnol., 28 (2010) 63-70.

28. G. Winter, C.M. Lobley, S.M. Prince, Decision making in xia2, Acta Crystallogr. D Biol. Crystallogr., 69 (2013) 1260-1273.

29. C. Vonrhein, C. Flensburg, P. Keller*, et al.*, Data processing and analysis with the autoPROC toolbox, Acta Crystallogr. D Biol. Crystallogr., 67 (2011) 293-302.

30. W. Kabsch, XDS, Acta Crystallogr. D Biol. Crystallogr., 66 (2010) 125-132.

31. P.R. Evans, G.N. Murshudov, How good are my data and what is the resolution?, Acta Crystallogr. D Biol. Crystallogr., 69 (2013) 1204-1214.

32. T.G. Battye, L. Kontogiannis, O. Johnson*, et al.*, iMOSFLM: a new graphical interface for diffraction-image processing with MOSFLM, Acta Crystallogr. D Biol. Crystallogr., 67 (2011) 271-281.

33. P.R. Evans, An introduction to data reduction: space-group determination, scaling and intensity statistics, Acta Crystallogr. D Biol. Crystallogr., 67 (2011) 282-292.

34. M.D. Winn, C.C. Ballard, K.D. Cowtan*, et al.*, Overview of the CCP4 suite and current developments, Acta Crystallogr. D Biol. Crystallogr., 67 (2011) 235-242.

35. A.J. McCoy, R.W. Grosse-Kunstleve, P.D. Adams*, et al.*, Phaser crystallographic software, J. Appl. Crystallogr., 40 (2007) 658-674.

36. P. Emsley, B. Lohkamp, W.G. Scott*, et al.*, Features and development of Coot, Acta Crystallogr. D Biol. Crystallogr., 66 (2010) 486-501.

37. G.N. Murshudov, P. Skubak, A.A. Lebedev*, et al.*, REFMAC5 for the refinement of macromolecular crystal structures, Acta Crystallogr. D Biol. Crystallogr., 67 (2011) 355-367.

38. V.B. Chen, W.B. Arendall, 3rd, J.J. Headd*, et al.*, MolProbity: all-atom structure validation for macromolecular crystallography, Acta Crystallogr. D Biol. Crystallogr., 66 (2010) 12-21.

39. S. Pronk, S. Pall, R. Schulz*, et al.*, GROMACS 4.5: a high-throughput and highly parallel open source molecular simulation toolkit, Bioinformatics, 29 (2013) 845-854.

40. M.J. Abraham, T. Murtola, R. Schulz*, et al.*, GROMACS: high performance molecular simulations through multi-level parallelism from laptops to supercomputers, SoftwareX, 1–2 (2015) 19-25.

41. K. Lindorff-Larsen, S. Piana, K. Palmo*, et al.*, Improved side-chain torsion potentials for the Amber ff99SB protein force field, Proteins, 78 (2010) 1950-1958.

42. W.L. Jorgensen, J. Chandrasekhar, J.D. Madura*, et al.*, Comparison of simple potential functions for simulating liquid water, J. Chem. Phys., 79 (1983) 926-935.

43. A.W. Sousa da Silva, W.F. Vranken, ACPYPE - AnteChamber PYthon Parser interfacE, BMC Res. Notes, 5 (2012) 367.

44. B. Hess, P-LINCS: a parallel linear constraint solver for molecular simulation, J. Chem. Theory Comput., 4 (2008) 116-122.

45. A.A. Alkhaldi, D.J. Creek, H. Ibrahim*, et al.*, Potent trypanocidal curcumin analogs bearing a monoenone linker motif act on *Trypanosoma brucei* by forming an adduct with trypanothione, Mol. Pharmacol., 87 (2015) 451-464.

46. A.A. Alkhaldi, J. Martinek, B. Panicucci*, et al.*, Trypanocidal action of bisphosphonium salts through a mitochondrial target in bloodstream form *Trypanosoma brucei*, Int. J. Parasitol. Drugs Drug Resist., 6 (2016) 23-34.

2
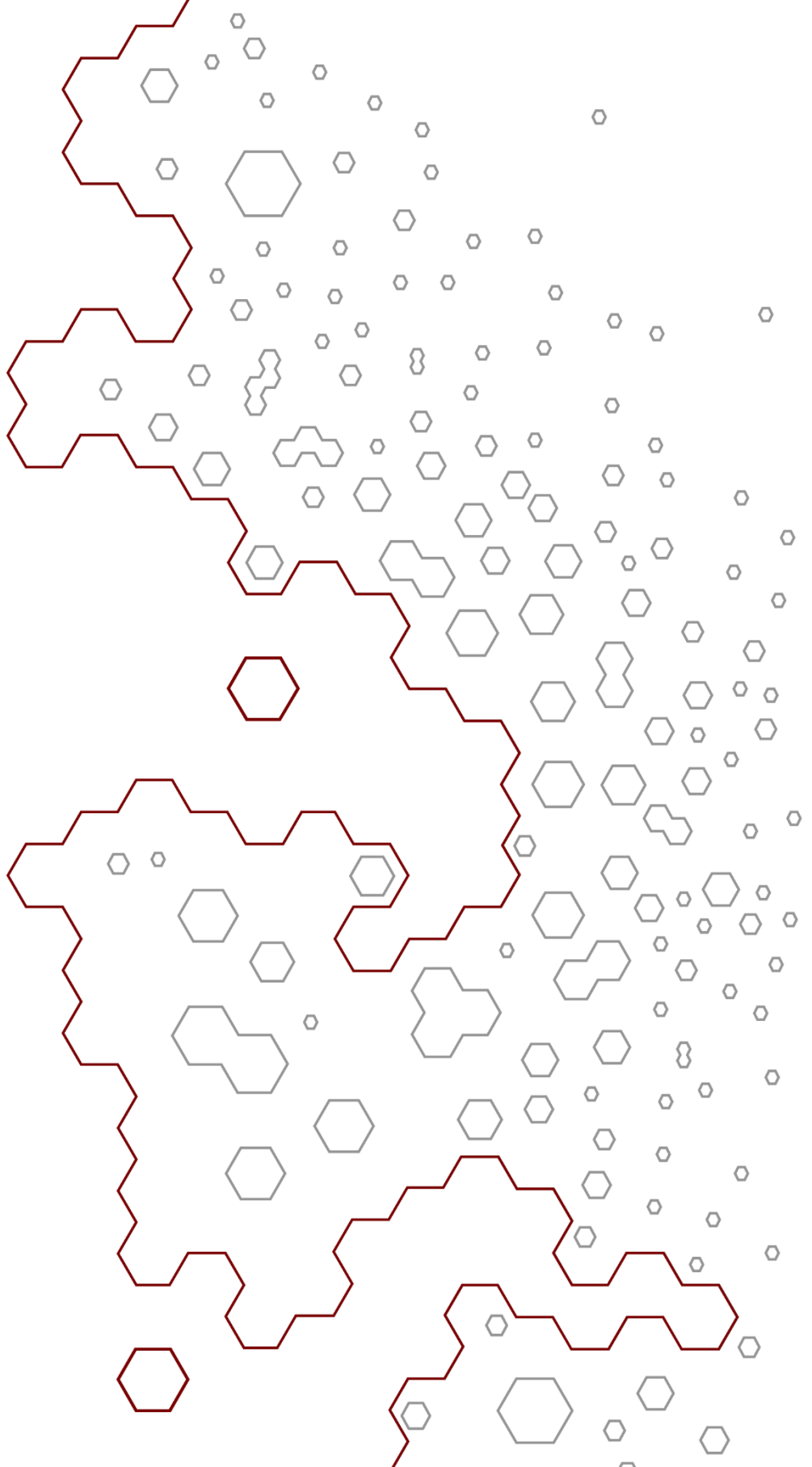
Chapter 3

Discovery of diaryl ether substituted tetrahydrophthalazinones as TbrPDEB1 inhibitors following structure-based virtual screening

Erik de Heuvel, Albert J. Kooistra, Ewald Edink, Sjors van Klaveren, Jeffrey Stuijt, Lindsey Burggraaff, Tiffany van der meer, Payman Sadek, Dorien Mabille, Guy Caljon, Louis Maes, Marco Siderius, Iwan J.P. de Esch, Geert Jan Sterk, Rob Leurs.

Abstract

Several members of the 3',5'-cyclic nucleotide phosphodiesterase (PDE) family play an essential role in cellular processes, which has labelled them as interesting targets for various diseases. The parasitic protozoan *Trypanosoma brucei*, causative agent of human African trypanosomiasis, contains several cyclic AMP specific PDEs from which TbrPDEB1 is validated as a drug target. The recent discovery of selective TbrPDEB1 inhibitors has increased their potential for a novel treatment for this disease. Compounds characterized by a rigid biphenyl tetrahydrophthalazinone core structure were used as starting point for the exploration of novel TbrPDEB1 inhibitors. Using a virtual screening campaign and structure-guided design, diaryl ether substituted phthalazinones were identified as novel TbrPDEB1 inhibitors with IC$_{50}$ values around 1 µM against *Trypanosoma brucei*. This study provides important structure-activity relationship (SAR) information for the future design of effective parasite-specific PDE inhibitors.

1. Introduction

Human African trypanosomiasis, also known as African sleeping sickness, is one of the neglected tropical diseases (NTDs) listed by the WHO and is caused by the protozoan *Trypanosoma brucei* (T.b.) *rhodesiense* and *T.b. gambiense*.[1] The majority of drugs that are currently on the market for HAT have been discovered over 30 years ago and have several major disadvantages including severe toxicity, subspecies selectivity, complex administration protocols and limited clinical efficacy.[2-4] The first oral drug fexinidazole has recently been approved for HAT and will significantly improve the status of the disease.[5] This new therapy benefits greatly from the ease of administration, but still has some drawbacks including potential relapse and a lower efficacy for late-stage patients compared to the commonly used NECT treatment.[6, 7] In addition, the reported increasing drug resistance could have a detrimental effect on the already limited arsenal of antiprotozoal drugs.[8, 9] The number of reported cases is slowly decreasing as result of active screening in endemic regions, still an estimated 65 million people are at risk of infection.[10] HAT has a history that is characterized by reoccurring epidemics and new control strategies and safer drugs are therefore still a necessity to eradicate this fatal disease.[1, 3, 11]

The family of 3',5'-cyclic nucleotide phosphodiesterases (PDEs) are involved in various essential regulatory processes in many different organisms making them interesting drug targets. The human 3',5'-cyclic nucleotide phosphodiesterases (hPDE) have been extensively studied as drug targets for a broad range of diseases, including COPD, heart failure and erectile dysfunction.[12-15] The *T. brucei* 3',5'-cyclic nucleotide phosphodiesterases B1 (TbrPDEB1) and TbrPDEB2 have previously been identified as potential new targets for the treatment of HAT as, in contrast to the other TbrPDE enzymes, they are essential for parasite virulence.[16] Simultaneous reduction in expression of TbrPDEB1 and TbrPDEB2 with siRNA resulted in distortions of the cell cycle and eventually cell death.[16, 17] The potential of TbrPDEB1 and TbrPDEB2 as drug targets against HAT was further demonstrated *in vivo* as siRNA-mediated gene silencing in mice prevented parasitemia and finally resulted in animal survival after parasite infection.[16] Simultaneous inhibition of both isoforms by small molecule inhibitors is conceived possible because of high structural similarity between both paralogues (88% structural identity of the

catalytic domain), resulting in equipotency as reported for NPD-001 (pIC$_{50}$ TbrPDEB1: 8.4; pIC$_{50}$ TBrPDEB2: 8.5).[18-20]

Obtaining selectivity for TbrPDEB1/2 over the human homologue hPDE4 is one of the challenges faced by using TbrPDEB1/2 as drug targets. The structural similarity between hPDE4 and TbrPDEB1 makes hPDE4 drug repurposing interesting as strategy, but strong hPDE4 inhibitory activity results in undesired side effects (e.g. emesis, headache and immune suppression).[21-23] Recently, a first series of molecules with selectivity for TbrPDEB1 over hPDE4 was reported by repurposing a tetrahydrophthalazinone scaffold that was originally developed as hPDE4 inhibitor.[24-26] Potency and selectivity over hPDE4 was obtained by addressing a parasite-specific pocket (P-pocket) in the substrate-binding site of TbrPDEB1 with a rigid biphenyl glycinamide installed on the tetrahydrophthalazinone (NPD-039, shown in Figure 1).[22, 24] NPD-039 (**1**) displays high nanomolar potency for TbrPDEB1 (pK$_i$ = 7.0) with more than 10-fold selectivity over hPDE4 (pK$_i$ = 5.7) with the glycinamide tail occupying the P-pocket in the crystal structure of **1** in the catalytic domain of TbrPDEB1.[24] Unfortunately, **1** shows a reduced efficacy against *T. brucei in vitro* (pIC$_{50}$ = 5.2) and its development as trypanocidal was therefore halted.[24]

In the present study, we describe one of our efforts to improve on **1** by introducing flexibility into the vector that directs to the P-pocket using a diaryl ether function. Two different design strategies were applied in parallel. Firstly, computer-aided drug design using the structure of NPD-039 co-crystalized in TbrPDEB1 (Figure 1, PDB: 5L8C) and commercially available heteroaromatic moieties (hAr, **2**) provided a selection of virtual hits for synthesis to explore accessibility of various aromatic structures in the active site of TbrPDEB1. Secondly, the pyrimidyl group in **3** was decorated with a selection of amide functionalities based on observations in previously reported studies to explore the directionality towards the P-pocket.[24, 27] Both compound classes were synthesized and tested to explore the interaction with TbrPDEB1, hPDE4 and their *in vitro* efficacy against *T. brucei*.
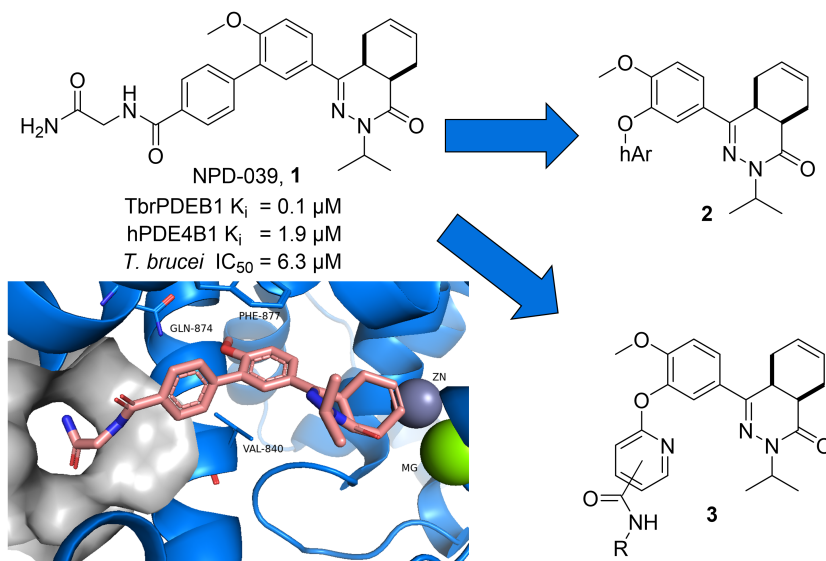
3

Figure 1: Design ideas based on reported biphenyl phthalazinone NPD-039 (**1**) based on virtual screening using the co-crystal structure of **1** (PDB: 5L8C) and heteroaryl chlorides (**2**) and structure-guided design (**3**)

2.   Results and discussion

2.1.   Virtual screening

The compound dataset for the virtual screening was based on commercially available heteroaryl chlorides which were combined with the core phenyltetrahydrophthalazinone scaffold using MOE Combinatorial Library module (Figure 2). Reaxys was used to search for commercially available building blocks to use in a straightforward nucleophilic aromatic substitution reaction with a phenol tetrahydrophthalazinone. The Reaxys search was focused on commercially available (via E-molecules) heteroaromatic chlorides with a molecular weight <228 Da to design a library of compounds with a maximum molecular weight of 500 Da. The combinatorial library consisted of almost 5000 compounds which were docked in the crystal structure of NPD-039 (**1**, PDB: 5L8C) using two different methods. Firstly, all compounds were docked using PLANTS and scored based on the similarity of the interaction fingerprint (IFP) compared with NPD-039. A high IFP similarity with NPD-039 suggests a similar binding mode and a higher probability of having similar affinity. All compounds were also scored using the overall docking score.

Using a combination of scoring criteria (an IFP similarity >0.78 and a docking score <-70) resulted in 114 selected compounds. In a second virtual screening approach, all computational library compounds were compared to the binding pose of NPD-039 in TbrPDEB1 using ROCS. The best scoring pose per compound was rescored in the crystal structure of TbrPDEB1 using PLANTS and the compounds with a docking score <-90 were selected, resulting in 105 compounds.
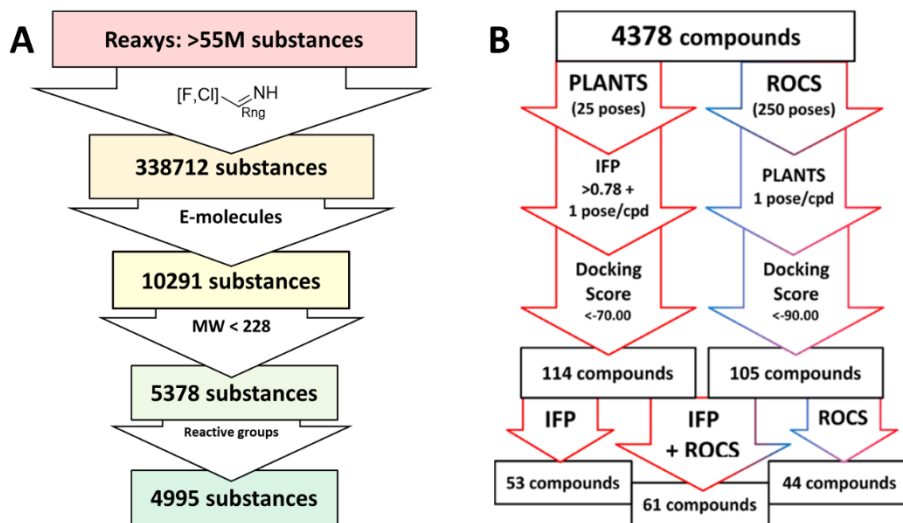
Figure 2: Schematic overview of the virtual screening. (A) Extraction of commercially available heteroaromatic chlorides and fluorides from Reaxys. Every arrow indicates a filter step based on substructure, commercial availability, molecular weight and a preliminary filter on reactive functionalities. (B) Schematic overview of the docking process based on PLANTS/IFP protocol or ROCS/PLANTS protocol of all compounds obtained from the Reaxys search.

Combining the hit sets from both virtual screening strategies (ROCS and PLANTS) resulted in 158 unique compounds that were visually inspected for their synthetic feasibility and binding mode in the crystal structure, resulting in a selection of 45 compounds. The compounds were divided into four clusters: 5-membered ring structures, 6-membered ring structures and fused 5- and 6-membered ring structures (5-ring linked or 6-ring linked). Several representatives from every cluster were selected for synthesis to assure the presence of every ring size in the final set of compounds (Figure 3).

Figure 3: Structures of the selected hits from the virtual screening

For some of the hits, reagents turned out to be more difficult to obtain or expensive; in those cases a more readily available building block to represent the same cluster was used. However, the replacement often resulted in the selection of simplified and rigid b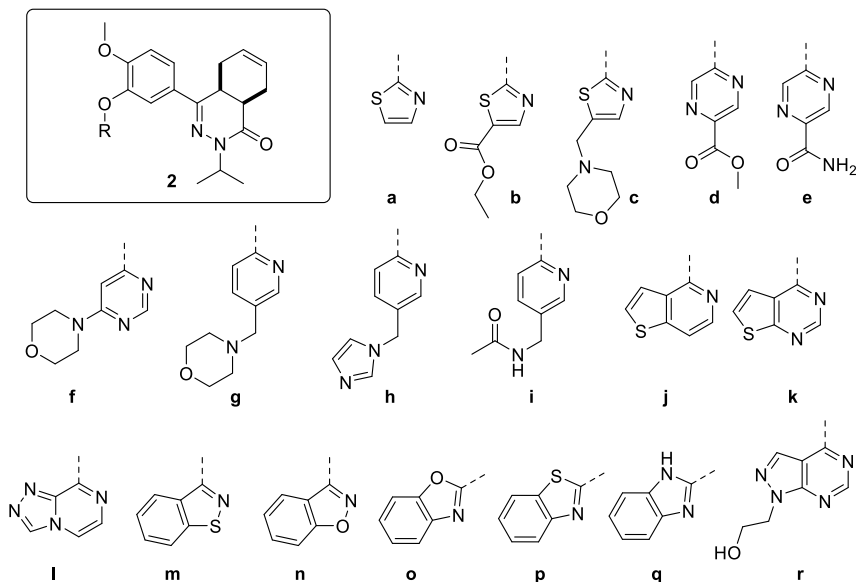uilding blocks that lack flexible substituents that can penetrate the P-pocket as observed for **1** (Figure 1). It was hypothesized that favorable binding to TbrPDEB1 could be obtained by introducing rigid aromatic systems, as previously observed for the biphenyl series.[24] The docking pose of these more rigid compounds (**2a**, **2j-q**, and to lesser extent conjugated esters **2b**, **2d** and amide **2e**) showed good directionality towards the P-pocket, as illustrated by the docking pose of **2d** (Figure 4A), but did not address or interact with residues in the P-pocket. Nevertheless, the docking pose of these compounds provide essential information for possible future modifications sites. The docked hits containing a flexible substituent (**2c**, **2f-i**, **2q**) showed good occupation of the P-pocket, as illustrated by the docking pose of **2h** (Figure 4B). The introduction of the ether bond between the aromatic functionalities causes a slight rotation of the anisole in the core scaffold. In most cases the ether bond is rotated towards the phenylalanine of the hydrophobic clamp, while for several of the larger fused 5- and 6-membered rings (**2j**, **2l**, **2m** and **2n**) the ether linker is rotated towards the valine (Figure 4C). Although the spatial filling of the linker is divergent from the phenyl linker of **1**

(Figure 4D) the occupancy of substituents is similar to the of the glycinamide tail of **1**. A detailed overview of the individual docking poses of **2a-r** can be found in the supporting information.
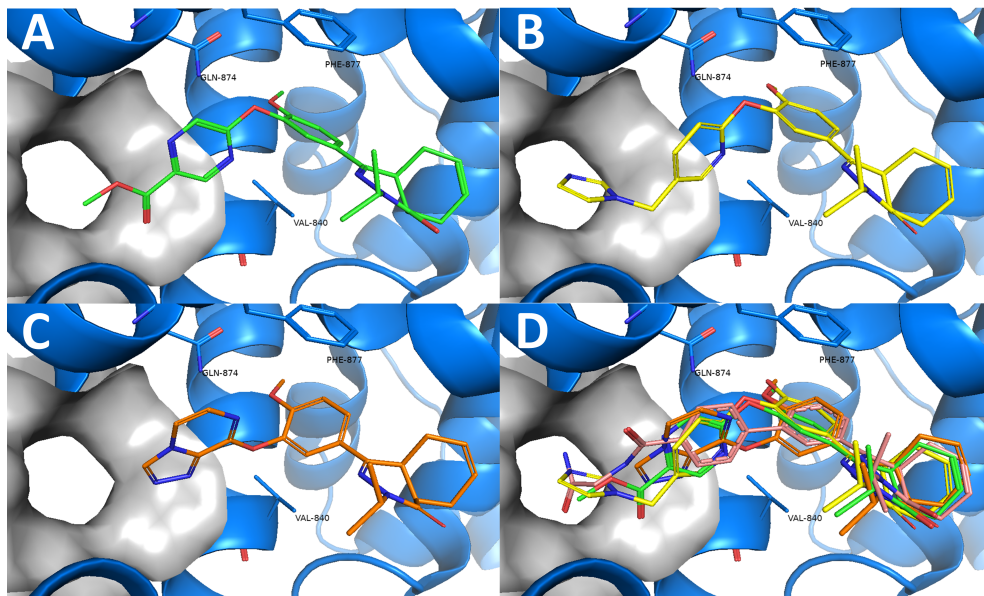
Figure 4: Examples of docked structures in the co-crystal structure of **1** in TbrPDEB1 (PDB: 5L8C). The P-pocket is indicated by the grey surface. A) The docking pose of pyrazine **2d** (green). B) The docking pose of **2h** (yellow). C) The docking pose of **2l** (orange). D) Overlay of the different docking poses of **2d**, **2h** and **2l** with reference compound **1** (salmon).

2.2. Chemistry

The synthesis of the compounds started with mesylation of guaiacol using mesyl chloride (Scheme 1). Mesylate **4** was used in a Friedel-Crafts acylation with maleic anhydride to obtain carboxylic acid **5**. Full isomerization towards the *E*-isomer was observed during the reaction. The *trans*-cyclohexene moiety of carboxylic acid **6** was installed using a Diels-Alder reaction with 1,3-butadiene, which was then used in a condensation reaction with isopropyl hydrazine to obtain tetrahydrophthalazinone **7**. The mesylate group was partially removed during the condensation reaction due to the basic conditions and a mixture of products was obtained. The mesylate group was completely removed by subjecting the mixture to a solution of NaOH in MeOH/THF. As shown for similar phenyl tetrahydrophthalazinones, *trans*-cyclohexene isomerizes to the *cis*-cyclohexene under basic conditions.[28] The *cis*-conformation was confirmed by a strong NOE-

coupling between the two bridgehead protons of tetrahydrophthalazinone **8**. The obtained phenol tetrahydrophthalazinone **8** was used as a building block for the synthesis of the various target compounds.
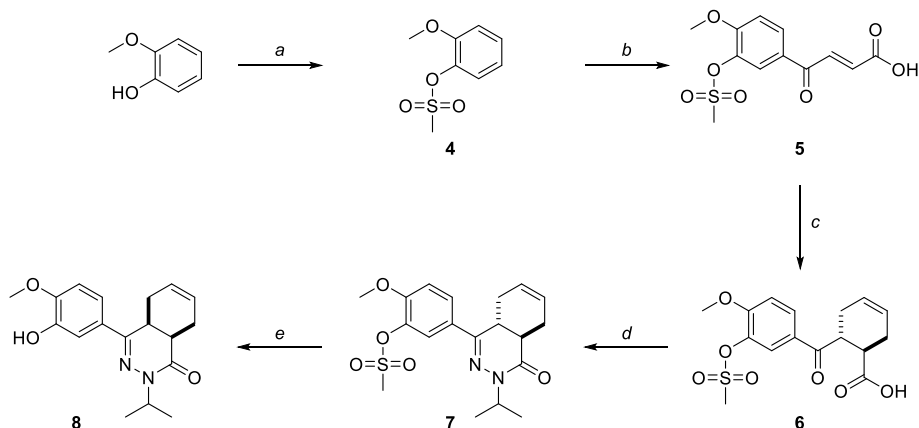
Scheme 1: *a*) Mesyl chloride, Et$_3$N, DCM, rt, 1 h, 78%; *b*) Maleic anhydride, AlCl$_3$, DCM, rt, 5 h, 40%; *c*) Buta-1,3-diene, THF, 140 °C, MW, 1.5 h, 92%; *d*) Isopropylhydrazine.HCl, Cs$_2$CO$_3$, EtOH, 100 °C, MW, 6 h, 75%; *e*) NaOH, H$_2$O, THF, MeOH, 50 °C, 2 h, 64%

The heteroaromatic ring systems were installed in the tetrahydrophthalazinone core structure using a nucleophilic aromatic substitution reaction at higher temperatures (Scheme 2). The reactivity of the various aromatic chlorides differed significantly, leading to varying reaction times and yields. Unfortunately, the synthesis of **2g**, **2i**, **2m-o**, **2q** was unsuccessful due to observed side reactions or instability of the starting material under the reaction conditions. The synthesis of 4- and 6-methyl ester functionalized chloropyridines did not provide the desired intermediates. Therefor the methyl ester was replaced by a nitrile (**3b** and **3d**) to provide a handle for further modifications. Both methyl esters (**3a** and **3c**) and nitriles (**3b** and **3d**) were successfully hydrolyzed with NaOH to obtain carboxylic acids **3e-h**. Furthermore, the nitriles were used in a Radziszewski reaction to quickly and efficiently obtain the carboxamides **3j** and **3l**. All other tail groups (**3i**, **3k** and **3m-w**) were installed in an amide coupling using EDC/HOBt. Unfortunately, the synthesis and functionalization of the 3-position on the pyridine using glycinamide was troublesome and unsuccessful.
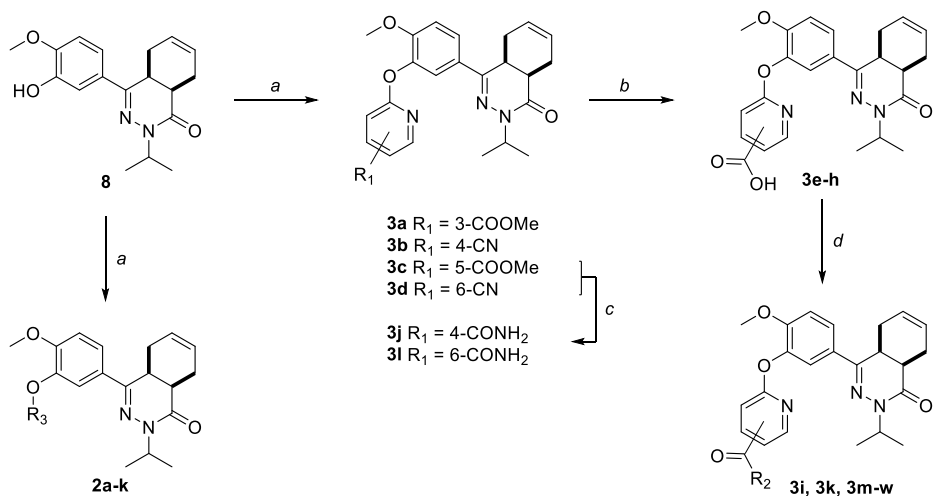
Scheme 2: *a*) Corresponding aryl chloride, Cs$_2$CO$_3$, DMF, 100 °C, 1-16 h, 23-82%; *b*) NaOH, H$_2$O, MeOH, rt, overnight, 71-99%; *c*) 30% aq. H$_2$O$_2$, K$_2$CO$_3$, DMSO, 0 °C, 10 min, **3j**: 71%, **3l**: 99%; *d*) Corresponding amine, EDC.HCl, HOBt.H$_2$O, DCM, rt, 16-72 h, 28-81%.

2.3. Biochemical activity

All compounds were initially tested for their biochemical activity against TbrPDEB1 in a single point assay at 10 μM. All of the 5-membered and 6-membered rings (**2a-f** and **2h**) from the virtual screening hits showed low to moderate inhibition of TbrPDEB1 at this concentration (Table 1), but the larger fused 5- and 6-membered rings (**2j-l** and **2p**) showed no inhibition at 10 μM. The observation of deviant binding poses for this cluster in the virtual screening and the absence of activity suggests that these linkers are too bulky to fit in the limited space towards the P-pocket. The best results were observed for pyrazine **2d** and pyridine **2h**, both having about 50% inhibition at 10 μM.

3

Discovery of diaryl ether substituted tetrahydrophthalazinones as TbrPDEB1 inhibitors following structure-based virtual screening

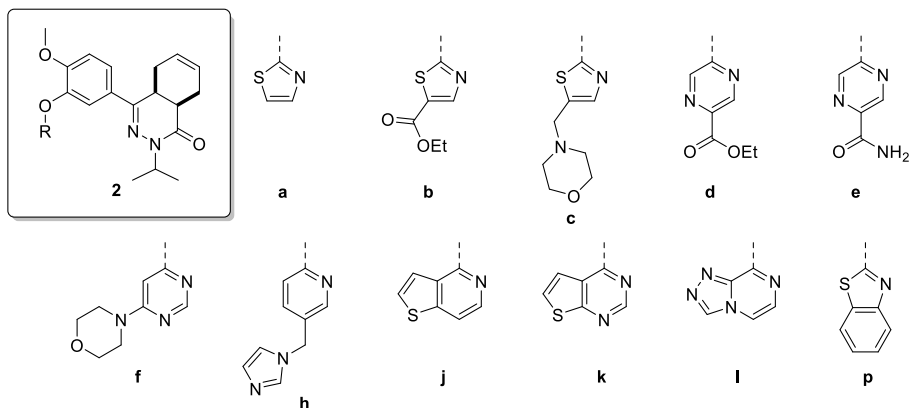Table 1: Single point activities of the virtual screening hits against TbrPDEB1 at 10 µM.
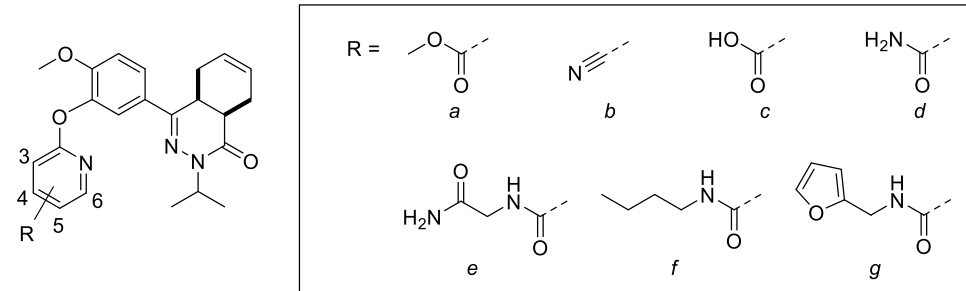
#	NPD-	TbrPDEB1 (% Inh.)	#	NPD-	TbrPDEB1 (% Inh.)
2a	1162	12 ± 3	2h	1164	49 ± 2
2b	1315	11 ± 0	2j	1157	No inhibition
2c	1163	40 ± 4	2k	1160	No inhibition
2d	1337	69 ± 1	2l	1158	No inhibition
2e	3162	18 ± 9	2p	1161	No inhibition
2f	1159	11 ± 8			

The computer-aided design of the pyridines on the different positions gave only a few active compounds (Table 2). With exception of **3m**, all substitutions on the 3- and 4-position of the pyridine ring resulted in no inhibition of TbrPDEB1 at 10 µM. A methyl ester substitution on the 5-position of the pyridine ring (**3c**) resulted in a moderate inhibition, while larger groups or a carboxylic acid were not tolerated on this position. The best results were obtained for substitutions on the 6-position next to the pyridine nitrogen (**3d**, **3h**, **3l**, **3o**, **3s** and **3w**). With exception of the carboxylic acid functionality, all substitutions on this position resulted in a moderate inhibitory effect, suggesting that this is the ideal vector to fit the side groups into the active site. Although we observed relatively small differences between the different analogues, the best activities were obtained for *n*-butyl and furfuryl substituted diaryl ethers **3s** and **3w**, which both showed slightly more than 50% inhibition at 10 µM.

Table 2: Single point activities of structure guided diaryl ether phthalazinones against TbrPDEB1 at 10 µM.

#	NPD-	R	Pos.	TbrPDEB1 (% inh)	#	NPD-	R	Pos.	TbrPDEB1 (% inh)
3a	1338	a	3	No inhibition	3m	1400	e	4	27 ± 0
3b	1340	b	4	No inhibition	3n	1392	e	5	5 ± 1
3c	1339	a	5	50 ± 1	3o	1397	e	6	40 ± 1
3d	1341	b	6	36 ± 6	3p	1389	f	3	No inhibition
3e	1342	c	3	No inhibition	3q	3167	f	4	No inhibition
3f	1394	c	4	No inhibition	3r	1390	f	5	No inhibition
3g	1343	c	5	11 ± 6	3s	1395	f	6	53 ± 3
3h	1393	c	6	No inhibition	3t	1344	g	3	No inhibition
3i	1345	d	3	No inhibition	3u	1444	g	4	No inhibition
3j	1398	d	4	No inhibition	3v	1391	g	5	No inhibition
3k	3165	d	5	No inhibition	3w	1396	g	6	51 ± 9
3l	1399	d	6	48 ± 10					

All compounds (**2d**, **2h**, **3c**, **3l**, **3s** and **3w**) that showed about 50% inhibition or higher at 10 µM in the single point assay were selected for a TbrPDEB1 and hPDE4 full dose response assay for selectivity determination and their *in vitro* activity against *T. brucei* parasites and *in vitro* cytotoxicity for MRC-5 cells. In line with the results in the 10 µM assay, all selected diaryl ethers showed interesting inhibitory activity against TbrPDEB1 with a pK_i values between 5.9 and 6.2 (Table 3). However, every compound showed at least a one log-unit higher inhibitory activity against hPDE4 and thus having an unfavorable selectivity profile. This suggests that the steric clash of the inhibitor with the protein in hPDE4, which is hypothesized to be

the cause of the selectivity for the biphenyl series (**1**, Fig. 1), could not be achieved as efficiently. The increased flexibility caused by the implemented ether functionality allows the molecule to bind in a more favorable conformation and thereby avoiding steric clash in hPDE4. In the phenotypic assays, this set of compounds, except **3s**, showed an activity comparable to **1** with pIC_{50} values in the range of 4.6 – 5.1. All compounds, with exception of **2h**, did not show cytotoxicity at the highest measured concentration (pCC_{50} <4.2), resulting in an acceptable cytotoxicity profile for **2d**, **3c**, **3l**, and **3w**., suggesting that the introduction of the ether functionality has no effect on the cellular activity when compared to **1**.

Table 3: In vitro activity of selected phthalazinones against TbrPDEB1, hPDE4, *T. brucei* parasites and MRC-5 cells.

#	TbrPDEB1 (pK_i)	hPDE4 (pK_i)	*T. brucei* pIC_{50}	MRC-5 pIC_{50}
2d	6.2 ± 0.1	7.5 ± 0.1	4.8 ± 0.4	<4.2
2h	5.9 ± 0.1	7.4 ± 0.1	5.1 ± 0.1	4.5 ± 0.1
3c	6.1 ± 0.1	7.0 ± 0.1	5.1 ± 0.1	<4.2
3l	6.1 ± 0.1	7.1 ± 0.1	4.8 ± 0.4	<4.2
3s	5.9 ± 0.1	7.1 ± 0.1	<4.2	<4.2
3w	6.0 ± 0.1	7.3 ± 0.1	4.6 ± 0.6	<4.2

3.   Conclusion

The computer-aided design of novel diaryl substituted tetrahydrophthalazinones resulted in the identification of several compounds with activities in the low micromolar range against TbrPDEB1 and devoid of cytotoxicity against MRC-5 cells. The results suggest a favorable position of modification for para-substituted 6-membered heteroaromatics (**2d**, **2h**, and **3c**) or 2,6-substituted pyridines (**3l**, **3s**, **3o** and **3w**). The current set of compounds provides additional insight in the SAR for development of new selective TbrPDEB1 inhibitors. These results are important in the design of TbrPDEB1 selective inhibitors with adequate selectivity (>30-fold over human PDE4) and efficacy (IC_{50} < 1 µM) against this parasite.

4.   Experimental

4.1.   *Phosphodiesterase activity assays*

The TbrPDEB1 catalytic domain phosphodiesterase activity assays were conducted based on a method reported by Sijm *et al.* with minor adaptations.[29] The PDELight™ HTS cAMP phosphodiesterase Kit (Lonza, Walkersville, USA) was performed at 25 °C in non-binding, low volume 384-well plates (Corning, Kennebunk, ME, USA). PDE activity measurements (TbrPDEB1_CD; K_m 3.45 μM, hPDE4B_CD; K_m 13.89 μM) were made in 'stimulation buffer' (50 mM Hepes, 100 mM NaCl, 10 mM $MgCl_2$, 0.5 mM EDTA, 0.05 mg/mL BSA, pH 7.5). Single concentration measurements were made at 10 μM inhibitor concentration (triplo measurements/assay, n=2). Dose-response curves were made in the range 100 μM - 10 pM (triplo measurements/assay, n=3). Compounds were diluted in DMSO (final in-test concentration 1%). Inhibitor dilutions (2.5 μL) were transferred to the 384-well plates, 2.5 μL PDE in stimulation buffer was added and mixed, 5 μL cAMP (at 2 × K_m up to 20 μM) added and the assay mixture was incubated for 20 min at 300 rpm. The reaction was terminated by addition of 5 μL Lonza Stop Buffer supplemented with 10 μM NPD-001. Then 5 μL of Lonza Detection reagent (diluted to 80% with reaction buffer) was added and the reaction incubated for 10 min at 300 rpm. Luminescence was read with a Victor3 luminometer using a 0.1 s/well program.

RLUs were measured in comparison to the DMSO-only control, NPD-001 always was taken along as positive control as a PDE inhibitor. The K_i values of the inhibitors analyzed are represented as the mean of at least three independent experiments with the associated standard error of the mean (S.E.M.). Due to solubility issues, we were not able to determine full dose-response curves for all compounds; K_i values for such inhibitors were obtained by curve fitting (Graphpad Prism 7.0) and the assumption of full inhibition to a level of inhibition by NPD-001.

4.2.   *Phenotypic cellular assays*

The phenotypic cellular assays were conducted as previously reported by Blaazer *et al.*[24] For the cellular assays, reference drugs as positive controls were suramin (Sigma-Aldrich, Germany) for *T. brucei* (pIC_{50} = 7.4 ± 0.2, n = 5) and tamoxifen (Sigma-Aldrich, Germany) for MRC-5 cells (pIC_{50} = 5.0 ± 0.1, n = 5). All compounds were tested at five concentrations (64, 16, 4, 1 and 0.25 μM) to establish a full dose-titration and determination of the IC_{50} and CC_{50}, data are represented as the mean of duplicate experiments ± S.E.M. The final in-test concentration of DMSO did not exceed 0.5%.

For the antitrypanosomal assay, *T.b. brucei* Squib-427 strain (suramin-sensitive) was cultured at 37 °C and 5% CO_2 in HMI-9 medium supplemented with 10% fetal calf serum (FCS). Approximately $1.5 × 10^4$ trypomastigotes were added to each well and parasite growth was assessed after 72 h at 37 °C by adding resazurin. Viability was assessed fluorimetrically 24 h after addition of resazurin. Fluorescence was measured (excitation 550 nm, emission 590 nm) and the results were expressed as percentage reduction in viability compared to control.

For the cellular cytotoxicity assay, MRC-5 SV2 cells, originally from a human diploid lung cell line, were cultivated in MEM supplemented with L-glutamine (20 mM), 16.5 mM sodium hydrogen carbonate and 5% FCS. For the assay, 10^4 MRC-5 cells/well were seeded onto the test plates containing the pre-diluted sample and incubated at 37 °C and 5% CO_2 for 72 h. Cell viability was assessed fluorimetrically

4 h after the addition of resazurin. Fluorescence was measured (excitation 550 nm, emission 590 nm) and the results were expressed as percentage reduction in cell viability compared to controls.

4.3. Chemistry

All reagents and solvents were obtained from commercial suppliers and were used as received. All reactions were magnetically stirred and carried out under an inert atmosphere. Reaction progress was monitored using thin-layer chromatography (TLC) and LC-MS analysis. LC-MS analysis was performed on a Shimadzu LC-20AD liquid chromatograph pump system, equipped with an Xbridge (C18) 5 μm column (50 mm, 4.6 mm), connected to a Shimadzu SPD-M20A diode array detector, and MS detection using a Shimadzu LC-MS-2010EV mass spectrometer. The LC-MS conditions were as follows: solvent A (water with 0.1% formic acid) and solvent B (MeCN with 0.1% formic acid), flow rate of 1.0 mL/min, start 5% B, linear gradient to 90% B in 4.5 min, then 1.5 min at 90% B, then linear gradient to 5% B in 0.5 min, then 1.5 min at 5% B; total run time of 8 min. Silica gel column chromatography was carried out with automatic purification systems using the indicated eluent. Reversed phase column purification was performed on Grace Davison iES system with C18 cartridges (60 Å, 40 μm) using the indicated eluent. Nuclear magnetic resonance (NMR) spectra were recorded as indicated on a Bruker Avance 500 (500 MHz for ^{1}H and 125.8 MHz for ^{13}C) instrument equipped with a Bruker CryoPlatform, or on a Bruker DMX300 (300 MHz for ^{1}H) or a Bruker Biospin (400 MHz for ^{1}H). Chemical shifts (δ in ppm) and coupling constants (J in Hz) are reported with residual solvent as internal standard (δ ^{1}H-NMR: CDCl$_3$ 7.26; DMSO-d_6 2.50; δ ^{13}C-NMR: CDCl$_3$ 77.16; DMSO-d_6 39.52). Abbreviations used for ^{1}H-NMR descriptions are as follows: s = singlet, d = doublet, t = triplet, q = quintet, hept = heptet dd = doublet of doublets, dt = doublet of triplets, tt = triplet of triplets, m = multiplet, app d = apparent doublet, br = broad signal. Exact mass measurements (HRMS) were performed on a Bruker micrOTOF-Q instrument with electrospray ionization (ESI): in positive ion mode and a capillary potential of 4,500 V. Microwave reactions were carried out in a Biotage Initiator$^+$ using sealed microwave vials. Systematic names for molecules were generated with ChemBioDraw Ultra 14.0.0.117 (PerkinElmer, Inc.). The reported yields refer to isolated pure products and are not optimized. The purity, reported as the LC peak area % at 254 nm, of all final compounds was ≥95% based on LC-MS. All compounds are isolated as a racemic mixture of cis-enantiomers.

4.3.1. 2-Methoxyphenyl methanesulfonate (**4**)

To an ice-cooled solution of 2-methoxyphenol (45 mL, 0.40 mol) and Et$_3$N (95 mL, 0.69 mol) in DCM (120 mL) was added methanesulfonyl chloride (41 mL, 0.52 mol) in a dropwise fashion to give an orange suspension, which was stirred at rt for 1 h. The reaction mixture was quenched by adding water (350 mL). The aqueous phase was extracted with DCM (2 × 300 mL) and the organic phases were combined and washed with aq. Na$_2$CO$_3$ (1 M, 300 mL) and brine (300 mL). The organic phase was dried over MgSO$_4$ and the solvent was removed in vacuo to yield the title compound (63 g, 78%) as an orange oil. ^{1}H NMR (500 MHz, CDCl$_3$): δ 7.35 – 7.23 (m, 2H), 7.06 – 6.93 (m, 2H), 3.89 (s, 3H), 3.17 (s, 3H). ^{13}C NMR (126 MHz, CDCl$_3$): δ 151.4, 138.3, 128.4, 124.5, 121.1, 112.9, 56.0, 38.2. LC-MS (ESI): t_R = 3.89 min, area: >98%, no ionisation.

4.3.2. *(E)*-4-(4-Methoxy-3-((methylsulfonyl)oxy)phenyl)-4-oxobut-2-enoic acid (**5**)

To a yellow solution of **4** (24.4 g, 121 mmol) and furan-2,5-dione (14.2 g, 145 mmol) in DCM (200 mL) was slowly added AlCl₃ (33.8 g, 253 mmol). The dark red solution was stirred at rt for 5 h. The dark red suspension was quenched by slowly pouring into ice-cooled aq. HCl (2 M, 400 mL). The organic phase was separated and the aqueous phase was extracted with DCM (200 mL) and EtOAc (2 × 200 mL). The organic phases were combined and concentrated *in vacuo* till crystallization was initiated. Further removal of solvents was stopped and the mixture was allowed further crystallisation to yield the title compound (14.3 g, 40%) as yellow crystals. ^{1}H NMR (500 MHz, DMSO-d_6): δ 8.11 (dd, *J* = 8.8, 2.2 Hz, 1H), 7.97 – 7.87 (m, 2H), 7.37 (d, *J* = 8.8 Hz, 1H), 6.69 (d, *J* = 15.5 Hz, 1H), 3.96 (s, 3H), 3.43 (s, 3H). ^{13}C NMR (126 MHz, DMSO-d_6): δ 187.4, 166.8, 156.7, 138.3, 136.2, 133.3, 130.7, 129.6, 124.6, 114.0, 57.1, 38.9. LC-MS (ESI): t_R = 3.37 min, area: >98%, *m/z* 301 [M + H]⁺.

4.3.3. *trans*-6-(4-Methoxy-3-((methylsulfonyl)oxy)benzoyl)cyclohex-3-enecarboxylic acid (**6**)

A mixture of **5** (10.0 g, 33.3 mmol) in a solution of buta-1,3-diene in THF (2 M, 33.3 mL, 66.6 mmol) was divided over two microwave vials. The reaction mixtures were stirred at 140 °C (pressure increased to ~11 bar) for 1.5 h by microwave irradiation. The two reactions were pooled and concentrated *in vacuo* to give a slightly yellow powder. This solid was triturated with toluene and filtrated to yield the title compound (10.8 g, 92%) as a white solid. ^{1}H NMR (500 MHz, DMSO-d_6): δ 12.29 (s, 1H), 8.08 (dd, *J* = 8.8, 2.2 Hz, 1H), 7.87 (d, *J* = 2.1 Hz, 1H), 7.33 (d, *J* = 8.7 Hz, 1H), 5.81 – 5.67 (m, 2H), 3.95 (s, 3H), 3.78 (td, *J* = 11.2, 5.4 Hz, 1H), 3.41 (s, 3H), 2.81 (td, *J* = 11.3, 5.5 Hz, 1H), 2.49 – 2.40 (m, 1H), 2.40 – 2.28 (m, 1H), 2.23 – 2.10 (m, 1H), 1.94 – 1.80 (m, 1H). ^{13}C NMR (126 MHz, DMSO-d_6): δ 200.9, 176.4, 156.0, 138.2, 129.9, 129.7, 125.8, 125.7, 124.1, 113.8, 57.0, 42.3, 41.6, 38.9, 29.4, 28.4. LC-MS (ESI): t_R = 3.89 min, area: 97%, *m/z* 355 [M + H]⁺.

4.3.4. *cis*-4-(3-Hydroxy-4-methoxyphenyl)-2-isopropyl-4a,5,8,8a-tetrahydrophthalazin-1(2*H*)-one (**8**)

A suspension of **6** (3.5 g, 10 mmol), Cs₂CO₃ (6.5 g, 20 mmol) and isopropylhydrazine.HCl (3.3 g, 30 mmol) in EtOH (10 mL) were charged in a microwave vial. This suspension was stirred in a microwave at 100 °C for 6 h. The reaction mixture was slowly poured into an ice-cooled aq. HCl solution (1 M, 100 mL) upon which white solids formed. These white solids where filtered of and dried in vacuo to give a mixture of the mesylated (**7**) and demesylated products (**8**).

To a solution of the crude product (2.95 g, 7.52 mmol) in dry THF (20 mL) and MeOH (15 mL) was added aq. NaOH (1 M, 20 mL). The reaction mixture was stirred at 50 °C for 2 h. THF and MeOH were removed *in vacuo*. The aqueous mixture was slowly poured into an ice-cooled aq. HCl (1 M, 100 mL) upon which yellow-white solids appeared. The solids were removed by filtration and dried *in vacuo*. The product was purified using flash column chromatography (EtOAc/cyclohexane: 0-100%) to yield the title compound (1.50 g, 47% over 2 steps) as a white powder. ^{1}H NMR (500 MHz, CDCl₃): δ 7.52 (d, *J* = 2.2 Hz, 1H), 7.30 (dd, *J* = 8.4, 2.2 Hz, 1H), 6.88 (d, *J* = 8.5 Hz, 1H), 5.82 (s, 1H), 5.81 – 5.64 (m, 2H), 5.05 (hept, *J* = 6.6 Hz, 1H), 3.95 (s, 3H), 3.29 (dt, *J* = 11.6, 5.8 Hz, 1H), 3.06 – 2.96 (m, 1H), 2.74 (t, *J* = 6.0 Hz, 1H), 2.26 – 2.12 (m, 2H), 2.07 – 1.97 (m, 1H), 1.33 (d, *J* = 6.6 Hz, 3H), 1.21 (d, *J* = 6.7 Hz, 3H). ^{13}C NMR (126 MHz, CDCl₃): δ 166.5, 153.6, 148.0, 145.8, 128.7, 126.0, 124.0, 118.2, 111.9, 110.2, 56.0,

46.6, 34.7, 31.0, 23.2, 22.4, 20.6, 20.2. LC-MS (ESI): t_R = 4.38 min, area: >98%, m/z 315 [M + H]$^+$. HRMS (ESI) m/z: [M + H]$^+$ calcd. for $C_{18}H_{23}N_2O_3$ 315.1703, found 315.1689.

4.3.5.   General procedure for nucleophilic aromatic substitution

To a suspension of **8** (1 equiv.) and Cs_2CO_3 (2.5 equiv.) in DMF (3 mL/equiv.) in a microwave vial was added the corresponding aromatic chloride (1 - 1.5 equiv.). This mixture was heated to 100 °C for 3 h under microwave irradiation, unless indicated otherwise. The reaction was quenched by slowly pouring it into ice-cooled aq. 1 M HCl solution and the product was extracted with EtOAc (3 ×). The organic phases were combined, washed twice with brine, dried over $MgSO_4$ and concentrated *in vacuo*. The crude product was purified as indicated.

4.3.6.   *cis*-2-Isopropyl-4-(4-methoxy-3-(thiazol-2-yloxy)phenyl)-4a,5,8,8a-tetrahydrophthalazin-1(2*H*)-one (**2a**)

This compound was synthesized according to the general procedure starting with **8** (0.15 g, 0.48 mmol) and 2-chlorothiazole (0.10 g, 0.81 mmol). The reaction mixture was stirred in a microwave at 100 °C for 11 h. The crude product was purified by column chromatography using EtOAc/n-heptane (gradient: 10-50%) to yield the title compound (110 mg, 58%) as a white solid. ^{1}H NMR (500 MHz, CDCl$_3$): δ 7.80 (t, J = 1.7 Hz, 1H), 7.69 (dt, J = 8.7, 1.8 Hz, 1H), 7.17 (s, 1H), 7.05 (dd, J = 8.7, 1.4 Hz, 1H), 6.79 (dd, J = 3.8, 1.8 Hz, 1H), 5.81 − 5.61 (m, 2H), 5.02 (hept, J = 6.6, 1.8 Hz, 1H), 3.89 − 3.80 (m, 3H), 3.27 (dt, J = 11.6, 5.8 Hz, 1H), 3.04 − 2.93 (m, 1H), 2.72 (t, J = 6.1 Hz, 1H), 2.24 − 2.10 (m, 2H), 2.07 − 1.96 (m, 1H), 1.30 (dd, J = 6.6, 1.8 Hz, 3H), 1.18 (dd, J = 6.7, 1.8 Hz, 3H). ^{13}C NMR (126 MHz, CDCl$_3$): δ 174.2, 166.4, 152.5, 152.3, 143.9, 137.4, 128.6, 126.0, 124.8, 123.9, 119.8, 112.8, 112.7, 56.2, 46.7, 34.7, 30.9, 23.1, 22.3, 20.6, 20.2. LC-MS (ESI): t_R = 4.97 min, area: >98%, m/z 398 [M + H]$^+$. HRMS (ESI) m/z: [M + H]$^+$ calcd. for $C_{21}H_{24}N_3O_3S$ 398.1533, found 398.1525.

4.3.7.   Ethyl   2-(5-(*cis*-3-isopropyl-4-oxo-3,4,4a,5,8,8a-hexahydrophthalazin-1-yl)-2-methoxyphenoxy)thiazole-5-carboxylate (**2b**)

This compound was synthesized according to the general procedure starting with **8** (400 mg, 1.27 mmol) and ethyl 2-chlorothiazole-5-carboxylate (293 mg, 1.53 mmol). The mixture was stirred 100 °C for 10 h. The crude product was purified by column chromatography using EtOAc/n-heptane (gradient: 10-50%) to obtain a white solid (250 mg, 35%). ^{1}H NMR (500 MHz, CDCl$_3$): δ 7.90 − 7.83 (m, 1H), 7.83 − 7.77 (m, 1H), 7.72 (dt, J = 8.7, 1.5 Hz, 1H), 7.11 − 7.02 (m, 1H), 5.82 − 5.61 (m, 2H), 5.11 − 4.94 (m, 1H), 4.39 − 4.22 (m, 2H), 3.86 (d, J = 1.8 Hz, 3H), 3.28 (dt, J = 11.6, 5.7 Hz, 1H), 3.07 − 2.92 (m, 1H), 2.74 (t, J = 6.0 Hz, 1H), 2.27 − 2.10 (m, 2H), 2.09 − 1.92 (m, 1H), 1.39 − 1.32 (m, 3H), 1.30 (dd, J = 6.6, 1.7 Hz, 3H), 1.19 (dd, J = 6.7, 1.7 Hz, 3H). ^{13}C NMR (126 MHz, CDCl$_3$): δ 177.7, 166.4, 161.3, 152.3, 152.0, 144.5, 143.4, 128.7, 126.0, 125.3, 123.8, 123.0, 119.7, 112.9, 61.4, 56.2, 46.7, 34.7, 31.0, 23.0, 22.3, 20.6, 20.2, 14.3. LC-MS (ESI): t_R = 5.37 min, area: 95%, m/z 470 [M + H]$^+$. HRMS (ESI) m/z: [M + H]$^+$ calcd. for $C_{24}H_{28}N_3O_5S$ 470.1744, found 470.1750.

4.3.8.   *cis*-2-Isopropyl-4-(4-methoxy-3-((5-(morpholinomethyl)thiazol-2-yl)oxy)phenyl)-4a,5,8,8a-tetrahydrophthalazin-1(2*H*)-one (**2c**)

This compound was synthesized according to the general procedure starting with **8** (150 mg, 0.477 mmol) and 4-((2-chlorothiazol-5-yl)methyl)morpholine (125 mg, 0.573 mmol). The crude product was purified by column chromatography using EtOAc/n-heptane (gradient: 10-50%) to yield the title compound (110 mg, 45%) as a white solid. ^{1}H NMR (500 MHz, CDCl$_3$): δ 7.79 (d, *J* = 2.2 Hz, 1H), 7.69 (dd, *J* = 8.6, 2.2 Hz, 1H), 7.05 (d, *J* = 8.7 Hz, 1H), 6.99 (s, 1H), 5.84 – 5.63 (m, 2H), 5.04 (hept, *J* = 6.5 Hz, 1H), 3.88 (s, 3H), 3.72 (t, *J* = 4.7 Hz, 4H), 3.59 (s, 2H), 3.27 (dt, *J* = 11.5, 5.7 Hz, 1H), 3.06 – 2.95 (m, 1H), 2.73 (t, *J* = 5.9 Hz, 1H), 2.50 (s, 4H), 2.25 – 2.12 (m, 2H), 2.08 – 1.96 (m, 1H), 1.31 (d, *J* = 6.6 Hz, 3H), 1.19 (d, *J* = 6.7 Hz, 3H). ^{13}C NMR (126 MHz, CDCl$_3$): δ 174.0, 166.4, 152.5, 152.3, 143.7, 128.6, 126.0, 124.7, 123.9, 119.8, 112.8, 66.8, 56.2, 55.4, 53.1, 46.7, 34.7, 31.0, 23.1, 22.3, 20.6, 20.2. LC-MS (ESI): t_R = 3.53 min, area: 97%, *m/z* 497 [M + H]$^+$. HRMS (ESI) *m/z*: [M + H]$^+$ calcd. for C$_{26}$H$_{33}$N$_4$O$_4$S 497.2217, found 497.2206.

4.3.9.   Methyl   5-(5-(*cis*-3-isopropyl-4-oxo-3,4,4a,5,8,8a-hexahydrophthalazin-1-yl)-2-methoxyphenoxy)pyrazine-2-carboxylate (**2d**)

This compound was synthesized according to the general procedure starting with **8** (150 mg, 0.477 mmol) and methyl 5-chloro-pyrazine-2-carboxylate (99 mg, 0.57 mmol). The mixture was heated to 50 °C for 1 h. The crude product was purified by column chromatography using EtOAc/cyclohexane (gradient: 0-30%) to give the title compound as a white solid (150 mg, 70%). ^{1}H NMR (500MHz, CDCl$_3$): δ 8.81 (d, *J* = 1.2 Hz, 1H), 8.55 (d, *J* = 1.2 Hz, 1H), 7.74 (d, *J* = 2.1 Hz, 1H), 7.70 (dd, *J* = 8.6, 2.2 Hz, 1H), 7.05 (d, *J* = 8.7 Hz, 1H), 5.83 – 5.62 (m, 2H), 5.03 (hept, *J* = 6.5 Hz, 1H), 4.01 (s, 3H), 3.78 (s, 3H), 3.29 (dt, *J* = 11.6, 5.7 Hz, 1H), 3.04 – 2.97 (m, 1H), 2.73 (t, *J* = 5.9 Hz, 1H), 2.24 – 2.14 (m, 2H), 2.09 – 1.99 (m, 1H), 1.30 (d, *J* = 6.6 Hz, 3H), 1.18 (d, *J* = 6.7 Hz, 3H). ^{13}C NMR (126 MHz, CDCl$_3$): δ 166.5, 164.4, 161.4, 152.6, 152.4, 144.3, 141.3, 137.3, 135.0, 128.8, 126.1, 124.9, 124.0, 120.2, 112.4, 56.1, 53.0, 46.8, 34.8, 31.1, 23.2, 22.4, 20.7, 20.3. LC-MS (ESI): t_R = 4.74 min, area: 96%, *m/z* 451 [M + H]$^+$. HRMS (ESI) *m/z*: [M + H]$^+$ calcd. for C$_{24}$H$_{27}$N$_4$O$_5$ 451.1976, found 451.1979.

4.3.10.   5-(5-(*cis*-3-Isopropyl-4-oxo-3,4,4a,5,8,8a-hexahydrophthalazin-1-yl)-2-methoxyphenoxy)pyrazine-2-carboxamide (**2e**)

This compound was synthesized according to the general procedure starting with **8** (100 mg, 0.318 mmol) and 5- chloropyrazine-2-carboxamide (60.1 mg, 0.382 mmol). The mixture was stirred at 50 °C for 5 h. The crude product was purified by column chromatography using EtOAc/cyclohexane (gradient: 0-50%) to give the title compound as a white solid (52 mg, 38%). ^{1}H NMR (500 MHz, CDCl$_3$) δ 9.08 (s, 1H), 8.61 (s, 1H), 7.76 (d, *J* = 2.2 Hz, 1H), 7.71 (dd, *J* = 8.6, 2.2 Hz, 1H), 7.07 (dd, *J* = 16.1, 6.3 Hz, 2H), 5.94 (d, *J* = 3.9 Hz, 1H), 5.85 – 5.75 (m, 1H), 5.74 – 5.64 (m, 1H), 5.05 (hept, *J* = 6.8 Hz, 1H), 3.80 (s, 3H), 3.38 – 3.25 (m, 1H), 3.09 – 2.95 (m, 1H), 2.77 (t, *J* = 5.9 Hz, 1H), 2.29 – 2.14 (m, 2H), 2.12 – 1.99 (m, 1H), 1.32 (d, *J* = 6.6 Hz, 3H), 1.21 (d, *J* = 6.7 Hz, 3H). ^{13}C NMR (126 MHz, CDCl3) δ 166.8, 165.1, 157.7, 152.5, 152.4, 141.2, 140.4, 138.1, 137.6, 128.7, 126.1, 124.5, 123.8, 120.1, 112.2, 56.0, 46.8, 34.7, 31.0, 23.1, 22.3, 20.6, 20.2. LC-MS (ESI): t_R = 4.24 min, area: 96%, *m/z* 436 [M + H]$^+$. HRMS (ESI) *m/z*: [M + H]$^+$ calcd. for C$_{23}$H$_{26}$N$_5$O$_4$ 436.1979, found 436.1989.

3

4.3.11. *cis*-2-Isopropyl-4-(4-methoxy-3-((6-morpholinopyrimidin-4-yl)oxy)phenyl)-4a,5,8,8a-tetrahydrophthalazin-1(2*H*)-one (**2f**)

This compound was synthesized according to the general procedure starting with **8** (150 mg, 0.477 mmol) and 4-(6-chloropyrimidin-4-yl)morpholine (95 mg, 0.50 mmol). The mixture was stirred at 100 °C for 5 h. Residual DMF was removed by co-evaporation with toluene to yield the title compound (165 mg, 72%) as a white powder. ^{1}H NMR (500 MHz, DMSO-d_6): δ 8.14 (d, *J* = 0.8 Hz, 1H), 7.72 (dd, *J* = 8.7, 2.2 Hz, 1H), 7.62 (d, *J* = 2.2 Hz, 1H), 7.19 (d, *J* = 8.7 Hz, 1H), 6.34 (s, 1H), 5.73 – 5.58 (m, 2H), 4.86 (hept, *J* = 6.6 Hz, 1H), 3.75 (s, 3H), 3.70 – 3.63 (m, 4H), 3.61 – 3.53 (m, 4H), 3.44 (dt, *J* = 11.5, 5.8 Hz, 1H), 2.80 (t, *J* = 6.0 Hz, 1H), 2.77 – 2.69 (m, 1H), 2.20 – 2.06 (m, 2H), 1.89 – 1.69 (m, 1H), 1.21 (d, *J* = 6.5 Hz, 3H), 1.11 (d, *J* = 6.7 Hz, 3H). ^{13}C NMR (126 MHz, DMSO-d_6): δ 170.0, 166.5, 164.4, 157.7, 153.5, 153.2, 141.8, 128.1, 126.3, 124.7, 124.5, 120.5, 113.2, 86.2, 66.2, 56.4, 46.1, 44.5, 34.3, 30.3, 23.0, 22.4, 20.9, 20.6. LC-MS (ESI): t_R = 4.69 min, area: 96%, *m/z* 478 [M + H]$^+$. HRMS (ESI) *m/z*: [M + H]$^+$ calcd. for $C_{26}H_{32}N_5O_4$ 478.2449, found 478.2454.

4.3.12. *cis*-4-(3-((5-((1*H*-Imidazol-1-yl)methyl)pyridin-2-yl)oxy)-4-methoxyphenyl)-2-isopropyl-4a,5,8,8a-tetrahydrophthalazin-1(2*H*)-one (**2h**)

This compound was synthesized according to the general procedure starting with **8** (150 mg, 0.477 mmol) and 5-((1*H*-imidazol-1-yl)methyl)-2-chloropyridine (111 mg, 0.573 mmol). The crude product was dissolved DMSO and subjected to reversed phase column chromatography using H$_2$O/MeCN + 0.1% formic acid (gradient: 0-100%) to obtain the title compound (62 mg, 27%) as a colourless oil. ^{1}H NMR (500 MHz, CDCl$_3$): δ 8.04 (s, 1H), 7.75 (s, 1H), 7.71 – 7.62 (m, 2H), 7.52 (dd, *J* = 8.6, 2.5 Hz, 1H), 7.11 (s, 1H), 7.08 – 7.01 (m, 1H), 7.01 – 6.84 (m, 2H), 5.82 – 5.58 (m, 2H), 5.10 (s, 2H), 5.07 – 4.92 (m, 1H), 3.82 – 3.70 (m, 3H), 3.34 – 3.19 (m, 1H), 3.04 – 2.90 (m, 1H), 2.71 (s, 1H), 2.25 – 2.11 (m, 2H), 2.08 – 1.93 (m, 1H), 1.33 – 1.21 (m, 3H), 1.17 (dt, *J* = 6.8, 2.0 Hz, 3H). ^{13}C NMR (126 MHz, CDCl$_3$) δ 166.4, 163.6, 152.9, 152.9, 146.6, 142.1, 138.9, 128.6, 128.5, 126.0, 125.6, 124.1, 124.0, 120.5, 119.2, 112.3, 111.2, 56.0, 48.1, 46.6, 34.7, 31.0, 23.1, 22.3, 20.6, 20.2. (One imidazole carbon not detected). LC-MS (ESI): t_R = 3.52 min, area: >98%, *m/z* 472 [M + H]$^+$. HRMS (ESI) *m/z*: [M + H]$^+$ calcd. for $C_{27}H_{30}N_5O_3$ 472.2343, found 472.2352.

4.3.13. *cis*-2-Isopropyl-4-(4-methoxy-3-(thieno[3,2-c]pyridin-4-yloxy)phenyl)-4a,5,8,8a-tetrahydrophthalazin-1(2*H*)-one (**2j**)

This compound was synthesized according to the general procedure starting with **8** (150 mg, 0.477 mmol) and 4-chlorothieno[3,2-c]pyridine (121 mg, 0.716 mmol). The mixture was stirred at rt for 2 h. The crude product was purified by column chromatography using EtOAc/n-heptane (gradient: 10-50%) to yield the title compound (110 mg, 50%) as a white solid. ^{1}H NMR (500 MHz, CDCl$_3$): δ 7.95 (d, *J* = 5.7 Hz, 1H), 7.77 (d, *J* = 2.2 Hz, 1H), 7.75 – 7.68 (m, 2H), 7.54 – 7.47 (m, 2H), 7.08 (d, *J* = 8.7 Hz, 1H), 5.82 – 5.63 (m, 2H), 5.04 (hept, *J* = 6.6 Hz, 1H), 3.80 (s, 3H), 3.31 (dt, *J* = 11.5, 5.7 Hz, 1H), 3.06 – 2.96 (m, 1H), 2.75 (t, *J* = 6.1 Hz, 1H), 2.26 – 2.15 (m, 2H), 2.11 – 1.99 (m, 1H), 1.31 (d, *J* = 6.5 Hz, 3H), 1.19 (d, *J* = 6.7 Hz, 3H). ^{13}C NMR (126 MHz, CDCl$_3$): δ 166.4, 158.2, 153.2, 153.0, 149.7, 142.3, 140.2, 128.5, 126.0, 124.3, 124.0, 121.1, 120.8, 112.6, 112.4, 56.1, 46.6, 34.7, 31.0, 23.1, 22.4, 20.6, 20.2. LC-MS

(ESI): t_R = 5.43 min, area: 97%, *m/z* 448 [M + H]⁺. HRMS (ESI) *m/z*: [M + H]⁺ calcd. for $C_{25}H_{26}N_3O_3S$ 448.1689, found 448.1689.

4.3.14. *cis*-2-Isopropyl-4-(4-methoxy-3-(thieno[2,3-d]pyrimidin-4-yloxy)phenyl)-4a,5,8,8a-tetrahydrophthalazin-1(2*H*)-one (**2k**)

This compound was synthesized according to the general procedure starting with **8** (150 mg, 0.477 mmol) and 4-chlorothieno[2,3-d]pyrimidine (122 mg, 0.716 mmol). The reaction mixture was stirred at rt for 1 h. The crude product was purified by column chromatography using EtOAc/n-heptane (gradient: 10-50%) to yield the title compound (50 mg, 23%) as a white solid. ¹H NMR (500 MHz, DMSO-d_6) δ 8.59 (s, 1H), 7.98 (d, *J* = 5.9 Hz, 1H), 7.86 – 7.79 (m, 2H), 7.69 (d, *J* = 5.9 Hz, 1H), 7.27 (d, *J* = 9.2 Hz, 1H), 5.73 – 5.58 (m, 2H), 4.86 (hept, *J* = 6.4 Hz, 1H), 3.74 (s, 3H), 3.45 (dt, *J* = 11.6, 5.8 Hz, 1H), 2.81 (t, *J* = 6.1 Hz, 1H), 2.78 – 2.68 (m, 1H), 2.21 – 2.09 (m, 2H), 1.88 – 1.76 (m, 1H), 1.21 (d, *J* = 6.6 Hz, 3H), 1.12 (d, *J* = 6.7 Hz, 3H). ¹³C NMR (126 MHz, DMSO-d_6): δ 169.4, 166.5, 163.3, 153.5, 153.4, 152.8, 141.1, 128.4, 127.9, 126.3, 125.4, 124.5, 120.8, 119.0, 118.5, 113.4, 56.5, 46.2, 34.3, 30.3, 23.0, 22.4, 20.9, 20.5. LC-MS (ESI): t_R = 5.22 min, area: >98%, *m/z* 449 [M + H]⁺. HRMS (ESI) *m/z*: [M + H]⁺ calcd. for $C_{24}H_{25}N_4O_3S$ 449.1642, found 449.1628.

4.3.15. *cis*-4-(3-([1,2,4]Triazolo[4,3-a]pyrazin-8-yloxy)-4-methoxyphenyl)-2-isopropyl-4a,5,8,8a-tetrahydrophthalazin-1(2*H*)-one (**2l**)

This compound was synthesized according to the general procedure starting with **8** (150 mg, 0.477 mmol) and 8-chloro-[1,2,4]triazolo[4,3-a]pyrazine (111 mg, 0.716 mmol). The reaction mixture was stirred at rt for 1 h. The reaction mixture was quenched by pouring into ice-cooled aq. HCl (1 M, 10 mL). The solids were filtered off and taken up in EtOAc (30 mL), which was washed with brine (2 x 30 mL), dried over MgSO₄ and concentrated in vacuo to give the title compound (170 mg, 82%) as a white solid. ¹H NMR (500 MHz, DMSO-d_6): δ 9.48 (s, 1H), 8.32 (d, *J* = 4.7 Hz, 1H), 7.85 (d, *J* = 2.2 Hz, 1H), 7.82 (dd, *J* = 8.6, 2.3 Hz, 1H), 7.34 (d, *J* = 4.7 Hz, 1H), 7.28 (d, *J* = 8.7 Hz, 1H), 5.76 – 5.57 (m, 2H), 4.87 (hept, *J* = 6.7 Hz, 1H), 3.77 (s, 3H), 3.45 (dt, *J* = 11.5, 5.8 Hz, 1H), 2.82 (s, 1H), 2.79 – 2.68 (m, 1H), 2.15 (d, *J* = 17.6 Hz, 2H), 1.83 (t, *J* = 13.9 Hz, 1H), 1.21 (d, *J* = 6.6 Hz, 3H), 1.12 (d, *J* = 6.8 Hz, 3H). ¹³C NMR (126 MHz, DMSO-d_6): δ 166.5, 153.4, 152.8, 152.4, 140.9, 138.8, 128.4, 126.8, 126.3, 125.4, 124.5, 120.8, 115.1, 113.5, 100.0, 56.5, 46.2, 34.3, 30.3, 23.0, 22.4, 20.9, 20.5. LC-MS (ESI): t_R = 4.08 min, area: >98%%, *m/z* 433 [M + H]⁺. HRMS (ESI) *m/z*: [M + H]⁺ calcd. for $C_{23}H_{25}N_6O_3$ 433.1983, found 433.1974.

4.3.16. *cis*-4-(3-(Benzo[d]thiazol-2-yloxy)-4-methoxyphenyl)-2-isopropyl-4a,5,8,8a-tetrahydrophthalazin-1(2*H*)-one (**2p**)

This compound was synthesized according to the general procedure starting with **8** (150 mg, 0.477 mmol) and 2-chlorobenzo[d]thiazole (81 mg, 0.48 mmol). In contrast to the general procedure, this reaction mixture was stirred at rt overnight. The title compound (132 mg, 61%) was obtained after work-up as a white powder. ¹H NMR (500 MHz, DMSO-d_6): δ 7.96 (d, *J* = 2.2 Hz, 1H), 7.92 (d, *J* = 8.0 Hz, 1H), 7.87 (dd, *J* = 8.7, 2.2 Hz, 1H), 7.66 (d, *J* = 8.0 Hz, 1H), 7.41 (t, *J* = 7.7 Hz, 1H), 7.36 – 7.27 (m, 2H), 5.74 – 5.57 (m, 2H), 4.87 (hept, *J* = 6.7 Hz, 1H), 3.83 (s, 3H), 3.48 (dt, *J* = 11.6, 5.7 Hz, 1H), 2.83 (s, 1H), 2.79 – 2.68 (m, 1H), 2.20 – 2.08 (m, 2H), 1.82 (t, *J* = 14.6 Hz, 1H), 1.22 (d, *J* = 6.6 Hz, 3H), 1.13 (d, *J* = 6.7 Hz, 3H). ¹³C NMR (126 MHz, DMSO-d_6): δ 172.5, 166.5, 153.2, 152.4, 149.0, 143.3, 132.3, 128.5,

126.9, 126.3, 126.1, 124.5, 124.5, 122.7, 121.5, 120.4, 114.1, 56.7, 46.2, 34.2, 30.3, 23.0, 22.4, 20.9, 20.5. LC-MS (ESI): t_R = 5.60 min, area: 98%, *m/z* 448 [M + H]$^+$. HRMS (ESI) *m/z*: [M + H]$^+$ calcd. for $C_{25}H_{26}N_3O_3S$ 448.1689, found 448.1677.

4.3.17. Methyl 2-(5-(*cis*-3-isopropyl-4-oxo-3,4,4a,5,8,8a-hexahydrophthalazin-1-yl)-2-methoxyphenoxy)nicotinate (**3a**)

This compound was synthesized according to the general procedure starting with **8** (1.20 g, 3.82 mmol) and methyl 2-chloronicotinate (0.74 mL, 5.7 mmol). The crude product was purified by column chromatography using EtOAc/cyclohexane (gradient: 30-55% + 1% AcOH) to give the title compound as a white solid (876 mg, 51%). ^{1}H NMR (500 MHz, DMSO-d_6): δ 8.28 (dd, J = 7.6, 1.9 Hz, 1H), 8.24 (dd, J = 4.8, 1.9 Hz, 1H), 7.73 (dd, J = 8.7, 2.1 Hz, 1H), 7.63 (d, J = 2.1 Hz, 1H), 7.24 – 7.17 (m, 2H), 5.72 – 5.59 (m, 2H), 4.86 (hept, J = 6.3 Hz, 1H), 3.87 (s, 3H), 3.70 (s, 3H), 3.45 (dt, J = 11.5, 5.7 Hz, 1H), 2.80 (t, J = 5.7 Hz, 1H), 2.77 – 2.68 (m, 1H), 2.19 – 2.07 (m, 2H), 1.87 – 1.77 (m, 1H), 1.21 (d, J = 6.5 Hz, 3H), 1.12 (d, J = 6.7 Hz, 3H). ^{13}C NMR (126 MHz, DMSO-d_6): δ 166.1, 164.6, 160.7, 153.2, 152.7, 151.0, 141.9, 141.7, 127.9, 125.9, 124.2, 124.1, 120.1, 118.6, 113.6, 112.9, 56.0, 52.5, 45.7, 33.9, 29.9, 22.6, 22.0, 20.5, 20.1. LC-MS (ESI): t_R = 5.13 min, area: >98%, *m/z* 450 [M + H]$^+$. HRMS (ESI) *m/z*: [M + H]$^+$ calcd. for $C_{25}H_{28}N_3O_5$ 450.2023, found 450.2023.

4.3.18. 2-(5-(c*is*-3-Isopropyl-4-oxo-3,4,4a,5,8,8a-hexahydrophthalazin-1-yl)-2-methoxyphenoxy)isonicotinonitrile (**3b**)

This compound was synthesized according to the general procedure starting with **8** (1.1 g, 3.4 mmol) and 2-chloroisonicotinonitrile (712 mg, 5.14 mmol). The crude product was purified by column chromatography using EtOAc/cyclohexane (gradient: 0-20% + 2% AcOH) to give the title compound as a white solid (620 mg, 44%). ^{1}H NMR (500 MHz, CDCl$_3$): δ 8.28 (d, *J* = 5.0 Hz, 1H), 7.71 – 7.66 (m, 2H), 7.21 – 7.17 (m, 2H), 7.04 (d, *J* = 8.5 Hz, 1H), 5.72 (dd, *J* = 54.2, 9.3 Hz, 2H), 5.03 (hept, *J* = 6.3 Hz, 1H), 3.79 (s, 3H), 3.28 (dt, *J* = 11.5, 5.6 Hz, 1H), 3.04 – 2.96 (m, 1H), 2.73 (t, *J* = 5.8 Hz, 1H), 2.23 – 2.13 (m, 2H), 2.08 – 1.99 (m, 1H), 1.29 (d, *J* = 6.6 Hz, 3H), 1.18 (d, *J* = 6.7 Hz, 3H). ^{13}C NMR (126 MHz, DMSO-d_6): δ 166.1, 163.0, 153.0, 152.6, 148.9, 141.3, 128.0, 126.0, 124.5, 124.1, 122.5, 120.1, 120.1, 116.5, 113.6, 113.0, 56.0, 45.8, 33.9, 29.9, 22.6, 22.0, 20.5, 20.1. LC-MS (ESI): t_R = 5.01 min, area: >98%, *m/z* 417 [M + H]$^+$. HRMS (ESI) *m/z*: [M + H]$^+$ calcd. for $C_{24}H_{25}N_4O_3$ 417.1921, found 417.1915.

4.3.19. Methyl 6-(5-(*cis*-3-isopropyl-4-oxo-3,4,4a,5,8,8a-hexahydrophthalazin-1-yl)-2-methoxyphenoxy)nicotinate (**3c**)

This compound was synthesized according to the general procedure starting with **8** (1.20 g, 3.82 mmol) and methyl 6-chloronicotinate (0.98 g, 5.7 mmol). The crude product was purified by column chromatography using EtOAc/cyclohexane (gradient: 30-55% + 1% AcOH) to give the title compound as a white solid (1.06 g, 62%). ^{1}H NMR (500 MHz, DMSO-d_6): δ 8.64 (d, *J* = 2.4 Hz, 1H), 8.29 (dd, *J* = 8.7, 2.3 Hz, 1H), 7.76 (dd, *J* = 8.7, 2.0 Hz, 1H), 7.71 (d, *J* = 2.0 Hz, 1H), 7.23 (d, *J* = 8.7 Hz, 1H), 7.15 (d, *J* = 8.7 Hz, 1H), 5.71 – 5.59 (m, 2H), 4.86 (hept, *J* = 6.5 Hz, 1H), 3.84 (s, 3H), 3.72 (s, 3H), 3.44 (dt, *J* = 11.4, 5.7 Hz, 1H), 2.80 (t, *J* = 6.0 Hz, 1H), 2.76 – 2.69 (m, 1H), 2.19 – 2.09 (m, 2H), 1.86 – 1.76 (m, 1H), 1.21 (d, *J* = 6.5 Hz, 3H), 1.11 (d, *J* = 6.7 Hz, 3H). ^{13}C NMR (126 MHz, CDCl$_3$) δ 166.1, 165.7, 164.9, 153.1, 152.6, 149.4, 141.5, 140.8, 128.0, 125.9, 124.6, 124.1, 120.9, 120.1, 113.1, 110.5, 56.0, 52.3, 45.8, 33.9, 29.9,

22.6, 22.0, 20.5, 20.1. LC-MS (ESI): t_R = 5.12 min, area: >98%, m/z 450 [M + H]$^+$. HRMS (ESI) m/z: [M + H]$^+$ calcd. for $C_{25}H_{28}N_3O_5$ 450.2023, found 450.2021.

4.3.20. 6-(5-(c*is*-3-Isopropyl-4-oxo-3,4,4a,5,8,8a-hexahydrophthalazin-1-yl)-2-methoxyphenoxy)picolinonitrile (**3d**)

This compound was synthesized according to the general procedure starting with **8** (1.2 g, 3.8 mmol) and 6-chloropicolinonitrile (793 mg, 5.73 mmol). The crude product was purified by column chromatography using EtOAc/cyclohexane (gradient: 0-20% + 2% TEA) to give the title compound (900 mg, 54%) as a white solid. ^{1}H NMR (500 MHz, DMSO-d_6): δ 8.07 (dd, J = 8.5, 7.3 Hz, 1H), 7.79 (dd, J = 8.7, 2.2 Hz, 1H), 7.76 (d, J = 7.3 Hz, 1H), 7.73 (d, J = 2.2 Hz, 1H), 7.42 (d, J = 8.4 Hz, 1H), 7.26 (d, J = 8.7 Hz, 1H), 5.72 – 5.58 (m, 2H), 4.87 (hept, J = 6.5 Hz, 1H), 3.75 (s, 3H), 3.45 (dt, J = 11.6, 5.8 Hz, 1H), 2.82 (t, J = 5.9 Hz, 1H), 2.78 – 2.68 (m, 1H), 2.13 (s, 2H), 1.87 – 1.78 (m, 1H), 1.22 (d, J = 6.6 Hz, 3H), 1.13 (d, J = 6.7 Hz, 3H). ^{13}C NMR (126 MHz, DMSO-d_6): δ 166.1, 163.0, 153.0, 152.5, 141.7, 141.1, 129.3, 128.0, 125.9, 124.7, 124.5, 124.1, 120.0, 117.1, 116.2, 113.2, 56.1, 45.8, 33.8, 29.9, 22.6, 22.0, 20.5, 20.1. LC-MS (ESI): t_R = 5.00 min, area: 96%, m/z 417 [M + H]$^+$. HRMS (ESI) m/z: [M + H]$^+$ calcd. for $C_{24}H_{25}N_4O_3$ 417.1921, found 417.1913.

4.3.21. 2-(5-(*cis*-3-Isopropyl-4-oxo-3,4,4a,5,8,8a-hexahydrophthalazin-1-yl)-2-methoxyphenoxy)nicotinic acid (**3e**)

To a solution of **3a** (875 mg, 1.95 mmol) in MeOH (20 mL) was added aq. NaOH (1.0 M, 10 mL, 10 mmol) and the reaction mixture was stirred at rt for 16 h. The reaction mixture was acidified with aq. 1 M HCl to pH 3 and was extracted with DCM (3 × 25 mL). The combined organic phases were dried over Na_2SO_4 and concentrated under reduced pressure to obtain the title compound as a white crystalline solid (690 mg, 81%). ^{1}H NMR (500 MHz, DMSO-d_6): δ 13.27 (s, 1H), 8.24 (dd, J = 7.5, 1.9 Hz, 1H), 8.19 (dd, J = 4.8, 1.9 Hz, 1H), 7.72 (dd, J = 8.7, 2.2 Hz, 1H), 7.63 (d, J = 2.2 Hz, 1H), 7.21 – 7.15 (m, 2H), 5.71 – 5.59 (m, 2H), 4.86 (hept, J = 6.6 Hz, 1H), 3.71 (s, 3H), 3.49 – 3.41 (m, 1H), 2.80 (t, J = 5.9 Hz, 1H), 2.77 – 2.69 (m, 1H), 2.19 – 2.07 (m, 2H), 1.86 – 1.77 (m, 1H), 1.21 (d, J = 6.6 Hz, 3H), 1.12 (d, J = 6.7 Hz, 3H). ^{13}C NMR (126 MHz, CDCl$_3$): δ 166.1, 165.8, 160.8, 153.2, 152.7, 150.4, 142.1, 141.6, 127.9, 125.9, 124.1, 124.1, 120.2, 118.5, 114.9, 112.8, 55.9, 45.8, 33.9, 29.9, 22.6, 22.0, 20.5, 20.1. LC-MS (ESI): t_R = 4.30 min, area: >98%, m/z 436 [M + H]$^+$. HRMS (ESI) m/z: [M + H]$^+$ calcd. for $C_{24}H_{26}N_3O_5$ 436.1867, found 436.1864.

4.3.22. 2-(5-(*cis*-3-Isopropyl-4-oxo-3,4,4a,5,8,8a-hexahydrophthalazin-1-yl)-2-methoxyphenoxy)isonicotinic acid (**3f**)

To a solution of **3b** (454 mg, 1.09 mmol) in 1,4-dioxane (14 mL) was added aq. NaOH (1.0 M, 14 mL, 14 mmol) and the reaction mixture was heated to 80 °C for 16 h. The reaction mixture was acidified with aq. HCl (1 M, 15 mL) and extracted with DCM (3 × 50 mL). The combined organic phases were dried over Na_2SO_4 and concentrated under reduced pressure to give the title compound as a white powder (487 mg, 99%). ^{1}H NMR (500 MHz, CDCl$_3$): δ 8.31 (d, J = 4.9 Hz, 1H), 7.72 (s, 1H), 7.68 (d, J = 8.6 Hz, 1H), 7.57 (d, J = 5.1 Hz, 2H), 7.04 (d, J = 8.6 Hz, 1H), 5.81 – 5.63 (m, 2H), 5.03 (hept, J = 6.7 Hz, 1H), 3.79 (s, 3H), 3.29 (dt, J = 11.4, 5.6 Hz, 1H), 3.05 – 2.97 (m, 1H), 2.74 (t, J = 5.3 Hz, 1H), 2.24 – 2.13 (m, 2H), 2.10 – 1.98 (m, 1H), 1.30 (d, J = 6.5 Hz, 3H), 1.18 (d, J = 6.7 Hz, 3H). ^{13}C NMR (126 MHz, CDCl$_3$):

δ 168.3, 166.7, 164.3, 153.1, 153.0, 148.5, 142.3, 140.4, 128.7, 126.1, 124.3, 124.1, 120.6, 117.8, 112.5, 111.4, 56.2, 46.9, 34.9, 31.1, 23.2, 22.5, 20.7, 20.3. LC-MS (ESI): t_R = 4.50 min, area: >98%, *m/z* 436 [M + H]$^+$. HRMS (ESI) *m/z*: [M + H]$^+$ calcd. for $C_{24}H_{26}N_3O_5$ 436.1867, found 436.1847.

4.3.23. 6-(5-(*cis*-3-Isopropyl-4-oxo-3,4,4a,5,8,8a-hexahydrophthalazin-1-yl)-2-methoxyphenoxy)nicotinic acid (**3g**)

To a solution of **3c** (1.1 g, 2.5 mmol) in MeOH (20 mL) was added aq. NaOH (1 M, 10 mL, 10 mmol) was added and the reaction mixture was stirred for 16 h. The reaction was quenched with aqueous 1 M HCl to pH 3 and was extracted with DCM (3 × 25 mL). The combined organic phases were dried over Na_2SO_4 and concentrated under reduced pressure. The crude product was purified by column chromatography using EtOAc/PhMe/cyclohexane + 1% AcOH (ratio: 0:1:1 to 1:1:1) to obtain the title compound as a white solid (791 mg, 74%). ^{1}H NMR (500 MHz, CDCl$_3$): δ 8.85 (d, *J* = 1.9 Hz, 1H), 8.33 (dd, *J* = 8.7, 2.2 Hz, 1H), 7.71 (d, *J* = 1.7 Hz, 1H), 7.69 (d, *J* = 8.6 Hz, 1H), 7.05 (d, *J* = 8.6 Hz, 2H), 5.72 (dd, *J* = 52.7, 9.9 Hz, 2H), 5.03 (hept, *J* = 6.6 Hz, 1H), 3.79 (s, 3H), 3.29 (dt, *J* = 11.5, 5.7 Hz, 1H), 3.07 – 2.97 (m, 1H), 2.74 (t, *J* = 5.9 Hz, 1H), 2.24 – 2.14 (m, 2H), 2.08 – 1.99 (m, 1H), 1.30 (d, *J* = 6.5 Hz, 3H), 1.18 (d, *J* = 6.7 Hz, 3H). ^{13}C NMR (126 MHz, CDCl$_3$): δ 169.8, 166.7, 166.6, 153.0, 152.9, 151.2, 142.1, 141.2, 128.7, 126.1, 124.5, 124.1, 120.5, 120.4, 112.5, 110.6, 56.2, 46.9, 34.9, 31.1, 23.2, 22.5, 20.7, 20.3. LC-MS (ESI): t_R = 4.48 min, area: >98%, *m/z* 436 [M + H]$^+$. HRMS (ESI) *m/z*: [M + H]$^+$ calcd. for $C_{24}H_{26}N_3O_5$ 436.1867, found 436.1864.

4.3.24. 6-(5-(*cis*-3-Isopropyl-4-oxo-3,4,4a,5,8,8a-hexahydrophthalazin-1-yl)-2-methoxyphenoxy)picolinic acid (**3h**)

To a solution of **3d** (600 mg, 1.44 mmol) in MeOH (20 mL) was added aq. NaOH (1 M, 10 mmol, 10 mL) and the reaction mixture was stirred at rt for 16 h. The reaction was quenched with aq. HCl (1 M, 10 mL) and the resulting mixture was extracted with DCM (3 × 50 mL). The combined organic phases were dried over Na_2SO_4 and concentrated under reduced pressure to give the title compound as an off-white solid (550 mg, 88%). ^{1}H NMR (300 MHz, CDCl$_3$): δ 10.13 (s, 1H), 8.03 – 7.88 (m, 2H), 7.75 – 7.63 (m, 2H), 7.24 (d, *J* = 1.8 Hz, 1H), 7.05 (d, *J* = 8.4 Hz, 1H), 5.94 – 5.49 (m, 2H), 5.04 (hept, *J* = 6.4 Hz, 1H), 3.79 (s, 3H), 3.30 (dt, *J* = 11.4, 5.7 Hz, 1H), 3.07 – 2.94 (m, 1H), 2.77 (t, *J* = 5.6 Hz, 1H), 2.29 – 2.12 (m, 2H), 2.11 – 1.98 (m, 1H), 1.31 (d, *J* = 6.6 Hz, 3H), 1.20 (d, *J* = 6.7 Hz, 3H). ^{13}C NMR (126 MHz, CDCl$_3$): δ 166.5, 163.6, 162.0, 152.8, 152.7, 143.7, 141.7, 141.6, 128.9, 126.2, 124.6, 124.0, 120.4, 118.5, 115.9, 112.4, 56.2, 46.9, 34.8, 31.2, 23.2, 22.4, 20.8, 20.3. LC-MS (ESI): t_R = 4.63 min, area: 96%, *m/z* 436 [M + H]$^+$. HRMS (ESI) *m/z*: [M + H]$^+$ calcd. for $C_{24}H_{26}N_3O_5$ 436.1867, found 436.1849.

4.3.25. 2-(5-(*cis*-3-Isopropyl-4-oxo-3,4,4a,5,8,8a-hexahydrophthalazin-1-yl)-2-methoxyphenoxy)nicotinamide (**3i**)

To a solution of **3e** (150 mg, 0.344 mmol) in DCM (3 mL) was added EDC·HCl (198 mg, 1.03 mmol), HOBt·H$_2$O (158 mg, 1.03 mmol) and a solution of NH$_3$ in MeOH (7 M, 0.98 mL, 6.9 mmol). The reaction mixture was stirred at rt for 72 h. The precipitate was filtered off and the resulting solution was concentrated under reduced pressure. The product was purified by column chromatography using EtOAc/cyclohexane (gradient: 20-50%) to obtain the title compound as a white solid (86 mg, 58%). ^{1}H NMR (500 MHz, CDCl$_3$): δ 8.59 (dd, *J* = 7.5, 1.6 Hz, 1H), 8.21 (dd, *J* = 4.7, 1.7 Hz, 1H), 7.86 – 7.76 (m,

2H), 7.70 (dd, *J* = 8.6, 1.9 Hz, 1H), 7.15 (dd, *J* = 7.5, 4.8 Hz, 1H), 7.04 (d, *J* = 8.7 Hz, 1H), 5.97 (s, 1H), 5.82 − 5.64 (m, 2H), 5.04 (hept, *J* = 6.4 Hz, 1H), 3.78 (s, 3H), 3.30 (dt, *J* = 11.5, 5.7 Hz, 1H), 3.01 (d, *J* = 17.4 Hz, 1H), 2.74 (t, *J* = 5.8 Hz, 1H), 2.24 − 2.15 (m, 2H), 2.10 − 1.99 (m, 1H), 1.31 (d, *J* = 6.5 Hz, 3H), 1.19 (d, *J* = 6.7 Hz, 3H). ^{13}C NMR (126 MHz, DMSO-d_6): δ 166.1, 165.2, 159.5, 153.2, 152.7, 149.1, 141.6, 140.7, 127.8, 125.9, 124.2, 124.1, 120.9, 118.9, 117.9, 112.8, 56.0, 45.8, 33.9, 30.0, 22.6, 22.0, 20.5, 20.1. LC-MS (ESI): t_R = 4.17 min, area: 98%, *m/z* 435 [M + H]$^+$. HRMS (ESI) *m/z*: [M + H]$^+$ calcd. for $C_{24}H_{27}N_4O_4$ 435.2027, found 435.2031.

4.3.26. 2-(5-(*cis*-3-Isopropyl-4-oxo-3,4,4a,5,8,8a-hexahydrophthalazin-1-yl)-2-methoxyphenoxy)isonicotinamide (**3j**)

To an ice-cooled solution of **3b** (100 mg, 0.240 mmol) in DMSO (1.2 mL) was added K_2CO_3 (133 mg, 0.96 mmol) and aq. H_2O_2 (30%, 0.25 mL) and the reaction mixture was stirred in an ice bath for 10 minutes. The reaction was diluted with ice-cold water (4 mL) and the resulting solids were filtered off and dried in a vacuum oven to obtain a sticky oil. The oil was dissolved in DCM/MeOH (ratio: 1:1) and concentrated to give an off-white solid, which was washed with water, dissolved in MeOH and concentrated to give the title compound as a white solid (103 mg, 99%). ^{1}H NMR (500 MHz, CDCl$_3$): δ 8.26 (d, *J* = 5.4 Hz, 1H), 7.72 (d, *J* = 2.2 Hz, 1H), 7.68 (dd, *J* = 8.6, 2.3 Hz, 1H), 7.39 − 7.30 (m, 2H), 7.04 (d, *J* = 8.6 Hz, 1H), 6.38 (s, 1H), 6.09 (s, 1H), 5.85 − 5.61 (m, 2H), 5.03 (hept, *J* = 6.6 Hz, 1H), 3.80 (s, 3H), 3.29 (dt, *J* = 11.6, 5.7 Hz, 1H), 3.06 − 2.94 (m, 1H), 2.74 (t, *J* = 6.1 Hz, 1H), 2.25 − 2.12 (m, 2H), 2.10 − 1.95 (m, 1H), 1.30 (d, *J* = 6.6 Hz, 3H), 1.19 (d, *J* = 6.7 Hz, 3H). ^{13}C NMR (126 MHz, CDCl$_3$): δ 167.1, 166.6, 164.3, 153.0, 153.0, 148.6, 144.4, 142.3, 128.8, 126.1, 124.2, 124.1, 120.6, 115.9, 112.5, 108.9, 56.2, 46.8, 34.9, 31.1, 23.2, 22.5, 20.7, 20.3. LC-MS (ESI): t_R = 4.13 min, area: 98%, *m/z* 435 [M + H]$^+$. HRMS (ESI) *m/z*: [M + H]$^+$ calcd. for $C_{24}H_{27}N_4O_4$ 435.2027, found 435.2015.

4.3.27. 6-(5-(cis-3-Isopropyl-4-oxo-3,4,4a,5,8,8a-hexahydrophthalazin-1-yl)-2-methoxyphenoxy)nicotinamide (**3k**)

This compound was synthesized according to the general procedure starting with **8** (100 mg, 0.318 mmol) and 6- chloronicotinamide (59.8 mg, 0.382 mmol). The crude product was purified by column chromatography using EtOAc/cyclohexane (gradient: 0-50%) to give the title compound (34 mg, 24%) as a white solid. ^{1}H NMR (500 MHz, CDCl$_3$) δ 8.54 (d, *J* = 2.5 Hz, 1H), 8.24 (dd, *J* = 8.6, 2.5 Hz, 1H), 8.03 (s, 1H), 7.75 (dd, *J* = 8.6, 2.1 Hz, 1H), 7.68 (d, *J* = 2.3 Hz, 1H), 7.47 (s, 1H), 7.22 (d, *J* = 8.7 Hz, 1H), 7.09 (d, *J* = 8.6 Hz, 1H), 5.75 − 5.57 (m, 2H), 4.86 (hept, *J* = 6.7 Hz, 1H), 3.73 (s, 3H), 3.50 − 3.41 (m, 1H), 2.80 (t, *J* = 6.1 Hz, 1H), 2.77 − 2.67 (m, 1H), 2.21 − 2.07 (m, 2H), 1.88 − 1.75 (m, 1H), 1.21 (d, *J* = 6.6 Hz, 3H), 1.12 (d, *J* = 6.8 Hz, 3H). ^{13}C NMR (126 MHz, CDCl$_3$) δ 171.2, 171.1, 169.7, 158.3, 157.9, 152.5, 146.9, 144.5, 133.1, 131.0, 130.1, 129.5, 129.2, 125.4, 118.1, 115.0, 61.1, 50.9, 39.0, 35.1, 27.8, 27.1, 25.6, 25.3. LC-MS (ESI): t_R = 4.17 min, area: 96%, *m/z* 435 [M + H]$^+$. HRMS (ESI) *m/z*: [M + H]$^+$ calcd. for $C_{24}H_{27}N_4O_4$ 435.2027, found 435.2028.

4.3.28. 6-(5-(*cis*-3-Isopropyl-4-oxo-3,4,4a,5,8,8a-hexahydrophthalazin-1-yl)-2-methoxyphenoxy)picolinamide (**3l**)

To an ice-cooled solution of **3d** (215 mg, 0.516 mmol) in DMSO (2.5 mL) was added K_2CO_3 (285 mg, 2.07 mmol) and aq. H_2O_2 (30%, 0.54 mL). The reaction mixture was stirred in an ice bath for 10

minutes. Ice-cold water (5 mL) was added and the resulting solids were filtered off, washed with water and dried in a vacuum oven to obtain the pure title compound as a white powder (160 mg, 71%). ^{1}H NMR (300 MHz, CDCl₃): δ 7.93 – 7.81 (m, 2H), 7.73 – 7.64 (m, 2H), 7.26 (s, 1H), 7.09 (d, *J* = 7.4 Hz, 1H), 7.03 (d, *J* = 8.4 Hz, 1H), 5.84 – 5.57 (m, 3H), 5.03 (hept, *J* = 6.3, 5.9 Hz, 1H), 3.78 (s, 3H), 3.29 (dt, *J* = 11.6, 5.8 Hz, 1H), 3.07 – 2.94 (m, 1H), 2.75 (t, *J* = 5.4 Hz, 1H), 2.26 – 2.11 (m, 2H), 2.11 – 1.94 (m, 1H), 1.30 (d, *J* = 6.5 Hz, 3H), 1.19 (d, *J* = 6.7 Hz, 3H). ¹³C NMR (126 MHz, CDCl₃): δ 166.5, 166.3, 162.0, 153.1, 152.9, 147.3, 142.2, 140.8, 128.7, 126.2, 124.1, 124.0, 120.6, 117.3, 113.9, 112.3, 56.2, 46.9, 34.9, 31.1, 23.2, 22.4, 20.8, 20.3. LC-MS (ESI): t_R = 4.50 min, area: 96%, *m/z* 435 [M + H]⁺. HRMS (ESI) *m/z*: [M + H]⁺ calcd. for $C_{24}H_{27}N_4O_4$ 435.2027, found 435.2020.

4.3.29. *N*-(2-Amino-2-oxoethyl)-2-(5-(*cis*-3-isopropyl-4-oxo-3,4,4a,5,8,8a-hexahydrophthalazin-1-yl)-2-methoxyphenoxy)isonicotinamide (**3m**)

This compound was prepared from **3f** (140 mg, 0.321 mmol) and glycinamide·HCl (42.6 mg, 0.386 mmol) as described for **3q**. The title compound was obtained as a white solid (120 mg, 76%). ^{1}H NMR (500 MHz, CDCl₃): δ 8.21 (d, *J* = 5.0 Hz, 1H), 7.69 (s, 1H), 7.66 (d, *J* = 8.6 Hz, 1H), 7.57 – 7.49 (m, 1H), 7.37 (s, 1H), 7.33 (d, *J* = 4.9 Hz, 1H), 7.01 (d, *J* = 8.6 Hz, 1H), 6.45 (s, 1H), 5.87 (s, 1H), 5.80 – 5.57 (m, 2H), 5.00 (hept, *J* = 6.4 Hz, 1H), 4.18 (d, *J* = 4.5 Hz, 2H), 3.76 (s, 3H), 3.27 (dt, *J* = 11.1, 5.3 Hz, 1H), 3.03 – 2.93 (m, 1H), 2.76 – 2.67 (m, 1H), 2.24 – 2.10 (m, 2H), 2.06 – 1.97 (m, 1H), 1.28 (d, *J* = 6.4 Hz, 3H), 1.16 (d, *J* = 6.6 Hz, 3H). ¹³C NMR (126 MHz, CDCl₃): δ 170.8, 166.6, 165.7, 164.2, 153.1, 153.0, 148.5, 144.5, 142.3, 128.7, 126.1, 124.2, 124.1, 120.6, 115.7, 112.5, 108.9, 56.1, 46.8, 43.2, 34.8, 31.1, 23.2, 22.4, 20.7, 20.3. LC-MS (ESI): t_R = 3.85 min, area: >98%, *m/z* 492 [M + H]⁺. HRMS (ESI) *m/z*: [M + H]⁺ calcd. for $C_{26}H_{30}N_5O_5$ 492.2241, found 492.2224.

4.3.30. *N*-(2-Amino-2-oxoethyl)-6-(5-(*cis*-3-isopropyl-4-oxo-3,4,4a,5,8,8a-hexahydrophthalazin-1-yl)-2-methoxyphenoxy)nicotinamide (**3n**)

This compound was prepared from **3g** (150 mg, 0.344 mmol) and glycinamide·HCl (762 mg, 6.89 mmol) as described for **3p**. The title compound was obtained after column chromatography using MeOH/DCM (gradient 0-10%) as a white solid (93 mg, 55%). ^{1}H NMR (500 MHz, DMSO-d_6): δ 8.78 (t, *J* = 5.9 Hz, 1H), 8.55 (d, *J* = 2.2 Hz, 1H), 8.25 (dd, *J* = 8.7, 2.4 Hz, 1H), 7.76 (dd, *J* = 8.7, 2.1 Hz, 1H), 7.69 (d, *J* = 2.1 Hz, 1H), 7.42 (s, 1H), 7.22 (d, *J* = 8.7 Hz, 1H), 7.11 (d, *J* = 8.6 Hz, 1H), 7.07 (s, 1H), 5.75 – 5.54 (m, 2H), 4.87 (hept, *J* = 6.6 Hz, 1H), 3.80 (d, *J* = 5.9 Hz, 2H), 3.73 (s, 3H), 3.45 (dt, *J* = 11.5, 5.7 Hz, 1H), 2.81 (t, *J* = 5.9 Hz, 1H), 2.79 – 2.69 (m, 1H), 2.20 – 2.09 (m, 2H), 1.88 – 1.78 (m, 1H), 1.21 (d, *J* = 6.5 Hz, 3H), 1.12 (d, *J* = 6.7 Hz, 3H).¹³C NMR (126 MHz, DMSO-d_6): δ 170.9, 166.1, 164.5, 164.5, 153.1, 152.7, 147.2, 141.7, 139.2, 127.9, 125.9, 124.9, 124.4, 124.1, 120.2, 113.0, 109.8, 56.0, 45.8, 42.3, 33.9, 29.9, 22.6, 22.0, 20.5, 20.1. LC-MS (ESI): t_R = 3.90 min, area: 95%, *m/z* 488 [M + H]⁺. HRMS (ESI) *m/z*: [M + H]⁺ calcd. for $C_{26}H_{30}N_5O_5$ 492.2241, found 492.2226.

4.3.31. *N*-(2-Amino-2-oxoethyl)-6-(5-(*cis*-3-isopropyl-4-oxo-3,4,4a,5,8,8a-hexahydrophthalazin-1-yl)-2-methoxyphenoxy)picolinamide (**3o**)

This compound was prepared from **3h** (160 mg, 0.367 mmol) and glycinamide·HCl (48.7 mg, 0.441 mmol) as described for **3q**. The title compound was obtained as a white solid (146 mg, 81%). ^{1}H NMR (300 MHz, CDCl₃): δ 7.99 (t, *J* = 5.5 Hz, 1H), 7.91 – 7.79 (m, 2H), 7.76 – 7.61 (m, 2H), 7.12 – 7.02 (m,

2H), 6.20 (s, 1H), 5.83 – 5.60 (m, 2H), 5.50 (s, 1H), 5.03 (hept, J = 7.0 Hz, 1H), 4.03 (d, J = 5.7 Hz, 2H), 3.81 (s, 3H), 3.31 (dt, J = 11.4, 5.2 Hz, 1H), 3.06 – 2.89 (m, 1H), 2.76 (t, J = 5.4 Hz, 1H), 2.27 – 2.11 (m, 2H), 2.09 – 1.97 (m, 1H), 1.29 (d, J = 6.5 Hz, 3H), 1.19 (d, J = 6.7 Hz, 3H). ^{13}C NMR (126 MHz, CDCl$_3$): δ 170.9, 166.6, 164.7, 162.0, 153.1, 153.0, 146.9, 142.0, 140.8, 128.7, 126.2, 124.3, 124.0, 120.4, 117.2, 114.1, 112.4, 56.2, 46.8, 43.3, 34.8, 31.1, 23.3, 22.5, 20.8, 20.3. LC-MS (ESI): t_R = 4.19 min, area: 97%, m/z 492 [M + H]$^+$. HRMS (ESI) m/z: [M + H]$^+$ calcd. for C$_{26}$H$_{30}$N$_5$O$_5$ 492.2241, found 492.2228.

4.3.32. *N*-Butyl-2-(5-(*cis*-3-isopropyl-4-oxo-3,4,4a,5,8,8a-hexahydrophthalazin-1-yl)-2-methoxyphenoxy)nicotinamide (**3p**)

To a solution of **3e** (150 mg, 0.344 mmol) in DCM (3 mL) was added EDC·HCl (198 mg, 1.03 mmol), HOBt·H$_2$O (158 mg, 1.03 mmol) and n-butylamine (0.69 mL, 7.0 mmol). The reaction mixture was stirred at rt for 72 h. The reaction mixture was diluted with DCM (25 mL) and washed with sat. aq. NH$_4$Cl (2 × 25 mL) and sat. aq. NaHCO$_3$ (2 × 25 mL). The organic phase was dried over MgSO$_4$ and concentrated under reduced pressure to give a yellow oil. The product was purified by column chromatography using EtOAc/cyclohexane (gradient: 20-50%) to obtain the title compound as a white solid (86 mg, 50%). ^{1}H NMR (500 MHz, DMSO-d_6): δ 8.37 – 8.24 (m, 1H), 8.18 – 8.09 (m, 2H), 7.78 (s, 1H), 7.74 (d, J = 8.5 Hz, 1H), 7.22 – 7.15 (m, 2H), 5.74 – 5.59 (m, 2H), 4.87 (hept, J = 6.7 Hz, 1H), 3.73 (s, 3H), 3.47 – 3.40 (m, 1H), 3.34 – 3.28 (m, 2H), 2.81 (t, J = 5.0 Hz, 1H), 2.79 – 2.69 (m, 1H), 2.23 – 2.06 (m, 2H), 1.90 – 1.78 (m, 1H), 1.55 – 1.47 (m, 2H), 1.38 – 1.30 (m, 2H), 1.22 (d, J = 6.3 Hz, 3H), 1.13 (d, J = 6.6 Hz, 3H), 0.88 (t, J = 7.3 Hz, 3H). ^{13}C NMR (126 MHz, CDCl$_3$): δ 166.5, 163.7, 160.0, 152.8, 152.6, 149.5, 142.2, 141.6, 128.6, 126.1, 124.4, 124.0, 121.1, 119.4, 116.9, 112.2, 56.1, 46.8, 39.8, 34.8, 31.6, 31.1, 23.2, 22.4, 20.7, 20.3, 20.3, 13.9. LC-MS (ESI): t_R = 5.19 min, area: >98%, m/z 491 [M + H]$^+$. HRMS (ESI) m/z: [M + H]$^+$ calcd. for C$_{28}$H$_{35}$N$_4$O$_4$ 491.2653, found 491.2652.

4.3.33. *N*-Butyl-2-(5-(*cis*-3-isopropyl-4-oxo-3,4,4a,5,8,8a-hexahydrophthalazin-1-yl)-2-methoxyphenoxy)isonicotinamide (**3q**)

To a solution of **3f** (140 mg, 0.321 mmol) in DMF (2.3 mL) and DIPEA (0.23 mL, 1.3 mmol) was added HATU (0.15 g, 0.39 mmol) and n-butyl amine (0.1 mL, 1.0 mmol). The reaction mixture was stirred at rt for 24 h. The reaction mixture was diluted with DCM (30 mL) and washed with sat. aq. NH$_4$Cl (30 mL). The aqueous phase was extracted with DCM (2 × 30 mL). The combined organic phases were washed with brine (2 × 80 mL), dried over Na$_2$SO$_4$ and concentrated under reduced pressure. The product was purified by column chromatography using EtOAc/cyclohexane (gradient 20-50%) to obtain the title compound as a white solid (91 mg, 58%). ^{1}H NMR (500 MHz, CDCl$_3$): δ 8.76 (t, J = 5.7 Hz, 1H), 8.18 (d, J = 5.2 Hz, 1H), 7.74 (dd, J = 8.6, 2.2 Hz, 1H), 7.67 (d, J = 2.1 Hz, 1H), 7.43 (dd, J = 5.2, 1.3 Hz, 1H), 7.36 (d, J = 1.1 Hz, 1H), 7.21 (d, J = 8.7 Hz, 1H), 5.73 – 5.57 (m, 2H), 4.85 (h, J = 6.7 Hz, 1H), 3.73 (s, 3H), 3.49 – 3.41 (m, 1H), 3.27 (q, J = 6.9 Hz, 2H), 2.80 (t, J = 6.1 Hz, 1H), 2.77 – 2.69 (m, 1H), 2.20 – 2.07 (m, 2H), 1.88 – 1.77 (m, 1H), 1.56 – 1.46 (m, 2H), 1.38 – 1.28 (m, 2H), 1.21 (d, J = 6.5 Hz, 3H), 1.11 (d, J = 6.7 Hz, 3H), 0.90 (t, J = 7.3 Hz, 3H). ^{13}C NMR (126 MHz, CDCl$_3$): δ 171.2, 169.1, 168.7, 158.3, 158.0, 152.9, 150.8, 147.1, 133.1, 131.1, 129.4, 129.2, 125.4, 121.4, 118.1, 113.3, 61.1, 50.9, 39.0, 36.2, 35.1, 31.5, 27.8, 27.1, 25.6, 25.3, 24.8, 18.9. LC-MS (ESI): t_R = 4.87 min, area: 97%, m/z 491 [M + H]$^+$. HRMS (ESI) m/z: [M + H]$^+$ calcd. for C$_{28}$H$_{35}$N$_4$O$_4$ 491.2653, found 491.2632.

4.3.34. *N*-Butyl-6-(5-(*cis*-3-isopropyl-4-oxo-3,4,4a,5,8,8a-hexahydrophthalazin-1-yl)-2-methoxyphenoxy)nicotinamide (**3r**)

This compound was prepared from **3g** (150 mg, 0.344 mmol) and n-butylamine (0.69 mL, 7.0 mmol) as described for **3p**. The title compound was obtained as a white solid (47 mg, 28%). ^{1}H NMR (300 MHz, CDCl$_3$): δ 8.50 (d, *J* = 1.8 Hz, 1H), 8.13 (dd, *J* = 8.6, 2.3 Hz, 1H), 7.75 – 7.63 (m, 2H), 7.02 (t, *J* = 7.9 Hz, 2H), 6.05 (t, *J* = 4.9 Hz, 1H), 5.82 – 5.61 (m, 2H), 5.03 (hept, *J* = 6.5 Hz, 1H), 3.78 (s, 3H), 3.45 (q, *J* = 6.8 Hz, 2H), 3.28 (dt, *J* = 11.4, 5.8 Hz, 1H), 3.07 – 2.93 (m, 1H), 2.73 (t, *J* = 5.7 Hz, 1H), 2.27 – 2.12 (m, 2H), 2.11 – 1.96 (m, 1H), 1.59 (p, *J* = 7.2 Hz, 2H), 1.47 – 1.33 (m, 2H), 1.29 (d, *J* = 6.5 Hz, 3H), 1.18 (d, *J* = 6.7 Hz, 3H), 0.95 (t, *J* = 7.3 Hz, 3H). ^{13}C NMR (126 MHz, CDCl$_3$): δ 166.5, 165.4, 165.2, 153.0, 152.9, 146.3, 142.2, 139.0, 128.8, 126.1, 125.6, 124.3, 124.1, 120.6, 112.5, 110.6, 56.2, 46.8, 40.0, 34.9, 31.8, 31.2, 23.2, 22.5, 20.7, 20.3, 20.3, 13.9. LC-MS (ESI): t_R = 4.75 min, area: 97%, *m/z* 547 [M + H]$^+$. HRMS (ESI) *m/z*: [M + H]$^+$ calcd. for C$_{28}$H$_{35}$N$_4$O$_4$ 491.2653, found 491.2634.

4.3.35. *N*-Butyl-6-(5-(*cis*-3-isopropyl-4-oxo-3,4,4a,5,8,8a-hexahydrophthalazin-1-yl)-2-methoxyphenoxy)picolinamide (**3s**)

This compound was prepared from **3h** (160 mg, 0.367 mmol) and *n*-butyl amine (0.10 mL, 1.0 mmol) as described for **3q**. The title compound was obtained as a white solid (129 mg, 72%). ^{1}H NMR (500 MHz, CDCl$_3$): δ 7.88 (d, *J* = 7.3 Hz, 1H), 7.82 (t, *J* = 7.8 Hz, 1H), 7.72 – 7.67 (m, 2H), 7.52 (t, *J* = 5.6 Hz, 1H), 7.04 (d, *J* = 9.2 Hz, 1H), 7.00 (d, *J* = 8.1 Hz, 1H), 5.81 – 5.63 (m, 2H), 5.03 (hept, *J* = 6.7 Hz, 1H), 3.79 (s, 3H), 3.33 (q, *J* = 6.8 Hz, 2H), 3.31 – 3.26 (m, 1H), 3.05 – 2.97 (m, 1H), 2.77 – 2.71 (m, 1H), 2.24 – 2.12 (m, 2H), 2.09 – 1.99 (m, 1H), 1.45 (p, *J* = 7.0 Hz, 2H), 1.30 (d, *J* = 6.6 Hz, 3H), 1.28 – 1.22 (m, 2H), 1.19 (d, *J* = 6.7 Hz, 3H), 0.88 (t, *J* = 7.4 Hz, 3H). ^{13}C NMR (126 MHz, CDCl$_3$): δ 166.5, 163.7, 161.9, 153.1, 152.9, 148.0, 142.2, 140.8, 128.7, 126.1, 124.1, 123.9, 120.7, 116.9, 112.9, 112.2, 56.1, 46.9, 38.9, 34.9, 31.5, 31.1, 23.2, 22.4, 20.7, 20.3, 20.1, 13.9. LC-MS (ESI): t_R = 5.23 min, area: >98%, *m/z* 491 [M + H]$^+$. HRMS (ESI) *m/z*: [M + H]$^+$ calcd. for C$_{28}$H$_{35}$N$_4$O$_4$ 491.2653, found 491.2629.

4.3.36. *N*-(Furan-2-ylmethyl)-2-(5-(*cis*-3-isopropyl-4-oxo-3,4,4a,5,8,8a-hexahydrophthalazin-1-yl)-2-methoxyphenoxy)nicotinamide (**3t**)

This compound was prepared from **3e** (150 mg, 0.344 mmol) and furfuryl amine (0.62 mL, 7.0 mmol) as described for **3i**. The title compound was obtained as a white solid (96 mg, 54%). ^{1}H NMR (500 MHz, CDCl$_3$): δ 8.81 (t, *J* = 5.6 Hz, 1H), 8.19 (d, *J* = 7.4 Hz, 1H), 8.16 (d, *J* = 4.7 Hz, 1H), 7.79 (s, 1H), 7.75 (d, *J* = 8.7 Hz, 1H), 7.58 (s, 1H), 7.21 (t, *J* = 6.2 Hz, 2H), 6.39 (s, 1H), 6.30 (s, 1H), 5.73 – 5.60 (m, 2H), 4.87 (hept, *J* = 6.1 Hz, 1H), 4.54 (d, *J* = 5.7 Hz, 2H), 3.71 (s, 3H), 3.43 (dt, *J* = 11.4, 5.6 Hz, 1H), 2.82 (t, *J* = 5.7 Hz, 1H), 2.78 – 2.70 (m, 1H), 2.21 – 2.08 (m, 2H), 1.89 – 1.78 (m, 1H), 1.39 (s, 2H), 1.22 (d, *J* = 6.5 Hz, 3H), 1.12 (d, *J* = 6.6 Hz, 3H). ^{13}C NMR (126 MHz, DMSO-*d*$_6$): δ 166.1, 163.7, 159.4, 153.2, 152.7, 152.2, 149.1, 142.2, 141.6, 140.6, 127.8, 125.9, 124.3, 124.1, 120.9, 118.9, 117.7, 112.8, 110.5, 106.8, 56.0, 45.8, 36.4, 33.9, 30.0, 22.6, 22.0, 20.5, 20.1. LC-MS (ESI): t_R = 4.96 min, area: >98%, *m/z* 515 [M + H]$^+$. HRMS (ESI) *m/z*: [M + H]$^+$ calcd. for C$_{29}$H$_{31}$N$_4$O$_5$ 515.2289, found 515.2290.

4.3.37. *N*-(Furan-2-ylmethyl)-2-(5-(*cis*-3-isopropyl-4-oxo-3,4,4a,5,8,8a-hexahydrophthalazin-1-yl)-2-methoxyphenoxy)isonicotinamide (**3u**)

This compound was prepared from **3f** (140 mg, 0.321 mmol) and furfuryl amine (0.10 mL, 1.1 mmol) as described for **3q**. The title compound was obtained as a white solid (102 mg, 62%). ^{1}H NMR (500 MHz, CDCl$_3$): δ 8.22 (d, J = 5.1 Hz, 1H), 7.69 (s, 1H), 7.66 (d, J = 8.6 Hz, 1H), 7.39 (s, 1H), 7.32 – 7.27 (m, 2H), 7.02 (d, J = 8.6 Hz, 1H), 6.62 (t, 1H), 6.34 (d, J = 15.6 Hz, 2H), 5.80 – 5.62 (m, 2H), 5.02 (hept, J = 6.2 Hz, 1H), 4.64 (d, J = 5.1 Hz, 2H), 3.77 (s, 3H), 3.27 (dt, J = 11.2, 5.5 Hz, 1H), 3.05 – 2.93 (m, 1H), 2.72 (t, J = 5.2 Hz, 1H), 2.25 – 2.11 (m, 2H), 2.09 – 1.96 (m, 1H), 1.28 (d, J = 6.5 Hz, 3H), 1.17 (d, J = 6.6 Hz, 3H). ^{13}C NMR (126 MHz, CDCl$_3$): δ 166.6, 165.1, 164.2, 153.0, 153.0, 150.5, 148.5, 145.2, 142.7, 142.3, 128.7, 126.1, 124.2, 124.1, 120.6, 115.7, 112.5, 110.8, 108.7, 108.3, 56.2, 46.8, 37.2, 34.9, 31.1, 23.2, 22.5, 20.7, 20.3. LC-MS (ESI): t_R = 4.75 min, area: >98%, m/z 515 [M + H]$^+$. HRMS (ESI) m/z: [M + H]$^+$ calcd. for C$_{29}$H$_{31}$N$_4$O$_5$ 515.2289, found 515.2276.

4.3.38. *N*-(Furan-2-ylmethyl)-6-(5-(*cis*-3-isopropyl-4-oxo-3,4,4a,5,8,8a-hexahydrophthalazin-1-yl)-2-methoxyphenoxy)nicotinamide (**3v**)

This compound was prepared from **3g** (150 mg, 0.344 mmol) and furfuryl amine (0.61 mL, 6.9 mmol) as described for **3p**. The title compound was obtained as a white solid (54 mg, 31%). ^{1}H NMR (500 MHz, CDCl$_3$): δ 8.54 (s, 1H), 8.15 (d, J = 8.4 Hz, 1H), 7.74 – 7.65 (m, 2H), 7.37 (s, 1H), 7.02 (t, J = 9.1 Hz, 2H), 6.41 (s, 1H), 6.34 (s, 1H), 6.30 (s, 1H), 5.83 – 5.59 (m, 2H), 5.02 (hept, J = 6.3 Hz, 1H), 4.63 (d, J = 4.6 Hz, 2H), 3.77 (s, 3H), 3.28 (dt, J = 10.7, 5.0 Hz, 1H), 3.00 (d, J = 18.9 Hz, 1H), 2.72 (s, 1H), 2.28 – 2.11 (m, 2H), 2.10 – 1.97 (m, 1H), 1.29 (d, J = 6.3 Hz, 3H), 1.17 (d, J = 6.5 Hz, 3H). ^{13}C NMR (126 MHz, DMSO-d_6): δ 166.1, 164.5, 164.2, 153.1, 152.7, 152.2, 147.1, 142.2, 141.7, 139.2, 128.0, 125.9, 124.9, 124.4, 124.1, 120.2, 113.0, 110.6, 109.9, 107.0, 56.0, 45.8, 36.0, 33.9, 29.9, 22.6, 22.0, 20.5, 20.1. LC-MS (ESI): t_R = 4.75 min, area: 98%, m/z 515 [M + H]$^+$. HRMS (ESI) m/z: [M + H]$^+$ calcd. for C$_{29}$H$_{31}$N$_4$O$_5$ 515.2289, found 515.2273.

4.3.39. *N*-(Furan-2-ylmethyl)-6-(5-(*cis*-3-isopropyl-4-oxo-3,4,4a,5,8,8a-hexahydrophthalazin-1-yl)-2-methoxyphenoxy)picolinamide (**3w**)

This compound was prepared from **3h** (160 mg, 0.367 mmol) and furfuryl amine (0.10 mL, 1.1 mmol) as described for **3q**. The title compound was obtained as a white solid (131 mg, 69%). ^{1}H NMR (500 MHz, CDCl$_3$): δ 7.92 – 7.89 (m, 1H), 7.85 – 7.81 (m, 1H), 7.79 (t, J = 5.7 Hz, 1H), 7.69 (d, J = 8.1 Hz, 2H), 7.32 (dd, J = 1.8, 0.7 Hz, 1H), 7.00 (s, 2H), 6.29 (dd, J = 3.2, 1.9 Hz, 1H), 6.18 – 6.13 (m, 1H), 5.81 – 5.62 (m, 2H), 5.04 (hept, J = 6.6 Hz, 1H), 4.52 (d, J = 5.7 Hz, 2H), 3.74 (s, 3H), 3.28 (dt, J = 11.5, 5.8 Hz, 1H), 3.05 – 2.97 (m, 1H), 2.73 (t, J = 5.9 Hz, 1H), 2.24 – 2.11 (m, 2H), 2.07 – 1.97 (m, 1H), 1.30 (d, J = 6.6 Hz, 3H), 1.19 (d, J = 6.7 Hz, 3H). ^{13}C NMR (126 MHz, CDCl$_3$): δ 166.5, 163.6, 161.9, 153.1, 152.9, 151.2, 147.6, 142.3, 142.1, 140.8, 128.7, 126.2, 124.1, 124.0, 120.5, 117.1, 113.2, 112.3, 110.5, 107.4, 56.0, 46.8, 36.5, 34.8, 31.1, 23.2, 22.4, 20.7, 20.3. LC-MS (ESI): t_R = 5.05 min, area: >98%, m/z 515 [M + H]$^+$. HRMS (ESI) m/z: [M + H]$^+$ calcd. for C$_{29}$H$_{31}$N$_4$O$_5$ 515.2289, found 515.2271.

5. Author contributions

E.d.H., S.v.K., J.S., G.J.S. and I.J.P.d.E. were involved in compound design, synthesis and analysis. E.d.H. and A.J.K. were involved in virtual screening and docking. T.v.d.M., P.S., and M.S. were involved in the biochemical assays. D.M., G.C. and L.M. were involved in the phenotypic cellular assays. L.M., G.J.S.,

I.J.P.d.E., D.G.B. and R.L. supervised the experiments and conceived the project. E.d.H., G.J.S., and R.L. integrated all data and wrote the manuscript.

6. References

1. P. Büscher, G. Cecchi, V. Jamonneau*, et al.*, Human African trypanosomiasis, The Lancet, 390 (2017) 2397-2409.
2. P. Babokhov, A.O. Sanyaolu, W.A. Oyibo*, et al.*, A current analysis of chemotherapy strategies for the treatment of human African trypanosomiasis, Pathogens and Global Health, 107 (2013) 242-252.
3. C.H. Baker, S.C. Welburn, The Long Wait for a New Drug for Human African Trypanosomiasis, Trends Parasitol, (2018).
4. G. Eperon, M. Balasegaram, J. Potet*, et al.*, Treatment options for second-stage gambiense human African trypanosomiasis, Expert Review of Anti-infective Therapy, 12 (2014) 1407-1417.
5. E.D. Deeks, Fexinidazole: First Global Approval, Drugs, 79 (2019) 215-220.
6. E. de Morais-Teixeira, A. Rabello, M.M.G. Aguiar, In vitro activity and in vivo efficacy of fexinidazole against New World Leishmania species, Journal of Antimicrobial Chemotherapy, 74 (2019) 2318-2325.
7. E. Pelfrene, M. Harvey Allchurch, N. Ntamabyaliro*, et al.*, The European Medicines Agency's scientific opinion on oral fexinidazole for human African trypanosomiasis, PLOS Neglected Tropical Diseases, 13 (2019) e0007381.
8. J.C. Munday, L. Settimo, H.P. de Koning, Transport proteins determine drug sensitivity and resistance in a protozoan parasite, Trypanosoma brucei, Frontiers in Pharmacology, 6 (2015).
9. H.P. de Koning, Drug resistance in protozoan parasites, Emerging Topics in Life Sciences, 1 (2017) 627.
10. W.H. Organization, Trypanosomiasis, human African (sleeping sickness), https://www.who.int/news-room/fact-sheets/detail/trypanosomiasis-human-african-(sleeping-sickness); 2020, Accessed on October 25, 2020
11. R. Brun, J. Blum, F. Chappuis*, et al.*, Human african trypanosomiasis, The Lancet, 375 (2010) 148-159.
12. M. Packer , J.R. Carver , R.J. Rodeheffer *, et al.*, Effect of Oral Milrinone on Mortality in Severe Chronic Heart Failure, New England Journal of Medicine, 325 (1991) 1468-1475.
13. A. Hatzelmann, C. Schudt, Anti-Inflammatory and Immunomodulatory Potential of the Novel PDE4 Inhibitor Roflumilast in Vitro, Journal of Pharmacology and Experimental Therapeutics, 297 (2001) 267-279.
14. P.M.A. Calverley, K.F. Rabe, U.-M. Goehring*, et al.*, Roflumilast in symptomatic chronic obstructive pulmonary disease: two randomised clinical trials, The Lancet, 374 (2009) 685-694.
15. M. Boolell, M.J. Allen, S.A. Ballard*, et al.*, Sildenafil: an orally active type 5 cyclic GMP-specific phosphodiesterase inhibitor for the treatment of penile erectile dysfunction, International Journal of Impotence Research, 8 (1996) 47-52.
16. M. Oberholzer, G. Marti, M. Baresic*, et al.*, The Trypanosoma brucei cAMP phosphodiesterases TbrPDEB1 and TbrPDEB2: flagellar enzymes that are essential for parasite virulence, The FASEB Journal, 21 (2007) 720-731.
17. S. Kunz, J.A. Beavo, M.A. D'Angelo*, et al.*, Cyclic nucleotide specific phosphodiesterases of the kinetoplastida: A unified nomenclature, Molecular and Biochemical Parasitology, 145 (2006) 133-135.
18. H.P. de Koning, M.K. Gould, G.J. Sterk*, et al.*, Pharmacological validation of Trypanosoma brucei phosphodiesterases as novel drug targets, Journal of Infectious Diseases, 206 (2012) 229-237.
19. K.M. Orrling, C. Jansen, X.L. Vu*, et al.*, Catechol pyrazolinones as trypanocidals: fragment-based design, synthesis, and pharmacological evaluation of nanomolar inhibitors of trypanosomal phosphodiesterase B1, Journal of Medicinal Chemistry, 55 (2012) 8745-8756.
20. J. Veerman, T. van den Bergh, K.M. Orrling*, et al.*, Synthesis and evaluation of analogs of the phenylpyridazinone NPD-001 as potent trypanosomal TbrPDEB1 phosphodiesterase inhibitors and in vitro trypanocidals, Bioorganic & Medicinal Chemistry, 24 (2016) 1573-1581.
21. V. Boswell-Smith, D. Spina, C.P. Page, Phosphodiesterase inhibitors, British Journal of Pharmacology, 147 (2006) S252-S257.
22. C. Jansen, H. Wang, A.J. Kooistra*, et al.*, Discovery of NovelTrypanosoma bruceiPhosphodiesterase B1 Inhibitors by Virtual Screening against the Unliganded TbrPDEB1 Crystal Structure, Journal of Medicinal Chemistry, 56 (2013) 2087-2096.
23. P.M. Seldon, P.J. Barnes, K. Meja*, et al.*, Suppression of lipopolysaccharide-induced tumor necrosis factor-alpha generation from human peripheral blood monocytes by inhibitors of phosphodiesterase 4: interaction with stimulants of adenylyl cyclase., Molecular Pharmacology, 48 (1995) 747-757.
24. A.R. Blaazer, A.K. Singh, E. de Heuvel*, et al.*, Targeting a subpocket in Trypanosoma brucei phosphodiesterase B1 (TbrPDEB1) enables the structure-based discovery of selective inhibitors with trypanocidal activity, Journal of Medicinal Chemistry, 61 (2018) 3870-3888.
25. M. Van der Mey, A. Hatzelmann, I.J. Van der Laan*, et al.*, Novel Selective PDE4 Inhibitors. 1. Synthesis, Structure-Activity Relationships, and Molecular Modeling of 4-(3, 4-Dimethoxyphenyl)-2 H-phthalazin-1-ones and Analogues, Journal of Medicinal Chemistry, 44 (2001) 2511-2522.

26. M. Van der Mey, A. Hatzelmann, G.P.M. Van Klink*, et al.*, Novel Selective PDE4 Inhibitors. 2. Synthesis and structure-activity relationships of 4-aryl-substituted cis-tetra- and cis-hexahydrophthalazinones, Journal of Medicinal Chemistry, 44 (2001) 2523-2535.
27. E. de Heuvel, A.K. Singh, E. Edink*, et al.*, Alkynamide phthalazinones as a new class of TbrPDEB1 inhibitors, Bioorganic & Medicinal Chemistry, 27 (2019) 3998-4012.
28. E. de Heuvel, A.K. Singh, P. Boronat*, et al.*, Alkynamide phthalazinones as a new class of TbrPDEB1 inhibitors (Part 2), Bioorganic & Medicinal Chemistry, 27 (2019) 4013-4029.
29. M. Sijm, J. Siciliano de Araújo, S. Kunz*, et al.*, Phenyldihydropyrazolones as Novel Lead Compounds Against Trypanosoma cruzi, ACS Omega, 4 (2019) 6585-6596.
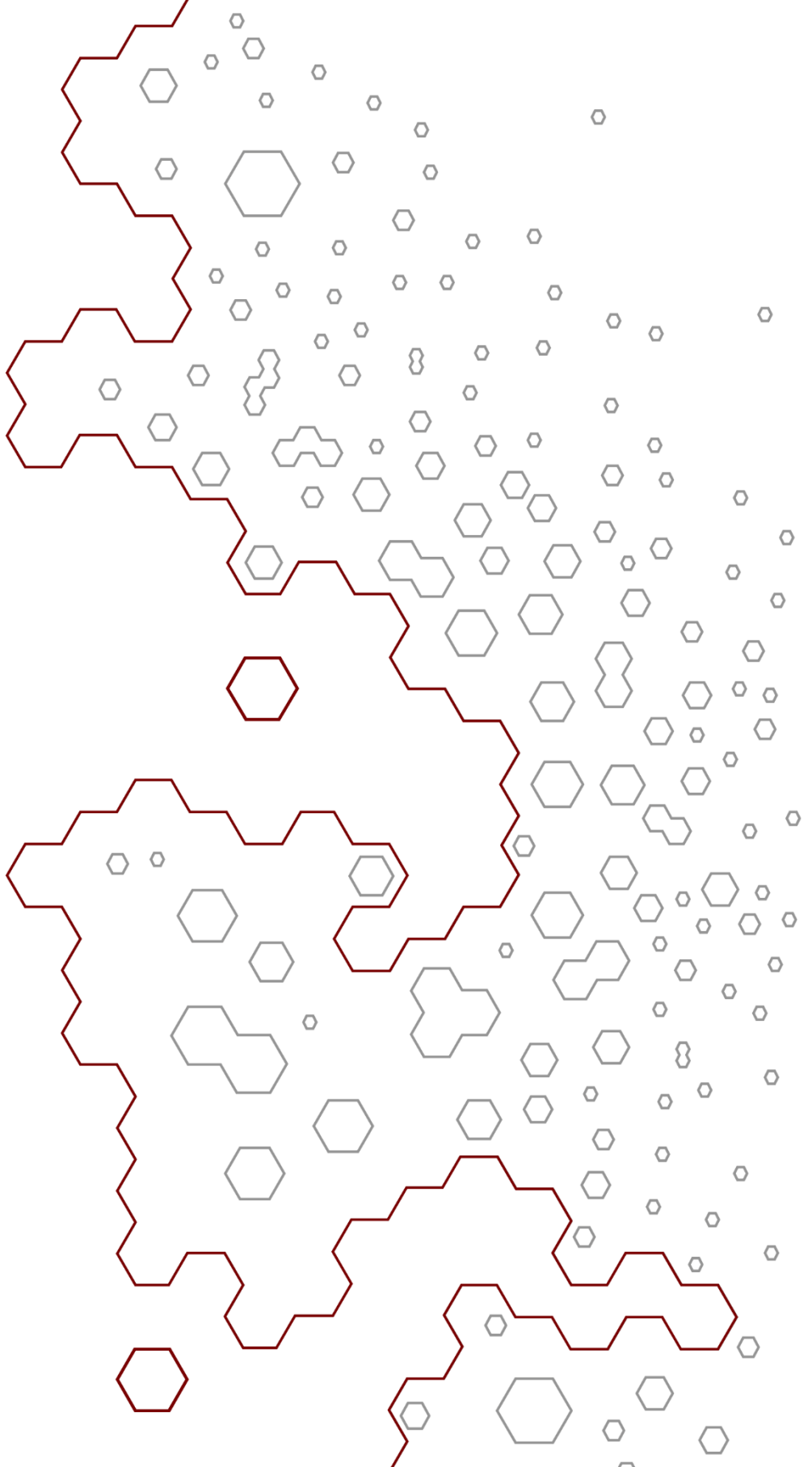
Chapter 4

Exploration of rigid linker structures for development of phthalazinone-based TbrPDEB1 inhibitors

Erik de Heuvel, Abhimanyu K. Singh, Ewald Edink, Tiffany van der Meer, Melanie van der Woude, Payman Sadek, Mikkel P. Krell-Jørgensen, Toine van den Bergh, Johan Veerman, Guy Caljon, Titilola D. Kalejaiye, Maikel Wijtmans, Louis Maes, Harry P. de Koning, Geert Jan Sterk, Marco Siderius, Iwan J.P. de Esch, David G. Brown, Rob Leurs.

Abstract

Several 3',5'-cyclic nucleotide phosphodiesterases (PDEs) have been validated as good drug targets for a large variety of diseases. *Trypanosoma brucei* PDEB1 (TbrPDEB1) has been designated as a promising drug target for the treatment of human African trypanosomiasis. Recently, the first class of selective nanomolar TbrPDEB1 inhibitors was obtained by targeting the parasite specific P-pocket. However, these biphenyl-substituted tetrahydrophthalazinone-based inhibitors did not show potent cellular activity against *Trypanosoma brucei (T. brucei)* parasites, leaving room for further optimization. Herein, we report the discovery of a new class of potent TbrPDEB1 inhibitors that display improved activities against *T. brucei* parasites. Exploring different linkers between the reported tetrahydrophthalazinone core scaffold and the amide tail group resulted in the discovery of alkynamide phthalazinones as new TbrPDEB1 inhibitors, which exhibit submicromolar activities versus *T. brucei* parasites and no cytotoxicity to human MRC-5 cells. Elucidation of the crystal structure of alkynamide **8b** (NPD-048) bound to the catalytic domain of TbrPDEB1 shows a bidentate interaction with the key-residue Gln874 and good directionality towards the P-pocket. Incubation of trypanosomes with alkynamide **8b** results in an increase of intracellular cAMP, validating a PDE-mediated effect *in vitro* and providing a new interesting compound series for further studies towards selective TbrPDEB1 inhibitors with potent phenotypic activity.

4

1. Introduction

Human African trypanosomiasis (HAT), one of the neglected tropical diseases (NTDs), is caused by two members of the trypanosomatids family, i.e. *Trypanosoma brucei (T.b.) rhodesiense* and *T.b. gambiense*.[1] This disease, also called African sleeping sickness, is fatal when left untreated and can have a big socioeconomic effect on rural populations in sub-Saharan Africa.[2] Although the disease was almost eradicated mid-1960s by active screening programs, it re-emerged in the 1980s as a result of discontinued disease surveillance and control programmes.[2, 3] Five drugs are commonly used for treatment of HAT, but all have major disadvantages including subspecies selectivity, disease stage selectivity, complex administration and toxicity.[4-7] First-stage treatments are generally not effective for the second-stage of the disease, while drugs for the second-stage of the disease are often toxic and require complex administration protocols.[2, 4, 8] Much of the HAT pharmacopoeia is becoming redundant because of drug resistance, necessitating new control strategies, including new drugs.[6, 9, 10]

Human 3',5'-cyclic nucleotide phosphodiesterases (hPDEs) have proven to be successful drug targets for a broad range of diseases, including COPD,[11, 12] heart failure[13] and erectile dysfunction.[14] In 2007 Oberholzer *et al.* published *T. brucei* PDEs as potential new targets for the treatment of HAT.[15] The parasite genome encodes four different class I PDE families, PDEA-D, and a simultaneous reduction in the expression of *Trypanosoma brucei* PDEB1 (TbrPDEB1) and TbrPDEB2 with siRNA results in fatal cell cycle defects.[15, 16] Furthermore, it was shown that gene silencing by siRNA prevents parasitemia in mice, further demonstrating the potential of TbrPDEB1 and TbrPDEB2 as a target for drugs against HAT.[15]

Several reports have been published about potential starting points for selective inhibitors of this class of parasitic proteins, albeit with mixed results.[17-24] De Koning *et al*. reported a potent nanomolar TbrPDEB1 inhibitor (NPD-001, **1**, Figure 1), which displays very similar anti-parasitic effects compared to cells treated with TbrPDEB1/2 siRNA, specifically a fatal inability to complete the abscission phase of the cell division.[25] However, the phthalazinone-based scaffold was originally developed as a human PDE4 (hPDE4) inhibitor,[26, 27] explaining why NPD-001 and close analogues exhibit sub-nanomolar activities for hPDE4.[24, 28] Such a strong hPDE4 activity of TbrPDEB1 inhibitors is disqualifying for a potential drug, as hPDE4

inhibition is associated with unacceptable side effects (e.g. emesis, gastro-intestinal disturbance, headache and immune suppression).[24, 29-31]
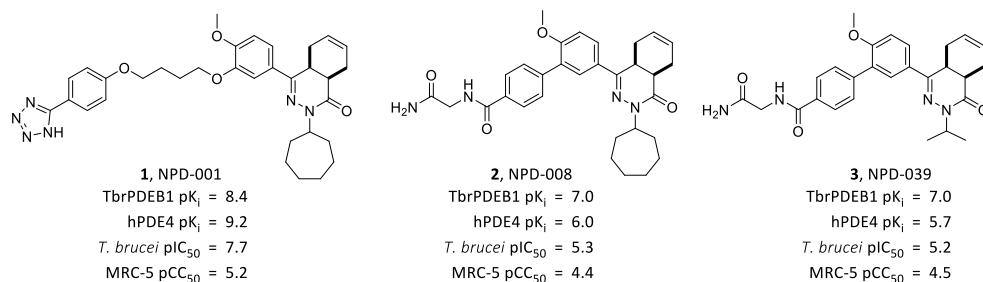

1, NPD-001
TbrPDEB1 pK_i = 8.4
hPDE4 pK_i = 9.2
T. brucei pIC_{50} = 7.7
MRC-5 pCC_{50} = 5.2

2, NPD-008
TbrPDEB1 pK_i = 7.0
hPDE4 pK_i = 6.0
T. brucei pIC_{50} = 5.3
MRC-5 pCC_{50} = 4.4

3, NPD-039
TbrPDEB1 pK_i = 7.0
hPDE4 pK_i = 5.7
T. brucei pIC_{50} = 5.2
MRC-5 pCC_{50} = 4.5

Figure 1. Previously reported TbrPDEB1 inhibitors.[25, 28, 32]

Structural comparison between hPDE4 and TbrPDEB1 reveals the presence of an additional parasite-specific pocket (P-pocket) near the active site, which can be exploited to obtain selective TbrPDEB1 inhibitors.[19, 33] Although docking studies had predicted P-pocket occupancy for **1**,[28] the recent elucidation of the X-ray structure of the ligand-protein complex shows the absence of P-pocket interactions by **1**, thereby explaining the lack of TbrPDEB1 selectivity over hPDE4.[32] Recently, we reported the first class of selective TbrPDEB1 inhibitors by rigidifying the catechol linker with a biphenyl system.[32] The two most potent and selective molecules (NPD-008 and NPD-039, **2** and **3** respectively) are shown in Figure 1. The co-crystal structures of **2** and **3** bound to the catalytic domain of TbrPDEB1 confirmed that the P-pocket is indeed occupied by the glycinamide tail. Unfortunately, both compounds show reduced phenotypic activity against *T. brucei* parasites *in vitro*, halting their further development as anti-*T. brucei* agents and indicating that improvement of the trypanocidal activity is desired. [32]

Herein, we describe the search and discovery of other rigidified molecules based on the same phthalazinone scaffold as **2** and **3**. This new class of TbrPDEB1 inhibitors exhibits submicromolar potency against *T. brucei* and induces a robust, dose-dependent increase in the intracellular cAMP levels of bloodstream form trypanosomes, at concentrations similar to its trypanocidal IC_{50}-value.

2. Results and discussion

2.1. Compound design and inhibitory activity against TbrPDEB1

Since targeting the P-pocket via the biphenyl linker resulted in the expected selectivity of the phthalazinone-based inhibitors **2** and **3** for TbrPDEB1 over hPDE4,

further optimization was started by installing small groups on the biphenyl linker. However, the possibilities to modify the benzamide ring seem very limited, since small changes in size and electron density of the ring dramatically decrease the activity against TbrPDEB1 (Table 1). The minor change of a proton (NPD-008, **2**) to an *ortho-* or *meta-*fluorine (**4a** and **4d**, respectively) substitution already results in a decrease in potency by at least 0.9 log units. A larger decrease in potency is observed for electron-donating substituents such as methyl and methoxy groups on either position (**4b**, **4c**, **4e** and **4f**). Subtle differences in potency are observed between *ortho-* and *meta-* substitutions, in favor of the modification on the *meta-*position. In addition, the flexibility of the amide bond was reduced by incorporating an isoindole as linker in an attempt to force the substituents to occupy the P-pocket (**5a-c**, Table 1). However, this too resulted in a more than 10-fold decrease in potency and adding an ether or amide tail group to N1 (**5b** and **5c**, respectively) did not improve activity either.
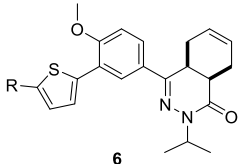
Table 1. Structure-activity relationship of substituted benzamide phthalazinones as TbrPDEB1 inhibitors.
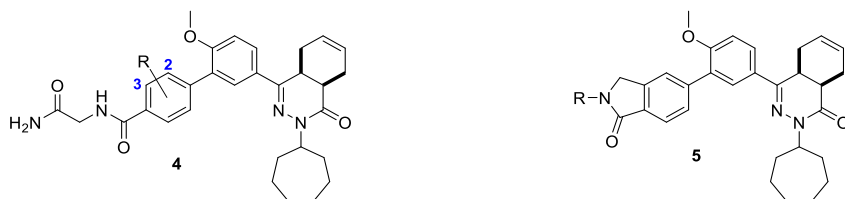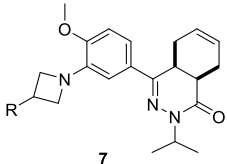
#	NPD-	R	pK$_i$ [a)]	#	NPD-	R	pK$_i$[a)]
2	008	H	7.0 [b)]	**5a**	051	H	5.8 ± 0.03
4a	932	2-F	5.7 ± 0.1	**5b**	056	CH$_2$CH$_2$OMe	5.9 ± 0.1
4b	948	2-Me	<5.0	**5c**	052	CH$_2$CONH$_2$	5.9 ± 0.01
4c	929	2-OMe	5.1 ± 0.1 [c)]				
4d	945	3-F	6.1 ± 0.1				
4e	931	3-Me	5.7 ± 0.1				
4f	930	3-OMe	5.2 ± 0.1 [c)]				

[a)]Mean and S.E.M. values of at least 3 independent experiments. [b)]Reported value[32] [c)]No full dose response curve obtained.

Table 2. Structure-activity relationship of phthalazinones with reduced linker size against TbrPDEB1.
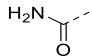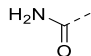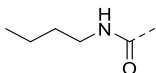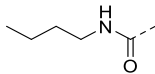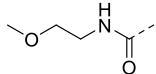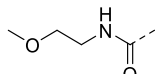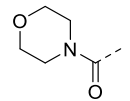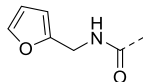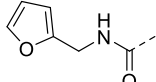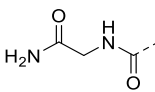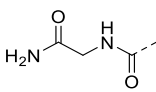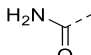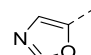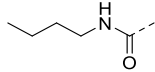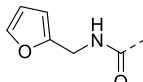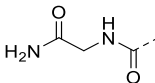
6

7

8

#	NPD-	R	pK_i [a]	#	NPD-	R	pK_i [a]
2	008	-	7.0 [b]	**8a**	064	H	5.4 ± 0.1 [c]
3	039	-	7.0 [b]	**8b**	048	H$_2$N–C(=O)–	6.2 ± 0.02
6a	1030	H$_2$N–C(=O)–	5.0 ± 0.06 [c]	**8c**	055	butyl-NH–C(=O)–	6.4 ± 0.02
6b	1027	butyl-NH–C(=O)–	<5.0	**8d**	050	MeO-ethyl-NH–C(=O)–	6.1 ± 0.1
6c	092	MeO-ethyl-NH–C(=O)–	<5.0	**8e**	054	morpholine-C(=O)–	6.0 ± 0.1
6d	1029	furfuryl-NH–C(=O)–	<5.0	**8f**	053	furfuryl-NH–C(=O)–	6.3 ± 0.01
6e	1028	H$_2$N–C(=O)–CH$_2$–NH–C(=O)–	<5.0	**8g**	046	H$_2$N–C(=O)–CH$_2$–NH–C(=O)–	6.2 ± 0.1
7a	1259	H$_2$N–C(=O)–	<5.0	**8h**	065	oxazolyl	<5.0
7b	1256	butyl-NH–C(=O)–	<5.0				
7c	1258	furfuryl-NH–C(=O)–	<5.0				
7d	1257	H$_2$N–C(=O)–CH$_2$–NH–C(=O)–	<5.0				

[a] Mean and S.E.M. values of at least 3 independent experiments. [b] Reported values.[32] [c] No full dose response curve obtained.

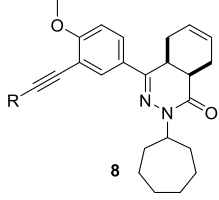As increasing linker size did not improve potency, linker size reductions were investigated. In view of the molecular weight, clogP and aqueous solubility of the molecules, it was decided to replace the cycloheptyl substituent of the phthalazinone scaffold with an isopropyl group for this series, as this modification has been shown to yield a small positive effect on the selectivity profile (compare **2** and **3**, Figure 1). In search for a bioisostere of the phenyl group a thiophene ring was introduced as linker, leading to dramatically reduced TbrPDEB1 activity (Table 2), with all thiophene compounds (**6a-e**) showing at least a 100-fold reduction in TbrPDEB1 activity compared to **3**, including **6e**, which represents a direct replacement of the phenyl moiety of **3** with a thiophene. A similar effect was observed when the phenyl ring was replaced by the non-aromatic azetidine group, as none of the azetidines (**7a-d**) display activities below 10 µM.

The results indicate that the vector that defines the accessibility of the P-pocket is not very tolerant to changes. To illustrate the differences in addressing the P-pocket, the unsubstituted thiophene amide and azetidine amide were docked in the crystal structure of TbrPDEB1 ligated with **2** (PDB id: 5G2B) using PLANTS. As illustrated in Figure 2, a subtle difference in directionality of the linker is observed for the thiophene and azetidine linkers, when compared to **2**. Both analogues bend the carboxamide group towards the protein helix and interact with the conserved residue Gln874, but the interaction seems unproductive as the thiophene-linked amide is in close proximity of the protein and most likely will sterically clash with it.
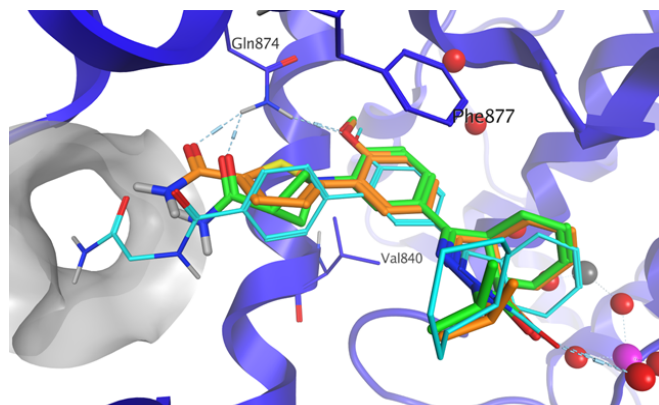
Figure 2. Binding prediction of the phthalazinones with a thiophene amide (orange) and azetidine amide (green) linker superposed on the X-ray structure of **2** (cyan) co-crystallized in the catalytic domain of TbrPDEB1 (modelled using the PLANTS software package). Key residues, active site water molecules and metals are shown for clarity.

Therefore, new derivatives with an alkyne functionality were designed that more closely obey the vector as defined by the phenyl-substituent in **2**. A reduction in TbrPDEB1 potency was observed for all alkynamides when compared to **2** (Table 2). However, modifying the terminal amide (NPD-048, **8b**) with different tail groups gave, as seen with the phenyl linker,[32] a small increase in potency. More flexible tail groups such as a *n*-butyl (**8c**) or furfuryl (**8f**) show a slightly higher activity (pK_i = 6.4 ± 0.1 and 6.3 ± 0.01, respectively) when compared with the more rigid tail groups such as morpholine (**8e**, pK_i = 6.0 ± 0.1). Both observations are in agreement with the previously observed SAR with the biphenyl linker reported by Blaazer *et al*.[32] In contrast to **2**, the highest potency in this new series of TbrPDEB1 inhibitors was not observed with a glycinamide tail (**8g**), but with an *n*-butyl (**8c**) or furfuryl tail (**8f**). Constraining the heteroatoms in an oxazole ring (**8h**) or absence of the amide (**8a**) further reduced inhibitory activity, which could indicate an important function for the amide functionality.

2.2. Biological evaluation

2.2.1. Selectivity alkynamides over hPDE4

To assess the selectivity of the alkynamides as inhibitors for TbrPDEB1 over hPDE4, the inhibitory activity of the alkynamides on hPDE4 was measured (Table 3). In contrast to the previously published selective TbrPDEB1 inhibitor NPD-008 (**2**), the primary carboxamide (**8b**) and the alkynamides **8c** – **8f** do not display the desired selectivity for inhibition for TbrPDEB1 over human PDE4 (Table 3). Only minor differences in the selectivity index (SI) are observed (range -0.3 – 0.3). Although the current set of alkynamides does not display the desired selectivity over hPDE4, when compared to the reference inhibitor NPD-001 (**1**) with a SI value of -0.8, the current alkynamide scaffold might offer future options to optimize the selectivity profile via structure-based design (*vide infra*).

2.2.2. Antitrypanosomal activity and cytotoxicity

As mentioned before, the biphenyls **2** or **3** show a reduced potency against the parasite (*T. brucei* pIC_{50} = 5.3 ± 0.2 and 5.2 ± 0.1, respectively) when compared to the potency against TbrPDEB1 (pK_i = 7.0 for both compounds) and an undesirably high cytotoxicity profile for human cells.[32] The alkynamides display submicromolar potencies against TbrPDEB1 and were therefore tested for their antitrypanosomal activity on *T. brucei* parasites, with MRC-5 cells as control for general cytotoxicity

towards human cells. The anti-parasitic activity of all the alkynamides was increased when compared to the corresponding biphenyl class (Table 3). The primary carboxamide **8b** (*T. brucei* pIC$_{50}$ 6.0 ± 0.3) is 6-fold more potent than NPD-008, but the cytotoxicity (MRC-5 pCC$_{50}$ = 5.0 ± 0.1) is also increased. Both **8c** and **8f** display an *in vitro* potency against *T. brucei* of 0.6 µM and are non-toxic to human MRC-5 cells at the highest concentration used (64 µM), resulting in an interesting phenotypic profile. Installing a glycinamide tail (**8g**) led to an almost equipotent molecule with decreased antitrypanosomal activity and increased cytotoxicity (*T. brucei* pIC$_{50}$ 5.4 ± 0.01 and MRC-5 pCC$_{50}$ = 5.4 ± 0.02). *N*-Methoxyethyl-substituted alkynamide **8d** was unexpectedly inactive on both cell lines for unknown reasons.

Table 3. Selectivity data for the synthesized alkynamides and their phenotypical activities (mean ± S.E.M).

#	TbrPDEB1 pK$_i$	hPDE4 pK$_i$	ΔpK$_i$	*T. brucei* (pIC$_{50}$)	MRC-5 (pCC$_{50}$)
2	7.0 [a)]	6.0 [a)]	1.0	5.3 ± 0.2 [a)]	4.4 [a)]
3	7.0 [a)]	5.7 [a)]	1.3	5.2 ± 0.1 [a)]	4.5 [a)]
8b	6.2 ± 0.02	6.5 ± 0.2	-0.3	6.0 ± 0.3	5.0 ± 0.1
8c	6.4 ± 0.02	6.2 ± 0.2	0.2	6.2 ± 0.3	<4.2
8d	6.1 ± 0.1	5.8 ± 0.3	0.3	<4.2	<4.2
8f	6.3 ± 0.01	6.4 ± 0.1	-0.1	6.2 ± 0.1	4.3 ± 0.2
8g	6.2 ± 0.1	ND	-	5.4 ± 0.01	5.4 ± 0.02

[a)] Reported values [32]

2.2.3. Intracellular cAMP levels

As reported previously, TbrPDEB1 inhibitors such as **1** and **2** are able to increase intracellular cAMP levels in *T. brucei* parasites,[25, 32] and we sought to confirm that NPD-048 (**8b**) was likewise acting on the parasite principally through inhibition of the *T. brucei* PDEs. Incubation of *T. brucei* parasites with 3.2 µM and 8 µM of **8b** resulted in highly significant increases in intracellular cAMP levels when compared to untreated control cells (19.8 pmol/5×10^6 cells (*P*<0.01) and 311 pmol/5×10^6 cells (*P*<0.001) *vs.* 6.66 pmol/5×10^6 cells, respectively).

2.2.4. Crystal structures

In order to investigate the binding mode of the alkynamides, we determined the co-crystal structures of the TbrPDEB1 and hPDE4D catalytic domains in complex with **8b**, at 2.10 and 2.16 Å resolution, respectively (Figure 3A, B). The PDE inhibitor

binds in an almost identical manner to both catalytic sites, maintaining the key hydrophobic interactions in the hydrophobic clamp region and a hydrogen bond interaction with the conserved Gln874, all mediated through its anisole moiety.
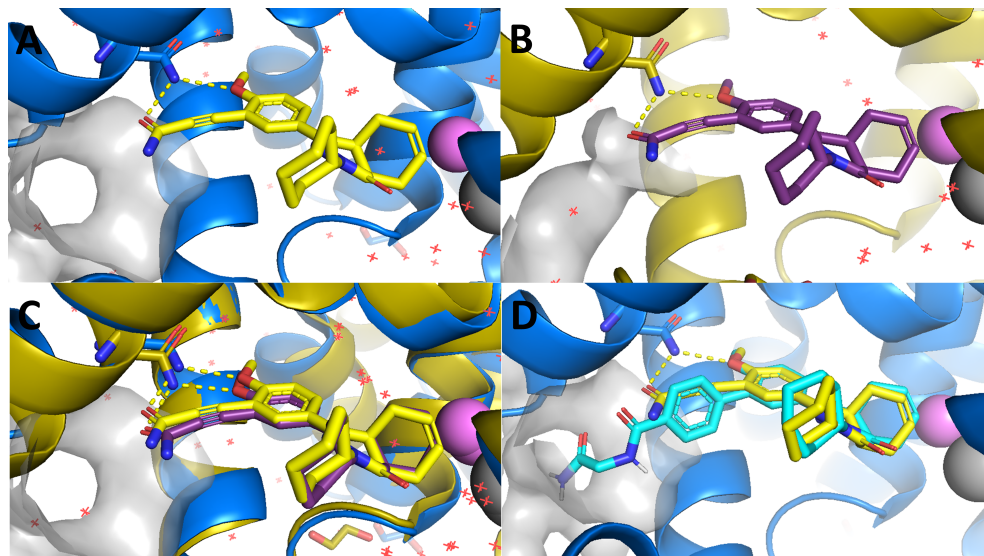
Figure 3: A) X-ray structure of **8b** in TbrPDEB1 (PDB id: 6FTM) and B) hPDE4D (PDB id: 6FTW). A molecular surface of the P-pocket region in TbrPDEB1 (grey) and hPDE4D (purple) is displayed to highlight the structural differences between both enzymes. C) Overlay of **8b** in TbrPDEB1 (blue) and hPDE4D (dark yellow). D) Overlay of **8b** and NPD-008 (**2**) in TbrPDEB1. Key residues for interaction with the substrate are shown and active site water molecules are shown as red crosses. Binding site metals zinc and magnesium are displayed as grey and magenta spheres, respectively.

Furthermore, the carbonyl of the alkynamide creates a second hydrogen bond interaction with the conserved Gln874. The co-crystal structures clearly show that the alkynamide inhibitor **8b** engages identically with both enzymes (Figure 3C). Moreover, the inability of **8b** to reach the P-pocket explains its lack of selectivity towards TbrPDEB1. The alignment of the binding pose of **8b** with the binding pose of **2** in TbrPDEB1 (Figure 3D) shows that **8b** adopts a binding mode which is slightly rotated to facilitate the double interaction with Gln874, positioning the carboxamide in front of the P-pocket. This positioning provides an interesting opportunity for optimization of the alkynamide phthalazinone scaffold. Further exploration by extension of the tail group to target the P-pocket is currently ongoing.

2.3. Synthesis

The racemic *cis*-cycloheptyl tetrahydrophthalazinone scaffold (building block **9**) was synthesized as described previously.[27, 28, 32] Derivatives **4** and **5** were synthesized via two different synthetic pathways. Firstly, a Suzuki reaction of **9** with the corresponding phenylboronic acid was performed to obtain carboxylic acid **10a** and methyl ester **10b**, which was hydrolyzed to carboxylic acid **10c** in quantitative yield (Scheme 1). The glycinamide tail was introduced by an amide coupling using EDC/HOAt to afford **4b** and **4d**. Secondly, building block **9** was converted to pinacol boronate ester **11** in moderate yield and a subsequent Suzuki reaction with the corresponding arylbromide **12a-d** (synthesized from the corresponding 4-bromobenzoic acid and glycinamide using EDC/HOAt) led to the desired compounds **4a**, **4c**, **4e** and **4f**. Isoindolinones (**5a-c**) were synthesized using a Suzuki reaction followed by an alkylation using the corresponding alkyl bromide.
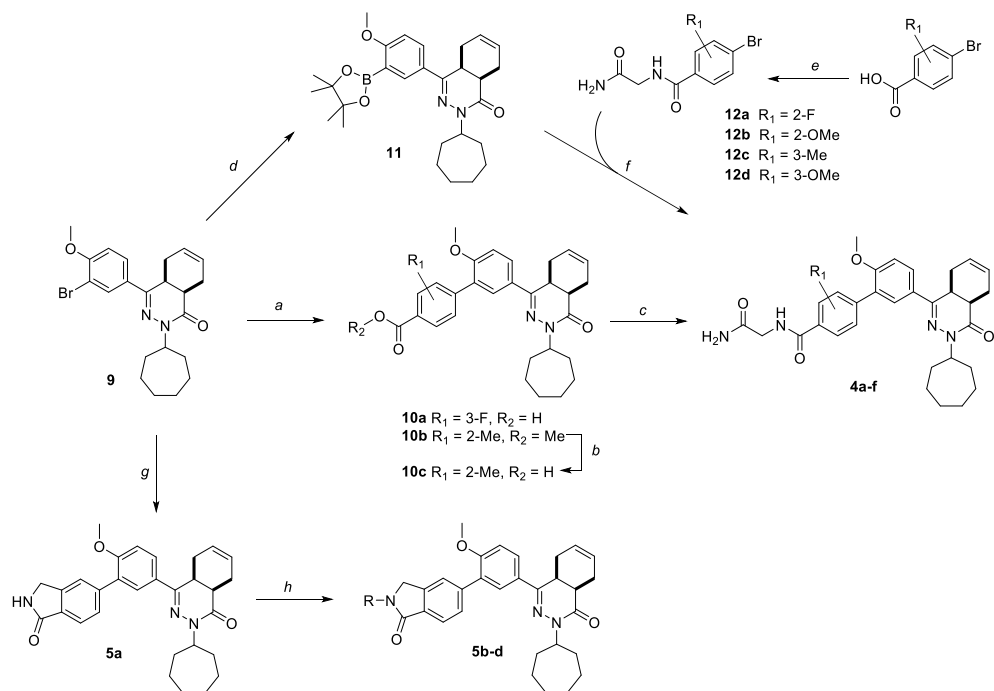
Scheme 1. Reagents and conditions: *a*) corresponding boronic acid, PdCl$_2$(dppf), Na$_2$CO$_3$, DME, H$_2$O, 100 °C, 5 h, **10a**: 46%, **10b**: 39%; *b*) NaOH, THF, MeOH, 50 °C, 16 h, 98%; *c*) For **4b** and **4d**: glycinamide.HCl, EDC.HCl, HOAt, Et$_3$N, DCM, rt, 1 h, **4b**: 83%, **4d**: 23%; *d*) Bis(pinacolato)diboron, PdCl$_2$(dppf), KOAc, dioxane, reflux, 2.5 h, 28%; *e*) glycinamide.HCl, EDC.HCl, HOAt, Et$_3$N, DCM, rt, overnight, 47-59%; *f*) For **4a**, **4c**, **4e** and **4f**: corresponding bromide, PdCl$_2$(dppf), Na$_2$CO$_3$, DME, H$_2$O, 100 °C, 5 h, 27-57%; *g*) 5-(4,4,5,5-tetramethyl-1,3,2-dioxaborolan-2-yl)isoindolin-1-one, PdCl$_2$(dppf), Na$_2$CO$_3$, DME, H$_2$O, 100 °C, 5 h, 73%; *h*) 1) NaH, DMF, rt, 30 min; 2) R-Br, rt, 1.5 h, 14-27%.

Incorporation of the alkyne functionality to carboxylic acid **13** could be achieved in a Sonogashira reaction of propiolic acid with **9** (Scheme 2). However, since **13** was found to slowly degrade over time, it was decided to use the crude material in a subsequent reaction with glycinamide to obtain **8g**, albeit in an extremely low yield. An alternative route towards the alkynamides avoiding the unstable carboxylic acid **13** involved synthesizing methyl ester **14** from pinacol boronate **11** (Scheme 1) in moderate yield, followed by an amidation in absence (for **8b**) or presence (for **8c-f**) of the Lewis acid trimethylaluminium. Unfortunately, synthesis of alkynamide **8g** was unsuccessful using this procedure. The primary alkyne **8a** was synthesized via a Sonogashira reaction with TMS-acetylene followed by deprotection of **15** with NaOH, both in high yield. The resulting alkyne in **8a** was converted into aldehyde **16** and used subsequently in the Van Leusen oxazole synthesis to obtain **8h**.
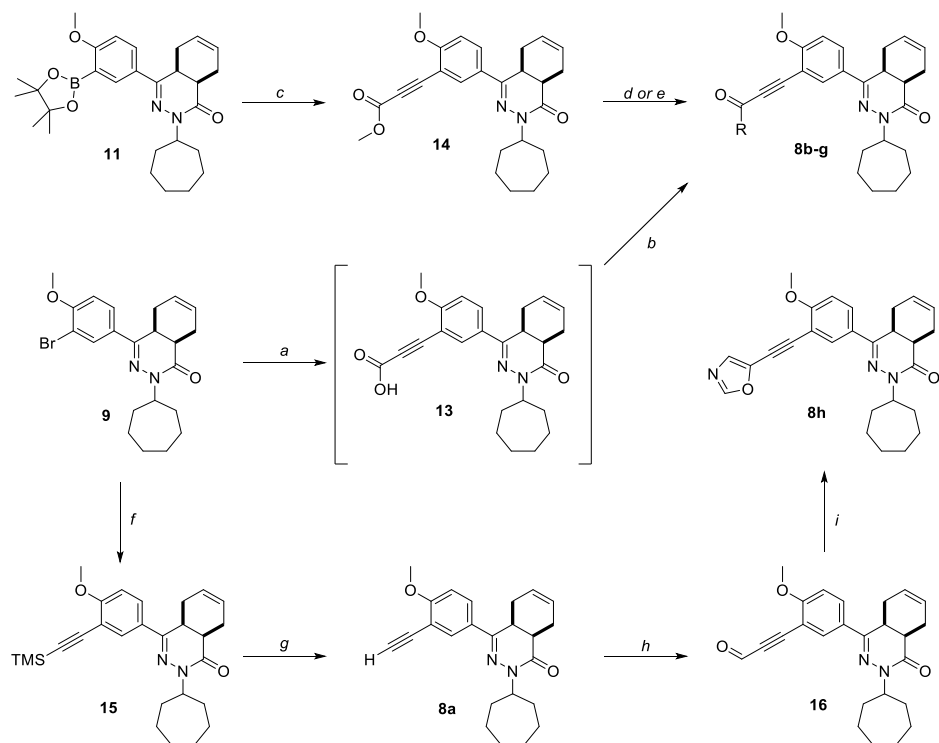
Scheme 2. Reagents and conditions: *a*) Propiolic acid, Pd(PPh₃)₂Cl₂, dppb, DBU, DMSO, 50 °C, 15 h, used crude; *b*) For **8g**: glycinamide.HCl, EDC.HCl, HOAt, Et₃N, DCM, rt, 30 h, 1% over 2 steps; *c*) Methyl propiolate, Pd(OAc)₂, K₂CO₃, AgO, 70 °C, 3 h, 53%; *d*) For **8b**: NH₃, MeOH, rt, 2 h, 89%; *e*) For **8c-8f**: corresponding amine, AlMe₃, PhMe, 50 °C, 1 d, 16-37%; *f*) Ethynyltrimethylsilane, Pd(PPh₃)₂Cl₂, CuI, TEA, 80 °C, 3 h, 80%; *g*) NaOH, MeOH, H₂O, rt, 2 h, 91% yield; *h*) 1) *n*-BuLi, THF, −78 °C, 30 min, 2) DMF, −78 °C, 1.5 h, 69%; *i*) 1-((isocyanomethyl)sulfonyl)-4-methylbenzene, K₂CO₃, MeOH, reflux, 1.5 h, 47%.

The racemic *cis*-isopropyl tetrahydrophthalazinone building block (**17**) was synthesized using the same procedure as described previously. Building block **17** was used in a Suzuki reaction using 5-boronothiophene-2-carboxylic acid, followed by an amide coupling to obtain **6a-e** (Scheme 3). The azetidine linker was introduced using a Buchwald-Hartwig cross coupling reaction with 3-cyanoazetidine to obtain nitrile **19**. The nitrile was hydrolyzed using NaOH and the formed carboxylic acid **20** was coupled to various amines using EDC/HOBt to obtain azetidines **7a-d**.
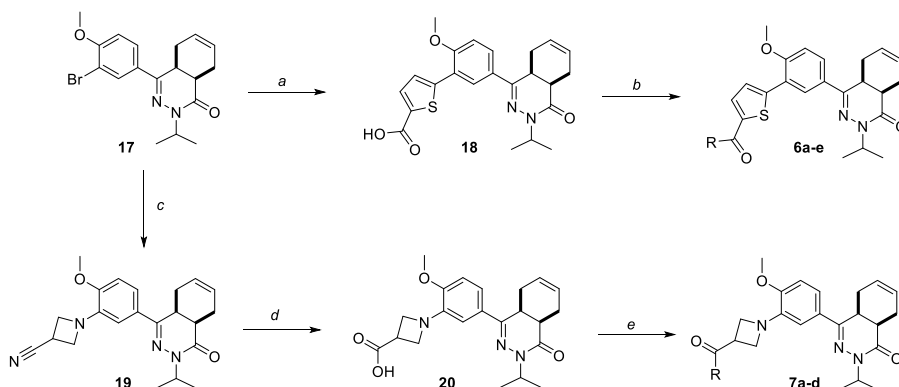
Scheme 3. Reagents and conditions: *a*) 5-boronothiophene-2-carboxylic acid , PdCl$_2$(dppf), Na$_2$CO$_3$, DME, H$_2$O, reflux, 5 h, 73%; *b*) Corresponding amine, EDC.HCl, HOBt, Et$_3$N, DCM, rt, 1 d, 15-76%; *c*) azetidine-3-carbonitrile.HCl, Cs$_2$CO$_3$, Pd(OAc)$_2$, XPhos, PhMe, 100 °C, 3 d, 46%; *d*) NaOH, H$_2$O, EtOH, 75 °C, 1 d, 47%; *e*) corresponding amine, EDC.HCl, HOBt, Et$_3$N, DCM, rt, 1 d, 31-70%.

3.   Conclusion

A class of tetrahydrophthalazinone-based TbrPDEB1 inhibitors with an alkynamide linker was identified as potent TbrPDEB1 inhibitors with good potency against *T. brucei* parasites and an interesting cytotoxicity profile. Alkynamide **8c** (NPD-055) inhibits TbrPDEB1 *in vitro,* shows a submicromolar trypanocidal activity (IC$_{50}$ = 0.6 µM) against *T. brucei* parasites and displays no cytotoxicity *versus* human MRC-5 cells (CC$_{50}$ >64 µM). The alkynamide **8b** (NPD-048) was co-crystallized in the catalytic domain of TbrPDEB1, showing a bidentate interaction of **8b** with the key residue Gln874 in the active site. Moreover, this bidentate interaction positions the carboxamide of **8b** in close proximity to the P-pocket of TbrPDEB1. The alkynamide **8b** is able to raise intracellular cAMP levels in living *T. brucei* parasites, supporting a PDE-mediated mode of action *in vitro*.

4.   Experimental

4.1.   *Protein production*

Cloning, expression and purification of recombinant TbrPDEB1 and hPDE4D catalytic domains were performed as previously described.[32]

4.2.   *Crystallisation, data collection and structure determination of inhibitor complexes*

TbrPDEB1 and hPDE4D catalytic domain crystals were grown in 24 well XRL plates (Molecular Dimensions) by vapor diffusion hanging drop technique, typically maintaining a protein to crystallisation solution ratio of 1:1 and a reservoir volume of 500 μL. Crystals of TbrPDEB1 were obtained in a condition containing 20% PEG 3350, 400 mM sodium formate, 300 mM guanidine and 100 mM MES pH 6.5 at 4 °C and were complexed with NPD-048 by soaking in the crystal growth solution containing 15 mM of the inhibitor for a period of 48 hours. The soaked crystals were then cryo protected, mounted on CryoLoop (Hampton Research) or LithoLoops (Molecular Dimensions) and vitrified in liquid nitrogen for data collection.

Crystals of hPDE4D catalytic domain were obtained in a condition containing 24% PEG 3350, 30% ethylene glycol and 100 mM HEPES pH 7.5 at 19 °C. Crystals were soaked with NPD-048 and archived in a way similar to that of TbrPDEB1.

X-ray diffraction data were collected at Diamond Light Source (Didcot, Oxfordshire, UK) beam lines I04 and I04-1 at 100 K using Pilatus 6M-F detector (Dectris, Baden, Switzerland) and were processed with XIA2 pipeline,[34] which incorporates XDS[35] and AIMLESS,[36] or were integrated using iMOSFLM [37] and reduced using POINTLESS, AIMLESS and TRUNCATE, all of which are part of CCP4.[38]

Structure of TbrPDEB1 and hPDE4D complexes with NPD-048 were determined by molecular replacement using CCP4 suite program PHASER[39] that utilised respective apo models (TbrPDEB1, PDB id: 4I15; hPDE4D, PDB id: 3SL3) as search templates. Stereochemical description of NPD-048 was generated by ACEDRG available within the CCP4 package[38] and ligand fitting and model adjustment were carried out in COOT[40] followed by maximum likelihood refinement with REFMAC.[41] Structural figures were prepared with PYMOL.[42] Coordinates of the structures have been deposited to the RCSB Protein Data Bank with following accession codes: 6FTM (TbrPDEB1–NPD-048) and 6FTW (hPDE4D–NPD-048).

4.2.1.   Accession codes

The coordinates of the crystal structures have been deposited to the RCSB Protein Data Bank under the following accession codes: 6FTM (TbrPDEB1–NPD-048); 6FTW (hPDE4D–NPD-048); The authors will release the atomic coordinates and experimental data upon article publication.

4.3.   *Phosphodiesterase activity assays*

The PDELight™ HTS cAMP phosphodiesterase Kit (Lonza, Walkersville, USA) was used. The assay was performed at 25 °C in non-binding, low volume 384 wells plates (Corning, Kennebunk, ME, USA). PDE activity measurements (TbrPDEB1_CD; K_m 3.45 μM, hPDE4B_CD; K_m 13.89 μM) were made in 'stimulation buffer' (50 mM Hepes, 100 mM NaCl, 10 mM MgCl, 0.5 mM EDTA, 0.05 mg/mL BSA, pH

7.5). Single concentration measurements were made at 10 µM inhibitor concentration (triplo measurements/assay, n=2). Dose response curves were made in the range 100 µM - 10 pM (triplo measurements/assay, n=3). Compounds were diluted in DMSO (final concentration 1%). Inhibitor dilutions (2.5 µL) were transferred to the 384 wells plate, 2.5 µL PDE in stimulation buffer was added and mixed, 5 µL cAMP (at $2 \times K_m$ up to 20 µM) is added and the assay mixture was incubated for 20 min at 300 rpm. The reaction was terminated by addition of 5 µL Lonza Stop Buffer supplemented with 10 µM NPD-001. Then 5 µL of Lonza Detection reagent (diluted to 80% with reaction buffer) was added and the reaction incubated for 10 min at 300 rpm. Luminescence was read with a Victor3 luminometer using a 0.1 s/well program. RLUs were measured in comparison to the DMSO-only control, NPD-001 always was taken along as positive control as a PDE inhibitor. The K_i values of the inhibitors analyzed are represented as the mean of at least three independent experiments with the associated standard error of the mean (S.E.M.) as indicated. Due to solubility issues, we were not able to determine full dose response curves for all compounds; K_i values for such inhibitors were obtained by curve fitting (Graphpad Prism 7.0) and the assumption of full inhibition to a level of inhibition by NPD-001.

4.4. Phenotypic cellular assays

For the cellular assays, the following reference drugs were used as positive controls: suramin (Sigma-Aldrich, Germany) for *T. brucei* (pIC_{50} = 7.4 ± 0.2, n = 5), and tamoxifen (Sigma-Aldrich, Germany) for MRC-5 cells (pIC_{50} = 5.0 ± 0.1, n = 5). All compounds were tested at five concentrations (64, 16, 4, 1 and 0.25 µM) to establish a full dose-titration and determination of the IC_{50} and CC_{50}, data are represented as the mean of duplicate experiments ± S.E.M. The final concentration of DMSO did not exceed 0.5% in the assays.

Antitrypanosomal cellular assay. *T.b. brucei* Squib-427 strain (suramin-sensitive) was cultured at 37 °C and 5% CO_2 in HMI-9 medium, supplemented with 10% fetal calf serum (FCS). Approximately 1.5×10^4 trypomastigotes were added to each well and parasite growth was assessed after 72 h at 37 °C by adding resazurin. Viability was assessed fluorimetrically 24 h after the addition of resazurin. Fluorescence was measured (excitation 550 nm, emission 590 nm) and the results were expressed as percentage reduction in viability compared to control.

MRC-5 cytotoxicity cellular assay. MRC-5 SV2 cells, originally from a human diploid lung cell line, were cultivated in MEM, supplemented with L-glutamine (20 mM), 16.5 mM sodium hydrogen carbonate and 5% FCS. For the assay, 10^4 MRC-5 cells/well were seeded onto the test plates containing the pre-diluted sample and incubated at 37 °C and 5% CO_2 for 72 h. Cell viability was assessed fluorimetrically 4 h after the of addition of resazurin. Fluorescence was measured (excitation 550 nm, emission 590 nm) and the results were expressed as percentage reduction in cell viability compared to control.

4.5. Intracellular cAMP assay

Quantification of intracellular cAMP was performed exactly as described previously, using the Direct Cyclic AMP Enzyme Immunoassay kit (Assay Designs).[25] Briefly, bloodstreams form trypanosomes were seeded at a density of 2×10^6 cells/mL in the log phase and incubated at 37 ºC and 5% CO_2 overnight followed by incubation with or without (negative control) potential PDE inhibitors at $2 \times$ and $5 \times IC_{50}$-values. After 4 h, 5×10^6 cells/mL were counted for both treated and control, transferred to

microfuge tubes and centrifuged at 2000×*g* for 10 min at 4 ºC in a Heraeus Biofuge centrifuge. The cell pellet was resuspended in 100 µL 0.1 M hydrochloric acid, placed on ice for 20 min, followed by centrifugation at 12,000 rpm for 10 min. The supernatant was stored at -20 ºC until assayed in duplicate using the Assays Design immunoassay kit, following the manufacturer's instructions. All experiments were performed at least three times independently.

4.6.   Chemistry

4.6.1.   General

All reagents and solvents were obtained from commercial suppliers and were used as received. All reactions were magnetically stirred and carried out under an inert atmosphere. Reaction progress was monitored using thin-layer chromatography (TLC) and LC-MS analysis. LC-MS analysis was performed on a Shimadzu LC-20AD liquid chromatograph pump system, equipped with an Xbridge (C18) 5 µm column (50 mm, 4.6 mm), connected to a Shimadzu SPD-M20A diode array detector, and MS detection using a Shimadzu LC-MS-2010EV mass spectrometer. The LC-MS conditions were as follows: solvent A (water with 0.1% formic acid) and solvent B (MeCN with 0.1% formic acid), flow rate of 1.0 mL/min, start 5% B, linear gradient to 90% B in 4.5 min, then 1.5 min at 90% B, then linear gradient to 5% B in 0.5 min, then 1.5 min at 5% B; total run time of 8 min. Silica gel column chromatography was carried out with automatic purification systems using the indicated eluent. Reversed phase column purification was performed on Grace Davison iES system with C18 cartridges (60 Å, 40 µm) using the indicated eluent. Nuclear magnetic resonance (NMR) spectra were recorded as indicated on a Bruker Avance 500 (500 MHz for ^{1}H and 125.8 MHz for ^{13}C) instrument equipped with a Bruker CryoPlatform , or on a Bruker DMX300 (300 MHz for ^{1}H) or a Bruker Biospin (400 MHz for ^{1}H). Chemical shifts (δ in ppm) and coupling constants (*J* in Hz) are reported with residual solvent as internal standard (δ ^{1}H-NMR: CDCl$_3$ 7.26; DMSO-*d*$_6$ 2.50; δ ^{13}C-NMR: CDCl$_3$ 77.16; DMSO-*d*$_6$ 39.52). Abbreviations used for ^{1}H-NMR descriptions are as follows: s = singlet, d = doublet, t = triplet, q = quintet, hept = heptet dd = doublet of doublets, dt = doublet of triplets, tt = triplet of triplets, m = multiplet, app d = apparent doublet, br = broad signal. Exact mass measurements (HRMS) were performed on a Bruker micrOTOF-Q instrument with electrospray ionization (ESI) in positive ion mode and a capillary potential of 4,500 V. Microwave reactions were carried out in a Biotage Initiator$^+$ using sealed microwave vials. Systematic names for molecules were generated with ChemBioDraw Ultra 14.0.0.117 (PerkinElmer, Inc.). The reported yields refer to isolated pure products and are not optimized. The purity, reported as the LC peak area % at 254 nm, of all final compounds was ≥ 95% based on LC-MS. All compounds are isolated as a racemic mixture of *cis*-enantiomers.

4.6.2.   Synthetic procedures

Building block **9** and **17** were prepared as described elsewhere.[27, 28, 32] All other compounds were prepared as described below.

4.6.2.1.   5'-(*cis*-3-Cycloheptyl-4-oxo-3,4,4a,5,8,8a-hexahydrophthalazin-1-yl)-3-fluoro-2'-methoxy-[1,1'-biphenyl]-4-carboxylic acid (**10a**)

To an argon purged solution of **9** (0.50 g, 1.7 mmol) and methyl 2-fluoro-4-(4,4,5,5-tetramethyl-1,3,2-dioxaborolan-2-yl)benzoate (0.40 g, 2.0 mmol) in DME (8 mL) was added aq. Na$_2$CO$_3$ (1.7 M, 2.0 mL)

and PdCl$_2$(dppf) (53 mg, 60 µmol). The reaction mixture was stirred and heated by microwave irradiation at 100 °C for 1 h. The reaction mixture was diluted with water (20 mL) and washed with EtOAc (60 mL). The aqueous phase was acidified to ∼ pH 1 with aq. HCl and extracted with EtOAc (3 × 50 mL). The combined organic phases were washed with water (40 mL), brine (40 mL), dried over Na$_2$SO$_4$, filtered and concentrated. The residue was purified on a reverse phase silica gel column eluting with MeCN/H$_2$O + 0.1% formic acid (gradient, 5-95%) to afford **10a** as a yellow solid (268 mg, 46%). ^{1}H NMR (300 MHz, CDCl$_3$): δ 8.09 (t, *J* = 8.1 Hz, 1H), 7.88 − 7.81 (m, 1H), 7.77 (s, 1H), 7.47 − 7.36 (m, 2H), 7.07 (d, *J* = 8.7 Hz, 1H), 5.84 − 5.63 (m, 2H), 4.89 − 4.75 (m, 1H), 3.89 (s, 3H), 3.39 − 3.25 (m, 1H), 3.09 − 2.95 (m, 1H), 2.75 (t, *J* = 5.4 Hz, 1H), 2.29 − 1.39 (m, 15H).

4.6.2.2. Methyl 5'-(*cis*-3-cycloheptyl-4-oxo-3,4,4a,5,8,8a-hexahydrophthalazin-1-yl)-2'-methoxy-2-methyl-[1,1'-biphenyl]-4-carboxylate (**10b**)

This compound was prepared from **9** (500 mg, 1.16 mmol) and methyl 3-methyl-4-(4,4,5,5-tetramethyl-1,3,2-dioxaborolan-2-yl)benzoate (384 mg, 1.39 mmol) as described for **10a**. The title compound was obtained as a white solid (228 mg, 39%). ^{1}H NMR (300 MHz, CDCl$_3$): δ 7.96 − 7.90 (m, 2H), 7.86 (dd, *J* = 8.7 Hz, 2.4 Hz, 1H), 7.56 (d, *J* = 2.4 Hz, 1H), 7.29 (d, *J* = 7.8 Hz, 1H), 7.03 (d, *J* = 8.7 Hz, 1H), 5.81 − 5.61 (m, 2H), 4.85 − 4.74 (m, 1H), 3.93 (s, 3H), 3.81 (s, 3H), 3.33 − 3.23 (m, 1H), 3.06 − 2.95 (m, 1H), 2.73 (t, *J* = 6.0 Hz, 1H), 2.20 (s, 3H), 2.18 − 1.41 (m, 15H).

4.6.2.3. 5'-(*cis*-3-Cycloheptyl-4-oxo-3,4,4a,5,8,8a-hexahydrophthalazin-1-yl)-2'-methoxy-2-methyl-[1,1'-biphenyl]-4-carboxylic acid (**10c**)

To a solution of **10b** (228 mg, 0.46 mmol) in MeOH (5 mL) and THF (12 mL) was added an aqueous solution of NaOH (2.0 M, 3.6 mL) and the reaction mixture was stirred overnight at 50 °C. The reaction mixture was cooled to rt, acidified with aq. HCl (4 M) and extracted with EtOAc (3 × 20 mL). The combined organic phases were washed with water (15 mL), brine (15 mL), dried over Na$_2$SO$_4$, filtered and concentrated to obtain **10c** as a white solid (219 mg, 98%). ^{1}H NMR (300 MHz, CDCl$_3$): δ 8.08 − 7.98 (m, 2H), 7.88 (dd, *J* = 8.7 Hz, 2.4 Hz, 1H), 7.58 (d, *J* = 2.4 Hz, 1H), 7.34 (d, *J* = 7.8 Hz, 1H), 7.05 (d, *J* = 8.7 Hz, 1H), 5.83 − 5.62 (m, 2H), 4.86 − 4.75 (m, 1H), 3.83 (s, 3H), 3.35 − 3.24 (m, 1H), 3.08 − 2.95 (m, 1H), 2.75 (t, *J* = 6.3 Hz, 1H), 2.23 (s, 3H), 2.19 − 1.42 (m, 15H).

4.6.2.4. *cis*-2-Cycloheptyl-4-(4-methoxy-3-(4,4,5,5-tetramethyl-1,3,2-dioxaborolan-2-yl)phenyl)-4a,5,8,8a-tetrahydrophthalazin-1(2*H*)-one (**11**)

To an argon-purged solution of **9** (1.7 g, 3.8 mmol) in 1,4-dioxane (30 mL) was added KOAc (0.75 g, 7.7 mmol), bis(pinacolato)diboron (1.1 g, 4.2 mmol) and PdCl$_2$(dppf) (0.14 g, 0.19 mmol). The mixture was heated to reflux for 2.5 hours. The reaction mixture was diluted with DCM (150 mL) and the mixture was washed with water (2 × 100 mL) and brine (100 mL). The organic phase was dried over Na$_2$SO$_4$, filtered and concentrated. The residue was purified on a silica gel column eluting with EtOAc/n-heptane (gradient, 10-30%) to afford **11** as a white solid (0.5 g, 28%). ^{1}H-NMR (400 MHz, CDCl$_3$): δ 8.01 − 7.95 (m, 2H), 6.92 (d, *J* = 8.7 Hz, 1H), 5.83 − 5.63 (m, 2H), 4.89 − 4.75 (m, 1H), 3.88 (s, 3H), 3.35 (q, *J* = 5.8 Hz, 1H), 3.03 (app d, 1H), 2.70 (t, *J* = 5.7 Hz, 1H), 2.23 − 1.21 (m, 24H). LC-MS (ESI): t_R = 2.54 min, area: >95%, *m/z* 479 [M + H]$^+$.

4.6.2.5.   *N*-(2-Amino-2-oxoethyl)-4-bromo-3-fluorobenzamide (**12a**)

To a solution of 4-bromo-3-fluorobenzoic acid (500 mg, 2.28 mmol) in DCM (25 mL) was added DIPEA (0.63 mL, 3.65 mmol), glycinamide.HCl (252 mg, 2.28 mmol), EDC.HCl (481 mg, 2.51 mmol) and HOAt (31 mg, 0.23 mmol). The reaction mixture was stirred overnight at rt and poured into water (120 mL). The solids were isolated by vacuum filtration to obtain **12a** as a white solid (338 mg, 58%). ^{1}H NMR (300 MHz, DMSO-d_6): δ 8.87 (t, *J* = 6.0 Hz, 1H), 7.88 – 7.81 (m, 2H), 7.68 (dd, *J* = 8.4 Hz, 2.1 Hz, 1H), 7.41 (br, 1H), 7.06 (br, 1H), 3.82 (d, *J* = 6.0 Hz, 2H).

4.6.2.6.   *N*-(2-Amino-2-oxoethyl)-4-bromo-3-methoxybenzamide (**12b**)

This compound was prepared from 4-bromo-3-methoxybenzoic acid (500 mg, 2.16 mmol) and glycinamide.HCl (300 mg, 2.74 mmol) as described for **12a**. The title compound was obtained as a white solid (385 mg, 59% yield). ^{1}H NMR (300 MHz, DMSO-d_6): δ 8.78 (t, *J* = 5.7 Hz, 1H), 7.70 (d, *J* = 8.1 Hz, 1H), 7.57 (d, *J* = 1.8 Hz, 1H), 7.46 – 7.35 (m, 2H), 7.05 (br, 1H), 3.92 (s, 3H), 3.81 (d, *J* = 6.0 Hz, 2H).

4.6.2.7.   *N*-(2-Amino-2-oxoethyl)-4-bromo-2-methylbenzamide (**12c**)

This compound was prepared from 4-bromo-2-methylbenzoic acid (500 mg, 2.33 mmol) and glycinamide.HCl (514 mg, 4.65 mmol) as described for **12a**. The title compound was obtained as a light-brown solid (300 mg, 47%). ^{1}H NMR (300 MHz, DMSO-d_6): δ 8.46 – 8.36 (m, 1H), 7.52 – 7.29 (m, 4H), 7.02 (br, 1H), 3.78 (d, *J* = 6.0 Hz, 2H), 2.35 (br, 3H).

4.6.2.8.   *N*-(2-Amino-2-oxoethyl)-4-bromo-2-methoxybenzamide (**12d**)

This compound was prepared from 4-bromo-2-methoxybenzoic acid (500 mg, 2.16 mmol) and glycinamide.HCl (478 mg, 4.33 mmol) as described for **12a**. The title compound was obtained as a white solid (350 mg, 55%). ^{1}H NMR (300 MHz, DMSO-d_6): δ 8.52 – 8.42 (m, 1H), 7.80 (d, *J* = 8.1 Hz, 1H), 7.43 – 7.34 (m, 2H), 7.27 (dd, *J* = 8.1 Hz, 1.8 Hz, 1H), 7.10 (br, 1H), 3.95 (s, 3H), 3.88 (d, *J* = 6.0 Hz, 2H).

4.6.2.9.   *N*-(2-Amino-2-oxoethyl)-5'-(*cis*-3-cycloheptyl-4-oxo-3,4,4a,5,8,8a-hexahydrophthalazin-1-yl)-2-fluoro-2'-methoxy-[1,1'-biphenyl]-4-carboxamide (**4a**)

To an argon purged solution of **11** (0.20 g, 0.42 mmol) and **12a** (0.12 g, 0.42 mmol) in DME (3.2 mL) was added an aqueous solution of Na$_2$CO$_3$ (1.6 M, 0.40 mL) and PdCl$_2$(dppf) (19 mg, 0.02 mmol). The reaction mixture was stirred at 100 °C for 1 h. The reaction mixture was diluted with water (8 mL) and washed with EtOAc (25 mL). The water phase was acidified to ~ pH 5 with HCl (aq. 2M) and extracted with EtOAc (4 × 20 mL). The combined organic phases were washed with water (3 × 20 mL), brine (20 mL), dried over Na$_2$SO$_4$ and concentrated. The residue was purified on a reverse phase silica gel column eluting with MeCN/H$_2$O + 0.1% formic acid (gradient, 5-95%) to afford **4a** as a light yellow solid (62 mg, 27%). ^{1}H NMR (500 MHz, DMSO-d_6): δ 8.84 (t, *J* = 6.0 Hz, 1H), 7.93 (dd, *J* = 8.7, 2.2 Hz, 1H), 7.81 – 7.71 (m, 3H), 7.51 (t, *J* = 7.6 Hz, 1H), 7.43 (s, 1H), 7.23 (d, *J* = 8.8 Hz, 1H), 7.09 (s, 1H), 5.72 – 5.58 (m, 2H), 4.67 (tt, *J* = 8.8, 4.8 Hz, 1H), 3.83 (d, *J* = 5.9 Hz, 2H), 3.80 (s, 3H), 3.47 (dt, *J* = 11.6, 5.8 Hz, 1H), 2.79 (t, *J* = 6.2 Hz, 1H), 2.76 – 2.68 (m, 1H), 2.19 – 2.08 (m, 2H), 1.95 – 1.64 (m, 7H), 1.59 – 1.39 (m, 6H). ^{13}C NMR (126 MHz, DMSO-d_6): δ 171.3, 166.0, 165.4, 160.5, 158.6, 158.1, 153.8, 136.0, 132.3, 128.9, 128.6, 128.3, 127.8, 126.3, 124.5, 124.3, 123.7, 114.9, 112.1, 56.4, 55.5, 42.9, 34.2, 33.3, 33.0, 30.3, 28.5, 28.5, 25.0, 24.9, 23.0, 22.4. LC-MS (ESI): t_R = 4.75 min, area: 97%, *m/z* 547 [M + H]$^+$. HRMS (ESI) *m/z*: [M + H]$^+$ calcd. for C$_{31}$H$_{36}$N$_4$O$_4$F 547.2715, found 547.2702.

4.6.2.10. *N*-(2-Amino-2-oxoethyl)-5'-(*cis*-3-cycloheptyl-4-oxo-3,4,4a,5,8,8a-hexahydrophthalazin-1-yl)-2'-methoxy-2-methyl-[1,1'-biphenyl]-4-carboxamide (**4b**)

To a solution of glycinamide.HCl (34.1 mg, 0.31 mmol) and **10c** (75 mg, 0.15 mmol) in DCM (3 mL) was added DIPEA (0.34 mmol, 60 µL), EDC.HCl (65 mg, 0.34 mmol) and HOAt (42 mg, 0.31 mmol). The mixture was stirred at rt for 1 h. The reaction mixture was diluted with water (10 mL) and extracted with EtOAc (3 × 25 mL). The combined organic phases were washed with water (15 mL), brine (15 mL), dried over Na$_2$SO$_4$, filtered and concentrated. The residue was purified on a reverse phase silica gel column eluting with MeCN/H$_2$O + 0.1% formic acid (gradient, 5-95%) to afford **4b** as a light yellow solid (71 mg, 83%). ^{1}H NMR (500 MHz, DMSO-*d*$_6$): δ 8.69 (t, *J* = 5.9 Hz, 1H), 7.90 (dd, *J* = 8.8, 2.2 Hz, 1H), 7.81 (s, 1H), 7.74 (dd, *J* = 7.8, 1.7 Hz, 1H), 7.60 (d, *J* = 2.1 Hz, 1H), 7.41 (s, 1H), 7.25 (d, *J* = 7.8 Hz, 1H), 7.21 (d, *J* = 8.7 Hz, 1H), 7.09 (s, 1H), 5.73 − 5.58 (m, 2H), 4.68 (tt, *J* = 9.6, 5.0 Hz, 1H), 3.83 (d, *J* = 5.8 Hz, 2H), 3.78 (s, 3H), 3.46 (dt, *J* = 11.6, 5.7 Hz, 1H), 2.80 (t, *J* = 6.1 Hz, 1H), 2.77 − 2.68 (m, 1H), 2.13 (s, 5H), 1.93 − 1.65 (m, 7H), 1.61 − 1.40 (m, 6H). ^{13}C NMR (126 MHz, DMSO-*d*$_6$): δ 171.5, 166.8, 166.0, 157.8, 154.0, 141.4, 136.7, 133.7, 130.3, 130.0, 129.0, 128.1, 127.6, 127.6, 126.4, 125.1, 124.5, 111.9, 56.1, 55.5, 42.9, 34.2, 33.3, 33.1, 30.3, 28.5, 28.5, 25.0, 24.9, 23.0, 22.4, 20.1. LC-MS (ESI): *t*$_R$ = 4.80 min, area: >98%, *m/z* 543 [M + H]$^+$. HRMS (ESI) *m/z*: [M + H]$^+$ calcd. for C$_{32}$H$_{39}$N$_4$O$_4$ 543.2966, found 543.2949.

4.6.2.11. *N*-(2-Amino-2-oxoethyl)-5'-(*cis*-3-cycloheptyl-4-oxo-3,4,4a,5,8,8a-hexahydrophthalazin-1-yl)-2,2'-dimethoxy-[1,1'-biphenyl]-4-carboxamide (**4c**)

This compound was prepared from **11** (100 mg, 0.21 mmol) and **12b** (60 mg, 0.21 mmol) as described for **4a**. The title compound was obtained as a light yellow solid (62 mg, 52%). ^{1}H NMR (500 MHz, DMSO-*d*$_6$): δ 8.75 (t, *J* = 6.0 Hz, 1H), 7.83 (dd, *J* = 8.7, 2.1 Hz, 1H), 7.64 (d, *J* = 2.3 Hz, 1H), 7.56 (s, 1H), 7.52 (d, *J* = 7.8 Hz, 1H), 7.40 (s, 1H), 7.27 (d, *J* = 7.7 Hz, 1H), 7.15 (d, *J* = 8.7 Hz, 1H), 7.08 (s, 1H), 5.72 − 5.58 (m, 2H), 4.71 − 4.62 (m, 1H), 3.84 (d, *J* = 5.8 Hz, 2H), 3.77 (s, 3H), 3.75 (s, 3H), 3.43 (dt, *J* = 11.7, 5.8 Hz, 1H), 2.81 − 2.68 (m, 2H), 2.20 − 2.07 (m, 2H), 1.94 − 1.64 (m, 7H), 1.61 − 1.37 (m, 6H). ^{13}C NMR (126 MHz, DMSO-*d*$_6$): δ 171.5, 166.6, 166.0, 158.4, 157.0, 154.0, 135.2, 131.3, 130.4, 128.6, 127.4, 127.4, 127.3, 126.4, 124.5, 119.8, 111.9, 110.6, 56.2, 56.1, 55.4, 42.9, 34.2, 33.3, 33.0, 30.4, 28.6, 28.5, 24.9, 24.9, 23.1, 22.4. LC-MS (ESI): *t*$_R$ = 4.65 min, area: 95%, *m/z* 559 [M + H]$^+$. HRMS (ESI) *m/z*: [M + H]$^+$ calcd. for C$_{32}$H$_{39}$N$_4$O$_5$ 559.2915, found 559.2913.

4.6.2.12. *N*-(2-Amino-2-oxoethyl)-5'-(*cis*-3-cycloheptyl-4-oxo-3,4,4a,5,8,8a-hexahydrophthalazin-1-yl)-3-fluoro-2'-methoxy-[1,1'-biphenyl]-4-carboxamide (**4d**)

This compound was prepared from **10a** (150 mg, 0.31 mmol) and glycinamide.HCl (68 mg, 0.61 mmol) as described for **4b**. The title compound was obtained as a light yellow solid (40 mg, 23%). ^{1}H NMR (500 MHz, DMSO-*d*$_6$): δ 8.43 − 8.34 (m, 1H), 7.92 (dd, *J* = 8.8, 2.3 Hz, 1H), 7.84 − 7.76 (m, 2H), 7.51 − 7.40 (m, 3H), 7.26 (d, *J* = 8.8 Hz, 1H), 7.19 − 7.12 (m, 1H), 5.75 − 5.58 (m, 2H), 4.69 (tt, *J* = 9.0, 4.4 Hz, 1H), 3.86 (d, *J* = 8.3 Hz, 5H), 3.53 (dt, *J* = 11.6, 5.7 Hz, 1H), 2.82 − 2.69 (m, 2H), 2.21 − 2.09 (m, 2H), 1.97 − 1.88 (m, 1H), 1.87 − 1.67 (m, 6H), 1.62 − 1.41 (m, 6H). ^{13}C NMR (126 MHz, DMSO-*d*$_6$): δ 170.9, 166.0, 163.7, 160.6, 158.6, 157.7, 153.9, 142.8, 130.7, 128.3, 128.1, 126.3, 125.8, 124.5, 121.8, 117.4, 112.7, 56.4, 55.4, 42.9, 34.2, 33.3, 33.1, 30.2, 28.7, 28.6, 25.0, 24.9, 23.0, 22.4. LC-MS (ESI): *t*$_R$ = 4.87 min,

area: >98%, *m/z* 547 [M + H]⁺. HRMS (ESI) *m/z*: [M + H]⁺ calcd. for $C_{31}H_{36}N_4O_4F$ 547.2707, found 547.2715.

4.6.2.13. *N*-(2-Amino-2-oxoethyl)-5'-(*cis*-3-cycloheptyl-4-oxo-3,4,4a,5,8,8a-hexahydrophthalazin-1-yl)-2'-methoxy-3-methyl-[1,1'-biphenyl]-4-carboxamide (**4e**)

This compound was prepared from **11** (200 mg, 0.42 mmol) and **12c** (113 mg, 0.42 mmol) as described for **4a**. The title compound was obtained as a light yellow solid (130 mg, 57%). ¹H NMR (500 MHz, DMSO-*d*₆): δ 8.39 (t, *J* = 6.0 Hz, 1H), 7.85 (dd, *J* = 8.7, 2.2 Hz, 1H), 7.74 (d, *J* = 2.1 Hz, 1H), 7.48 (d, *J* = 7.8 Hz, 1H), 7.40 – 7.30 (m, 3H), 7.20 (d, *J* = 8.7 Hz, 1H), 7.06 (s, 1H), 5.73 – 5.57 (m, 2H), 4.73 – 4.64 (m, 1H), 3.85 – 3.75 (m, 5H), 3.52 – 3.43 (m, 1H), 2.82 – 2.69 (m, 2H), 2.40 (s, 3H), 2.20 – 2.07 (m, 2H), 1.95 – 1.65 (m, 7H), 1.62 – 1.38 (m, 6H). ¹³C NMR (126 MHz, DMSO-*d*₆): δ 171.3, 169.6, 166.0, 157.8, 154.0, 139.3, 135.9, 135.7, 131.7, 130.0, 128.1, 127.8, 127.6, 127.4, 126.8, 126.4, 124.5, 112.3, 56.3, 55.3, 42.6, 34.2, 33.3, 33.0, 30.3, 28.7, 28.7, 24.9, 24.8, 23.0, 22.4, 20.1. LC-MS (ESI): t_R = 4.83 min, area: 98%, *m/z* 543 [M + H]⁺. HRMS (ESI) *m/z*: [M + H]⁺ calcd. for $C_{32}H_{39}N_4O_4$ 543.2950, found 543.2966.

4.6.2.14. *N*-(2-Amino-2-oxoethyl)-5'-(*cis*-3-cycloheptyl-4-oxo-3,4,4a,5,8,8a-hexahydrophthalazin-1-yl)-2',3-dimethoxy-[1,1'-biphenyl]-4-carboxamide (**4f**)

This compound was prepared from **11** (200 mg, 0.42 mmol) and **12d** (120 mg, 0.42 mmol) as described for **4a**. The title compound was obtained as a light yellow solid (137 mg, 58%). ¹H NMR (500 MHz, DMSO-*d*₆): δ 8.57 (t, *J* = 5.3 Hz, 1H), 7.93 (d, *J* = 8.0 Hz, 1H), 7.89 (dd, *J* = 8.7, 2.2 Hz, 1H), 7.83 (d, *J* = 2.1 Hz, 1H), 7.42 (s, 1H), 7.28 – 7.18 (m, 3H), 7.14 (s, 1H), 5.74 – 5.59 (m, 2H), 4.70 (tt, *J* = 8.5, 4.9 Hz, 1H), 3.97 (s, 3H), 3.92 (d, *J* = 5.2 Hz, 2H), 3.85 (s, 3H), 3.50 (dt, *J* = 11.5, 5.7 Hz, 1H), 2.83 – 2.71 (m, 2H), 2.22 – 2.09 (m, 2H), 1.97 – 1.68 (m, 7H), 1.62 – 1.41 (m, 6H). ¹³C NMR (126 MHz, DMSO-*d*₆): δ 171.1, 166.0, 164.7, 157.8, 157.4, 153.9, 142.7, 131.0, 129.6, 128.2, 127.9, 127.7, 126.4, 124.5, 122.2, 120.9, 113.6, 112.5, 56.5, 56.4, 55.4, 43.1, 34.3, 33.3, 33.1, 30.3, 28.8, 28.7, 24.9, 24.8, 23.0, 22.4. LC-MS (ESI): t_R = 4.86 min, area: 97%, *m/z* 559 [M + H]⁺. HRMS (ESI) *m/z*: [M + H]⁺ calcd. for $C_{32}H_{39}N_4O_5$ 559.2915, found 559.2887.

4.6.2.15. *cis*-2-Cycloheptyl-4-(4-methoxy-3-(1-oxoisoindolin-5-yl)phenyl)-4a,5,8,8a-tetrahydrophthalazin-1(2*H*)-one (**5a**)

To an argon purged solution of **9** (1.4 g, 3.1 mmol) in DME (15 mL) was added 5-(4,4,5,5-tetramethyl-1,3,2-dioxaborolan-2-yl)isoindolin-1-one (0.84 g, 3.2 mmol), PdCl₂(dppf) (0.11 g, 0.15 mmol) and aq. Na₂CO₃ (2 M, 9.3 mmol, 4.6 mL). The reaction mixture was stirred at 100 °C for 5 h. The reaction mixture was diluted with DCM (250 mL) and washed with sat. aq. NH₄Cl (150 mL), water (150 mL) and brine (200 mL). The organic phase was dried over Na₂SO₄, filtered and concentrated. The residue was purified on a reverse phase silica gel column eluting with MeCN/H₂O + 0.1% formic acid (gradient, 5-95%) to afford **5a** as a light brown solid (1.2 g, 73%). ¹H NMR (500 MHz, DMSO-*d*₆): δ 8.61 (s, 1H), 7.92 (dd, *J* = 8.7, 2.2 Hz, 1H), 7.76 (d, *J* = 2.2 Hz, 1H), 7.72 (d, *J* = 7.9 Hz, 1H), 7.68 (s, 1H), 7.59 (d, *J* = 7.8 Hz, 1H), 7.26 (d, *J* = 8.8 Hz, 1H), 5.75 – 5.59 (m, 2H), 4.69 (tt, *J* = 10.0, 4.7 Hz, 1H), 4.43 (s, 2H), 3.83 (s, 3H), 3.50 (dt, *J* = 11.5, 5.7 Hz, 1H), 3.34 (s, 1H), 2.80 (t, *J* = 6.1 Hz, 1H), 2.77 – 2.69 (m, 1H), 2.21 – 2.09 (m, 2H), 1.96 – 1.67 (m, 6H), 1.62 – 1.40 (m, 6H). ¹³C NMR (126 MHz, DMSO-*d*₆): δ 170.2, 166.0, 157.7, 154.0, 144.5, 141.4, 131.9, 129.9, 129.5, 128.5, 128.0, 127.6, 126.4, 125.0, 124.5, 122.8, 112.6, 56.4,

55.4, 45.4, 34.2, 33.3, 33.1, 30.3, 28.6, 28.6, 25.0, 24.9, 23.0, 22.4. LC-MS (ESI): t_R = 5.05 min, area: >98%, *m/z* 484 [M + H]⁺. HRMS (ESI) *m/z*: [M + H]⁺ calcd. for $C_{30}H_{34}N_3O_3$ 484.2595, found 484.2585.

4.6.2.16. *cis*-2-Cycloheptyl-4-(4-methoxy-3-(2-(2-methoxyethyl)-1-oxoisoindolin-5-yl)phenyl)-4a,5,8,8a-tetrahydrophthalazin-1(2*H*)-one (**5b**)

To an ice-cooled solution of **5a** (0.10 g, 0.19 mmol) in DMF (1.5 mL) was added NaH (23 mg, 0.57 mmol, 60 %). The mixture was stirred for 0.5 h at rt prior to the addition of 1-bromo-2-methoxyethane (40 μL, 0.41 mmol). The reaction mixture was stirred at rt for 1.5 h. The reaction mixture was quenched with water (20 mL) and extracted with DCM (2 × 30 mL). The combined organic phases were washed with brine (25 mL), dried over Na_2SO_4, filtered and concentrated. The residue was purified on a silica gel column eluting with EtOAc/n-heptane (gradient, 25-66%) to afford **5b** as a white solid (31 mg, 27%). ¹H NMR (500 MHz, DMSO-*d₆*): δ 7.91 (dt, *J* = 8.8, 1.8 Hz, 1H), 7.76 (t, *J* = 1.9 Hz, 1H), 7.75 – 7.68 (m, 2H), 7.60 (d, *J* = 7.8 Hz, 1H), 7.25 (dd, *J* = 8.8, 1.2 Hz, 1H), 5.74 – 5.59 (m, 2H), 4.73 – 4.65 (m, 1H), 4.57 (s, 2H), 3.84 (d, *J* = 1.3 Hz, 3H), 3.72 (t, *J* = 5.4 Hz, 2H), 3.59 (t, *J* = 5.4 Hz, 2H), 3.50 (dt, *J* = 11.6, 5.8 Hz, 1H), 3.29 (s, 3H), 2.83 – 2.71 (m, 2H), 2.22 – 2.09 (m, 2H), 1.97 – 1.67 (m, 7H), 1.61 – 1.42 (m, 6H). ¹³C NMR (126 MHz, DMSO-*d₆*): δ 167.5, 166.0, 157.7, 154.0, 142.4, 141.3, 131.6, 129.9, 129.6, 128.5, 128.0, 127.6, 126.4, 124.7, 124.5, 122.7, 112.6, 70.6, 58.4, 56.4, 55.5, 50.8, 41.8, 34.3, 33.3, 33.1, 30.4, 28.6, 28.6, 25.0, 24.9, 23.0, 22.4. LC-MS (ESI): t_R = 5.39 min, area: 95%, *m/z* 542 [M + H]⁺. HRMS (ESI) *m/z*: [M + H]⁺ calcd. for $C_{33}H_{40}N_3O_4$ 542.3013, found 542.3000.

4.6.2.17. 2-(5-(5-(*cis*-3-Cycloheptyl-4-oxo-3,4,4a,5,8,8a-hexahydrophthalazin-1-yl)-2-methoxyphenyl)-1-oxoisoindolin-2-yl)acetamide (**5c**)

This compound was prepared from **5a** (0.10 mg, 0.21 mmol) and 2-bromoacetamide (31 mg, 0.23 mmol) as described for **5b**. The title compound was obtained as a white solid (29 mg, 26%). ¹H NMR (500 MHz, DMSO-*d₆*): δ 7.91 (dd, *J* = 8.7, 2.2 Hz, 1H), 7.78 (d, *J* = 2.3 Hz, 1H), 7.75 (d, *J* = 7.9 Hz, 1H), 7.71 (s, 1H), 7.61 (d, *J* = 7.8 Hz, 1H), 7.57 (s, 1H), 7.26 (d, *J* = 8.7 Hz, 1H), 7.17 (s, 1H), 5.74 – 5.59 (m, 2H), 4.69 (tt, *J* = 8.8, 4.9 Hz, 1H), 4.57 (s, 2H), 4.16 (s, 2H), 3.84 (s, 3H), 3.50 (dt, *J* = 11.5, 5.7 Hz, 1H), 2.83 – 2.70 (m, 2H), 2.22 – 2.10 (m, 2H), 1.97 – 1.67 (m, 7H), 1.61 – 1.41 (m, 6H). ¹³C NMR (126 MHz, DMSO-*d₆*): δ 170.4, 168.0, 166.0, 157.8, 154.0, 142.7, 141.5, 131.3, 130.0, 129.6, 128.5, 128.0, 127.7, 126.4, 124.7, 124.5, 122.9, 112.6, 56.4, 55.5, 51.0, 45.0, 34.3, 33.3, 33.1, 30.4, 28.6, 28.6, 25.0, 24.9, 23.0, 22.4. LC-MS (ESI): t_R = 4.75 min, area: >98%, *m/z* 541 [M + H]⁺. HRMS (ESI) *m/z*: [M + H]⁺ calcd. for $C_{32}H_{37}N_4O_4$ 541.2809, found 541.2788.

4.6.2.18. *N*-(2-Amino-2-oxoethyl)-3-(5-(*cis*-3-cycloheptyl-4-oxo-3,4,4a,5,8,8a-hexahydrophthalazin-1-yl)-2-methoxyphenyl)propiolamide (**8g**)

A N₂-flushed mixture of **9** (1.0 g, 2.32 mmol), Pd(PPh₃)₂Cl₂ (49.0 mg, 0.07 mmol), propiolic acid (0.16 mL, 2.55 mmol), DBU (1.73 mL, 11.59 mmol) and dppb (79.0 mg, 0.19 mmol) in DMSO (6 mL) was stirred at 50 °C for 15 h. The reaction mixture was diluted with EtOAc (300 mL) and washed with sat. aq. NaHCO₃ (150 mL). The aqueous phase was acidified using sat. aq. NH₄Cl (~250 mL) and extracted with EtOAc (2 × 400 mL). The combined organic phases were dried over Na_2SO_4, filtered and concentrated to obtain the crude material of carboxylic acid **13 (**320 mg). A portion of the residue (100 mg) was dissolved in DMF (3 mL) and glycinamide.HCl (52 mg, 0.48 mmol), DIPEA (0.10 mL, 0.60 mmol), EDC (50 mg, 0.26 mmol) and HOAt (32 mg, 0.24 mmol) were added. This mixture was stirred

at rt for 30 h. The reaction mixture was diluted with water (25 mL) and extracted with EtOAc (3 × 75 mL). The combined organic phases were combined and washed with water (4 × 25 mL) and brine (3 × 25 mL). The organic phase was dried over Na_2SO_4 and concentrated. The residue was purified on a silica gel column eluting with MeOH/DCM (gradient, 0-1.5%) to afford **8g** as a white solid (6 mg). The extrapolated yield of this reaction is 1.5%. ^{1}H NMR (500 MHz, DMSO-d_6): δ 8.91 (t, *J* = 6.1 Hz, 1H), 7.98 (dd, *J* = 8.9, 2.3 Hz, 1H), 7.95 (d, *J* = 2.3 Hz, 1H), 7.43 (s, 1H), 7.23 (d, *J* = 8.9 Hz, 1H), 7.09 (s, 1H), 5.74 − 5.58 (m, 2H), 4.67 (tt, *J* = 9.0, 4.4 Hz, 1H), 3.92 (s, 3H), 3.72 (d, *J* = 6.0 Hz, 2H), 3.45 (dt, *J* = 11.7, 5.8 Hz, 1H), 2.81 (t, *J* = 6.1 Hz, 1H), 2.74 (app. d, 1H), 2.14 (app. t, 2H), 1.98 − 1.89 (m, 1H), 1.83 − 1.67 (m, 6H), 1.61 − 1.43 (m, 7H). ^{13}C NMR (126 MHz, DMSO-d_6): δ 170.5, 166.1, 161.8, 153.1, 153.1, 131.6, 130.0, 127.9, 126.4, 124.4, 112.4, 109.5, 88.2, 80.7, 56.6, 55.7, 42.3, 34.1, 33.3, 33.1, 30.3, 28.4, 28.3, 25.0, 24.9, 22.9, 22.4. LC-MS (ESI): t_R = 4.44 min, area: >98%, *m/z* 477 [M + H]+. HRMS (ESI) *m/z*: [M + H]+ calcd. for $C_{27}H_{33}N_4O_4$ 477.2496, found 477.2480.

4.6.2.19. Methyl-3-(5-(*cis*-3-cycloheptyl-4-oxo-3,4,4a,5,8,8a-hexahydrophthalazin-1-yl)-2-methoxyphenyl)propiolate (**14**)

To a solution of **11** (900 mg, 1.88 mmol) in anhydrous acetonitrile (15 mL) was added Pd(II)(OAc)$_2$ (21 mg, 94 μmol), K_2CO_3 (520 mg, 3.76 mmol), Ag(II)O (654 mg, 2.82 mmol) and methyl propiolate (174 mg, 2.07 mmol, 0.18 mL). The mixture was heated to 70 °C for 2.5 h. The reaction mixture was filtered over Hyflo. The filtrate was diluted with EtOAc (15 mL) and washed with water (2 × 10 mL) and brine (10 mL). The organic phase was dried over Na_2SO_4, filtered and concentrated. The residue was purified on a silica gel column eluting with EtOAc/n-heptane (gradient, 10-20%) to afford **14** as a white solid (489 mg, 53%). ^{1}H-NMR (300 MHz, DMSO-d_6): δ 8.05 (dd, *J* = 2.3 Hz, *J* = 8.8 Hz, 1H), 8.01 (d, *J* = 2.3 Hz, 1H), 7.26 (d, *J* = 8.8 Hz, 1H), 5.81 − 5.53 (m, 2H), 4.13 − 4.01 (m, 1H), 3.93 (s, 3H), 3.78 (s, 3H), 3.48 (q, *J* = 5.6 Hz, 1H), 2.82 − 2.68 (m, 2H), 2.21 − 2.05 (m, 2H), 1.98 − 1.36 (m, 13H). LC-MS (ESI): t_R = 3.95 min, area: >95%, *m/z* 435 [M + H]+.

4.6.2.20. 3-(5-(*cis*-3-Cycloheptyl-4-oxo-3,4,4a,5,8,8a-hexahydrophthalazin-1-yl)-2-methoxyphenyl)propiolamide (**8b**)

Compound **14** (60 mg, 0.12 mmol) was dissolved in a solution of NH_3 in MeOH (7 M, 2 mL). This mixture was stirred at rt for 2 h. The solvent was evaporated to obtain **8b** as a white solid (52 mg, 89%). ^{1}H NMR (500 MHz, CDCl$_3$): δ 7.99 − 7.84 (m, 2H), 7.02 − 6.90 (m, 1H), 6.35 (s, 1H), 6.14 (s, 1H), 5.85 − 5.59 (m, 2H), 4.88 − 4.72 (m, 1H), 3.94 (s, 3H), 3.25 (dt, *J* = 11.5, 5.7 Hz, 1H), 3.05 − 2.92 (m, 1H), 2.72 (t, *J* = 6.0 Hz, 1H), 2.26 − 2.08 (m, 2H), 2.05 − 1.95 (m, 2H), 1.92 − 1.84 (m, 1H), 1.82 − 1.69 (m, 4H), 1.69 − 1.43 (m, 6H), 1.34 − 1.20 (m, 2H). ^{13}C NMR (126 MHz, CDCl$_3$): δ 165.9, 161.9, 155.2, 152.3, 132.0, 129.5, 127.9, 126.0, 123.8, 111.0, 109.5, 86.5, 82.3, 56.4, 56.1, 34.6, 33.2, 33.0, 30.9, 28.2, 28.1, 25.1, 25.0, 22.9, 22.3. LC-MS (ESI): t_R = 4.82 min, area: >98%, *m/z* 420 [M + H]+. HRMS (ESI) *m/z*: [M + H]+ calcd. for $C_{25}H_{30}N_3O_3$ 420.2282, found 420.2278.

4.6.2.21. *N*-Butyl-3-(5-(*cis*-3-cycloheptyl-4-oxo-3,4,4a,5,8,8a-hexahydrophthalazin-1-yl)-2-methoxyphenyl)propiolamide (**8c**)

To an ice-cooled solution of **14** (60 mg, 0.12 mmol) and butan-1-amine (15 μL, 0.15 mmol) in toluene (2 mL) was slowly added AlMe$_3$ in toluene (2 M, 93 μL, 0.19 mmol,). The reaction mixture was stirred at 50 °C for 1 day. The reaction mixture was diluted with water (10 mL) and extracted with EtOAc (3 ×

15 mL). The combined organic phases were washed with brine (25 mL), dried over Na_2SO_4, filtered and concentrated. The residue was purified on a silica gel column eluting with MeOH/DCM (gradient, 0-1.5%) to afford **8c** as a white solid (10 mg, 17%). ^{1}H NMR (500 MHz, DMSO-d_6): δ 8.75 (t, *J* = 5.8 Hz, 1H), 7.95 (dd, *J* = 8.9, 2.3 Hz, 1H), 7.90 (d, *J* = 2.3 Hz, 1H), 7.21 (d, *J* = 9.0 Hz, 1H), 5.73 – 5.57 (m, 2H), 4.65 (tt, *J* = 9.7, 4.5 Hz, 1H), 3.90 (s, 3H), 3.47 – 3.39 (m, 1H), 3.16 – 3.07 (m, 2H), 2.78 (t, *J* = 6.1 Hz, 1H), 2.76 – 2.67 (m, 1H), 2.20 – 2.03 (m, 2H), 1.96 – 1.85 (m, 1H), 1.85 – 1.18 (m, 16H), 0.87 (t, *J* = 7.3 Hz, 3H). ^{13}C NMR (126 MHz, DMSO-d_6): δ 166.0, 161.7, 153.1, 152.6, 131.5, 129.8, 127.8, 126.3, 124.4, 112.4, 109.6, 88.4, 79.9, 56.5, 55.6, 39.1, 34.1, 33.3, 33.1, 31.3, 30.3, 28.4, 28.3, 25.0, 24.9, 22.8, 22.4, 20.0, 14.1. LC-MS (ESI): t_R = 5.56 min, area: >98%, *m/z* 476 [M + H]+. HRMS (ESI) *m/z*: [M + H]+ calcd. for $C_{29}H_{38}N_3O_3$ 476.2908, found 476.2887.

4.6.2.22. 3-(5-(*cis*-3-Cycloheptyl-4-oxo-3,4,4a,5,8,8a-hexahydrophthalazin-1-yl)-2-methoxyphenyl)-*N*-(2-methoxyethyl)propiolamide (**8d**)

This compound was prepared from **14** (60 mg, 0.12 mmol) and 2-methoxyethanamine (13 µL, 0.15 mmol) as described for **8c**. The title compound was obtained as a white solid (11 mg, 19%). ^{1}H NMR (500 MHz, DMSO-d_6): δ 8.83 (t, *J* = 5.7 Hz, 1H), 8.02 – 7.89 (m, 2H), 7.21 (d, *J* = 8.9 Hz, 1H), 5.75 – 5.56 (m, 2H), 4.66 (tt, *J* = 9.5, 4.8 Hz, 1H), 3.90 (s, 3H), 3.47 – 3.37 (m, 3H), 3.33 – 3.26 (m, 2H), 3.25 (s, 3H), 2.84 – 2.67 (m, 2H), 2.19 – 2.05 (m, 2H), 1.97 – 1.86 (m, 1H), 1.84 – 1.37 (m, 13H). ^{13}C NMR (126 MHz, DMSO-d_6): δ 166.0, 161.8, 153.1, 152.9, 131.5, 129.9, 127.8, 126.3, 124.4, 112.4, 109.6, 88.3, 80.2, 70.5, 58.3, 56.6, 55.6, 39.2, 34.1, 33.3, 33.1, 30.3, 28.4, 28.3, 25.0, 24.9, 22.8, 22.4. LC-MS (ESI): t_R = 5.12 min, area: >98%, *m/z* 478 [M + H]+. HRMS (ESI) *m/z*: [M + H]+ calcd. for $C_{28}H_{36}N_3O_4$ 478.2700, found 478.2678.

4.6.2.23. *cis*-2-Cycloheptyl-4-(4-methoxy-3-(3-morpholino-3-oxoprop-1-yn-1-yl)phenyl)-4a,5,8,8a-tetrahydrophthalazin-1(2*H*)-one (**8e**)

This compound was prepared from **14** (60 mg, 0.12 mmol) and morpholine (11 µL, 0.12 mmol) as described for **8c**. The title compound was obtained as a white solid (22 mg, 37%). ^{1}H NMR (500 MHz, DMSO-d_6): δ 8.03 – 7.96 (m, 2H), 7.24 (d, *J* = 8.7 Hz, 1H), 5.74 – 5.57 (m, 2H), 4.65 (m, *J* = 9.3, 4.3 Hz, 1H), 3.92 (s, 3H), 3.83 (t, *J* = 4.8 Hz, 2H), 3.69 (t, *J* = 4.8 Hz, 2H), 3.64 – 3.53 (m, 4H), 3.48 (dt, *J* = 11.6, 5.8 Hz, 1H), 2.79 (t, *J* = 6.1 Hz, 1H), 2.77 – 2.69 (m, 1H), 2.21 – 2.05 (m, 2H), 1.98 – 1.87 (m, 1H), 1.85 – 1.65 (m, 6H), 1.63 – 1.39 (m, 6H). ^{13}C NMR (126 MHz, DMSO-d_6): δ 166.1, 162.1, 153.1, 152.4, 131.5, 130.4, 128.0, 126.3, 124.5, 112.4, 109.2, 86.7, 85.7, 66.7, 66.2, 56.8, 55.5, 47.2, 42.0, 34.2, 33.3, 33.1, 30.1, 28.5, 28.5, 25.0, 24.9, 22.8, 22.4. LC-MS (ESI): t_R = 5.23 min, area: >98%, *m/z* 490 [M + H]+. HRMS (ESI) *m/z*: [M + H]+ calcd. for $C_{29}H_{36}N_3O_4$ 490.2700, found 490.2684.

4.6.2.24. 3-(5-(*cis*-3-Cycloheptyl-4-oxo-3,4,4a,5,8,8a-hexahydrophthalazin-1-yl)-2-methoxyphenyl)-*N*-(furan-2-ylmethyl)propiolamide (**8f**)

This compound was prepared from **14** (60 mg, 0.12 mmol) and furan-2-ylmethanamine (13 µL, 0.15 mmol) as described for **8c**. The title compound was obtained as a white solid (10 mg, 16%). ^{1}H NMR (500 MHz, CDCl3): δ 8.01 – 7.83 (m, 2H), 7.39 (s, 1H), 6.95 (d, *J* = 8.6 Hz, 1H), 6.42 (t, *J* = 5.7 Hz, 1H), 6.38 – 6.28 (m, 2H), 5.84 – 5.62 (m, 2H), 4.85 – 4.74 (m, 1H), 4.55 (d, *J* = 5.6 Hz, 2H), 3.93 (s, 3H), 3.24 (dt, *J* = 11.5, 5.7 Hz, 1H), 3.07 – 2.94 (m, 1H), 2.71 (t, *J* = 6.1 Hz, 1H), 2.27 – 2.09 (m, 2H), 2.05 – 1.93 (m, 2H), 1.93 – 1.83 (m, 1H), 1.83 – 1.69 (m, 4H), 1.69 – 1.43 (m, 6H). ^{13}C NMR (126 MHz, CDCl3): δ

165.9, 161.8, 153.1, 152.3, 150.3, 142.4, 132.0, 129.3, 127.9, 126.0, 123.7, 111.0, 110.6, 109.6, 108.1, 86.8, 81.6, 56.4, 56.1, 36.7, 34.6, 33.2, 33.0, 30.9, 28.2, 28.1, 25.1, 25.0, 22.9, 22.3. LC-MS (ESI): t_R = 5.35 min, area: >98%, m/z 500 [M + H]+. HRMS (ESI) m/z: [M + H]+ calcd. for $C_{30}H_{34}N_3O_4$ 500.2544, found 500.2539.

4.6.2.25. cis-2-Cycloheptyl-4-(4-methoxy-3-((trimethylsilyl)ethynyl)phenyl)-4a,5,8,8a-tetrahydrophthalazin-1(2H)-one (15)

To an argon purged solution of Pd(PPh3)2Cl2 (15 mg, 21 mmol) and **9** (0.10 g, 0.21 mmol) in Et3N (2.0 mL, 14 mmol) was added ethynyltrimethylsilane (60 µL, 0.43 mmol) and CuI (4.0 mg, 0.02 mmol). The reaction mixture was stirred at 80 °C for 3 h. The reaction mixture was filtered over Celite and partitioned between EtOAc (40 mL) and sat. aq. NH4Cl/H2O (1:2, 30 mL). The organic phase was washed with water (30 mL) and brine (30 mL), dried over Na2SO4, filtered and concentrated. The residue was purified on a silica gel column eluting with EtOAc/n-heptane (gradient, 5-25%) to afford **15** as a white solid (77 mg, 80%). 1H NMR (400 MHz, DMSO-d_6): δ 7.87 (dd, J = 8.8, 1.8 Hz, 1H), 7.79 (d, J = 1.8 Hz, 1H), 7.15 (d, J = 8.9 Hz, 1H), 5.76 – 5.56 (m, 2H), 4.77 – 4.57 (m, 1H), 3.86 (s, 3H), 3.48 – 3.40 (m, 1H), 2.84 – 2.63 (m, 2H), 2.27 – 1.13 (m, 15H), 0.23 (s, 9H). LC-MS (ESI): t_R = 2.74 min, area: >97%, m/z 449 [M + H]+.

4.6.2.26. cis-2-Cycloheptyl-4-(3-ethynyl-4-methoxyphenyl)-4a,5,8,8a-tetrahydrophthalazin-1(2H)-one (8a)

To a suspension of **15** (1.2 g, 3.04 mmol) in MeOH (15 mL) was added NaOH (1.0 M, 6 mL). The mixture was stirred at rt for 2 h. The reaction mixture was diluted with EtOAc (100 mL) and washed with water (2 × 50 mL) and brine (50 mL). The organic phase was dried over MgSO4, filtered and concentrated to obtain **8a** (890 mg, 91%) as a light yellow solid. 1H NMR (500 MHz, DMSO-d_6): δ 7.91 – 7.85 (m, 2H), 7.19 – 7.12 (m, 1H), 5.74 – 5.59 (m, 2H), 4.68 (tt, J = 9.2, 4.6 Hz, 1H), 4.31 (s, 1H), 3.88 (s, 3H), 3.44 (dt, J = 11.5, 5.7 Hz, 1H), 2.82 – 2.70 (m, 2H), 2.22 – 2.05 (m, 2H), 1.97 – 1.87 (m, 1H), 1.85 – 1.66 (m, 6H), 1.63 – 1.41 (m, 6H). 13C NMR (126 MHz, DMSO-d_6): δ 166.0, 161.6, 153.3, 131.2, 128.7, 127.7, 126.3, 124.4, 112.0, 111.5, 85.4, 80.2, 56.4, 55.6, 34.2, 33.3, 33.1, 30.3, 28.5, 28.5, 25.0, 24.9, 22.9, 22.4. LC-MS (ESI): t_R = 5.60 min, area: 95%, m/z 377 [M + H]+. HRMS (ESI) m/z: [M + H]+ calcd. for $C_{24}H_{29}N_2O_2$ 377.2224, found 377.2213.

4.6.2.27. 3-(5-(cis-3-Cycloheptyl-4-oxo-3,4,4a,5,8,8a-hexahydrophthalazin-1-yl)-2-methoxyphenyl)propiolaldehyde (16)

Compound **8a** (100 mg, 0.266 mmol) was dissolved in THF (2 mL) and the mixture was cooled to -78 °C. To this mixture was added 1.6 M n-BuLi in hexane (0.20 mL, 0.32 mmol,) and the mixture was stirred for 30 min prior to the addition of DMF (0.031 mL, 0.40 mmol). After 1.5 h, the reaction mixture was poured into acidified ice water (50 mL) and was neutralized to pH 6-7. The product was extracted with EtOAc (3 × 50 mL). The combined organic phases were washed with brine (100 mL), dried over Na2SO4, filtered and concentrated. The product was purified with flash column chromatography (5-40% EtOAc/Hept) and to give **16** as a white solid (74 mg, 69%). 1H NMR (300 MHz, DMSO-d_6): δ 9.45 (s, 1H), 8.07 – 8.03 (m, 2H), 7.27 (d, J = 8.9 Hz, 1H), 5.71 – 5.60 (m, 2H), 4.65 (hept, J = 4.5 Hz, 1H), 3.94 (s, 3H), 3.47 (dt, J = 11.4, 5.8 Hz, 1H), 2.80 – 2.67 (m, 2H), 2.15 – 2.04 (m, 2H), 1.96 – 1.43 (m, 13H)

4.6.2.28. *cis*-2-Cycloheptyl-4-(4-methoxy-3-(oxazol-5-ylethynyl)phenyl)-4a,5,8,8a-
tetrahydrophthalazin-1(2*H*)-one (**8h**)

To a solution of **16** (74 mg, 0.18 mmol) in MeOH (3 mL) was added 1-((isocyanomethyl)sulfonyl)-4-methylbenzene (38 mg, 0.19 mmol) and K_2CO_3 (28 mg, 0.20 mmol). This mixture was heated to reflux for 1.5 h. The mixture was diluted with EtOAc (25 mL) and washed with sat. aq. NH_4Cl (25 mL), water (25 mL) and brine (25 mL). The organic phase was dried over Na_2SO_4, filtered and concentrated to gain a brown oil. The product was purified with reverse phase column purification to obtain the product as a white solid after lyophilisation (38 mg, 47%). ^1H NMR (500 MHz, DMSO-d_6): δ 8.54 (s, 1H), 7.96 (s, 2H), 7.67 (s, 1H), 7.24 (d, *J* = 8.6 Hz, 1H), 5.75 – 5.58 (m, 2H), 4.68 (tt, *J* = 9.3, 4.5 Hz, 1H), 3.93 (s, 3H), 3.48 (dt, *J* = 11.5, 5.8 Hz, 1H), 2.80 (t, *J* = 6.0 Hz, 1H), 2.77 – 2.69 (m, 1H), 2.21 – 2.07 (m, 2H), 1.99 – 1.88 (m, 1H), 1.86 – 1.66 (m, 6H), 1.63 – 1.42 (m, 6H). ^{13}C NMR (126 MHz, DMSO-d_6): δ 166.1, 161.2, 153.7, 153.2, 134.3, 131.4, 130.9, 129.7, 127.9, 126.3, 124.4, 112.4, 110.2, 94.2, 79.9, 56.7, 55.6, 34.2, 33.3, 33.1, 30.2, 28.4, 28.4, 25.0, 24.9, 22.8, 22.4. LC-MS (ESI): t_R = 5.58 min, area: 97%, *m/z* 444 [M + H]$^+$. HRMS (ESI) *m/z*: [M + H]$^+$ calcd. for $C_{27}H_{30}N_3O_3$ 444.2282, found 444.2266.

4.6.2.29. *cis*-5-(5-(3-Isopropyl-4-oxo-3,4,4a,5,8,8a-hexahydrophthalazin-1-yl)-2-methoxyphenyl)thiophene-2-carboxylic acid (**18**)

To a solution of **17** (1.00 g, 2.65 mmol) and 5-borono-thiophene-2-carboxylic acid (0.830 g, 4.85 mmol) in DME (10 mL) was added aq. Na_2CO_3 (1 M, 6.6 mL, 6.63 mmol) and $PdCl_2$(dppf) (97.0 mg, 0.133 mmol). The reaction mixture was heated to 120 °C in the microwave for 3 h and then filtered over Celite using EtOAc (100 mL). The filtrate was washed with 1 M aq. HCl (2 × 150 mL), brine (10 mL), dried over $MgSO_4$, filtered and concentrated *in vacuo*. The residue was purified on a silica gel column eluting with EtOAc/n-heptane + 5% AcOH (gradient, 5-35%) to afford **18** as a white solid (610 mg, 49%). ^1H NMR (500 MHz, DMSO-d_6): δ 8.21 (d, *J* = 2.2 Hz, 1H), 7.89 (dd, *J* = 8.8, 2.2 Hz, 1H), 7.74 (d, *J* = 4.0 Hz, 1H), 7.70 (d, *J* = 4.0 Hz, 1H), 7.26 (d, *J* = 8.8 Hz, 1H), 5.74 – 5.60 (m, 2H), 4.89 (hept, *J* = 6.7 Hz, 1H), 3.99 (s, 3H), 3.58 (dt, *J* = 11.6, 5.8 Hz, 1H), 2.81 (t, *J* = 6.1 Hz, 1H), 2.79 – 2.72 (m, 1H), 2.23 – 2.10 (m, 2H), 1.86 – 1.77 (m, 1H), 1.25 (d, *J* = 6.5 Hz, 3H), 1.16 (d, *J* = 6.7 Hz, 3H). ^{13}C NMR (126 MHz, DMSO-d_6): δ 166.2, 163.4, 156.4, 153.4, 144.1, 134.6, 132.6, 127.8, 127.6, 126.4, 125.9, 125.3, 124.2, 121.6, 112.7, 56.2, 45.8, 34.0, 29.8, 22.6, 22.0, 20.6, 20.2. LC-MS (ESI): t_R = 4.81 min, area: >98%, *m/z* 425 [M + H]$^+$. HRMS (ESI) *m/z*: [M + H]$^+$ calcd. for $C_{23}H_{25}N_2O_4S$ 425.1530, found 425.1541.

4.6.2.30. 5-(5-(*cis*-3-Isopropyl-4-oxo-3,4,4a,5,8,8a-hexahydrophthalazin-1-yl)-2-methoxyphenyl)thiophene-2-carboxamide (**6a**)

To a solution of **18** (88.0 mg, 0.207 mmol) in DCM (2 mL) was added HOBt (73.0 mg, 0.540 mmol) and EDC.HCl (100 mg, 0.522 mmol). This mixture was stirred for 2 h at rt before NH_3 in MeOH (7 M, 0.5 mL, 3.50 mmol) was added. The reaction mixture was stirred for 22 h. EtOAc (2 × 10 mL) was added and the organic phase was washed with sat. aq. NH_4Cl (2 × 10 mL) and brine (5 mL), dried over $MgSO_4$, filtered and concentrated *in vacuo*. The residue was purified on a silica gel column eluting with EtOAc/n-heptane (gradient, 35-100%) to afford **6a** as a white solid (58 mg, 72%). ^1H NMR (500 MHz, CDCl$_3$): δ 8.13 (d, *J* = 2.2 Hz, 1H), 7.79 (dd, *J* = 8.7, 2.3 Hz, 1H), 7.55 (d, *J* = 4.0 Hz, 1H), 7.51 (d, *J* = 4.0 Hz, 1H), 7.04 (d, *J* = 8.8 Hz, 1H), 6.04 (s, 2H), 5.83 – 5.76 (m, 1H), 5.72 – 5.65 (m, 1H), 5.05 (hept, *J* = 6.6 Hz, 1H), 4.00 (s, 3H), 3.33 (dt, *J* = 11.6, 5.8 Hz, 1H), 3.07 – 2.98 (m, 1H), 2.76 (t, *J* = 6.0 Hz, 1H), 2.26

– 2.15 (m, 2H), 2.08 – 2.01 (m, 1H), 1.34 (d, J = 6.6 Hz, 3H), 1.22 (d, J = 6.7 Hz, 3H). ^{13}C NMR (126 MHz, CDCl$_3$): δ 166.5, 164.3, 157.0, 153.2, 144.6, 136.9, 129.1, 128.2, 127.3, 126.2, 126.1, 126.1, 124.0, 122.6, 111.7, 56.0, 46.9, 34.9, 31.2, 23.2, 22.5, 20.8, 20.4. LC-MS (ESI): t_R = 4.47 min, area: 97%, m/z 424 [M + H]$^+$. HRMS (ESI) m/z: [M + H]$^+$ calcd. for C$_{23}$H$_{26}$N$_3$O$_3$S 424.1689, found 424.1683.

4.6.2.31. *N*-Butyl-5-(5-(*cis*-3-isopropyl-4-oxo-3,4,4a,5,8,8a-hexahydrophthalzin-1-yl)-2-methoxyphenyl)thiophene-2-carboxamide (**6b**)

This compound was prepared from **18** (88.0 mg, 0.207 mmol) and butan-1-amine (0.5 mL, 4.72 mmol) as described for **6a**. The title compound was obtained as a white solid (77 mg, 76%). ^{1}H NMR (500 MHz, CDCl$_3$): δ 8.11 (d, J = 2.3 Hz, 1H), 7.76 (dd, J = 8.7, 2.3 Hz, 1H), 7.51 (d, J = 4.0 Hz, 1H), 7.47 (d, J = 4.0 Hz, 1H), 7.02 (d, J = 8.7 Hz, 1H), 6.29 – 6.17 (m, 1H), 5.85 – 5.73 (m, 1H), 5.73 – 5.62 (m, 1H), 5.04 (hept, J = 6.8 Hz, 1H), 3.98 (s, 3H), 3.44 (q, J = 6.7 Hz, 2H), 3.33 (dt, J = 11.6, 5.8 Hz, 1H), 3.07 – 2.96 (m, 1H), 2.75 (t, J = 5.9 Hz, 1H), 2.27 – 2.13 (m, 2H), 2.08 – 1.99 (m, 1H), 1.60 (p, J = 7.4 Hz, 2H), 1.40 (h, J = 7.4 Hz, 2H), 1.33 (d, J = 6.6 Hz, 3H), 1.21 (d, J = 6.7 Hz, 3H), 0.95 (t, J = 7.4 Hz, 3H). ^{13}C NMR (126 MHz, CDCl$_3$): δ 166.5, 162.3, 156.9, 153.3, 143.1, 138.5, 128.1, 127.6, 127.0, 126.1, 126.1, 126.0, 124.0, 122.8, 111.7, 55.9, 46.8, 39.8, 34.8, 31.9, 31.1, 23.2, 22.4, 20.7, 20.3, 20.2, 13.9. LC-MS (ESI): t_R = 5.30 min, area: >98%, m/z 480 [M + H]$^+$. HRMS (ESI) m/z: [M + H]$^+$ calcd. for C$_{27}$H$_{34}$N$_3$O$_3$S 480.2315, found 480.2306.

4.6.2.32. 5-(5-(*cis*-3-Isopropyl-4-oxo-3,4,4a,5,8,8a-hexahydrophthalzin-1-yl)-2-methoxyphenyl)-*N*-(2-methoxyethyl)thiophene-2-carboxamide (**6c**)

This compound was prepared from **18** (212 mg, 0.50 mmol) and 2-methoxyethylamine (75 mg, 1.0 mmol) as described for **6a**. The title compound was obtained as a white solid (36 mg, 15%). ^{1}H NMR (250 MHz, CDCl$_3$): δ 8.12 (d, J = 2.05 Hz, 1H), 7.77 (dd, J = 2.21, 8.69 Hz, 1H), 7.53 – 7.43 (m, 2H), 7.03 (d, J = 8.69 Hz, 1H), 6.43 (t, J = 4.98 Hz, 1H), 5.86 – 5.60 (m, 2H), 5.15 – 4.95 (m, 1H), 3.99 (s, 3H), 3.72 – 3.50 (m, 4H), 3.40 (s, 3H), 3.37 – 3.26 (m, 1H), 3.10 – 2.92 (m, 1H), 2.76 (t, J = 5.77 Hz, 1H), 2.32 – 2.07 (m, 3H), 1.34 (d, J = 6.63 Hz, 3H), 1.27 – 1.12 (m, 3H). ^{13}C NMR (126 MHz, CDCl$_3$): δ 166.8, 162.6, 157.3, 153.5, 143.8, 138.4, 128.5, 128.2, 127.4, 126.3, 124.3, 123.0, 112.0, 77.7, 77.4, 71.6, 59.3, 56.2, 47.1, 40.0, 35.1, 31.5, 23.5, 22.7, 21.0, 20.6. LC-MS (ESI): t_R = 5.10 min, area: >98%, m/z 482 [M + H]$^+$. HRMS (ESI) m/z: [M + H]$^+$ calcd. for C$_{26}$H$_{32}$N$_3$O$_4$ 482.2108, found 482.2091.

4.6.2.33. *N*-(Furan-2-ylmethyl)-5-(5-(*cis*-3-isopropyl-4-oxo-3,4,4a,5,8,8a-hexahydrophthalzin-1-yl)-2-methoxyphenyl)thiophene-2-carboxamide (**6d**)

This compound was prepared from **18** (117 mg, 0.276 mmol) and furan-2-ylmethanamine (0.06 mL, 0.63 mmol) as described for **6a**. The title compound was obtained as a white solid (82 mg, 57%). ^{1}H NMR (500 MHz, CDCl$_3$): δ 8.12 (d, J = 2.3 Hz, 1H), 7.78 (dd, J = 8.7, 2.3 Hz, 1H), 7.52 (d, J = 4.0 Hz, 1H), 7.48 (d, J = 4.0 Hz, 1H), 7.42 – 7.33 (m, 1H), 7.03 (d, J = 8.7 Hz, 1H), 6.43 (t, J = 5.6 Hz, 1H), 6.35 (dd, J = 3.2, 1.8 Hz, 1H), 6.31 (d, J = 3.3 Hz, 1H), 5.84 – 5.75 (m, 1H), 5.75 – 5.61 (m, 1H), 5.05 (hept, J = 6.7 Hz, 1H), 4.64 (d, J = 5.4 Hz, 2H), 3.99 (s, 3H), 3.33 (dt, J = 11.6, 5.8 Hz, 1H), 3.09 – 2.94 (m, 1H), 2.76 (t, J = 6.0 Hz, 1H), 2.28 – 2.13 (m, 2H), 2.08 – 2.00 (m, 1H), 1.34 (d, J = 6.6 Hz, 3H), 1.21 (d, J = 6.7 Hz, 3H). ^{13}C NMR (126 MHz, CDCl$_3$): δ 166.5, 162.0, 157.0, 153.2, 151.2, 143.7, 137.6, 128.2, 128.2, 127.1, 126.1, 126.1, 126.0, 126.0, 124.0, 122.7, 111.7, 110.7, 107.9, 56.0, 46.9, 37.0, 34.9, 31.2, 23.2, 22.4, 20.7, 20.4. LC-MS (ESI): t_R = 5.08 min, area: 97%, m/z 504 [M + H]$^+$. HRMS (ESI) m/z: [M + H]$^+$ calcd. for

$C_{28}H_{30}N_3O_4S$ 504.1952, found 504.1927.

4.6.2.34. N-(2-Amino-2-oxoethyl)-5-(5-(cis-3-isopropyl-4-oxo-3,4,4a,5,8,8a-hexahydrophthalazin-1-yl)-2-methoxyphenyl)thiophene-2-carboxamide (6e)

This compound was prepared from **18** (114 mg, 0.269 mmol) and glycinamide.HCl (74 mg, 0.67 mmol) as described for **6a**. The title compound was obtained as a white solid (88 mg, 63%). ^1H NMR (500 MHz, CDCl$_3$): δ 8.11 (d, J = 2.2 Hz, 1H), 7.77 (dd, J = 8.7, 2.3 Hz, 1H), 7.62 (d, J = 4.0 Hz, 1H), 7.49 (d, J = 4.0 Hz, 1H), 7.24 (t, J = 5.3 Hz, 2H), 7.02 (d, J = 8.8 Hz, 1H), 6.61 (s, 1H), 5.85 – 5.75 (m, 2H), 5.71 – 5.65 (m, 1H), 5.04 (hept, J = 6.7 Hz, 1H), 4.18 (d, J = 5.1 Hz, 2H), 3.97 (s, 3H), 3.32 (dt, J = 11.6, 5.8 Hz, 1H), 3.05 – 2.97 (m, 1H), 2.75 (t, J = 6.0 Hz, 1H), 2.25 – 2.14 (m, 2H), 2.07 – 1.99 (m, 1H), 1.33 (d, J = 6.6 Hz, 3H), 1.21 (d, J = 6.7 Hz, 3H). ^{13}C NMR (126 MHz, CDCl$_3$): δ 171.5, 166.5, 162.9, 157.0, 153.2, 144.2, 137.0, 128.7, 128.2, 127.2, 126.1, 126.0, 124.0, 122.6, 111.7, 56.0, 46.9, 43.4, 34.9, 31.2, 23.2, 22.5, 20.8, 20.4. LC-MS (ESI): t_R = 4.19 min, area: 95%, m/z 481 [M + H]$^+$. HRMS (ESI) m/z: [M + H]$^+$ calcd. for $C_{25}H_{29}N_4O_4$ 481.1904, found 481.1924.

4.6.2.35. cis-1-(5-(3-Isopropyl-4-oxo-3,4,4a,5,8,8a-hexahydrophthalazin-1-yl)-2-methoxyphenyl)azetidine-3-carbonitrile (19)

To a solution of **17** (2.60 g, 6.89 mmol) in dry toluene (15 mL) was added Xantphos (0.798 g, 1.38 mmol), Pd(II)(OAc)$_2$ (0.155 g, 0.689 mmol), Cs$_2$CO$_3$ (4.49 g, 13.8 mmol) and azetidine-3-carbonitrile.HCl (0.577 g, 6.89 mmol). The mixture was stirred at 100 °C for 68 h. The reaction mixture was filtered over celite with EtOAc (2 × 50 mL). The filtrate was washed with sat. aq. NH$_4$Cl (2 × 25 mL) and brine (20 mL). The organic phase was dried over MgSO$_4$, filtered and concentrated *in vacuo*. The residue was purified on a silica gel column eluting with EtOAc/n-heptane (gradient, 5-40%) to afford **19** as a white solid (1.21 g, 46%). ^1H NMR (500 MHz, CDCl$_3$): δ 7.23 (dd, J = 8.4, 2.1 Hz, 1H), 7.04 (d, J = 2.1 Hz, 1H), 6.81 (d, J = 8.4 Hz, 1H), 5.83 – 5.62 (m, 2H), 5.04 (hept, J = 6.6 Hz, 1H), 4.29 (td, J = 7.9, 4.2 Hz, 2H), 4.12 (td, J = 7.2, 1.7 Hz, 2H), 3.85 (s, 3H), 3.61 – 3.51 (m, 1H), 3.28 (dt, J = 11.5, 5.8 Hz, 1H), 3.05 – 2.96 (m, 1H), 2.72 (t, J = 5.9 Hz, 1H), 2.25 – 2.10 (m, 2H), 2.06 – 1.96 (m, 1H), 1.32 (d, J = 6.6 Hz, 3H), 1.20 (d, J = 6.7 Hz, 3H). ^{13}C NMR (126 MHz, CDCl$_3$): δ 166.5, 153.7, 151.0, 139.8, 128.2, 126.1, 124.1, 120.0, 119.1, 110.6, 110.2, 56.7, 56.6, 55.7, 46.8, 34.8, 31.1, 23.3, 22.5, 20.7, 20.3, 19.1. LC-MS (ESI): t_R = 4.45 min, area: >98%, m/z 379 [M + H]$^+$. HRMS (ESI) m/z: [M + H]$^+$ calcd. for $C_{22}H_{27}N_4O_2$ 379.2129, found 379.2128.

4.6.2.36. cis-1-(5-(3-Isopropyl-4-oxo-3,4,4a,5,8,8a-hexahydrophthalazin-1-yl)-2-methoxyphenyl)azetidine-3-carboxylic acid (20)

A solution of **19** (1.05 g, 2.77 mmol) in EtOH (2.7 mL) and aq. NaOH (1 M, 2.7 mL, 2.7 mmol) was stirred at 75 °C for 24 h. EtOAc (2 × 10 mL) was added and the organic phase was washed with sat. aq. NH$_4$Cl (2 × 10 mL) and brine (5 mL). The combined organic phases were dried over MgSO$_4$, filtered and concentrated *in vacuo* to afford **20** as a white solid (0.55 g, 47%). ^1H NMR (500 MHz, DMSO-d_6): δ 7.18 (d, J = 8.3 Hz, 1H), 6.95 – 6.88 (m, 1H), 6.86 (d, J = 8.5 Hz, 1H), 5.71 – 5.64 (m, 1H), 5.64 – 5.57 (m, 1H), 4.85 (hept, J = 6.8 Hz, 1H), 4.06 – 3.94 (m, 2H), 3.92 – 3.85 (m, 2H), 3.73 (s, 3H), 3.37 (dt, J = 11.6, 5.7 Hz, 1H), 3.31 – 3.25 (m, 1H), 2.80 – 2.65 (m, 2H), 2.23 – 2.10 (m, 1H), 2.10 – 2.01 (m, 1H), 1.84 – 1.72 (m, 1H), 1.21 (d, J = 6.7 Hz, 3H), 1.11 (d, J = 6.7 Hz, 3H). ^{13}C NMR (126 MHz, DMSO-d_6): δ 166.0, 154.0,

150.4, 141.4, 127.5, 126.0, 124.2, 117.4, 111.0, 109.2, 56.5, 55.6, 45.7, 45.4, 34.0, 30.0, 22.9, 22.1, 20.5, 20.2. LC-MS (ESI): t_R = 4.55 min, area: 96%, m/z 398 [M + H]$^+$. HRMS (ESI) m/z: [M + H]$^+$ calcd. for $C_{22}H_{28}N_3O_4$ 398.2074, found 398.2060.

4.6.2.37. 1-(5-(*cis*-3-Isopropyl-4-oxo-3,4,4a,5,8,8a-hexahydrophthalazin-1-yl)-2-methoxyphenyl)azetidine-3-carboxamide (**7a**)

This compound was prepared from **20** (110 mg, 0.277 mmol) and NH$_3$ in MeOH (7 M, 1.6 mL, 11 mmol) as described for **6a**. The title compound was obtained as a white solid (63 mg, 56%). ^{1}H NMR (500 MHz, DMSO-d_6): δ 7.45 (s, 1H), 7.21 (dd, J = 8.5, 2.1 Hz, 1H), 7.00 (s, 1H), 6.95 − 6.86 (m, 2H), 5.77 − 5.54 (m, 2H), 4.86 (hept, J = 6.7 Hz, 1H), 4.00 (q, J = 7.4 Hz, 2H), 3.84 (q, J = 6.9 Hz, 2H), 3.76 (s, 3H), 3.42 − 3.37 (m, 2H), 2.81 − 2.67 (m, 2H), 2.22 − 2.02 (m, 2H), 1.85 − 1.74 (m, 1H), 1.23 (d, J = 6.4 Hz, 3H), 1.13 (d, J = 6.8 Hz, 3H). ^{13}C NMR (126 MHz, DMSO-d_6): δ 173.7, 166.0, 154.0, 150.4, 141.2, 127.5, 126.0, 124.2, 117.6, 111.0, 109.3, 55.9, 55.8, 55.6, 45.7, 34.3, 34.0, 30.0, 22.8, 22.0, 20.5, 20.2. LC-MS (ESI): t_R = 4.13 min, area: >98%, m/z 397 [M + H]$^+$. HRMS (ESI) m/z: [M + H]$^+$ calcd. for $C_{22}H_{29}N_4O_3$ 397.2234, found 397.2216.

4.6.2.38. *N*-Butyl-1-(5-(*cis*-3-isopropyl-4-oxo-3,4,4a,5,8,8a-hexahydrophthalazin-1-yl)-2-methoxyphenyl)azetidine-3-carboxamide (**7b**)

This compound was prepared from **20** (94.0 mg, 0.236 mmol) and butan-1-amine (0.5 mL, 5.20 mmol) as described for **6a**. The title compound was obtained as a white solid (34 mg, 31%). ^{1}H NMR (500 MHz, DMSO-d_6): δ 7.94 (t, J = 5.6 Hz, 1H), 7.21 (dd, J = 8.4, 2.1 Hz, 1H), 6.99 − 6.84 (m, 2H), 5.74 − 5.57 (m, 2H), 4.86 (hept, J = 5.3 Hz, 1H), 4.01 (q, J = 7.4 Hz, 2H), 3.83 (q, J = 6.7 Hz, 2H), 3.76 (s, 3H), 3.46 − 3.38 (m, 2H), 3.05 (q, J = 6.6 Hz, 2H), 2.82 − 2.67 (m, 2H), 2.21 − 2.02 (m, 2H), 1.86 − 1.74 (m, 1H), 1.37 (p, J = 7.0 Hz, 2H), 1.32 − 1.18 (m, 5H), 1.12 (d, J = 6.7 Hz, 3H), 0.86 (t, J = 7.3 Hz, 3H). ^{13}C NMR (126 MHz, DMSO-d_6): δ 171.3, 166.0, 154.1, 150.4, 141.2, 127.5, 126.0, 124.2, 117.6, 111.1, 109.4, 55.9, 55.8, 55.6, 45.7, 38.3, 34.4, 34.0, 31.2, 30.0, 22.8, 22.0, 20.5, 20.2, 19.6, 13.8. LC-MS (ESI): t_R = 5.02 min, area: >98%, m/z 453 [M + H]$^+$. HRMS (ESI) m/z: [M + H]$^+$ calcd. for $C_{26}H_{37}N_4O_3$ 453.2860, found 453.2846.

4.6.2.39. *N*-(Furan-2-ylmethyl)-1-(5-(*cis*-3-isopropyl-4-oxo-3,4,4a,5,8,8a-hexahydrophthalazin-1-yl)-2-methoxyphenyl)azetidine-3-carboxamide (**7c**)

This compound was prepared from **20** (110 mg, 0.277 mmol) and furan-2-ylmethanamine (0.06 mL, 0.679 mmol) as described for **6a**. The title compound was obtained as a white solid (93 mg, 64%). ^{1}H NMR (500 MHz, DMSO-d_6): δ 8.47 (t, J = 5.6 Hz, 1H), 7.58 (d, J = 1.4 Hz, 1H), 7.22 (dd, J = 8.5, 2.2 Hz, 1H), 6.91 (d, J = 2.1 Hz, 1H), 6.89 (d, J = 8.5 Hz, 1H), 6.39 (dd, J = 3.2, 1.9 Hz, 1H), 6.24 (d, J = 3.1 Hz, 1H), 5.72 − 5.66 (m, 1H), 5.66 − 5.58 (m, 1H), 4.86 (hept, J = 6.7 Hz, 1H), 4.28 (d, J = 5.5 Hz, 2H), 4.02 (q, J = 7.3 Hz, 2H), 3.86 (q, J = 6.7 Hz, 2H), 3.76 (s, 3H), 3.47 − 3.38 (m, 2H), 2.79 − 2.69 (m, 2H), 2.21 − 2.02 (m, 2H), 1.85 − 1.74 (m, 1H), 1.23 (d, J = 6.6 Hz, 3H), 1.13 (d, J = 6.7 Hz, 3H). ^{13}C NMR (126 MHz, DMSO-d_6): δ 171.5, 166.0, 154.0, 152.2, 150.4, 142.2, 141.1, 127.5, 126.0, 124.2, 117.6, 111.1, 110.5, 109.4, 107.0, 55.8, 55.7, 55.6, 45.7, 35.6, 34.3, 34.0, 30.0, 22.8, 22.0, 20.5, 20.2. LC-MS (ESI): t_R = 4.85 min, area: 97%, m/z 477 [M + H]$^+$. HRMS (ESI) m/z: [M + H]$^+$ calcd. for $C_{27}H_{33}N_4O_4$ 477.2496, found 477.2481.

4.6.2.40. *N*-(2-Amino-2-oxoethyl)-1-(5-(*cis*-3-isopropyl-4-oxo-3,4,4a,5,8,8a-hexahydrophthalazin-1-yl)-2-methoxyphenyl)azetidine-3-carboxamide (**7d**)

This compound was prepared from **20** (110 mg, 0.277 mmol) and glycinamide.HCl (76 mg, 1.0 mmol) as described for **6a**. The title compound was obtained as a white solid (90 mg, 70%). ^{1}H NMR (500 MHz, DMSO-d_6): δ 8.19 (t, *J* = 5.9 Hz, 1H), 7.36 (s, 1H), 7.21 (dd, *J* = 8.5, 2.1 Hz, 1H), 7.05 (s, 1H), 6.91 (d, *J* = 2.1 Hz, 1H), 6.89 (d, *J* = 8.5 Hz, 1H), 5.75 – 5.65 (m, 1H), 5.65 – 5.56 (m, 1H), 4.86 (hept, *J* = 6.7 Hz, 1H), 4.02 (q, *J* = 7.3 Hz, 2H), 3.86 (q, *J* = 6.7 Hz, 2H), 3.76 (s, 3H), 3.65 (d, *J* = 5.8 Hz, 2H), 3.48 (p, *J* = 7.4 Hz, 1H), 3.41 – 3.36 (m, 4H), 2.79 – 2.68 (m, 2H), 2.22 – 2.02 (m, 2H), 1.86 – 1.73 (m, 1H), 1.23 (d, *J* = 6.6 Hz, 3H), 1.13 (d, *J* = 6.7 Hz, 3H). ^{13}C NMR (126 MHz, DMSO-d_6): δ 172.0, 171.0, 166.0, 154.1, 150.4, 141.2, 127.5, 126.0, 124.2, 117.6, 111.0, 109.3, 55.9, 55.8, 55.6, 45.7, 42.0, 34.4, 34.0, 30.0, 22.9, 22.1, 20.5, 20.2. LC-MS (ESI): t_R = 3.90 min, area: >98%, *m/z* 454 [M + H]$^+$. HRMS (ESI) *m/z*: [M + H]$^+$ calcd. for $C_{24}H_{32}N_5O_4$ 454.2449, found 454.2442.

5.   **Author contributions**

E.d.H., E.E., M.P.K.J., T.v.d.B., J.V., G.J.S. and I.J.P.d.E. were involved in compound design, synthesis and analysis. A.K.S. and D.G.B. were involved in protein production, crystallization, data collection and refinement for structural studies. E.d.H., A.K.S. and D.G.B. were involved in crystal structure analysis. T.v.d.M., M.v.d.W., P.S. and M.S. were involved in the biochemical assays. G.C. and L.M. were involved in the phenotypic cellular assays and T.D.K. performed the target validation experiments, supervised by H.P.d.K. E.E., M.W., M.S., L.M., G.J.S., I.J.P.d.E., D.G.B. and R.L. supervised the experiments and conceived the project. E.d.H., A.K.S., G.J.S., I.J.P.d.E., H.P.d.K., D.G.B. and R.L. integrated all data and wrote the manuscript.

6. References

1. P. Büscher, G. Cecchi, V. Jamonneau*, et al.*, Human African trypanosomiasis, The Lancet, 390 (2017) 2397-2409.
2. R. Brun, J. Blum, F. Chappuis*, et al.*, Human african trypanosomiasis, The Lancet, 375 (2010) 148-159.
3. N. Feasey, M. Wansbrough-Jones, D.C. Mabey*, et al.*, Neglected tropical diseases, British Medical Bulletin, 93 (2010) 179-200.
4. P. Babokhov, A.O. Sanyaolu, W.A. Oyibo*, et al.*, A current analysis of chemotherapy strategies for the treatment of human African trypanosomiasis, Pathogens and Global Health, 107 (2013) 242-252.
5. A.H. Fairlamb, Chemotherapy of human African trypanosomiasis: current and future prospects, Trends Parasitol, 19 (2003) 488-494.
6. V. Delespaux, H.P. de Koning, Drugs and drug resistance in African trypanosomiasis, Drug Resistance Updates, 10 (2007) 30-50.
7. G. Eperon, M. Balasegaram, J. Potet*, et al.*, Treatment options for second-stage gambiense human African trypanosomiasis, Expert Review of Anti-infective Therapy, 12 (2014) 1407-1417.
8. P.G.E. Kennedy, Human African trypanosomiasis of the CNS: current issues and challenges, Journal of Clinical Investigation, 113 (2004) 496-504.
9. H.P. de Koning, Drug resistance in protozoan parasites, Emerging Topics in Life Sciences, 1 (2017) 627.
10. J.C. Munday, L. Settimo, H.P. de Koning, Transport proteins determine drug sensitivity and resistance in a protozoan parasite, Trypanosoma brucei, Frontiers in Pharmacology, 6 (2015).
11. P.M.A. Calverley, K.F. Rabe, U.-M. Goehring*, et al.*, Roflumilast in symptomatic chronic obstructive pulmonary disease: two randomised clinical trials, The Lancet, 374 (2009) 685-694.
12. A. Hatzelmann, C. Schudt, Anti-Inflammatory and Immunomodulatory Potential of the Novel PDE4 Inhibitor Roflumilast in Vitro, Journal of Pharmacology and Experimental Therapeutics, 297 (2001) 267-279.
13. M. Packer , J.R. Carver , R.J. Rodeheffer , *et al.*, Effect of Oral Milrinone on Mortality in Severe Chronic Heart Failure, New England Journal of Medicine, 325 (1991) 1468-1475.
14. M. Boolell, M.J. Allen, S.A. Ballard*, et al.*, Sildenafil: an orally active type 5 cyclic GMP-specific phosphodiesterase inhibitor for the treatment of penile erectile dysfunction, International Journal of Impotence Research, 8 (1996) 47-52.
15. M. Oberholzer, G. Marti, M. Baresic*, et al.*, The Trypanosoma brucei cAMP phosphodiesterases TbrPDEB1 and TbrPDEB2: flagellar enzymes that are essential for parasite virulence, The FASEB Journal, 21 (2007) 720-731.
16. S. Kunz, J.A. Beavo, M.A. D'Angelo*, et al.*, Cyclic nucleotide specific phosphodiesterases of the kinetoplastida: A unified nomenclature, Molecular and Biochemical Parasitology, 145 (2006) 133-135.
17. E. Amata, N.D. Bland, R.K. Campbell*, et al.*, Evaluation of pyrrolidine and pyrazolone derivatives as inhibitors of trypanosomal phosphodiesterase B1 (TbrPDEB1), Tetrahedron Letters, 56 (2015) 2832-2835.
18. E. Amata, N.D. Bland, C.T. Hoyt*, et al.*, Repurposing human PDE4 inhibitors for neglected tropical diseases: Design, synthesis and evaluation of cilomilast analogues as Trypanosoma brucei PDEB1 inhibitors, Bioorganic & Medicinal Chemistry Letters, 24 (2014) 4084-4089.
19. C. Jansen, H. Wang, A.J. Kooistra*, et al.*, Discovery of NovelTrypanosoma bruceiPhosphodiesterase B1 Inhibitors by Virtual Screening against the Unliganded TbrPDEB1 Crystal Structure, Journal of Medicinal Chemistry, 56 (2013) 2087-2096.
20. S.O. Ochiana, N.D. Bland, L. Settimo*, et al.*, Repurposing human PDE4 inhibitors for neglected tropical diseases. Evaluation of analogs of the human PDE4 inhibitor GSK-256066 as inhibitors of PDEB1 of Trypanosoma brucei, Chemical Biology & Drug Design, (2014).
21. C. Wang, T.D. Ashton, A. Gustafson*, et al.*, Synthesis and evaluation of human phosphodiesterases (PDE) 5 inhibitor analogs as trypanosomal PDE inhibitors. Part 1. Sildenafil analogs, Bioorganic & Medicinal Chemistry Letters, 22 (2012) 2579-2581.
22. J.L. Woodring, N.D. Bland, S.O. Ochiana*, et al.*, Synthesis and assessment of catechol diether compounds as inhibitors of trypanosomal phosphodiesterase B1 (TbrPDEB1), Bioorganic & Medicinal Chemistry Letters, 23 (2013) 5971-5974.
23. A.R. Blaazer, K.M. Orrling, A. Shanmugham*, et al.*, Fragment-Based Screening in Tandem with Phenotypic Screening Provides Novel Antiparasitic Hits, Journal of Biomolecular Screening, 20 (2015) 131-140.
24. K.M. Orrling, C. Jansen, X.L. Vu*, et al.*, Catechol pyrazolinones as trypanocidals: fragment-based design, synthesis, and pharmacological evaluation of nanomolar inhibitors of trypanosomal phosphodiesterase B1, Journal of Medicinal Chemistry, 55 (2012) 8745-8756.
25. H.P. de Koning, M.K. Gould, G.J. Sterk*, et al.*, Pharmacological validation of Trypanosoma brucei phosphodiesterases as novel drug targets, Journal of Infectious Diseases, 206 (2012) 229-237.

4

26. M. Van der Mey, A. Hatzelmann, I.J. Van der Laan*, et al.*, Novel Selective PDE4 Inhibitors. 1. Synthesis, Structure-Activity Relationships, and Molecular Modeling of 4-(3, 4-Dimethoxyphenyl)-2 H-phthalazin-1-ones and Analogues, Journal of Medicinal Chemistry, 44 (2001) 2511-2522.

27. M. Van der Mey, A. Hatzelmann, G.P.M. Van Klink*, et al.*, Novel Selective PDE4 Inhibitors. 2. Synthesis and structure-activity relationships of 4-aryl-substituted cis-tetra- and cis-hexahydrophthalazinones, Journal of Medicinal Chemistry, 44 (2001) 2523-2535.

28. J. Veerman, T. van den Bergh, K.M. Orrling*, et al.*, Synthesis and evaluation of analogs of the phenylpyridazinone NPD-001 as potent trypanosomal TbrPDEB1 phosphodiesterase inhibitors and in vitro trypanocidals, Bioorganic & Medicinal Chemistry, 24 (2016) 1573-1581.

29. J.E. Souness, S. Rao, Proposal for Pharmacologically Distinct Conformers of PDE4 Cyclic AMP Phosphodiesterases, Cellular Signalling, 9 (1997) 227-236.

30. V. Boswell-Smith, D. Spina, C.P. Page, Phosphodiesterase inhibitors, British Journal of Pharmacology, 147 (2006) S252-S257.

31. P.M. Seldon, P.J. Barnes, K. Meja*, et al.*, Suppression of lipopolysaccharide-induced tumor necrosis factor-alpha generation from human peripheral blood monocytes by inhibitors of phosphodiesterase 4: interaction with stimulants of adenylyl cyclase., Molecular Pharmacology, 48 (1995) 747-757.

32. A.R. Blaazer, A.K. Singh, E. de Heuvel*, et al.*, Targeting a subpocket in Trypanosoma brucei phosphodiesterase B1 (TbrPDEB1) enables the structure-based discovery of selective inhibitors with trypanocidal activity, Journal of Medicinal Chemistry, 61 (2018) 3870-3888.

33. T. Seebeck, G.J. Sterk, H. Ke, Phosphodiesterase inhibitors as a new generation of antiprotozoan drugs: exploiting the benefit of enzymes that are highly conserved between host and parasite, Future Medicinal Chemistry, 3 (2011) 1289-1306.

34. G. Winter, C.M.C. Lobley, S.M. Prince, Decision making in xia2, Acta Crystallographica Section D, 69 (2013) 1260-1273.

35. W. Kabsch, Integration, scaling, space-group assignment and post-refinement, Acta Crystallographica Section D, 66 (2010) 133-144.

36. P.R. Evans, G.N. Murshudov, How good are my data and what is the resolution?, Acta Crystallographica Section D, 69 (2013) 1204-1214.

37. T.G.G. Battye, L. Kontogiannis, O. Johnson*, et al.*, iMOSFLM: a new graphical interface for diffraction-image processing with MOSFLM, Acta Crystallographica Section D, 67 (2011) 271-281.

38. M.D. Winn, C.C. Ballard, K.D. Cotwan*, et al.*, Overview of the CCP4 suite and current developments, Acta Crystallographica Section D, 67 (2011) 235-242.

39. A.J. McCoy, R.W. Grosse-Kunstleve, P.D. Adams*, et al.*, Phaser crystallographic software, Journal of Applied Crystallography, 40 (2007) 658-674.

40. P. Emsley, B. Lohkamp, W.G. Scott*, et al.*, Features and development of Coot, Acta Crystallographica Section D, 66 (2010) 486-501.

41. G.N. Murshudov, P. Skubak, A.A. Lebedev*, et al.*, REFMAC5 for the refinement of macromolecular crystal structures, Acta Crystallographica Section D, 67 (2011) 355-367.

42. The PyMOL Molecular Graphics System, Version 1.7, Schrödinger, LLC.
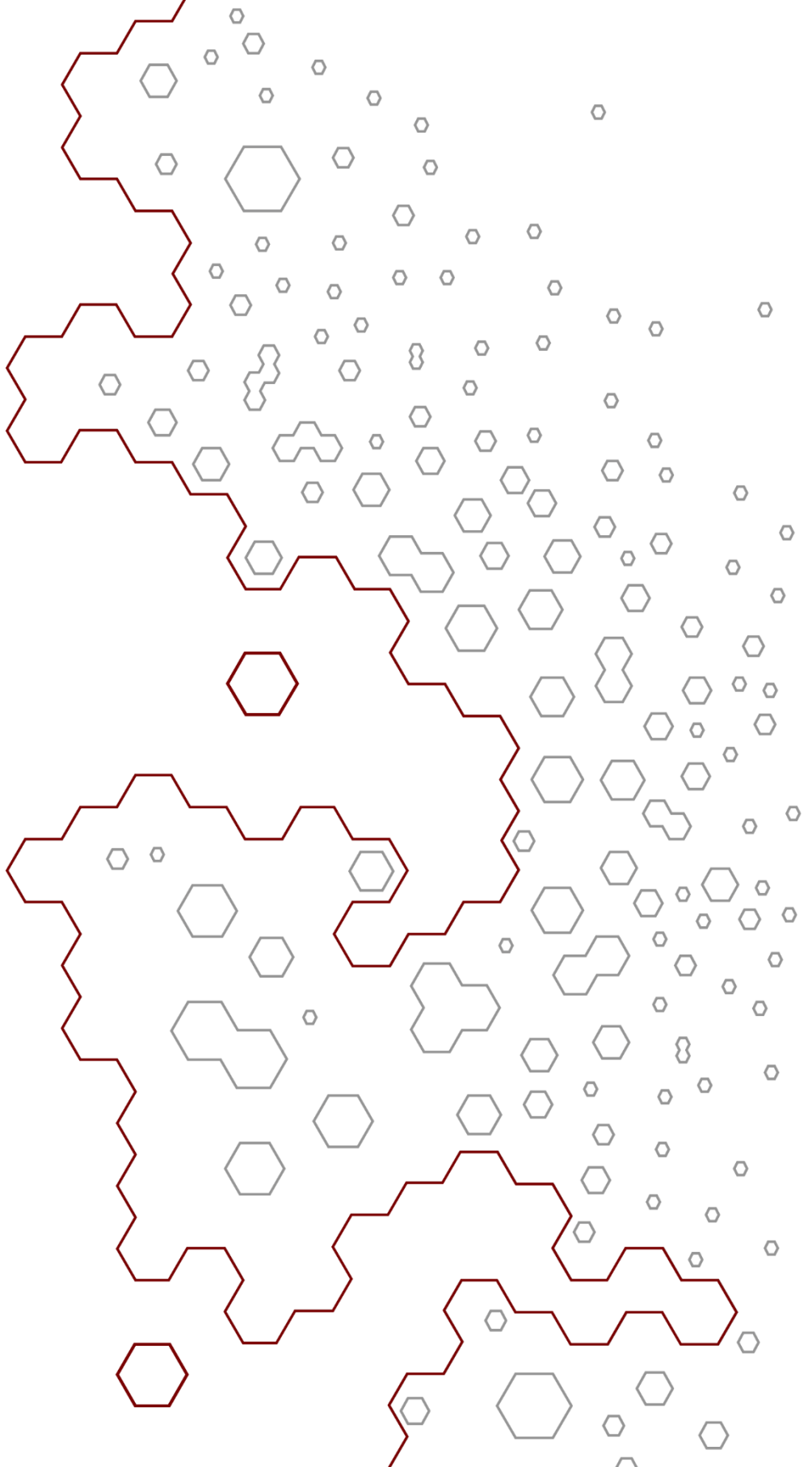
Chapter 5

Development of alkynamide phthalazinones as a new class of TbrPDEB1 inhibitors

Erik de Heuvel, Abhimanyu K. Singh, Pierre Boronat, Albert J. Kooistra, Tiffany van der Meer, Payman Sadek, Antoni R. Blaazer, Nathan C. Shaner, Daphne S. Bindels, Guy Caljon, Louis Maes, Geert Jan Sterk, Marco Siderius, Michael Oberholzer, Iwan J.P. de Esch, David G. Brown, Rob Leurs.

Abstract

Inhibitors against *Trypanosoma brucei* phosphodiesterase B1 (TbrPDEB1) and B2 (TbrPDEB2) have gained interest as new treatments for human African trypanosomiasis. The recently reported alkynamide tetrahydrophthalazinones, which show submicromolar activities against TbrPDEB1 and anti-*T. brucei* activity, have been used as starting point for the discovery of new TbrPDEB1 inhibitors. Structure-based design indicated that the alkynamide-nitrogen atom can be readily decorated, leading to the discovery of **37**, a potent TbrPDEB1 inhibitor with submicromolar activities against *T. brucei* parasites. Furthermore, **37** is more potent against TbrPDEB1 than hPDE4 and shows no cytotoxicity on human MRC-5 cells. The crystal structures of the catalytic domain of TbrPDEB1 co-crystalized with several different alkynamides show a bidentate interaction with key-residue Gln874, but no interaction with the parasite-specific P-pocket, despite being (uniquely) a more potent inhibitor for the parasite PDE. Incubation of blood stream form trypanosomes by **37** increases intracellular cAMP levels and results in the distortion of the cell cycle and cell death, validating phosphodiesterase inhibition as mode of action.

5

1. Introduction

The two causative agents of human African trypanosomiasis (HAT), i.e. *Trypanosoma brucei* (*T.b.*) *rhodesiense* and *T.b. gambiense* are endemic in sub-Saharan Africa.[1, 2] The drugs against HAT currently available on the market have major disadvantages, including limited clinical efficacy in certain disease stages, complex administration protocols and toxicity.[1, 3-5] Additionally, the small repertoire of available drugs against HAT suffers from emerging drug resistance.[6-10] While the number of new HAT cases has dropped considerably in the last few years,[11] there remains an interest in developing novel and non-toxic trypanocidal agents.[6-10] Several enzymes have been identified as potential targets for development of such new treatments.[12-16] For example, *T. brucei* 3'5'-cyclic nucleotide phosphodiesterase B1 and B2 (TbrPDEB1 and TbrPDEB2) have been validated as essential enzymes of the parasite and can be exploited as a drug target.[16, 17] The high sequence homology (88%) between the catalytic sites of the TbrPDEB1 and B2 creates a high degree of equipotency against the paralogues.[17-19] However, selectivity for the parasite PDE over the human orthologues, especially human PDE4 (hPDE4), is required to limit unwanted side effects (e.g. emesis, gastrointestinal disturbance and immune suppression).[19-23]

Cilomilast, **1**
TbrPDEB1 IC$_{50}$ = 16 µM
hPDE4B IC$_{50}$ = 0.090 µM

2
TbrPDEB1 IC$_{50}$ = 0.95 µM
hPDE4B IC$_{50}$ = 0.038 µM
T. brucei IC$_{50}$ = 26 µM

Rolipram, **3**
TbrPDEB1 IC$_{50}$ >100 µM
hPDE4 IC$_{50}$ = 0.13 µM

4
TbrPDEB1 IC$_{50}$ = 0.049 µM
hPDE4B IC$_{50}$ = 0.0046 µM
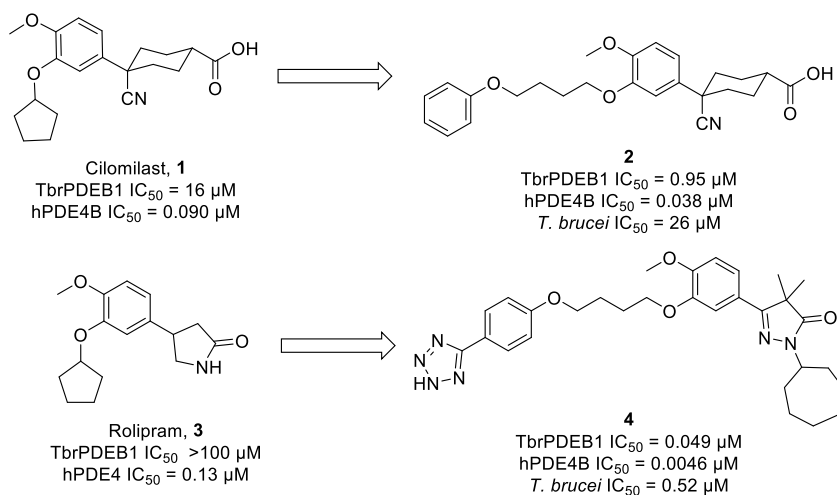*T. brucei* IC$_{50}$ = 0.52 µM

Figure 1: Repurposing hPDE4 inhibitors for the development of potent TbrPDEB1 inhibitors for the treatment of human African trypanosomiasis.[19, 24]

Over the years, several studies reported different hPDE4 inhibitors as starting point for TbrPDEB1 inhibitors, resulting in a number of potent inhibitors, e.g. cilomilast analogue **2** and rolipram analogue **4** (Figure 1).[19, 24] However, selectivity for TbrPDEB1 over hPDE4 in combination with antiparasitic activity has been a challenge.[19, 24]

Recently, we have shown that the activity profile for TbrPDEB1 over hPDE4 can be obtained by targeting a parasite-specific P-pocket present near the active site of TbrPDEB1.[25, 26] Biphenyl tetrahydrophthalazinone NPD-008 (**5**) (Figure 2) exhibits a submicromolar potency for TbrPDEB1 (pK_i = 7.0) and a 10-fold selectivity over hPDE4 (pK_i = 6.0).[25] The crystal structure of **5** (PDB: 5G2B) in the catalytic domain of TbrPDEB1 shows that the glycinamide tail occupies the P-pocket thereby explaining the observed selectivity for TbrPDEB1 over hPDE4 (Figure 2).[25] Successful targeting of the P-pocket was also observed in the crystal structure of TbrPDEB1 co-crystallized with NPD-937 (**6**, PDB: 5L8Y), indicating that a longer and more spacious tail group is also able to enter the P-pocket resulting in selectivity for TbrPDEB1 over hPDE4 (TbrPDEB1 pK_i = 6.4 *vs* hPDE4 pK_i = 5.5).[25] However, **5** and **6** show an unfortunate reduced phenotypic activity against *T. brucei* (pIC_{50} = 5.3 and pIC_{50} = 5.1, respectively), thereby halting further development of these compounds as trypanocidals.[25] Further research to replace the phenyl linker and tail group of **5** by an alkynamide resulted in the discovery of NPD-048 (**7**) which displays a submicromolar potency against TbrPDEB1 (TbrPDEB1 pK_i = 6.2).[27] Although this alkynamide does not show a similar activity profile (hPDE4 pK_i = 6.5) as observed with **5**, the phenotypic activity against *T. brucei* (pIC_{50} = 6.0) improved considerably compared with **5**. Moreover, the co-crystal structure of **7** (PDB: 6FTM) in the catalytic domain of TbrPDEB1 indicates that the scaffold forms a good bidentate interaction with the conserved glutamine residue Gln874 while the alkynamide nitrogen atom offers a promising vector to grow the compound towards the P-pocket.[27]
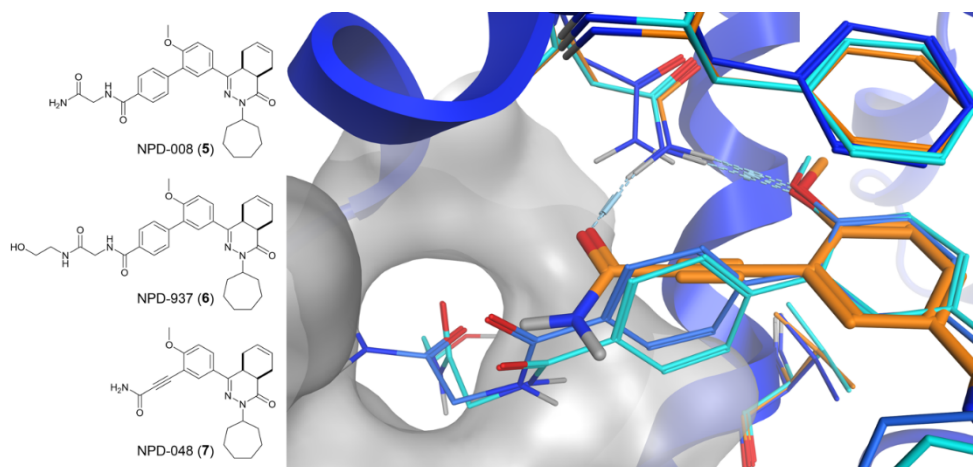
Figure 2: The structures of the reported tetrahydrophthalazinone-based TbrPDEB1 inhibitors with a phenylamide (**5** and **6**) or alkynamide linker (**7**) and their binding pose in the catalytic domain of TbrPDEB1. Key active site residues and the P-pocket are shown for clarity. NPD-008 (**5**) is displayed in blue, NPD-937 (**6**) in cyan and NPD-048 (**7**) in orange.

Herein, we report the structure-based design of new alkynamide tetrahydrophthalazinones with different amide substituents in an attempt to obtain ligands with a better antiparasitic activity.

2. Results and discussion

2.1. In silico exploration of the amide vector

The crystal structures of TbrPDEB1 ligated with **5**, **6** and **7** (PDB-codes 5G2B, 5L8Y, and 6FTM respectively)[25, 27] were used to explore suitable amines to decorate the scaffold of **7** to fit the vector towards the P-pocket described by the alkynamide. All three crystal structures were used as basis because the P-pocket volume varies, indicating the flexibility of the P-pocket residues. Reaxys was used to extract all commercially available (eMolecules) primary or secondary amines with a molecular mass below 158 dalton. Using the *combinatorial library module* of Molecular Operating Environment (MOE) software package of Chemical Computing Group, the amines were virtually coupled to the alkyne tetrahydrophthalazinone scaffold to make a combinatorial library consisting of 16153 substituted alkynamides. These molecules were docked using PLANTS[28] into each of the three aforementioned TbrPDEB1 structures and all resulting docking poses were scored using Interaction Fingerprints[29] (IFP) for the core scaffold of the molecules. After applying combined scoring cut-offs[30] (PLANTS ≤ -90 and IFP ≥ 0.5) and filtering for binding poses in which the ligand was in contact with Gln874, there were 2291 unique molecules

left. The docking results of the 3 different crystal structures were compared and the overlapping hits were visually inspected (see Figure 3A). Six compounds, consisting of aliphatic and aromatic substitutions of varying complexity, were hits in all three sets of docking results (Figure 3B). Compounds with a second (primary or secondary) amine or additional chiral center were removed from the results to increase synthetic feasibility and to eliminate compounds with more than two diastereomers, nominating only **11** and **12** for synthesis. Non-chiral amines that were hits in two of the three sets of docking results (88 compounds) contained a higher abundance of aromatic tail groups (66%) *versus* aliphatic tail groups (33%), thereby predicting a better occupancy of the P-pocket by aromatic groups than aliphatic groups. Most amines contained a second heteroatom that can function as a hydrogen bond acceptor, but no clear preference for flexible or (ring) strained amines was observed. These results were used as inspiration for the compounds synthesized from readily available amines.
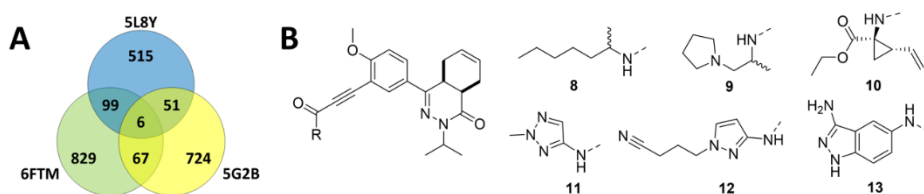
Figure 3: Virtual screening results. A) Number of hits of the docking in different TbrPDEB1 crystal structures indicated by PDB-code. B) Structures of the 6 amines found in all three databases.

2.2. Chemistry

The previously reported synthetic pathway towards phthalazinone alkynamides contained several steps with low yield and long reaction times.[25, 27] Revision of these steps resulted in the design of a new synthetic route (Scheme 1) with reduced reaction times, easier purifications and improved yields. In this new scheme 2-bromoanisole was used in a Friedel-Craft acylation with maleic anhydride to obtain carboxylic acid **14** in good yield. The conversion towards the *E*-isomer was also reported by Onoue *et al.*[31] and confirmed by NMR based on the ^3J-coupling constant of 15.4 Hz between the vinylic hydrogens, typical for *trans* alkene protons. The cyclohexene moiety was introduced by a Diels-Alder reaction with butadiene to form carboxylic acid **15** in quantitative yield. The subsequent condensation with hydrazine and alkylation with isopropylbromide was performed as reported previously.[25, 27] It was decided to install an isopropyl group instead of a cycloheptyl

substituent of the phthalazinone scaffold for this series of alkynamides, as this modification has been shown to yield a small positive effect on the activity profile.[25, 27] Conversion of the stereochemical configuration from the *trans*-cyclohexene to the *cis*-cyclohexene occurs under strongly basic conditions. Comparison of the NMR-spectra of *trans*-tetrahydrophthalazinone **16** with the *cis*-tetrahydrophthalazinone synthesized according to previous reported methods[25] showed distinct differences in shift of aromatic protons (spectra in Supporting Info).
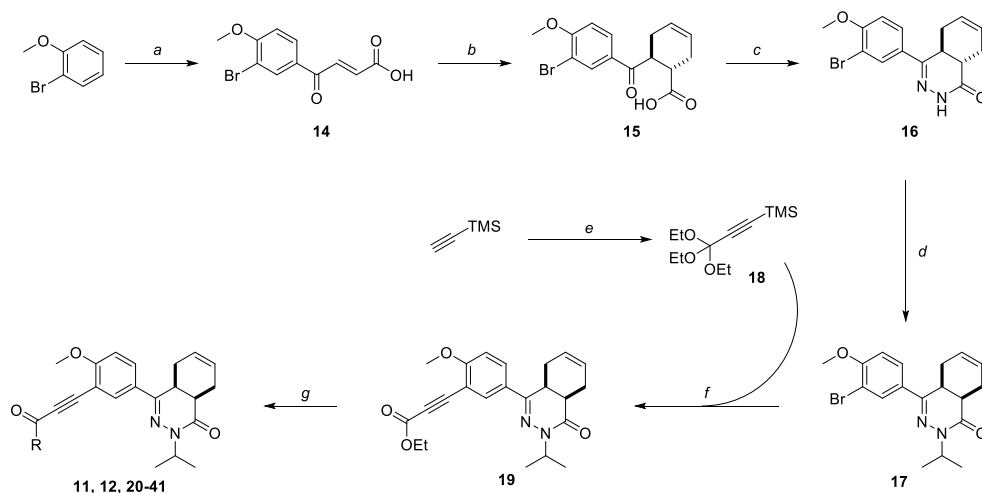
Scheme 1: Reagents and conditions: *a*) maleic anhydride, AlCl$_3$, DCM, rt, overnight, 66%; *b*) 13% butadiene in THF, 140 °C (MW), 30 min, 97%; *c*) N$_2$H$_4$.H$_2$O, EtOH, reflux, 4 h, 86%; *d*) 1) NaH, DMF, rt, 30 min, 2) isopropylbromide, DMF, rt, 4 h, 81%; *e*) 1) *i*PrMgBr, Et$_2$O, 10 °C, 30 min; 2) tetraethoxymethane, Et$_2$O, rt, 1 h, 93%; *f*) PdCl$_2$(dppf), CuI, CsF, Et$_3$N, DMF, 120 °C (MW), 4 h, 70%; *g*) corresponding amine, K$_2$CO$_3$, AlMe$_3$, (Et$_3$N for HCl-salts), DCM, rt, overnight, 9-84%

Alkylation of **16** with excess of sodium hydride resulted in a fast conversion towards the *cis*-tetrahydrophthalazinone, which was confirmed by nuclear magnetic resonance (NMR) spectroscopy using Nuclear Overhauser Enhancement (NOE) experiments. Upon saturation of the signal of proton H4a in **15** and **16**, a weak NOE correlation with H8a was observed in the NOE difference spectrum. Saturation of the signal of proton H4a in **17** resulted in a strong NOE correlation with H8a and thereby confirming the *cis*-configuration of **17** (spectra in Supporting Info). Furthermore, the observed ^3J-values of H4a are in agreement with the *trans*-isomer for **16** with one small and two large coupling constants (^3J = 14.6, 11.4 and 5.4 Hz), indicating one axial-equatorial and two axial-axial positioned protons.[32] The opposite was observed for *cis*-isomer **17** with one larger and two smaller coupling constants (^3J = 11.5 and 2 × 5.8 Hz) as a result of one axial-axial coupling and two

axial-equatorial protons. The alkyne functionality was introduced using combined Sonogashira/Hiyama reaction conditions with TMS-protected triethyl-orthopropiolate **18**, which was synthesized in a Grignard reaction from TMS-acetylene in high yield, to obtain ethyl ester **19**. The various amides were obtained by coupling the corresponding amines to ester **19** using AlMe$_3$ in DCM.

2.3. PDE-activity assay

The PDE-activity on TbrPDEB1 and hPDE4 of the synthesized alkynamides was measured to assess their potency and selectivity as TbrPDEB1 inhibitors. Aliphatic alkynamides **20-27** showed comparable submicromolar potencies against TbrPDEB1 in a pK$_i$ range of 6.0 to 6.5 (Table 1). Most alkynamides showed similar or lower potency for hPDE4 compared to TbrPDEB1, with the best selectivity index (SI, TbrPDEB1 pK$_i$ − hPDE4 pK$_i$) observed for the tetrahydrofuranyl-substituted analogue **26** (SI = 0.5).
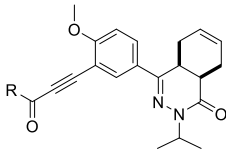
The alkynamides that contain aromatic rings in the tail group (**11**, **12** and **28-41**, Table 2) showed in general higher potencies for TbrPDEB1 (pK$_i$ range 6.1 − 7.0) when compared to the aliphatic alkynamides. Interestingly, both compounds that were directly selected from the virtual screening (**11** and **12**) showed the lowest potency on TbrPDEB1 observed for the aromatic series of alkynamides.
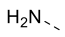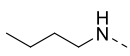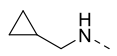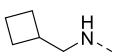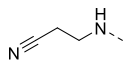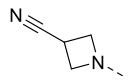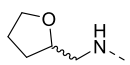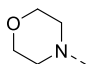
There was no difference observed between a furan and thiophene ring (**28** and **30**), both having a nanomolar potency against TbrPDEB1 (pK$_i$ = 6.9). Introducing a methyl group on the furan (**29**) or elongating the tail group for the thiophene (**31**) slightly reduced the potency for TbrPDEB1. Implementing a thiazole ring (**32**-**34**) in the tail group did not improve the potency or selectivity of the alkynamides. Methylpyrrole **35** was equally potent against TbrPDEB1 as 2-methylfuran **28** and 2-methylthiophene **30**, but with a slightly better SI (Table 2, SI = 0.7). Imidazole **36** with a more flexible tail displayed a reduced activity and selectivity. The highest potencies were observed for pyridinyl alkynamides **38** (NPD-1169, pK$_i$ = 7.0) and **39** (NPD-1334, pK$_i$ = 7.0), which were slightly more potent than the benzyl analogue **37** (pK$_i$ = 6.8), while the less flexible 3-methoxyphenyl analogue **40** displayed a pK$_i$ of 6.7 against TbrPDEB1. Fluorophenyl **41** showed a slightly reduced potency and selectivity when compared with benzyl analogue **37**.

Table 1: Structure-activity relationship of alkynamides with aliphatic tail groups for TbrPDEB1 and hPDE4
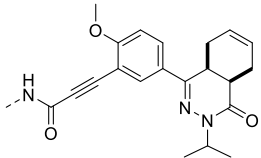
#	NPD	R	pK_i[a] TbrPDEB1	pK_i[a] hPDE4
20	1170	H_2N–	6.3 ± 0.05	6.5 ± 0.1
21	1024	propyl–NH–	6.5 ± 0.04	6.3 ± 0.1
22	1038	cyclopropylmethyl–NH–	6.4 ± 0.1	6.5 ± 0.1
23	1042	cyclobutylmethyl–NH–	6.5 ± 0.1	6.1 ± 0.1
24	1167	N≡C–CH_2CH_2–NH–	6.0 ± 0.1	6.1 ± 0.1
25	1041	3-cyanoazetidin-1-yl	6.2 ± 0.1	6.4 ± 0.1
26	1043	tetrahydrofuran-2-ylmethyl–NH–	6.4 ± 0.1	5.9 ± 0.2
27	1336	morpholin-4-yl	6.0 ± 0.1	6.1 ± 0.1
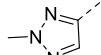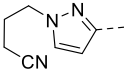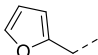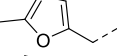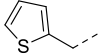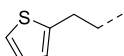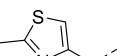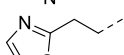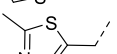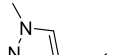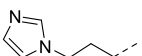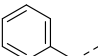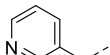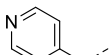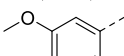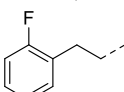
[a]Mean and S.E.M. values of at least 3 independent experiments.

When compared to the previously synthesized primary alkynamide **7** with a SI of -0.3 (Figure 4), most compounds (except **11**) show a slightly improved selectivity index for TbrPDEB1 over hPDE4 and several compounds display a comparable selectivity to **5** (SI = 1.0). The SI observed for **39** was 0.8 log unit, making this 4-pyridinyl alkynamide approximately 6-times more potent against TbrPDEB1 than hPDE4.

Development of alkynamide phthalazinones as potential new class selective TbrPDEB1 inhibitors.

Table 2: Structure-activity relationship of alkynamides with aromatic tail groups

| # | NPD | R | pK$_i$ ± S.E.M.[a] | |
			TbrPDEB1	hPDE4
11	3154		5.6 ± 0.1[b]	6.3 ± 0.1
12	3155		6.1 ± 0.02	5.9 ± 0.2
28	1016		6.9 ± 0.04	6.4 ± 0.1
29	1174		6.7 ± 0.2	6.7 ± 0.1
30	1322		6.9 ± 0.04	6.3 ± 0.1
31	1320		6.4 ± 0.01	6.1 ± 0.1
32	1171		6.5 ± 0.1	6.0 ± 0.1
33	1319		6.6 ± 0.1	6.4 ± 0.2
34	3153		6.7 ± 0.01	6.6 ± 0.3
35	1321		6.9 ± 0.1	6.2 ± 0.1
36	1323		6.4 ± 0.03	6.2 ± 0.2
37	1335		6.8 ± 0.1	6.1 ± 0.2
38	1169		7.0 ± 0.1	6.3 ± 0.1
39	1334		7.0 ± 0.1	6.2 ± 0.1
40	1018		6.7 ± 0.1	6.0 ± 0.1
41	1039		6.5 ± 0.1	6.1 ± 0.1

[a]Mean and S.E.M. values of at least 3 independent experiments. [b]No full dose response curve obtained.

5
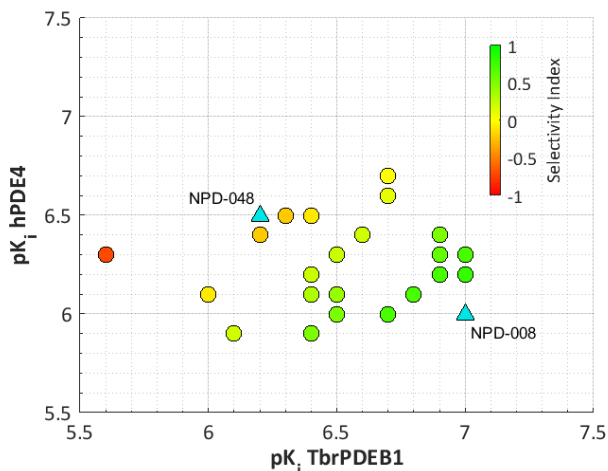
Figure 4: Biochemical activity against TbrPDEB1 and hPDE4 of all alkynamides and reference compounds NPD-008 (**5**) and NPD-048 (**7**). The selectivity index (pK$_i$ TbrPDEB1 − pK$_i$ hPDE4) is indicated by color.

2.4. Co-crystal structures in TbrPDEB1 and hPDE4

We successfully obtained co-crystal structures of **37**, **40** and **41** (PDB: 6GXQ, 6RFN and 6RFW, respectively, Figure 5) and the previously reported NPD-053 (**42**) and NPD-055 (**43**) (PDB: 6RB6 and 6RGK, respectively) in the catalytic domain of TbrPDEB1 and co-crystal structures of **37** and **42** bound in the catalytic domain of hPDE4 (PDB: 6HWO and 6RCW respectively). While our design indicated that decoration of the alkynamide nitrogen of **7** is possible in TbrPDEB1 because of the presence of the parasite-specific P-pocket, the crystal structures of **37** show that the amide substituent does not occupy the P-pocket (Figure 5A).

While a bidentate interaction with the key Gln874 of TbrPDEB1 is maintained, the amide substituent folds back in a hydrophobic collapse. A highly similar binding pose is observed in the co-crystal structure of **37** in hPDE4 (Figure 5B). The comparison of the co-crystal structures of **42** in hPDE4 and TbrPDEB1 gave a similar result. While the ligands do not seem to exploit the parasite-specific P-pocket, the crystal structures do not give an explanation for the improved activity profile for TbrPDEB1 over hPDE4. The tail groups seem to fold back towards Phe877 of the hydrophobic clamp, but no substantial additional interactions are observed. In addition, an overlay of the binding poses of **37**, **40**, **41**, **42** and **43** in the catalytic domain of TbrPDEB1 (Figure 5C) shows that they occupy the same space in the binding site.

Development of alkynamide phthalazinones as potential new class selective TbrPDEB1 inhibitors.
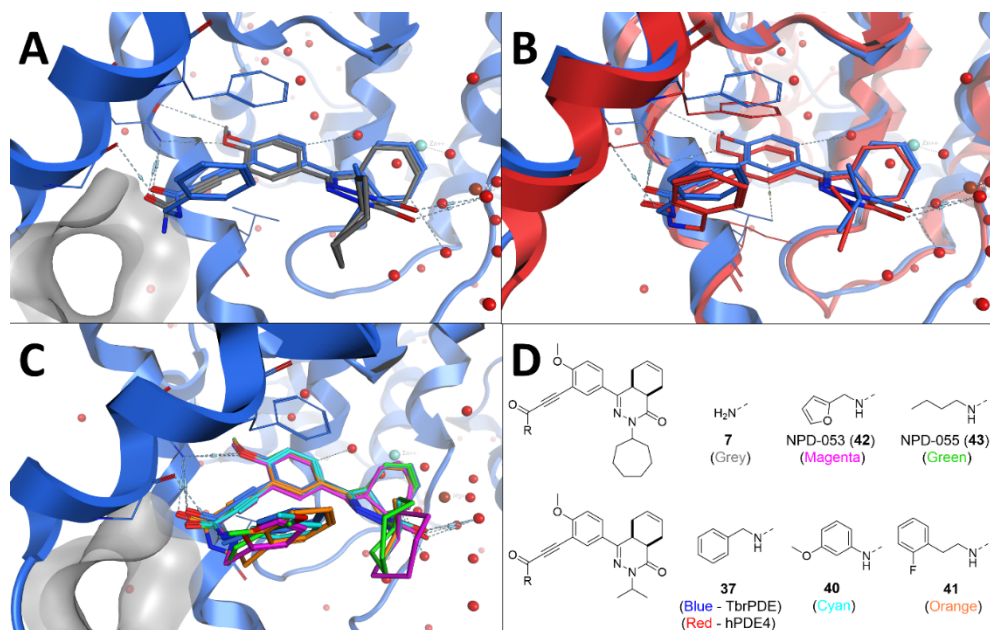
Figure 5: Crystal structures of alkynamides in the catalytic domain of TbrPDEB1 (blue) and hPDE4 (red). Key residues, active site water molecules and metals are shown for clarity. A) Overlay of **7** (grey) and **37** (blue) in TbrPDEB1 with the P-pocket shown in grey. B) Binding pose of **37** in the catalytic domain of TbrPDEB1 (blue) and hPDE4 (red). C) Overlay of all obtained crystal structures of alkynamides **37** (blue), **40** (cyan) and **41** (orange), **42** (magenta) and **43** (green) bound to the catalytic domain of TbrPDEB1. D) Structures of the co-crystallized compounds and their color of visualization.

2.5. Surface plasmon resonance biosensor analysis

To increase our understanding of ligand-PDE binding and the molecular features that have an influence on the resulting activity profiles, we performed interaction analyses using a surface plasmon resonance (SPR) biosensor assay (Figure 6). Biotinylated proteins were captured by neutravidin, immobilized on CM5 chip surface. Interaction assays were performed by injecting suitable concentration series for each compound. Compounds **20** and **37** were injected for respectively 60 and 320 seconds to reach steady-state equilibrium and their dissociation was monitored (300 seconds for **20** and 900 seconds for **37**) to determine the pK_D values. The affinity of the unsubstituted alkynamide **20** at hPDE4D ($pK_D = 6.6 \pm 0.1$) was ~0.5 log unit higher compared to the affinity obtained for its binding to TbrPDEB1 ($pK_D = 6.1 \pm 0.1$). Going from **20** to the benzyl substituted analog **37**, the affinity for TbrPDEB1 ($pK_D = 7.1 \pm 0.1$) improved 10-fold, while at hPDE4D ($pK_D = 7.1 \pm 0.1$) the affinity of **37** was only 0.5 log-unit higher. These findings indicate that the

benzyl substitution of the alkynamide has a pronounced effect on TbrPDEB1 binding, as **37** is equipotent at TbrPDEB1 and hPDE4. Interestingly, while the obtained crystal structures do not easily explain the improved biochemical activity profile of the new TbrPDEB1 inhibitors, the SPR biosensor analysis indicates notable differences in binding kinetics, as a much slower off-rates for TbrPDEB1 and hPDE4 can be observed when comparing the dissociation kinetics of **20** and **37**. The results indicate that binding kinetics represent an opportunity to design new compounds with improved activity profiles. We are currently developing *in silico* methods (including but not limited to molecular dynamics studies) to translate these kinetic binding data to molecular understanding.
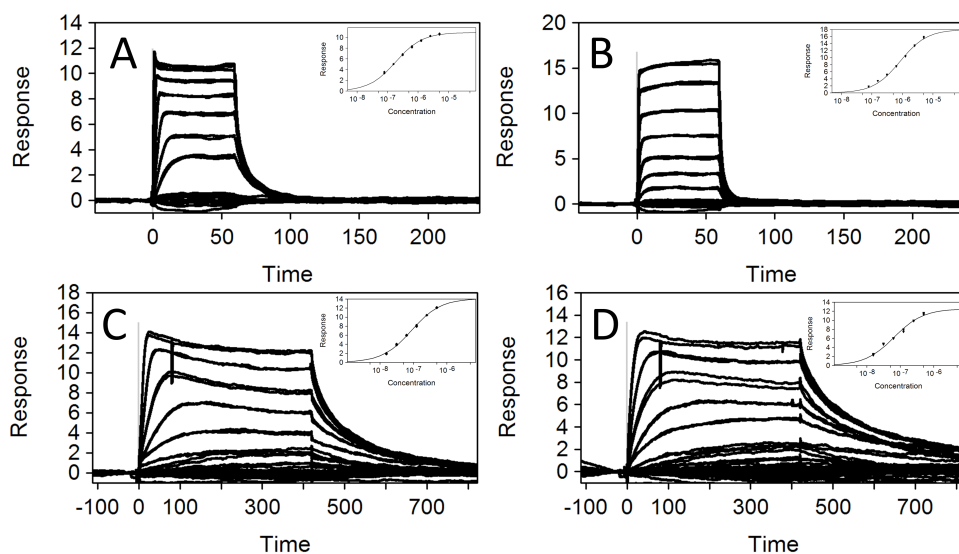
Figure 6: Sensorgrams of compound **20** binding to hPDE4D (A) and TbrPDEB1 (B), and compound **37** binding to hPDE4D (C) and TbrPDEB1 (D). Inset shows steady-state affinity analyses of SPR biosensor interaction data; blank injections are also shown. Measurements using two independent biosensor chips and three different stock solutions indicate good reproducibility.

2.6. Phenotypical data

All alkynamides were tested *in vitro* for their trypanocidal activity against *T. brucei* trypomastigotes (Table 3). The best results were obtained for **37** and **39**, which both displayed submicromolar activities and were not cytotoxic to MRC-5 cells. Aliphatic alkynamides (**20-27**) showed a lower activity when compared to alkynamides with aromatic tail groups (**11**, **12** and **28-41**), as observed in the biochemical assay.

Table 3: Trypanocidal activity of all alkynamides against *T. brucei* parasites and their cytotoxicity against human MRC-5 cells (mean ± S.E.M).

#	cLogP	cLogS	TPSA	*T. brucei* (pIC$_{50}$)	MRC-5 (pCC$_{50}$)
20	2.4	-4.3	85	5.2 ± 0.1	4.5 ± 0.1
21	3.9	-5.4	71	5.1 ± 0.1	<4.2
22	3.4	-5.2	71	5.1 ± 0.1	<4.2
23	3.8	-5.7	71	5.2 ± 0.1	<4.2
24	2.4	-4.5	95	4.6 ± 0.1	4.5 ± 0.1
25	2.4	-4.9	86	5.1 ± 0.1	5.1 ± 0.1
26	3.0	-4.9	80	5.1 ± 0.1	4.5 ± 0.1
27	2.6	-4.7	71	5.0 ± 0.1	4.5 ± 0.1
11	3.0	-4.3	102	<4.2	5.0 ± 0.2
12	3.7	-5.2	113	5.7 ± 0.1	5.1 ± 0.1
28	3.4	-5.3	84	5.6 ± 0.1	<4.2
29	3.6	-5.5	84	5.5 ± 0.3	<4.2
30	4.2	-5.9	71	6.0 ± 0.4	4.2 ± 0.1
31	4.5	-5.8	71	5.6 ± 0.1	<4.2
32	3.2	-4.7	84	5.7 ± 0.1	4.9 ± 0.1
33	3.3	-4.6	84	5.3 ± 0.2	5.0 ± 0.1
34	3.4	-4.8	84	5.7 ± 0.1	5.1 ± 0.1
35	2.7	-4.0	89	5.8 ± 0.3	4.7 ± 0.1
36	2.6	-4.5	89	5.1 ± 0.1	6.6 ± 0.1
37	4.3	-5.9	71	6.2 ± 0.1	<4.2
38	3.1	-4.7	84	5.9 ± 0.1	5.4 ± 0.2
39	3.1	-4.7	84	6.0 ± 0.4	4.5 ± 0.4
40	4.5	-6.0	80	5.8 ± 0.1	<4.2
41	4.7	-6.1	71	5.7 ± 0.1	<4.2

As displayed in Figure 7A, the alkynamides showed a good correlation (R^2 = 0.7) between TbrPDEB1 and *T. brucei* activity. No correlation was observed between important physicochemical properties (cLogP, cLogS and TPSA) and their anti-*T. brucei* activity (Figure 7B-D). Most alkynamides showed low or no cytotoxicity on MRC-5 cells, except imidazole **36** that displayed a substantially higher cytotoxicity

when compared with other alkynamides. When compared to alkynamide **7** (CC_{50} = 5.0) most decorated alkynamides show an improved cytotoxicity profile.
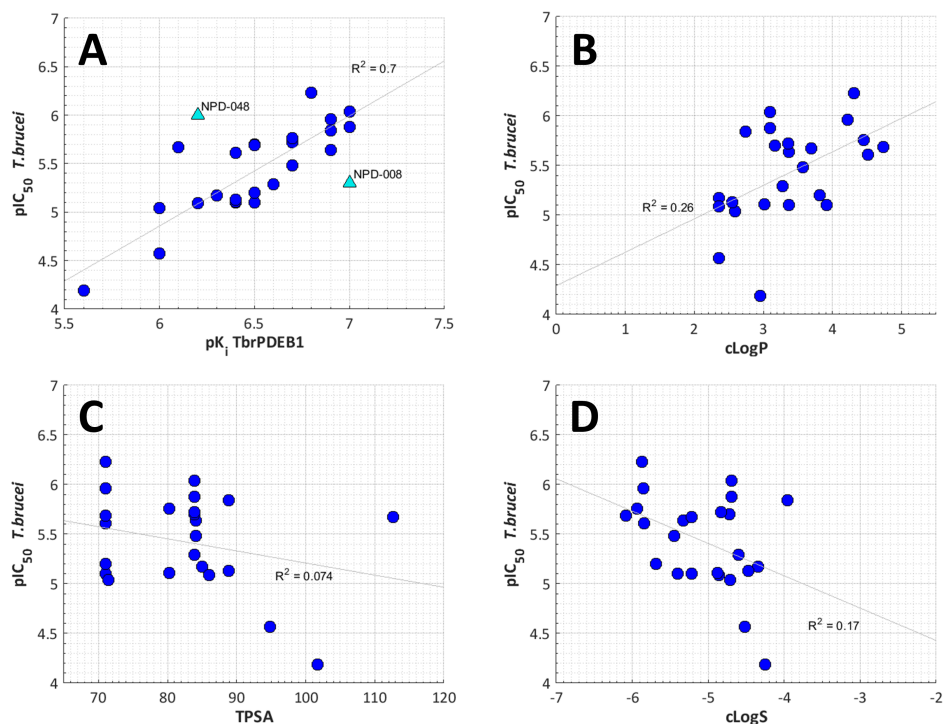
Figure 7: Correlation between cellular activity against *T. brucei* parasites of all alkynamides and A) TbrPDEB1 activity, reference compounds NPD-048 and NPD-008 shown as blue triangles, B) cLogP, C) TPSA and D) cLogS.

2.7. Intracellular real-time cAMP assay

To confirm on-target activity of **37** and **39** in live parasites, procyclic form trypanosomes expressing a FRET-based cAMP sensor were incubated with 1 and 10 µM inhibitor **37** and **39** (Figure 8). Both inhibitors induce a rapid and sustained increase in intracellular cAMP in the reporter cell line versus the negative control (DMSO), as indicated by an increase in 488/535nm emission ratio. Both inhibitors were compared with a known non-selective TbrPDEB1 inhibitor (NPD-001), which was previously reported to increase intracellular cAMP levels in bloodstream and procyclic form trypanosomes.[18, 33] Both inhibitors **37** and **39** show a higher response at 1 µM when compared with reference inhibitor NPD-001 and an equal response at 10 µM.
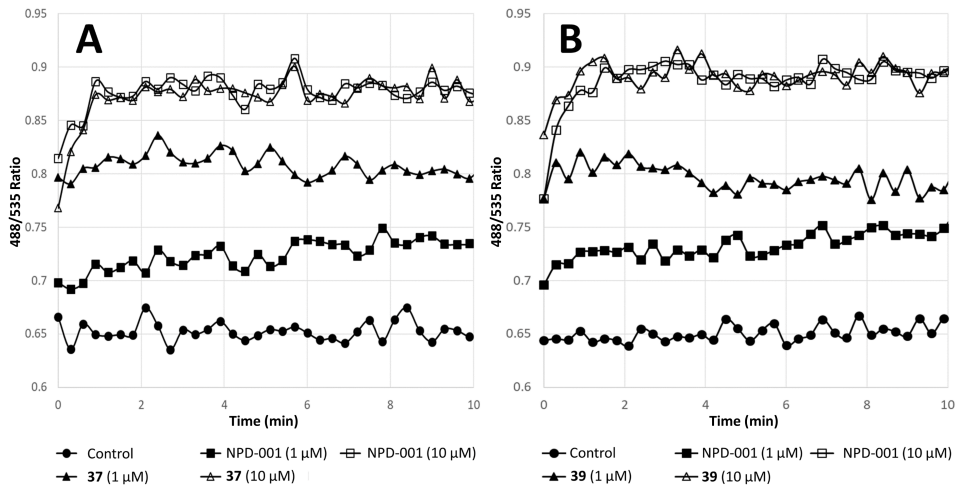
Figure 8: Intracellular cAMP levels in procyclic form trypanosomes upon incubation with inhibitor A) **37** and B) **39** at two concentrations (1 μM and 10 μM) compared to NPD-001 and control cells.

To determine the activity of inhibitor **37** and **39** on bloodstream form trypanosomes, parasites were incubated with inhibitor **37** and **39** for 24-48h prior to fixation and cellular analysis by fluorescence microscopy. After incubation with inhibitor **37** and **39**, bloodstream form trypanosomes exhibit a lethal block in cytokinesis, indicated by multi-nucleated and multi-flagellated parasites (Figure 9). The trypanocidal effects of **37** and **39** are in line with previous observations after genetic and pharmacological modulation of TbrPDEB1 and TbrPDEB2 expression or function in bloodstream form trypanosomes.[16, 19]
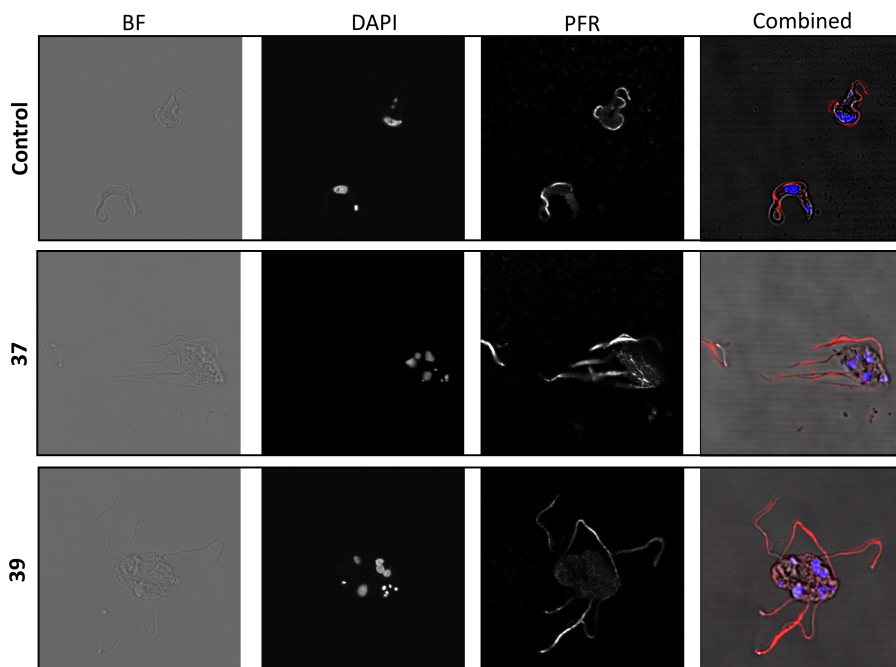
Figure 9: Fluorescence microscopy of control trypanosomes and trypanosomes incubated with **37** or **39** after 24-48 h visualized with different stains. First column shows cells under normal microscope conditions. Second and third column show the cells with DAPI and PFR stains respectively to visualize cell nuclei (DAPI) and the flagellum (PFR). Overlay of the different imaging techniques is shown in the fourth column.

3. Conclusion

The structure-based design of alkynamide phthalazinones as TbrPDEB1 inhibitors delivered several compounds with a submicromolar activity against TbrPDEB1 and a modest selectivity over its human homologue hPDE4. Unexpectedly, alkynamide **37** did not show the predicted P-pocket occupation by the tail group in the co-crystal structure with TbrPDEB1 and a very similar binding mode was observed in the co-crystal structure with hPDE4. This observation indicates that targeting of the P-pocket of TbrPDEB1 is difficult to achieve with alkynamide tetrahydrophthalazinones. Moreover, the observed (moderate) selectivity of the benzyl and the two pyridinyl-substituted alkynamides **37**, **38** and **39** suggests that other, as of yet unidentified interactions of PDE inhibitors with TbrPDEB1 and hPDE4 can also result in (moderate) parasite selectivity. The alkynamides show a good correlation between their biochemical activity against TbrPDEB1 and their *in*

vitro activity against *T. brucei* parasites. Benzyl alkynamide **37** (NPD-1335) is 5-fold more potent against TbrPDEB1 (pK_i = 6.9) than hPDE4 (pK_i = 6.2) and displays a greatly improved cytotoxicity profile (pIC_{50} *T. brucei* = 6.2 *vs* pCC_{50} MRC-5 < 4.2) when compared to the unsubstituted alkynamide **7** (pIC_{50} *T. brucei* = 6.0 *vs* pCC_{50} MRC-5 < 5.0). Furthermore, incubation of procyclic forms with **37** and **39** results in elevation of the intracellular cAMP levels in the cells. In bloodstream forms, incubation with **37** and **39** leads to a block in cytokinesis, which is associated with formation of multiple flagella and nuclei, both supporting a PDE-mediated mode of action*.*

5

4. Experimental

4.1. Docking

The dockings were performed similar to the combined screening protocol as previously published for GPCRs.[30] In short, the dockings were performed using PLANTS[28] (version 1.2) and the resulting docking poses were post-processed with IFP[29] (version 2.2). Every molecule was docked 5 times generating 10 docking poses during each iteration (speed setting 2, RMSD 1.0) into each of the three crystal structures (chain B for 5G2B and 5L8Y and chain A for 6FTM) based on the pocket definition as defined for PDEStrIAn.[34] All docking poses were scored using the ChemPLP scoring function and only poses with a score ≤ -90 were further investigated. The positioning of the core scaffold was evaluated by performing an IFP similarity comparison to the co-crystallized ligands limited to solely the residues in the direct vicinity of the core scaffold. Poses with an IFP score lower than 0.5 or where the ligand did not interact with the conserved glutamine (Q.50) or the hydrophobic clamp (HC.32, HC.52) were removed. A final interaction filter was applied to select only those binding modes in which the Q2 pocket was targeted by having at least one IFP contact with Q2.45 or Q2.46. From the initial combinatorial library of 16153 alkynamides 2291 compounds remained for further processing.

4.2. Protein production

Cloning, expression and purification of recombinant TbrPDEB1 and hPDE4D catalytic domains were performed as previously described.[25]

4.3. Crystallization, data collection and structure determination

Apo crystals of TbrPDEB1 and hPDE4D were grown in 24 well XRL plates (Molecular Dimensions, Newmarket, Suffolk, UK) by vapor diffusion hanging drop technique. Typically, protein and crystallization solution were mixed in 1:1 ratio and drops were setup against 500 μL reservoir solution. Crystals of TbrPDEB1 were obtained in a condition containing 20% PEG 3350, 400 mM sodium formate, 300 mM guanidine and 100 mM MES pH 6.5 at 4 °C and soaked with different inhibitors to obtain protein-inhibitor complexes. hPDE4D crystals obtained in a condition containing 24% PEG 3350, 30% ethylene glycol and 100 mM HEPES pH 7.5 at 19 °C were complexed with different inhibitors in a similar way. The soaked crystals were then cryo protected, mounted on CryoLoop (Hampton Research, Aliso Viejo, CA, USA) or LithoLoops (Molecular Dimensions) and vitrified in liquid nitrogen for data collection. All X-ray diffraction data sets were collected at Diamond Light Source (DLS; Didcot, Oxfordshire, UK) at beam lines I03 using a Pilatus 6M detector (Dectris, Baden, Switzerland) or at I04-1 using a Pilatus 6M-F detector (Dectris) at 100 K temperature. Datasets were processed with xia2[35] or autoPROC[36] pipelines available at DLS , which incorporates XDS[37] and AIMLESS,[38] or were integrated using iMOSFLM[39] and reduced using POINTLESS, AIMLESS and TRUNCATE, all of which are part of CCP4 suite.[40] Structures of inhibitor complexes with TbrPDEB1 and hPDE4D were determined by molecular replacement in CCP4 suite program PHASER[41] by using the respective apo models (TbrPDEB1, PDB id: 4I15; hPDE4D, PDB id: 3SL3) as search templates. Stereochemical restrains for the inhibitors were generated by ACEDRG available within the CCP4 package and ligand fitting and model adjustment were carried out in COOT[42] followed by their refinement in REFMAC.[43] Structural figures were prepared with PYMOL[44]. Coordinates of the structures have been deposited to the RCSB Protein Data Bank with following accession codes: 6GXQ (TbrPDEB1-NPD-1335), 6RFN (TbrPDEB1-NPD-1018),

Development of alkynamide phthalazinones as potential new class selective TbrPDEB1 inhibitors.

6RFW (TbrPDEB1-NPD-1039), 6RB6 (TbrPDEB1-NPD-053), 6RGK (TbrPDEB1-NPD-055), 6HWO (hPDE4D-NPD-1335) and 6RCW (hPDE4D-NPD-053).

4.4. Phosphodiesterase activity assays

Phosphodiesterase activity assays are performed using the PDELight™ HTS cAMP phosphodiesterase Kit (Lonza, Walkersville, USA): The assay is performed at 25 °C in non-binding, low volume 384 wells plates (Corning, Kennebunk, ME, USA). PDE activity measurements (TbrPDEB1_CD; K_m 3.45 μM, hPDE4B_CD; K_m 13.89 μM) are made in 'stimulation buffer' (50 mM Hepes, 100 mM NaCl, 10 mM MgCl, 0.5 mM EDTA, 0.05 mg/mL BSA, pH 7.5). Single concentration measurements are made at 10 μM inhibitor concentration (triplo measurements/assay, n=2). Dose response curves are made in the range 100 μM - 10 pM (triplo measurements/assay, n=3). Compounds are diluted in DMSO (final concentration 1%). Inhibitor dilutions (2.5 μL) are transferred to the 384 wells plate, 2.5 μL PDE in stimulation buffer is added and mixed, 5 μL cAMP (at $2 \times K_m$ up to 20 μM) is added and the assay is incubated for 20 min at 300rpm. The reaction is terminated by then addition of 5 μL Lonza Stop Buffer supplemented with 10 μM NPD-001. Then 5 μL of Lonza Detection reagent (diluted to 80% with reaction buffer) is added and the reaction incubated for 10 min at 300rpm. Luminescence is read with a Victor3 luminometer using a 0.1 s/well program.

RLUs were measured in comparison to the DMSO-only control, NPD-001 always was taken along as positive control as a PDE inhibitor. The K_i values of the inhibitors analyzed are represented as the mean of at least three independent experiments with the associated standard error of the mean (SEM) as indicated.

4.5. Phenotypic cellular assays.

For the cellular assays, the following reference drugs were used as positive controls: suramin (Sigma-Aldrich, Germany) for T. brucei (pIC_{50} = 7.4 ± 0.2, n = 5), and tamoxifen (Sigma-Aldrich, Germany) for MRC-5 cells (pCC_{50} = 5.0 ± 0.1, n = 5). All compounds were tested at five concentrations (64, 16, 4, 1 and 0.25 μM) to establish determination of the IC_{50} and CC_{50}. Data are represented as the mean of duplicate experiments ± S.E.M. The final concentration of DMSO did not exceed 0.5% in the assays.

In vitro antitrypanosomal assay. *T. brucei* Squib-427 strain (suramin-sensitive) was cultured at 37 °C and 5% CO_2 in HMI-9 medium, supplemented with 10% heat-inactivated fetal calf serum (FCSi). About 1.5×10^4 trypomastigotes were added to each well and parasite growth was assessed after 72 h at 37 °C by adding resazurin. Viability was assessed fluorimetrically 24 h after the addition of resazurin. Fluorescence was measured (excitation 550 nm, emission 590 nm) and the results were expressed as percentage reduction in viability compared to control.

In vitro MRC-5 cytotoxicity assay. MRC-5 SV2 cells, originally from a human diploid lung cell line, were cultivated in MEM, supplemented with L-glutamine (20 mM), 16.5 mM sodium hydrogen carbonate and 5% FCSi. For the assay, 10^4 MRC-5 cells/well were seeded onto the 96-well test plates containing the pre-diluted sample and incubated at 37 °C and 5% CO2 for 72 h. Cell viability was assessed fluorimetrically 4 h after the of addition of resazurin. Fluorescence was measured (excitation 550 nm, emission 590 nm) and the results were expressed as percentage reduction in cell viability compared to control.

Development of alkynamide phthalazinones as potential new class selective TbrPDEB1 inhibitors.

4.6. Intracellular cAMP and fluorescence microscopy

4.6.1. Cell lines

Procyclic 2913 *T. b. brucei*[45] were cultivated in SDM-79 supplemented with 5% FCSi .[46] Bloodstream-form *T. b. brucei* 221 single marker cell line[45] were cultivated in HMI-9 medium supplemented with 10% FCSi .[46] The cAMP FRET reporter cell line was developed by transfecting 2913 procyclic form *T. b. brucei* with linearized pLEW-100 containing epac1camps. Selection for transfected cells and cloning by limited dilution was done as published previously.[46] Expression of epac1-camps was validated using fluorescence microscopy.

4.6.2. Plasmids

For tetracycline inducible expression of the cAMP FRET sensor, the Epac1camps sensor[47] was cloned into pLEW-100[45] as described.[33]

4.6.3. Chemicals

NPD-001, **37**, **39** were dissolved in DMSO to 1 and 10 mM and stored at -80 °C.

4.6.4. FRET assay

cAMP FRET assays were performed in triplicates for each time point and 3 independent experiments, as described previously[33]: As controls, NPD-001 (positive control,[18] and DMSO (solvent for **37**, **39**, NPD-001)) were included. The following modifications to the published method[33] were made: the cAMP reporter cell line was cultivated in SDM-79 containing 5% FCSi . After induction of Epac1-camps expression with tetracycline[46] for 24h-48h, the cells were washed once and resuspended in PBS containing 5% FCSi to 1.5×10^8 cells/mL. 150 μL of cells was added to each well of a 96-well black microtiter plate. 50 μL of NPD-001, **37**, **39** and DMSO diluted in PBS containing 5% FCSi was added to the wells (final concentration of compounds: 10 μM).

4.6.5. Microscopy

Bloodstream-form *T. b. brucei* 221 single marker cell line were cultivated for 24 h in the presence of 1μM NPD-001, **37**, **39** or DMSO as control. Methodology used for cell fixation and staining has been described previously,[48] with the following modifications: blocking and antibody staining was done in PBS containing 5% bovine serum albumin (BSA). Antibodies used were rat anti-PFR 1:500[49] and anti-rat Alexa594 1:500 (Invitrogen). NucBlue Fixed Cell Stain (Invitrogen) was added to Vectashield mounting medium (for DNA stain). Images were acquired using a Leica confocal microscope and standard procedures. Images were processed using ImageJ.

4.7. Surface plasmon resonance

All experiments were performed with a Biacore T200 surface plasmon resonance biosensor instrument (GE healthcare). Proteins were immobilized on CM5 series S sensor chips. Consumables were obtained from GE Healthcare. All solutions were freshly prepared, degassed, and filtered. The neutravidin immobilization was run on HBS-N at a flowspeed of 10 μL/min at 25 °C. The matrix of the sensor chip was activated by injecting on all flow channels a mixture of 0.1 M *N*-hydroxysuccinimide (NHS) and 0.4 M 1-ethyl-3-(3-(dimethylamino)propyl) carbodiimidehydrochloride (EDC) at a flow rate

of 10 µM for 420 seconds. Subsequently, neutravidin (0.30 mg/mL) in a 10 mM NaAc solution (pH 5.0) was injected for 120 seconds. Unreacted activated groups of the dextran matrix were deactivated by injection of ethanolamine.HCl (1 M) for 420 s.

The catalytic domains of hPDE4D and TbrPDEB1 were produced and purified as previously described.[25] the proteins were buffer exchanged using a Amicon Ultra 0.5 mL centrifugal filter (Merk) to HBS-N, 5% glycerol (v/v), 4 µM $MgCl_2.6H_2O$, 100 nM $ZnCl_2$, 2 mM 2-mercaptoethanol and diluted to 1 mg/mL. EZ-Link Sulfo-NHS-Biotin (Thermo Fisher Scientific) was diluted to 1.5 mM in the same buffer, mixed with the protein in a 1:1 molar ratio, and incubated at 4 °C overnight. Biotinylated proteins were buffer exchanged to 0.5 M Tris-HCl (pH 8.0), 150 mM NaCl, 4 mM $MgCl_2.6H_2O$, 100 nM $ZnCl_2$, 5% glycerol (v/v), 2 mM 2-mercaptoethanol, and desalted using 0.5 mL Zeba Spin desalting columns (Thermo Scientific). Proteins were diluted to 0.5 mg/mL and injected on the flow channels until 3000 RU in the same buffer at 15 °C. Biocytin (0.05 mg/mL) was injected for 120 seconds on all flow channels at 15 °C.

All compounds were dissolved in DMSO (stock solutions of 10 mM) and diluted in 0.5 M Tris-HCl (pH 8.0), 150 mM NaCl, 4 mM $MgCl_2.6H_2O$, 100 nM $ZnCl_2$, 5% glycerol (v/v), 2 mM 2-Mercaptoethanol, 0.005% Tween-20 (v/v), 2% DMSO (v/v). Suitable concentration series and injection times were determined for each compound separately. In multicycle experiments, a 7-point concentration range of each compound was measured. On a first CM5 chip, a first stock solution was used to obtain a dose response curve in duplicate. On a second CM5 chip, two other independent stock solutions were used to measure dose response curves in duplicate. Compound **20** was injected for 60 seconds and its dissociation was monitored for 300 seconds. Compound **37** was injected for 420 seconds and its dissociation was monitored for 900 seconds. All titrations were run at 25 °C at a flow speed of 50 µL/min. Data analyses were performed with Scrubber2. Signals were subtracted from reference surface and blanc injections. DMSO correction was performed. The affinity was determined by fitting a Langmuir binding equation to steady state binding signals at different concentrations. All SPR experiments are shown in the supplementary data with individually measured pK_D and the error reported is the error in the fit of the binding isotherm.

4.8. Chemistry.

4.8.1. General

All reagents and solvents were obtained from commercial suppliers and were used as received. All reactions were magnetically stirred and carried out under an inert atmosphere. Reaction progress was monitored using thin-layer chromatography (TLC) and LC-MS analysis. LC-MS analysis was performed on a Shimadzu LC-20AD liquid chromatograph pump system, equipped with an Xbridge (C18) 5 µm column (50 mm, 4.6 mm), connected to a Shimadzu SPD-M20A diode array detector, and MS detection using a Shimadzu LC-MS-2010EV mass spectrometer. The LC-MS conditions were as follows: solvent A (water with 0.1% formic acid) and solvent B (acetonitrile with 0.1% formic acid), flow rate of 1.0 mL/min, start 5% B, linear gradient to 90% B in 4.5 min, then 1.5 min at 90% B, then linear gradient to 5% B in 0.5 min, then 1.5 min at 5% B; total run time of 8 min. Silica gel column chromatography was carried out with automatic purification systems using the indicated eluent. Reversed phase column purification was performed on Grace Davison iES system with C18 cardridges (60 Å, 40 µm) using the

indicated eluent. Nuclear magnetic resonance (NMR) spectra were recorded as indicated on a Bruker Avance 500 (500 MHz for ^{1}H and 125.8 MHz for ^{13}C) instrument equipped with a Bruker CryoPlatform, or on a Bruker Avance III HD (600 MHz for ^{1}H) instrument equipped with a Bruker CryoPlatform. Chemical shifts (δ in ppm) and coupling constants (*J* in Hz) are reported with residual solvent as internal standard (δ ^{1}H-NMR: CDCl$_3$ 7.26; DMSO-d_6 2.50; δ ^{13}C-NMR: CDCl$_3$ 77.16; DMSO-d_6 39.52). Abbreviations used for ^{1}H-NMR descriptions are as follows: s = singlet, d = doublet, t = triplet, q = quintet, hept = heptet dd = doublet of doublets, dt = doublet of triplets, tt = triplet of triplets, m = multiplet, app d = apparent doublet, br = broad signal. Exact mass measurement (HRMS) was performed on a Bruker micrOTOF-Q instrument with electrospray ionization (ESI) in positive ion mode and a capillary potential of 4,500 V. Systematic names for molecules were generated with ChemBioDraw Ultra 14.0.0.117 (PerkinElmer, Inc.). The reported yields refer to isolated pure products and yields were not optimized. The purity, reported as the LC peak area % at 254 nm, of all final compounds was ≥ 95% based on LC-MS. All compounds are isolated as a racemic mixture of *cis*-enantiomers.

4.8.2. Synthetic procedures

4.8.2.1. (*E*)-4-(3-Bromo-4-methoxyphenyl)-4-oxobut-2-enoic acid (**14**)

To an ice-cooled mixture of 1-bromo-2-methoxybenzene (65 mL, 0.52 mol) and furan-2,5-dione (77 g, 0.78 mol) in DCM (465 mL) was added AlCl$_3$ (84 g, 0.63 mol). The reaction mixture was stirred at rt overnight. The orange suspension was quenched in 3 M aq. HCl (1.5 L) and extracted using EtOAc (4 × 1 L). The combined organic layers were dried over Na$_2$SO$_4$, filtered and concentrated to obtain a dark yellow solid. Trituration with Et$_2$O provided the product as a light yellow solid (97.5 g, 66%). ^{1}H NMR (500 MHz, CDCl$_3$): δ 7.89 (d, *J* = 2.2 Hz, 1H), 7.69 (dd, *J* = 8.7, 2.2 Hz, 1H), 7.53 (d, *J* = 15.4 Hz, 1H), 6.74 (d, *J* = 8.7 Hz, 1H), 6.51 (d, *J* = 15.4 Hz, 1H), 3.69 (s, 3H). ^{13}C NMR (126 MHz, DMSO-d_6): δ 187.2, 167.1, 166.7, 160.2, 136.3, 133.8, 133.0, 131.3, 130.6, 112.9, 111.8, 57.3. LC-MS (ESI): t_R = 4.09 min, area: >98%, *m/z*: 285/287 [M + H]$^+$. HRMS (ESI): *m/z*: [M + H]$^+$ calcd. for C$_{11}$H$_{10}$BrO$_4$ 284.9757, found 284.9763

4.8.2.2. *trans*-6-(3-Bromo-4-methoxybenzoyl)cyclohex-3-ene-1-carboxylic acid (**15**)

A mixture of **14** (70.0 g, 221 mmol) and buta-1,3-diene in THF (~ 13% w/w, 150 mL, 300 mmol) was divided over 8 microwave vials. Each vial was stirred under microwave irradiation at 140 °C for 30 min (the internal pressure reached ~ 10 bar). The reaction mixtures were pooled and concentrated *in vacuo* to obtain the crude product. Trituration with toluene provided the product as a white solid (72.4 g, 97%). ^{1}H NMR (500 MHz, DMSO-d_6): δ 12.30 (s, 1H), 8.16 (s, 1H), 8.07 (d, *J* = 8.7 Hz, 1H), 7.23 (d, *J* = 8.5 Hz, 1H), 5.79 − 5.66 (m, 2H), 3.95 (s, 3H), 3.83 − 3.72 (m, 1H), 2.92 − 2.75 (m, 1H), 2.54 − 2.10 (m, 3H), 1.93 − 1.79 (m, 1H). ^{13}C NMR (126 MHz, DMSO-d_6): δ 200.8, 176.4, 159.61 133.4, 130.6, 130.3, 125.8, 125.7, 112.8, 111.6, 57.2, 42.2, 41.6, 29.4, 28.4. LC-MS (ESI): t_R = 4.53 min, area: >98%, *m/z*: 339/341 [M + H]$^+$. HRMS (ESI): *m/z*: [M + H]$^+$ calcd. for C$_{15}$H$_{16}$BrO$_4$ 339.0226, found 339.0213

4.8.2.3. *trans*-4-(3-Bromo-4-methoxyphenyl)-4a,5,8,8a-tetrahydrophthalazin-1(2*H*)-one (**16**)

A solution of **15** (70 g, 0.21 mol) and hydrazine monohydrate (32 mL, 0.62 mol) in EtOH (400 mL) was stirred at reflux for 4 h. The reaction mixture was cooled in the refridgerator and filtered to obtain the

pure product as a white solid (60 g, 86%). *Note: Partial conversion of stereochemistry during the condensation reaction was observed only once (out of 5) during a small scale reaction (<3 mmol).* ^{1}H NMR (600 MHz, DMF-d_7) δ 10.98 (s, 1H), 7.74 (d, *J* = 2.1 Hz, 1H), 7.52 (dd, *J* = 8.5, 2.1 Hz, 1H), 7.22 (d, *J* = 8.5 Hz, 1H), 5.82 – 5.64 (m, 2H), 3.98 (s, 3H), 3.14 (ddd, *J* = 14.6, 11.4, 5.4 Hz, 1H), 2.57 (td, *J* = 14.2, 13.3, 5.4 Hz, 2H), 2.51 – 2.43 (m, 1H), 2.22 – 2.10 (m, 1H), 1.94 – 1.84 (m, 1H). ^{13}C NMR (126 MHz, DMSO-d_6): δ 168.9, 155.9, 153.8, 132.3, 130.9, 128.7, 126.1, 125.9, 112.4, 110.5, 56.8, 36.2, 34.3, 30.3, 26.2. LC-MS (ESI): t_R = 4.29 min, area: >98%, *m/z*: 335/337 [M + H]$^+$. HRMS (ESI): *m/z*: [M + H]$^+$ calcd. for $C_{15}H_{16}BrN_2O_2$ 335.0390, found 335.0378

4.8.2.4. *cis*-4-(3-Bromo-4-methoxyphenyl)-2-isopropyl-4a,5,8,8a-tetrahydrophthalazin-1(2*H*)-one (**17**)

To a solution of **16** (50.0 g, 0.15 mol) in DMF (500 mL) was added NaH (15 g, 0.37 mol) and the reaction mixture was stirred at rt for 30 min. 2-bromopropane (21 mL, 22 mmol) was added to the reaction mixture and the reaction mixture was stirred at rt for 4 h. The reaction mixture was quenched with aq. HCl (0.5 M, 1.5 L) on ice. The suspension was filtered and the residue was dissolved in MeOH/DCM. The solution was dried over Na_2SO_4, filtered and concentrated *in vacuo.* The residue was triturated with Et$_2$O to obtain the product as white crystals (46 g, 81%). ^{1}H NMR (600 MHz, CDCl$_3$) δ 8.04 (s, 1H), 7.74 (d, *J* = 8.6 Hz, 1H), 6.94 (d, *J* = 8.6 Hz, 1H), 5.85 – 5.65 (m, 2H), 5.05 (hept, *J* = 6.3 Hz, 1H), 3.95 (s, 3H), 3.28 (dt, *J* = 11.5, 5.8 Hz, 1H), 3.07 – 2.96 (m, 1H), 2.74 (t, *J* = 6.1 Hz, 1H), 2.26 – 2.12 (m, 2H), 2.08 – 1.96 (m, 1H), 1.33 (d, *J* = 6.6 Hz, 3H), 1.22 (d, *J* = 6.7 Hz, 3H). ^{13}C NMR (126 MHz, DMSO-d_6): δ 166.5, 156.8, 152.9, 130.4, 129.2, 127.3, 126.3, 124.4, 113.0, 111.6, 56.9, 46.2, 34.3, 30.3, 22.9, 22.4, 20.9, 20.6. LC-MS (ESI): t_R = 5.30 min, area: >98%, *m/z*: 377/379 [M + H]$^+$. HRMS (ESI): *m/z*: [M + H]$^+$ calcd. for $C_{18}H_{22}BrN_2O_2$ 377.0859, found 377.0871

4.8.2.5. Trimethyl(3,3,3-triethoxyprop-1-yn-1-yl)silane (**18**)

Magnesium (1.38 g, 56.7 mmol) was activated using a mortar and pestle and was suspended in dry Et$_2$O (25 mL). 2-bromopropane (5.33 mL, 56.7 mmol) was slowly added to the stirring reaction mixture while cooling with water (the reaction mixture starts to reflux). The reaction mixture was stirred in a cold water bath for 30 min prior to the addition of ethynyltrimethylsilane (6.68 mL, 47.3 mmol). This reaction mixture was stirred for an additional 30 min to form a thick grey suspension, which was diluted with Et$_2$O (25 mL) prior to slow addition of tetraethoxymethane (10.9 mL, 52.0 mmol). After 1 h the reaction mixture turned into a dark brown/colourless mixture (two phases). The reaction mixture was poured in saturated aq. NH$_4$Cl (500 mL) and was extracted with Et$_2$O (2 × 500 mL). The organic phase was concentrated and the product was isolated as a light yellow liquid (10.5 g, 93%). ^{1}H NMR (500 MHz, DMSO-d_6): δ 3.55 (q, *J* = 7.1 Hz, 6H), 1.12 (t, *J* = 7.2 Hz, 9H), 0.18 (s, 9H). ^{13}C NMR (126 MHz, DMSO-d_6): δ 107.8, 99.2, 88.0, 58.3, 14.7, -0.5. HRMS (ESI): *m/z*: [M + Na]$^+$ calcd. for $C_{12}H_{24}NaO_3Si$ 267.1387, found 267.1376

4.8.2.6. Ethyl 3-(5-(*cis*-3-isopropyl-4-oxo-3,4,4a,5,8,8a-hexahydrophthalazin-1-yl)-2-methoxyphenyl)propiolate (**19**)

To a N$_2$-purged solution of **17** (0.50 g, 1.3 mmol) in DMF (2 mL) and Et$_3$N (2 mL) was added subsequently **18** (0.65 g, 2.7 mmol), PdCl$_2$(dppf) (49 mg, 0.66 mmol), CuI (25 mg, 0.13 mmol) and CsF (0.30 g, 1.99 mmol). The mixture was stirred in the microwave at 120 °C for 4 h. The reaction mixture

was poured in 1 M aq. HCl (250 mL) and extracted with EtOAc (2 × 250 mL). The organic phase was washed with brine (250 mL), dried over MgSO$_4$, filtered and concentrated to obtain the crude product as a brown solid. The crude product was purified using flash column chromatography (0-50% EtOAc/Hept). The product was obtained as a light yellow solid (0.37 g, 70%). ^{1}H NMR (500 MHz, DMSO-d_6): δ 8.10 – 7.99 (m, 2H), 7.25 (d, J = 8.9 Hz, 1H), 5.74 – 5.56 (m, 2H), 4.88 (hept, J = 6.6 Hz, 1H), 4.25 (q, J = 7.1 Hz, 2H), 3.93 (s, 3H), 3.51 (dt, J = 11.5, 5.8 Hz, 1H), 2.80 (t, J = 6.0 Hz, 1H), 2.78 – 2.69 (m, 1H), 2.23 – 2.06 (m, 2H), 1.86 – 1.72 (m, 1H), 1.33 – 1.20 (m, 6H), 1.15 (d, J = 6.8 Hz, 3H). ^{13}C NMR (126 MHz, DMSO-d_6): δ 166.6, 162.5, 153.6, 153.0, 132.3, 131.1, 128.1, 126.3, 124.5, 112.6, 108.1, 84.9, 82.9, 62.5, 56.8, 46.2, 34.3, 30.2, 22.8, 22.4, 20.9, 20.6, 14.4. LC-MS (ESI): t$_R$ = 5.31 min, area: >98%, m/z: 395 [M + H]$^+$. HRMS (ESI): m/z: [M + H]$^+$ calcd. for C$_{23}$H$_{27}$N$_2$O$_4$ 395.1965, found 395.1952

4.8.2.7. 3-(5-(*cis*-3-Isopropyl-4-oxo-3,4,4a,5,8,8a-hexahydrophthalazin-1-yl)-2-methoxyphenyl)propiolamide (**20**)

Ester **19** (0.50 g, 1.27 mmol) was dissolved in a solution of NH$_3$ in MeOH (7 M, 4 mL, 28.0 mmol) and stirred at rt for 2 h. The reaction mixture was concentrated and the crude product was purified using flash column chromatography (gradient: 0-50% EtOAc/Hept). The product was obtained as a white solid (390 mg, 84%). ^{1}H NMR (500 MHz, DMSO-d_6): δ 8.14 (s, 1H), 8.01 – 7.91 (m, 2H), 7.69 (s, 1H), 7.20 (d, J = 8.8 Hz, 1H), 5.75 – 5.57 (m, 2H), 4.88 (p, J = 6.6 Hz, 1H), 3.90 (s, 3H), 3.45 (dt, J = 11.6, 5.7 Hz, 1H), 2.81 (t, J = 6.0 Hz, 1H), 2.78 – 2.68 (m, 1H), 2.25 – 1.99 (m, 2H), 1.80 (t, J = 14.8 Hz, 1H), 1.24 (d, J = 6.4 Hz, 4H), 1.14 (d, J = 6.7 Hz, 3H). ^{13}C NMR (126 MHz, DMSO-d_6): δ 166.5, 161.7, 154.4, 153.1, 131.6, 129.9, 127.8, 126.3, 124.4, 112.3, 109.7, 88.5, 80.0, 56.6, 46.2, 34.2, 30.3, 22.9, 22.3, 20.9, 20.6. LC-MS (ESI): t$_R$ = 4.19 min, area: >98%, m/z: 366 [M + H]$^+$. HRMS (ESI): m/z: [M + H]$^+$ calcd. for C$_{21}$H$_{24}$N$_3$O$_3$ 366.1812, found 366.1797

4.8.3. General procedure for alkynamide synthesis

To a N$_2$-purged solution of **19** (1 equiv.) in DCM (4 mL per equiv. of **19**) was added K$_2$CO$_3$ (5 equiv.) and the corresponding amine (2.5 equiv.) (3 equiv. of Et$_3$N was added for HCl salts). AlMe$_3$ (2.5 equiv.) was slowly added and the reaction mixture was stirred at rt overnight. The reaction mixture was carefully poured in 1 M aq. HCl (100 mL) and extracted with EtOAc (100 mL). The organic phase was washed with brine (100 mL), dried over MgSO$_4$, filtered and concentrated to obtain the crude product as a brown solid. The crude product was purified using flash column chromatography.

4.8.3.1. *N*-Butyl-3-(5-(*cis*-3-isopropyl-4-oxo-3,4,4a,5,8,8a-hexahydrophthalazin-1-yl)-2-methoxyphenyl)propiolamide (**21**)

This compound was synthesized according to the general procedure using **19** (0.25 g, 0.63 mmol) and butan-1-amine as the corresponding amine. Column chromatography was performed using EtOAc/n-hept (gradient: 0-50%) to obtain a white solid (182 mg, 68%). ^{1}H NMR (500 MHz, CDCl$_3$): δ 7.94 (d, J = 2.4 Hz, 1H), 7.90 (dd, J = 8.8, 2.4 Hz, 1H), 6.96 (t, J = 8.1 Hz, 1H), 6.12 – 5.87 (m, 1H), 5.84 – 5.64 (m, 2H), 5.05 (hept, J = 6.7 Hz, 1H), 3.95 (s, 3H), 3.38 (q, J = 6.9 Hz, 2H), 3.27 (dt, J = 11.5, 5.7 Hz, 1H), 3.07 – 2.96 (m, 1H), 2.74 (t, J = 5.8 Hz, 1H), 2.28 – 2.10 (m, 2H), 2.09 – 1.94 (m, 1H), 1.57 (p, J = 7.3 Hz, 2H), 1.41 (hept, J = 7.6 Hz, 2H), 1.36 – 1.15 (m, 7H), 0.96 (t, J = 7.3 Hz, 3H), 0.89 (t, J = 6.9 Hz, 1H). ^{13}C NMR (126 MHz, CDCl$_3$): δ 166.4, 161.7, 153.4, 152.4, 132.0, 129.4, 129.1, 127.9, 126.0, 123.8, 110.9, 109.8, 87.3, 80.6, 56.1, 46.7, 43.2, 39.7, 34.7, 32.8, 31.4, 31.0, 23.0, 22.3, 20.6, 20.2, 20.1, 13.8. LC-MS (ESI):

t_R = 4.97 min, area: >98%, *m/z*: 422 [M + H]+. HRMS (ESI): *m/z*: [M + H]+ calcd. for $C_{25}H_{32}N_3O_3$ 422.2438, found 422.2428

4.8.3.2. *N*-(Cyclopropylmethyl)-3-(5-(*cis*-3-isopropyl-4-oxo-3,4,4a,5,8,8a-hexahydrophthalazin-1-yl)-2-methoxyphenyl)propiolamide (**22**)

This compound was synthesized according to the general procedure using **19** (0.20 g, 0.51 mmol) and cyclopropylmethanamine as the corresponding amine. Column chromatography was performed using EtOAc/n-hept (gradient: 0-50%) to obtain a white solid (105 mg, 49%). 1H NMR (500 MHz, CDCl3): δ 8.01 – 7.85 (m, 2H), 6.95 (dd, *J* = 8.9, 4.9 Hz, 1H), 6.35 – 6.18 (m, 1H), 5.82 – 5.61 (m, 2H), 5.03 (hept, *J* = 6.7 Hz, 1H), 3.94 (s, 3H), 3.49 – 3.16 (m, 3H), 3.04 – 2.94 (m, 1H), 2.72 (t, *J* = 5.8 Hz, 1H), 2.26 – 2.09 (m, 2H), 2.07 – 1.92 (m, 1H), 1.32 (d, *J* = 6.6 Hz, 3H), 1.19 (d, *J* = 6.7 Hz, 3H), 1.08 – 0.95 (m, 1H), 0.61 – 0.47 (m, 2H), 0.36 – 0.19 (m, 2H). 13C NMR (126 MHz, CDCl3): δ 166.4, 161.7, 153.3, 152.4, 132.0, 129.1, 128.0, 126.0, 123.8, 110.9, 109.8, 87.3, 80.8, 56.1, 48.3, 46.7, 44.8, 34.7, 31.0, 23.0, 22.3, 20.6, 20.2, 10.5, 3.6. LC-MS (ESI): t_R = 4.80 min, area: 98%, *m/z*: 420 [M + H]+. HRMS (ESI): *m/z*: [M + H]+ calcd. for $C_{25}H_{30}N_3O_3$ 420.2282, found 420.2277

4.8.3.3. *N*-(Cyclobutylmethyl)-3-(5-(*cis*-3-isopropyl-4-oxo-3,4,4a,5,8,8a-hexahydrophthalazin-1-yl)-2-methoxyphenyl)propiolamide (**23**)

This compound was synthesized according to the general procedure using **19** (0.20 g, 0.51 mmol) and cyclobutylmethanamine as the corresponding amine. Column chromatography was performed using EtOAc/n-hept (gradient: 0-50%) to obtain a white solid (115 mg, 52%). 1H NMR (500 MHz, CDCl3): δ 8.05 – 7.84 (m, 2H), 6.96 (t, *J* = 9.3 Hz, 1H), 6.08 (q, *J* = 6.5, 6.0 Hz, 1H), 5.83 – 5.63 (m, 2H), 5.04 (hept, *J* = 6.6 Hz, 1H), 3.94 (s, 3H), 3.40 (dd, *J* = 7.3, 5.9 Hz, 2H), 3.33 – 3.21 (m, 1H), 3.08 – 2.94 (m, 1H), 2.73 (q, *J* = 6.0 Hz, 1H), 2.63 – 2.46 (m, *J* = 7.7 Hz, 1H), 2.28 – 1.65 (m, 10H), 1.32 (d, *J* = 6.6 Hz, 3H), 1.20 (d, *J* = 6.7 Hz, 3H). 13C NMR (126 MHz, CDCl3): δ 166.4, 161.7, 153.5, 152.4, 132.0, 129.1, 127.9, 126.0, 123.8, 110.9, 109.8, 87.3, 80.8, 56.1, 46.7, 45.2, 35.8, 34.7, 31.0, 25.7, 23.0, 22.3, 20.6, 20.2, 18.3. LC-MS (ESI): t_R = 5.11 min, area: >98%, *m/z*: 434 [M + H]+. HRMS (ESI): *m/z*: [M + H]+ calcd. for $C_{26}H_{32}N_3O_3$ 434.2438, found 434.2428

4.8.3.4. *N*-(2-Cyanoethyl)-3-(5-(*cis*-3-isopropyl-4-oxo-3,4,4a,5,8,8a-hexahydrophthalazin-1-yl)-2-methoxyphenyl)propiolamide (**24**)

This compound was synthesized according to the general procedure using **19** (0.20 g, 0.51 mmol) and 3-aminopropanenitrile as the corresponding amine. Column chromatography was performed using EtOAc/n-hept (gradient: 0-50%) to obtain a white solid (47 mg, 22%). 1H NMR (500 MHz, DMSO-*d6*): δ 9.12 (t, *J* = 5.8 Hz, 1H), 8.04 – 7.93 (m, 2H), 7.21 (d, *J* = 8.9 Hz, 1H), 5.74 – 5.57 (m, 2H), 4.88 (hept, *J* = 6.6 Hz, 1H), 3.91 (s, 3H), 3.46 (dt, *J* = 11.6, 5.7 Hz, 1H), 3.39 (d, *J* = 6.3 Hz, 1H), 2.80 (t, *J* = 6.4 Hz, 1H), 2.77 – 2.67 (m, 3H), 2.21 – 2.05 (m, 2H), 1.87 – 1.73 (m, 1H), 1.24 (d, *J* = 6.5 Hz, 3H), 1.14 (d, *J* = 6.7 Hz, 3H). 13C NMR (126 MHz, DMSO-*d6*): δ 166.5, 161.8, 153.1, 153.0, 131.7, 130.1, 127.9, 126.3, 124.4, 119.7, 112.4, 109.3, 87.8, 80.8, 56.6, 46.2, 35.6, 34.2, 30.3, 22.8, 22.3, 20.9, 20.6, 17.8. LC-MS (ESI): t_R = 4.35 min, area: >98%, *m/z*: 419 [M + H]+. HRMS (ESI): *m/z*: [M + H]+ calcd. for $C_{24}H_{27}N_4O_3$ 419.2078, found 419.2065

4.8.3.5. 1-(3-(5-(*cis*-3-Isopropyl-4-oxo-3,4,4a,5,8,8a-hexahydrophthalazin-1-yl)-2-methoxyphenyl)propioloyl)azetidine-3-carbonitrile (**25**)

This compound was synthesized according to the general procedure using **19** (0.20 g, 0.51 mmol) and azetidine-3-carbonitrile.HCl as the corresponding amine. Column chromatography was performed using EtOAc/n-hept (gradient: 0-50%) to obtain a white solid (126 mg, 58%). ^{1}H NMR (500 MHz, CDCl$_3$): δ 7.98 – 7.87 (m, 2H), 6.97 (d, *J* = 8.8 Hz, 1H), 5.83 – 5.63 (m, 2H), 5.04 (hept, *J* = 6.6 Hz, 1H), 4.67 – 4.52 (m, 2H), 4.43 (t, *J* = 9.7 Hz, 1H), 4.34 (dd, *J* = 10.2, 6.2 Hz, 1H), 3.95 (s, 3H), 3.60 (tt, *J* = 9.1, 6.2 Hz, 1H), 3.26 (dt, *J* = 11.5, 5.8 Hz, 1H), 3.05 – 2.96 (m, 1H), 2.74 (t, *J* = 6.0 Hz, 1H), 2.26 – 2.10 (m, 2H), 2.04 – 1.96 (m, 1H), 1.32 (d, *J* = 6.6 Hz, 3H), 1.20 (d, *J* = 6.7 Hz, 3H). ^{13}C NMR (126 MHz, CDCl$_3$): δ 166.4, 162.0, 154.1, 152.2, 131.8, 129.7, 128.0, 126.0, 123.8, 119.0, 110.9, 109.3, 87.5, 83.5, 56.2, 53.4, 51.7, 46.7, 34.7, 31.0, 23.0, 22.3, 20.6, 20.2, 17.5. LC-MS (ESI): t$_R$ = 4.59 min, area: >98%, *m/z*: 431 [M + H]$^+$. HRMS (ESI): *m/z*: [M + H]$^+$ calcd. for C$_{25}$H$_{27}$N$_4$O$_3$ 431.2078, found 431.2073

4.8.3.6. 3-(5-(*cis*-3-Isopropyl-4-oxo-3,4,4a,5,8,8a-hexahydrophthalazin-1-yl)-2-methoxyphenyl)-*N*-((tetrahydrofuran-2-yl)methyl)propiolamide (**26**)

This compound was synthesized according to the general procedure using **19** (0.20 g, 0.51 mmol) and (tetrahydrofuran-2-yl)methanamine.HCl as the corresponding amine. Column chromatography was performed using EtOAc/n-hept (gradient: 0-50%) to obtain a white solid (120 mg, 53%). ^{1}H NMR (500 MHz, CDCl$_3$): δ 8.05 – 7.83 (m, 2H), 6.95 (t, *J* = 8.9 Hz, 1H), 6.43 (t, *J* = 6.0 Hz, 1H), 5.83 – 5.61 (m, 2H), 5.03 (hept, *J* = 6.7 Hz, 1H), 3.98 – 3.87 (m, 4H), 3.84 (dd, *J* = 8.8, 6.9 Hz, 1H), 3.75 (q, *J* = 7.8 Hz, 1H), 3.65 – 3.54 (m, 1H), 3.38 (q, *J* = 6.5 Hz, 2H), 3.26 (dt, *J* = 11.5, 5.7 Hz, 1H), 3.05 – 2.94 (m, 1H), 2.72 (t, *J* = 6.0 Hz, 1H), 2.61 – 2.50 (m, 1H), 2.25 – 2.05 (m, 3H), 2.04 – 1.93 (m, 1H), 1.71 – 1.59 (m, 1H), 1.31 (d, *J* = 6.6 Hz, 3H), 1.19 (d, *J* = 6.7 Hz, 3H). ^{13}C NMR (126 MHz, CDCl$_3$): δ 166.4, 161.7, 153.7, 152.4, 132.0, 129.2, 127.9, 126.0, 123.8, 110.9, 109.7, 87.1, 81.2, 77.4, 77.1, 71.3, 67.8, 56.1, 46.7, 42.7, 38.9, 34.7, 30.9, 29.9, 23.0, 22.3, 20.6, 20.2. LC-MS (ESI): t$_R$ = 4.46 min, area: >98%, *m/z*: 450 [M + H]$^+$. HRMS (ESI): *m/z*: [M + H]$^+$ calcd. for C$_{26}$H$_{32}$N$_3$O$_4$ 450.2387, found 450.2387

4.8.3.7. *cis*-2-Isopropyl-4-(4-methoxy-3-(3-morpholino-3-oxoprop-1-yn-1-yl)phenyl)-4a,5,8,8a-tetrahydrophthalazin-1(2*H*)-one (**27**)

This compound was synthesized according to the general procedure using **19** (0.10 g, 0.25 mmol) and morpholine as the corresponding amine. Column chromatography was performed using EtOAc/n-hept (gradient: 0-50%) to obtain a white solid (56 mg, 51%). ^{1}H NMR (500 MHz, CDCl$_3$): δ 7.96 (d, *J* = 2.2 Hz, 1H), 7.91 (dd, *J* = 8.8, 2.3 Hz, 1H), 6.96 (d, *J* = 8.9 Hz, 1H), 5.84 – 5.61 (m, 2H), 5.04 (hept, *J* = 6.7 Hz, 1H), 3.94 (d, *J* = 3.4 Hz, 5H), 3.82 – 3.75 (m, 2H), 3.72 (s, 4H), 3.27 (dt, *J* = 11.5, 5.7 Hz, 1H), 3.07 – 2.94 (m, 1H), 2.74 (t, *J* = 6.0 Hz, 1H), 2.28 – 2.09 (m, 2H), 2.05 – 1.94 (m, 1H), 1.33 (d, *J* = 6.6 Hz, 3H), 1.21 (d, *J* = 6.7 Hz, 3H). ^{13}C NMR (126 MHz, CDCl$_3$): δ 166.4, 161.9, 153.3, 152.3, 131.8, 129.3, 128.0, 126.0, 123.8, 110.9, 109.9, 87.3, 85.2, 67.0, 66.5, 56.1, 47.3, 46.7, 42.0, 34.7, 31.0, 23.0, 22.3, 20.6, 20.2. LC-MS (ESI): t$_R$ = 4.56 min, area: >98%, *m/z*: 436 [M + H]$^+$. HRMS (ESI): *m/z*: [M + H]$^+$ calcd. for C$_{25}$H$_{30}$N$_3$O$_4$ 436.2231, found 436.2217

4.8.3.8. 3-(5-(*cis*-3-Isopropyl-4-oxo-3,4,4a,5,8,8a-hexahydrophthalazin-1-yl)-2-methoxyphenyl)-*N*-(2-methyl-2*H*-1,2,3-triazol-4-yl)propiolamide (**11**)

This compound was synthesized according to the general procedure using **19** (0.10 g, 0.25 mmol) and 2-methyl-2*H*-1,2,3-triazol-4-amine.HCl as the corresponding amine. Column chromatography was performed using EtOAc/n-hept (gradient: 10-80%) to obtain a white solid (42 mg, 37%). ^{1}H NMR (500 MHz, CDCl$_3$): δ 8.33 (s, 1H), 7.94 (s, 1H), 7.91 (d, *J* = 2.3 Hz, 1H), 7.86 (dd, *J* = 8.8, 2.4 Hz, 1H), 6.90 (d, *J* = 8.9 Hz, 1H), 5.78 – 5.57 (m, 2H), 4.98 (hept, *J* = 6.7 Hz, 1H), 4.06 (s, 3H), 3.89 (s, 3H), 3.26 – 3.15 (m, 1H), 2.99 – 2.89 (m, 1H), 2.68 (t, *J* = 6.0 Hz, 1H), 2.20 – 2.04 (m, 2H), 2.01 – 1.89 (m, 1H), 1.26 (d, *J* = 6.6 Hz, 3H), 1.14 (d, *J* = 6.7 Hz, 3H). ^{13}C NMR (126 MHz, CDCl$_3$): δ 166.4, 162.0, 152.2, 149.8, 143.2, 132.2, 129.7, 128.1, 126.0, 125.4, 123.8, 111.0, 109.2, 86.5, 83.4, 56.4, 46.8, 41.7, 34.7, 31.0, 23.0, 22.3, 20.6, 20.2. LC-MS (ESI): t$_R$ = 4.54 min, area: >97%, *m/z*: 447 [M + H]$^+$. HRMS (ESI): *m/z*: [M + H]$^+$ calcd. for C$_{24}$H$_{27}$N$_6$O$_3$ 447.2139, found 447.2131

4.8.3.9. *N*-(1-(3-Cyanopropyl)-1*H*-pyrazol-3-yl)-3-(5-(*cis*-3-isopropyl-4-oxo-3,4,4a,5,8,8a-hexahydrophthalazin-1-yl)-2-methoxyphenyl)propiolamide (**12**)

This compound was synthesized according to the general procedure using **19** (0.10 g, 0.25 mmol) and 4-(3-amino-1*H*-pyrazol-1-yl)butanenitrile as the corresponding amine. Column chromatography was performed using EtOAc/n-hept (gradient: 10-80%) to obtain a white solid (11 mg, 9%). ^{1}H NMR (500 MHz, CDCl$_3$): δ 8.29 (s, 1H), 7.99 (d, *J* = 2.3 Hz, 1H), 7.93 (dd, *J* = 8.8, 2.3 Hz, 1H), 7.37 (s, 1H), 6.98 (d, *J* = 8.8 Hz, 1H), 6.76 (s, 1H), 5.85 – 5.66 (m, 2H), 5.06 (hept, *J* = 6.6 Hz, 1H), 4.20 (t, *J* = 6.2 Hz, 2H), 3.97 (s, 3H), 3.33 – 3.25 (m, 1H), 3.07 – 2.98 (m, 1H), 2.76 (t, *J* = 5.9 Hz, 1H), 2.35 (t, *J* = 6.8 Hz, 2H), 2.28 – 2.13 (m, 4H), 2.08 – 1.97 (m, 1H), 1.35 (d, *J* = 6.6 Hz, 3H), 1.23 (d, *J* = 6.7 Hz, 3H). ^{13}C NMR (126 MHz, CDCl$_3$): δ 166.4, 162.0, 152.3, 150.0, 132.2, 131.0, 129.5, 128.0, 126.0, 123.8, 118.6, 111.0, 109.4, 98.2, 87.0, 82.6, 56.1, 49.9, 46.8, 34.7, 31.0, 25.9, 23.0, 22.3, 20.6, 20.2, 14.5. LC-MS (ESI): t$_R$ = 4.49 min, area: >98%, *m/z*: 499 [M + H]$^+$. HRMS (ESI): *m/z*: [M + H]$^+$ calcd. for C$_{28}$H$_{31}$N$_6$O$_3$ 499.2452, found 499.2449

4.8.3.10. *N*-(Furan-2-ylmethyl)-3-(5-(*cis*-3-isopropyl-4-oxo-3,4,4a,5,8,8a-hexahydrophthalazin-1-yl)-2-methoxyphenyl)propiolamide (**28**)

This compound was synthesized according to the general procedure using **19** (0.20 g, 0.51 mmol) and furfurylamine as the corresponding amine. Column chromatography was performed using EtOAc/n-hept (gradient: 0-50%) to obtain a white solid (112 mg, 50%). ^{1}H NMR (500 MHz, CDCl$_3$): δ 8.02 – 7.85 (m, 2H), 7.39 (d, *J* = 1.8 Hz, 1H), 7.01 – 6.91 (m, 1H), 6.42 (d, *J* = 6.8 Hz, 1H), 6.38 – 6.27 (m, 2H), 5.85 – 5.61 (m, 2H), 5.05 (p, *J* = 6.6 Hz, 1H), 4.55 (d, *J* = 5.6 Hz, 2H), 3.93 (s, 3H), 3.26 (dt, *J* = 11.5, 5.7 Hz, 1H), 3.11 – 2.91 (m, 1H), 2.73 (t, J= 6.0 Hz, 1H), 2.27 – 2.10 (m, 2H), 2.04 – 1.95 (m, 1H), 1.33 (d, *J* = 6.6 Hz, 3H), 1.20 (d, *J* = 6.7 Hz, 3H). ^{13}C NMR (126 MHz, CDCl$_3$): δ 166.4, 161.8, 153.1, 152.4, 150.3, 142.5, 132.0, 129.3, 127.9, 126.0, 123.8, 110.9, 110.6, 109.6, 108.1, 86.8, 81.5, 56.1, 46.7, 36.7, 34.7, 31.0, 23.0, 22.3, 20.6, 20.2. LC-MS (ESI): t$_R$ = 4.78 min, area: >98%, *m/z*: 446 [M + H]$^+$. HRMS (ESI): *m/z*: [M + H]$^+$ calcd. for C$_{26}$H$_{28}$N$_3$O$_4$ 446.2074, found 446.2055

4.8.3.11. 3-(5-(*cis*-3-Isopropyl-4-oxo-3,4,4a,5,8,8a-hexahydrophthalazin-1-yl)-2-methoxyphenyl)-*N*-((5-methylfuran-2-yl)methyl)propiolamide (**29**)

This compound was synthesized according to the general procedure using **19** (0.20 g, 0.51 mmol) and (5-methylfuran-2-yl)methanamine as the corresponding amine. Column chromatography was performed using EtOAc/n-hept (gradient: 0-50%) to obtain a white solid (112 mg, 48%). ^{1}H NMR (500 MHz, DMSO-d_6): δ 9.21 (t, J = 5.8 Hz, 1H), 8.02 – 7.93 (m, 2H), 7.20 (d, J = 8.8 Hz, 1H), 6.15 (d, J = 3.0 Hz, 1H), 6.03 – 5.97 (m, 1H), 5.74 – 5.58 (m, 2H), 4.87 (hept, J = 6.6 Hz, 1H), 4.27 (d, J = 5.7 Hz, 2H), 3.90 (s, 3H), 3.44 (dt, J = 11.6, 5.8 Hz, 1H), 2.80 (t, J = 6.0 Hz, 1H), 2.78 – 2.69 (m, 1H), 2.23 (d, J = 1.0 Hz, 3H), 2.19 – 2.04 (m, 2H), 1.85 – 1.74 (m, 1H), 1.23 (d, J = 6.5 Hz, 3H), 1.14 (d, J = 6.8 Hz, 3H). ^{13}C NMR (126 MHz, DMSO-d_6): δ 166.5, 161.8, 153.1, 152.6, 151.3, 145.0, 131.6, 130.0, 127.9, 126.3, 124.4, 112.3, 109.5, 108.7, 106.9, 88.0, 80.7, 56.6, 46.2, 36.1, 34.2, 30.3, 22.9, 22.3, 20.9, 20.6, 13.8. LC-MS (ESI): t_R = 4.96 min, area: >98%, m/z: 460 [M + H]$^+$. HRMS (ESI): m/z: [M + H]$^+$ calcd. for C$_{27}$H$_{30}$N$_3$O$_4$ 460.2231, found 460.2216

4.8.3.12. 3-(5-(*cis*-3-Isopropyl-4-oxo-3,4,4a,5,8,8a-hexahydrophthalazin-1-yl)-2-methoxyphenyl)-*N*-(thiophen-2-ylmethyl)propiolamide (**30**)

This compound was synthesized according to the general procedure using **19** (0.15 g, 0.38 mmol) and thiophen-2-ylmethanamine as the corresponding amine. Column chromatography was performed using EtOAc/n-hept (gradient: 0-50%) to obtain a white solid (76 mg, 43%). ^{1}H NMR (500 MHz, CDCl$_3$): δ 7.92 (d, J = 2.4 Hz, 1H), 7.89 (dd, J = 8.8, 2.4 Hz, 1H), 7.27 – 7.23 (m, 1H), 7.08 – 7.02 (m, 1H), 6.97 (dd, J = 5.2, 3.4 Hz, 1H), 6.94 (d, J = 8.9 Hz, 1H), 6.54 (t, J = 5.8 Hz, 1H), 5.82 – 5.64 (m, 2H), 5.03 (p, J = 6.6 Hz, 1H), 4.71 (d, J = 5.7 Hz, 2H), 3.91 (s, 3H), 3.25 (dt, J = 11.4, 5.7 Hz, 1H), 3.04 – 2.95 (m, 1H), 2.71 (t, J = 6.0 Hz, 1H), 2.24 – 2.10 (m, 2H), 2.04 – 1.93 (m, 1H), 1.32 (d, J = 6.5 Hz, 3H), 1.19 (d, J = 6.7 Hz, 3H). ^{13}C NMR (126 MHz, CDCl$_3$): δ 166.4, 161.8, 153.0, 152.4, 139.6, 132.0, 129.3, 127.9, 127.0, 126.7, 126.0, 125.6, 123.8, 110.9, 109.6, 86.9, 81.6, 56.1, 46.7, 38.5, 34.7, 30.9, 23.0, 22.3, 20.6, 20.2. LC-MS (ESI): t_R = 5.00 min, area: >98%, m/z: 462 [M + H]$^+$. HRMS (ESI): m/z: [M + H]$^+$ calcd. for C$_{26}$H$_{28}$N$_3$O$_3$S 462.1846, found 462.1836

4.8.3.13. 3-(5-(*cis*-3-Isopropyl-4-oxo-3,4,4a,5,8,8a-hexahydrophthalazin-1-yl)-2-methoxyphenyl)-*N*-(2-(thiophen-2-yl)ethyl)propiolamide (**31**)

This compound was synthesized according to the general procedure using **19** (0.15 g, 0.38 mmol) and 2-(thiophen-2-yl)ethanamine as the corresponding amine. Column chromatography was performed using EtOAc/n-hept (gradient: 0-50%) to obtain a white solid (87 mg, 48%). ^{1}H NMR (500 MHz, CDCl$_3$): δ 7.92 (d, J = 2.4 Hz, 1H), 7.88 (dd, J = 8.8, 2.4 Hz, 1H), 7.21 – 7.14 (m, 1H), 6.99 – 6.91 (m, 2H), 6.88 (dd, J = 3.3, 1.2 Hz, 1H), 6.36 (t, J = 6.1 Hz, 1H), 5.81 – 5.62 (m, 2H), 5.04 (p, J = 6.6 Hz, 1H), 3.91 (s, 3H), 3.64 (q, J = 6.6 Hz, 2H), 3.25 (dt, J = 11.5, 5.7 Hz, 1H), 3.10 (t, J = 6.8 Hz, 2H), 3.05 – 2.95 (m, 1H), 2.72 (q, J = 7.7, 5.9 Hz, 1H), 2.25 – 1.97 (m, 3H), 1.32 (dd, J = 6.6, 2.6 Hz, 3H), 1.20 (dd, J = 6.7, 2.9 Hz, 3H). ^{13}C NMR (126 MHz, CDCl$_3$): δ 166.4, 161.8, 153.4, 152.4, 140.9, 132.0, 129.2, 127.9, 127.1, 126.0, 125.5, 124.1, 123.8, 110.9, 109.7, 87.2, 81.1, 56.1, 46.7, 41.3, 34.7, 30.9, 26.9, 23.0, 22.3, 20.6, 20.2. LC-MS (ESI): t_R = 5.09 min, area: >98%, m/z: 476 [M + H]$^+$. HRMS (ESI): m/z: [M + H]$^+$ calcd. for C$_{27}$H$_{30}$N$_3$O$_3$S 476.2002, found 476.1990

4.8.3.14. 3-(5-(*cis*-3-Isopropyl-4-oxo-3,4,4a,5,8,8a-hexahydrophthalazin-1-yl)-2-methoxyphenyl)-*N*-((2-methylthiazol-4-yl)methyl)propiolamide (**32**)

This compound was synthesized according to the general procedure using **19** (0.20 g, 0.51 mmol) and (2-methylthiazol-4-yl)methanamine.2HCl as the corresponding amine. Column chromatography was performed using EtOAc/n-hept (gradient: 0-50%) to obtain a white solid (142 mg, 59%). ^{1}H NMR (500 MHz, DMSO-d_6): δ 9.29 (t, J = 6.0 Hz, 1H), 8.03 – 7.91 (m, 2H), 7.25 (d, J = 0.9 Hz, 1H), 7.21 (d, J = 8.8 Hz, 1H), 5.73 – 5.57 (m, 2H), 4.88 (p, J = 6.6 Hz, 1H), 4.37 (dd, J = 6.0, 1.0 Hz, 2H), 3.91 (s, 3H), 3.44 (dt, J = 11.7, 5.8 Hz, 1H), 2.81 (t, J = 6.1 Hz, 1H), 2.77 – 2.68 (m, 1H), 2.63 (s, 3H), 2.21 – 2.05 (m, 2H), 1.87 – 1.71 (m, 1H), 1.24 (d, J = 6.6 Hz, 3H), 1.14 (d, J = 6.7 Hz, 3H). ^{13}C NMR (126 MHz, DMSO-d_6): δ 166.5, 166.0, 161.8, 153.1, 152.9, 152.7, 131.6, 130.0, 127.9, 126.3, 124.4, 115.6, 112.4, 109.6, 88.1, 80.6, 56.6, 46.2, 34.2, 30.3, 22.9, 22.3, 20.9, 20.6, 19.2. LC-MS (ESI): t_R = 4.57 min, area: >97%, *m/z*: 477 [M + H]$^+$. HRMS (ESI): *m/z*: [M + H]$^+$ calcd. for $C_{26}H_{29}N_4O_3S$ 477.1955, found 477.1939

4.8.3.15. 3-(5-(*cis*-3-Isopropyl-4-oxo-3,4,4a,5,8,8a-hexahydrophthalazin-1-yl)-2-methoxyphenyl)-*N*-(2-(thiazol-2-yl)ethyl)propiolamide (**33**)

This compound was synthesized according to the general procedure using **19** (0.15 g, 0.38 mmol) and 2-(thiazol-2-yl)ethanamine as the corresponding amine. Column chromatography was performed using EtOAc/n-hept (gradient: 0-50%) to obtain a white solid (81 mg, 45%). ^{1}H NMR (500 MHz, CDCl$_3$): δ 7.93 (d, J = 2.3 Hz, 1H), 7.89 (dd, J = 8.8, 2.4 Hz, 1H), 7.74 (d, J = 3.3 Hz, 1H), 6.94 (d, J = 8.8 Hz, 1H), 6.91 (t, J = 6.1 Hz, 1H), 5.83 – 5.64 (m, 2H), 5.05 (hept, J = 6.6 Hz, 1H), 3.94 (s, 3H), 3.85 (q, J = 6.1 Hz, 2H), 3.34 – 3.23 (m, 3H), 3.06 – 2.96 (m, 1H), 2.73 (t, J = 6.0 Hz, 1H), 2.27 – 2.11 (m, 2H), 2.06 – 1.97 (m, 1H), 1.33 (d, J = 6.7 Hz, 3H), 1.21 (d, J = 6.6 Hz, 3H). ^{13}C NMR (126 MHz, CDCl$_3$): δ 167.7, 166.4, 161.8, 153.4, 152.4, 142.4, 132.0, 129.2, 127.9, 126.0, 123.8, 119.0, 110.9, 109.8, 87.2, 81.2, 56.1, 46.7, 38.7, 34.7, 32.3, 31.0, 23.0, 22.3, 20.6, 20.2. LC-MS (ESI): t_R = 4.59 min, area: >98%, *m/z*: 477 [M + H]$^+$. HRMS (ESI): *m/z*: [M + H]$^+$ calcd. for $C_{26}H_{29}N_4O_3S$ 477.1955, found 477.1941

4.8.3.16. *N*-((2,4-Dimethylthiazol-5-yl)methyl)-3-(5-(*cis*-3-isopropyl-4-oxo-3,4,4a,5,8,8a-hexahydrophthalazin-1-yl)-2-methoxyphenyl)propiolamide (**34**)

This compound was synthesized according to the general procedure using **19** (0.10 g, 0.25 mmol) and (2,4-dimethylthiazol-5-yl)methanamine as the corresponding amine. Column chromatography was performed using EtOAc/n-hept (gradient: 10-80%) to obtain a white solid (36 mg, 29%). ^{1}H NMR (500 MHz, CDCl$_3$): δ 7.93 (d, J = 2.3 Hz, 1H), 7.90 (dd, J = 8.8, 2.4 Hz, 1H), 6.95 (d, J = 8.8 Hz, 1H), 6.27 (t, J = 5.7 Hz, 1H), 5.83 – 5.76 (m, 1H), 5.72 – 5.64 (m, 1H), 5.05 (p, J = 6.7 Hz, 1H), 4.61 (d, J = 5.6 Hz, 2H), 3.94 (s, 3H), 3.30 – 3.23 (m, 1H), 3.07 – 2.97 (m, 1H), 2.74 (t, J = 6.1 Hz, 1H), 2.66 (s, 3H), 2.41 (s, 3H), 2.26 – 2.10 (m, 2H), 2.07 – 1.95 (m, 1H), 1.33 (d, J = 6.6 Hz, 3H), 1.21 (d, J = 6.7 Hz, 3H). ^{13}C NMR (126 MHz, CDCl$_3$): δ 166.4, 164.5, 161.8, 153.0, 152.3, 149.7, 132.1, 129.4, 128.0, 126.1, 126.0, 123.8, 110.9, 109.5, 86.6, 81.9, 56.1, 46.7, 35.3, 34.7, 31.0, 23.0, 22.3, 20.6, 20.2, 19.1, 14.9 LC-MS (ESI): t_R = 4.39 min, area: >98%, *m/z*: 491 [M + H]$^+$. HRMS (ESI): *m/z*: [M + H]$^+$ calcd. for $C_{27}H_{31}N_4O_3S$ 491.2111, found 491.2102

171

5

4.8.3.17. 3-(5-(*cis*-3-Isopropyl-4-oxo-3,4,4a,5,8,8a-hexahydrophthalazin-1-yl)-2-methoxyphenyl)-*N*-((1-methyl-1*H*-pyrazol-4-yl)methyl)propiolamide (**35**)

This compound was synthesized according to the general procedure using **19** (0.15 g, 0.38 mmol) and (1-methyl-1*H*-pyrazol-4-yl)methanamine as the corresponding amine. Column chromatography was performed using EtOAc/n-hept (gradient: 10-80%) to obtain a white solid (73 mg, 42%). ^{1}H NMR (500 MHz, CDCl$_3$): δ 7.89 (d, *J* = 2.3 Hz, 1H), 7.86 (dd, *J* = 8.8, 2.4 Hz, 1H), 7.40 (d, *J* = 15.1 Hz, 2H), 6.97 – 6.89 (m, 1H), 6.61 (t, *J* = 5.7 Hz, 1H), 5.79 – 5.58 (m, 2H), 5.00 (p, *J* = 6.7 Hz, 1H), 4.36 (d, *J* = 5.7 Hz, 2H), 3.88 (s, 3H), 3.84 (s, 3H), 3.27 – 3.17 (m, 1H), 3.02 – 2.91 (m, 1H), 2.69 (t, *J* = 5.9 Hz, 1H), 2.23 – 2.06 (m, 2H), 2.01 – 1.90 (m, 1H), 1.29 (d, *J* = 6.6 Hz, 3H), 1.17 (d, *J* = 6.7 Hz, 3H). ^{13}C NMR (126 MHz, CDCl$_3$): δ 166.4, 161.7, 153.2, 152.4, 138.8, 131.9, 129.7, 129.2, 127.9, 126.0, 123.8, 117.7, 110.9, 109.7, 87.1, 81.2, 56.0, 46.7, 38.9, 34.6, 34.3, 30.9, 22.9, 22.2, 20.6, 20.2. LC-MS (ESI): t$_R$ = 4.37 min, area: >98%, *m/z*: 460 [M + H]$^+$. HRMS (ESI): *m/z*: [M + H]$^+$ calcd. for C$_{26}$H$_{30}$N$_5$O$_3$ 460.2343, found 460.2337

4.8.3.18. *N*-(3-(1*H*-Imidazol-1-yl)propyl)-3-(5-(*cis*-3-isopropyl-4-oxo-3,4,4a,5,8,8a-hexahydrophthalazin-1-yl)-2-methoxyphenyl)propiolamide (**36**)

This compound was synthesized according to the general procedure using **19** (0.15 g, 0.38 mmol) and 3-(1*H*-imidazol-1-yl)propan-1-amine as the corresponding amine. Column chromatography was performed using EtOAc/n-hept (gradient: 10-100%)to obtain a white solid (101 mg, 56%). ^{1}H NMR (500 MHz, CDCl$_3$): δ 7.86 (d, *J* = 2.4 Hz, 1H), 7.82 (dd, *J* = 8.8, 2.3 Hz, 1H), 7.45 (s, 1H), 7.08 (t, *J* = 6.2 Hz, 1H), 7.01 (s, 1H), 6.93 – 6.84 (m, 2H), 5.75 – 5.54 (m, 2H), 4.96 (p, *J* = 6.7 Hz, 1H), 3.97 (t, *J* = 6.9 Hz, 2H), 3.85 (s, 3H), 3.27 (q, *J* = 6.5 Hz, 2H), 3.23 – 3.14 (m, 1H), 2.97 – 2.86 (m, 1H), 2.65 (t, *J* = 6.0 Hz, 1H), 2.19 – 2.03 (m, 2H), 2.03 – 1.97 (m, 2H), 1.96 – 1.86 (m, 1H), 1.24 (d, *J* = 6.6 Hz, 3H), 1.17 – 1.09 (m, 3H). ^{13}C NMR (126 MHz, CDCl$_3$): δ 166.4, 161.7, 153.9, 152.4, 137.2, 132.0, 129.4, 129.3, 128.0, 126.0, 123.8, 118.9, 111.0, 109.7, 87.1, 81.3, 56.1, 46.7, 44.4, 36.9, 34.7, 30.9, 30.9, 23.0, 22.3, 20.6, 20.2. LC-MS (ESI): t$_R$ = 3.59 min, area: >98%, *m/z*: 474 [M + H]$^+$. HRMS (ESI): *m/z*: [M + H]$^+$ calcd. for C$_{27}$H$_{32}$N$_5$O$_3$ 474.2500, found 474.2496

4.8.3.19. *N*-Benzyl-3-(5-(*cis*-3-isopropyl-4-oxo-3,4,4a,5,8,8a-hexahydrophthalazin-1-yl)-2-methoxyphenyl)propiolamide (**37**)

This compound was synthesized according to the general procedure using **19** (0.10 g, 0.25 mmol) and phenylmethanamine as the corresponding amine. Column chromatography was performed using EtOAc/n-hept (gradient: 0-50%) to obtain a white solid (80 mg, 69%). ^{1}H NMR (500 MHz, CDCl$_3$): δ 7.94 (d, *J* = 2.2 Hz, 1H), 7.90 (dd, *J* = 8.8, 2.3 Hz, 1H), 7.41 – 7.29 (m, 5H), 6.94 (d, *J* = 8.8 Hz, 1H), 6.41 (t, *J* = 5.8 Hz, 1H), 5.83 – 5.63 (m, 2H), 5.04 (hept, *J* = 6.7 Hz, 1H), 4.56 (d, *J* = 5.7 Hz, 2H), 3.92 (s, 3H), 3.26 (dt, *J* = 11.5, 5.7 Hz, 1H), 3.06 – 2.95 (m, 1H), 2.72 (t, *J* = 5.9 Hz, 1H), 2.26 – 2.10 (m, 2H), 2.07 – 1.95 (m, 1H), 1.33 (d, *J* = 6.5 Hz, 3H), 1.20 (d, *J* = 6.7 Hz, 3H). ^{13}C NMR (126 MHz, CDCl$_3$): δ 166.4, 161.8, 153.3, 152.4, 137.3, 132.0, 129.2, 128.8, 128.1, 127.9, 127.8, 126.0, 123.8, 110.9, 109.7, 87.0, 81.4, 56.1, 46.7, 44.0, 34.7, 31.0, 23.0, 22.3, 20.6, 20.2. LC-MS (ESI): t$_R$ = 4.93 min, area: >98%, *m/z*: 456 [M + H]$^+$. HRMS (ESI): *m/z*: [M + H]$^+$ calcd. for C$_{28}$H$_{30}$N$_3$O$_3$ 456.2282, found 456.2275

4.8.3.20. 3-(5-(*cis*-3-Isopropyl-4-oxo-3,4,4a,5,8,8a-hexahydrophthalazin-1-yl)-2-methoxyphenyl)-*N*-(pyridin-3-ylmethyl)propiolamide (**38**)

This compound was synthesized according to the general procedure using **19** (0.20 g, 0.51 mmol) and pyridin-3-ylmethanamine.HCl as the corresponding amine. Column chromatography was performed using EtOAc/n-hept (gradient: 0-50%) to obtain a white solid (142 mg, 61%). ^{1}H NMR (500 MHz, DMSO-*d6*): δ 9.37 (t, *J* = 6.1 Hz, 1H), 8.52 (d, *J* = 2.2 Hz, 1H), 8.48 (dd, *J* = 4.7, 1.7 Hz, 1H), 8.02 – 7.92 (m, 2H), 7.70 (dt, *J* = 7.8, 2.0 Hz, 1H), 7.43 – 7.33 (m, 1H), 7.20 (d, *J* = 8.8 Hz, 1H), 5.75 – 5.56 (m, 2H), 4.87 (hept, *J* = 6.6 Hz, 1H), 4.37 (d, *J* = 6.0 Hz, 2H), 3.90 (s, 3H), 3.44 (dt, *J* = 11.5, 5.7 Hz, 1H), 2.80 (t, *J* = 6.1 Hz, 1H), 2.78 – 2.68 (m, 1H), 2.21 – 2.05 (m, 2H), 1.86 – 1.72 (m, 1H), 1.23 (d, *J* = 6.7 Hz, 3H), 1.13 (d, *J* = 6.8 Hz, 3H). ^{13}C NMR (126 MHz, DMSO-*d6*): δ 166.5, 161.8, 153.1, 152.9, 149.4, 148.8, 135.8, 134.6, 131.6, 130.1, 127.9, 126.3, 124.4, 124.0, 112.3, 109.4, 87.9, 80.8, 56.6, 46.2, 40.6, 34.2, 30.3, 22.8, 22.3, 20.9, 20.5. LC-MS (ESI): t_R = 3.72 min, area: >98%, *m/z*: 457 [M + H]$^+$. HRMS (ESI): *m/z*: [M + H]$^+$ calcd. for C$_{27}$H$_{29}$N$_4$O$_3$ 457.2234, found 457.2220

4.8.3.21. 3-(5-(*cis*-3-Isopropyl-4-oxo-3,4,4a,5,8,8a-hexahydrophthalazin-1-yl)-2-methoxyphenyl)-*N*-(pyridin-4-ylmethyl)propiolamide (**39**)

This compound was synthesized according to the general procedure using **19** (0.10 g, 0.25 mmol) and pyridin-4-ylmethanamine as the corresponding amine. Column chromatography was performed using EtOAc/n-hept (gradient: 0-50%) to obtain a white solid (67 mg, 58%). ^{1}H NMR (500 MHz, CDCl$_3$): δ 8.62 (s, 2H), 7.95 (d, *J* = 2.3 Hz, 1H), 7.91 (dd, *J* = 8.8, 2.4 Hz, 1H), 7.29 (s, 2H), 6.98 – 6.90 (m, 1H), 6.67 (t, *J* = 6.3 Hz, 1H), 5.83 – 5.64 (m, 2H), 5.05 (hept, *J* = 6.7 Hz, 1H), 4.58 (d, *J* = 6.1 Hz, 2H), 3.94 (s, 3H), 3.26 (dq, *J* = 11.9, 5.9 Hz, 1H), 3.06 – 2.96 (m, 1H), 2.74 (t, *J* = 6.0 Hz, 1H), 2.26 – 2.10 (m, 2H), 2.06 – 1.99 (m, 1H), 1.33 (d, *J* = 6.6 Hz, 3H), 1.21 (d, *J* = 6.6 Hz, 3H). ^{13}C NMR (126 MHz, CDCl$_3$): δ 166.4, 161.8, 153.6, 152.3, 149.9, 146.6, 132.1, 129.7, 129.5, 128.0, 126.0, 123.8, 111.0, 109.4, 86.6, 82.2, 56.1, 46.7, 42.6, 34.7, 31.0, 23.0, 22.3, 20.6, 20.2. LC-MS (ESI): t_R = 3.64 min, area: >98%, *m/z*: 457 [M + H]$^+$. HRMS (ESI): *m/z*: [M + H]$^+$ calcd. for C$_{27}$H$_{29}$N$_4$O$_3$ 457.2234, found 457.2220

4.8.3.22. 3-(5-(*cis*-3-Isopropyl-4-oxo-3,4,4a,5,8,8a-hexahydrophthalazin-1-yl)-2-methoxyphenyl)-*N*-(3-methoxyphenyl)propiolamide (**40**)

This compound was synthesized according to the general procedure using **19** (0.20 g, 0.51 mmol) and 3-methoxyaniline as the corresponding amine. Column chromatography was performed using EtOAc/n-hept (gradient: 0-50%) to obtain a white solid (98 mg, 41%). ^{1}H NMR (500 MHz, CDCl$_3$): δ 7.97 (d, *J* = 2.6 Hz, 2H), 7.92 (dd, *J* = 8.8, 2.3 Hz, 1H), 7.33 (t, *J* = 2.3 Hz, 1H), 7.24 (t, *J* = 8.1 Hz, 1H), 7.09 (dd, *J* = 7.9, 1.9 Hz, 1H), 6.97 (d, *J* = 8.9 Hz, 1H), 6.71 (dd, *J* = 8.2, 2.4 Hz, 1H), 5.85 – 5.63 (m, 2H), 5.06 (hept, *J* = 6.6 Hz, 1H), 3.96 (s, 3H), 3.82 (s, 3H), 3.28 (dt, *J* = 11.6, 5.7 Hz, 1H), 3.07 – 2.97 (m, 1H), 2.74 (t, *J* = 6.0 Hz, 1H), 2.27 – 2.12 (m, 2H), 2.05 – 1.96 (m, 1H), 1.34 (d, *J* = 6.6 Hz, 3H), 1.22 (d, *J* = 6.7 Hz, 3H). ^{13}C NMR (126 MHz, CDCl$_3$): δ 166.4, 161.9, 160.1, 152.4, 151.0, 138.6, 132.1, 129.8, 129.5, 128.0, 126.0, 123.8, 112.1, 111.0, 110.6, 109.5, 105.8, 87.7, 82.0, 56.1, 55.4, 46.8, 34.7, 31.0, 23.0, 22.3, 20.6, 20.2. LC-MS (ESI): t_R = 5.10 min, area: >98%, *m/z*: 472 [M + H]$^+$. HRMS (ESI): *m/z*: [M + H]$^+$ calcd. for C$_{28}$H$_{30}$N$_3$O$_4$ 472.2231, found 472.2243

4.8.3.23. *N*-(2-Fluorophenethyl)-3-(5-(*cis*-3-isopropyl-4-oxo-3,4,4a,5,8,8a-hexahydrophthalazin-1-yl)-2-methoxyphenyl)propiolamide (**41**)

This compound was synthesized according to the general procedure using **19** (0.20 g, 0.51 mmol) and 2-(2-fluorophenyl)ethanamine as the corresponding amine. Column chromatography was performed using EtOAc/n-hept (gradient: 0-50%) to obtain a white solid (110 mg, 45%). ^{1}H NMR (500 MHz, CDCl$_3$): δ 8.00 – 7.84 (m, 2H), 7.27 – 7.16 (m, 2H), 7.14 – 6.99 (m, 2H), 6.95 (dd, *J* = 13.4, 8.9 Hz, 1H), 6.31 (q, *J* = 7.0 Hz, 1H), 5.85 – 5.61 (m, 2H), 5.04 (p, *J* = 6.7 Hz, 1H), 3.91 (s, 3H), 3.62 (q, *J* = 6.8 Hz, 2H), 3.27 (tt, *J* = 11.5, 5.7 Hz, 1H), 3.07 – 2.87 (m, 3H), 2.73 (dt, *J* = 11.9, 5.9 Hz, 1H), 2.28 – 2.09 (m, 2H), 2.04 – 1.94 (m, 1H), 1.32 (dd, *J* = 6.6, 3.4 Hz, 3H), 1.20 (dd, *J* = 6.9, 4.2 Hz, 3H). ^{13}C NMR (126 MHz, CDCl$_3$): δ 166.4, 161.8, 153.5, 152.4, 132.0, 131.1, 129.2, 128.4, 127.9, 126.0, 125.4, 124.3, 123.8, 115.5, 115.3, 110.9, 109.8, 87.2, 81.0, 56.1, 46.7, 39.9, 34.7, 30.9, 29.0, 23.0, 22.3, 20.6, 20.2. LC-MS (ESI): t_R = 5.07 min, area: >98%, *m/z*: 488 [M + H]$^+$. HRMS (ESI): *m/z*: [M + H]$^+$ calcd. for C$_{29}$H$_{31}$FN$_3$O$_3$ 488.2344, found 488.2341

5. Author contributions

E.d.H., G.J.S. and I.J.P.d.E. were involved in compound design, synthesis and analysis. A.K.S. and D.G.B. were involved in protein production, crystallization, data collection and refinement for structural studies. E.d.H., A.K.S. and D.G.B. were involved in crystal structure analysis. E.d.H. and A.J.K. were involved in virtual screening and docking. T.v.d.M., P.S., and M.S. were involved in the biochemical assays. G.C. and L.M. were involved in the phenotypic cellular assays. P.B. and A.R.B. were involved in SPR analysis. M.O., NS and DB were involved in the target validation experiments. L.M., G.J.S., I.J.P.d.E., D.G.B. and R.L. supervised the experiments and conceived the project. E.d.H., A.K.S. G.J.S., I.J.P.d.E., and R.L. integrated all data and wrote the manuscript.

Development of alkynamide phthalazinones as potential new class selective TbrPDEB1 inhibitors.

6. References

1. R. Brun, J. Blum, F. Chappuis, *et al.*, Human african trypanosomiasis, The Lancet, 375 (2010) 148-159.
2. P. Büscher, G. Cecchi, V. Jamonneau *et al.*, Human African trypanosomiasis, The Lancet, 390 (2017) 2397-2409.
3. P. Babokhov, A.O. Sanyaolu, W.A. Oyibo, *et al.*, A current analysis of chemotherapy strategies for the treatment of human African trypanosomiasis, Pathogens and Global Health, 107 (2013) 242-252.
4. P.G.E. Kennedy, Human African trypanosomiasis of the CNS: current issues and challenges, Journal of Clinical Investigation, 113 (2004) 496-504.
5. C.H. Baker, S.C. Welburn, The Long Wait for a New Drug for Human African Trypanosomiasis, Trends Parasitol, (2018).
6. B.M. Anene, D.N. Onah, Y. Nawa, Drug resistance in pathogenic African trypanosomes: what hopes for the future?, Veterinary Parasitology, 96 (2001) 83-100.
7. N. Baker, H.P. de Koning, P. Maser, *et al.*, Drug resistance in African trypanosomiasis: the melarsoprol and pentamidine story, Trends Parasitol, 29 (2013) 110-118.
8. H.P. de Koning, Drug resistance in protozoan parasites, Emerging Topics in Life Sciences, 1 (2017) 627.
9. M.K. Gould, A. Schnaufer, Independence from kinetoplast DNA maintenance and expression is associated with multidrug resistance in trypanosoma brucei in vitro, antimicrob Agents Chemother, 58 (2014) 2925-2928.
10. A.Y. Sokolova, S. Wyllie, S. Patterson, *et al.*, Cross-resistance to nitro drugs and implications for treatment of human African trypanosomiasis, Antimicrobial agents and chemotherapy, 54 (2010) 2893-2900.
11. WHO, Trypanosomiasis, human African (sleeping sickness), https://www.who.int/news-room/fact-sheets/detail/trypanosomiasis-human-african-(sleeping-sickness); 2018, Accessed on 03-02-2018
12. P.W. Bowyer, E.W. Tate, R.J. Leatherbarrow, *et al.*, N-myristoyltransferase: a prospective drug target for protozoan parasites, ChemMedChem, 3 (2008) 402-408.
13. A.J. Caceres, P.A. Michels, V. Hannaert, Genetic validation of aldolase and glyceraldehyde-3-phosphate dehydrogenase as drug targets in Trypanosoma brucei, Mol Biochem Parasitol, 169 (2010) 50-54.
14. C. Merritt, L.E. Silva, A.L. Tanner, *et al.*, Kinases as Druggable Targets in Trypanosomatid Protozoan Parasites, Chemical Reviews, 114 (2014) 11280-11304.
15. J.C. Pizarro, T. Hills, G. Senisterra, *et al.*, Exploring the Trypanosoma brucei Hsp83 potential as a target for structure guided drug design, PLoS neglected tropical diseases, 7 (2013) e2492.
16. M. Oberholzer, G. Marti, M. Baresic, *et al.*, The Trypanosoma brucei cAMP phosphodiesterases TbrPDEB1 and TbrPDEB2: flagellar enzymes that are essential for parasite virulence, The FASEB Journal, 21 (2007) 720-731.
17. N.D. Bland, C. Wang, C. Tallman, *et al.*, Pharmacological validation of Trypanosoma brucei phosphodiesterases B1 and B2 as druggable targets for African sleeping sickness, J Med Chem, 54 (2011) 8188-8194.
18. H.P. de Koning, M.K. Gould, G.J. Sterk, *et al.*, Pharmacological validation of Trypanosoma brucei phosphodiesterases as novel drug targets, Journal of Infectious Diseases, 206 (2012) 229-237.
19. K.M. Orrling, C. Jansen, X.L. Vu, *et al.*, Catechol pyrazolinones as trypanocidals: fragment-based design, synthesis, and pharmacological evaluation of nanomolar inhibitors of trypanosomal phosphodiesterase B1, Journal of Medicinal Chemistry, 55 (2012) 8745-8756.
20. V. Boswell-Smith, D. Spina, C.P. Page, Phosphodiesterase inhibitors, British Journal of Pharmacology, 147 (2006) S252-S257.
21. P.M. Seldon, P.J. Barnes, K. Meja, *et al.*, Suppression of lipopolysaccharide-induced tumor necrosis factor-alpha generation from human peripheral blood monocytes by inhibitors of phosphodiesterase 4: interaction with stimulants of adenylyl cyclase., Molecular Pharmacology, 48 (1995) 747-757.
22. J.E. Souness, S. Rao, Proposal for Pharmacologically Distinct Conformers of PDE4 Cyclic AMP Phosphodiesterases, Cellular Signalling, 9 (1997) 227-236.
23. J. Veerman, T. van den Bergh, K.M. Orrling, *et al.*, Synthesis and evaluation of analogs of the phenylpyridazinone NPD-001 as potent trypanosomal TbrPDEB1 phosphodiesterase inhibitors and in vitro trypanocidals, Bioorganic & Medicinal Chemistry, 24 (2016) 1573-1581.
24. E. Amata, N.D. Bland, C.T. Hoyt, *et al.*, Repurposing human PDE4 inhibitors for neglected tropical diseases: Design, synthesis and evaluation of cilomilast analogues as Trypanosoma brucei PDEB1 inhibitors, Bioorganic & Medicinal Chemistry Letters, 24 (2014) 4084-4089.
25. A.R. Blaazer, A.K. Singh, E. de Heuvel, *et al.*, Targeting a subpocket in Trypanosoma brucei phosphodiesterase B1 (TbrPDEB1) enables the structure-based discovery of selective inhibitors with trypanocidal activity, Journal of Medicinal Chemistry, 61 (2018) 3870-3888.

26. C. Jansen, H. Wang, A.J. Kooistra, *et al.*, Discovery of NovelTrypanosoma bruceiPhosphodiesterase B1 Inhibitors by Virtual Screening against the Unliganded TbrPDEB1 Crystal Structure, Journal of Medicinal Chemistry, 56 (2013) 2087-2096.

27. E. De Heuvel, A.K. Singh, E.E. Edink, *et al.*, Alkynamide phthalazinones as a new class of TbrPDEB1 inhibitors, part 1, Biorg. Med. Chem., In press (2019).

28. O. Korb, T. Stützle, T.E. Exner, Empirical Scoring Functions for Advanced Protein−Ligand Docking with PLANTS, Journal of Chemical Information and Modeling, 49 (2009) 84-96.

29. G. Marcou, D. Rognan, Optimizing fragment and scaffold docking by use of molecular interaction fingerprints, Journal of chemical information and modeling, 47 (2007) 195-207.

30. A.J. Kooistra, H.F. Vischer, D. McNaught-Flores, *et al.*, Function-specific virtual screening for GPCR ligands using a combined scoring method, Scientific Reports, 6 (2016) 28288.

31. O. Ken-ichi, S. Taichi, Z.C. Shan, *et al.*, An Efficient Synthesis of β-Aroylacrylic Acid Ethyl Ester by the Friedel–Crafts Reaction in the Presence of Diethyl Sulfate, Chemistry Letters, 35 (2006) 22-23.

32. A.C. Huitric, J.B. Carr, W.F. Trager, *et al.*, Configurational and conformational analysis: Axial-axial and axial-equatorial coupling constants in six-membered ring compounds, Tetrahedron, 19 (1963) 2145-2151.

33. M. Oberholzer, E.A. Saada, K.L. Hill, Cyclic AMP Regulates Social Behavior in African Trypanosomes, mBio, 6 (2015).

34. C. Jansen, A.J. Kooistra, G.K. Kanev, *et al.*, PDEStrIAn: A Phosphodiesterase Structure and Ligand Interaction Annotated Database As a Tool for Structure-Based Drug Design, Journal of Medicinal Chemistry, 59 (2016) 7029-7065.

35. G. Winter, C.M.C. Lobley, S.M. Prince, Decision making in xia2, Acta Crystallographica Section D, 69 (2013) 1260-1273.

36. C. Vonrhein, C. Flensburg, P. Keller, *et al.*, Data processing and analysis with the autoPROC toolbox, Acta Crystallographica Section D, 67 (2011) 293-302.

37. W. Kabsch, Integration, scaling, space-group assignment and post-refinement, Acta Crystallographica Section D, 66 (2010) 133-144.

38. P.R. Evans, G.N. Murshudov, How good are my data and what is the resolution?, Acta Crystallographica Section D, 69 (2013) 1204-1214.

39. T.G.G. Battye, L. Kontogiannis, O. Johnson, *et al.*, iMOSFLM: a new graphical interface for diffraction-image processing with MOSFLM, Acta Crystallographica Section D, 67 (2011) 271-281.

40. M.D. Winn, C.C. Ballard, K.D. Cowtan, *et al.*, Overview of the CCP4 suite and current developments, Acta Crystallographica Section D, 67 (2011) 235-242.

41. A.J. McCoy, R.W. Grosse-Kunstleve, P.D. Adams, *et al.*, Phaser crystallographic software, Journal of Applied Crystallography, 40 (2007) 658-674.

42. P. Emsley, B. Lohkamp, W.G. Scott, *et al.*, Features and development of Coot, Acta Crystallographica Section D, 66 (2010) 486-501.

43. G.N. Murshudov, P. Skubak, A.A. Lebedev, *et al.*, REFMAC5 for the refinement of macromolecular crystal structures, Acta Crystallographica Section D, 67 (2011) 355-367.

44. The PyMOL Molecular Graphics System, Version 1.7, Schrödinger, LLC.

45. E. Wirtz, S. Leal, C. Ochatt, *et al.*, A tightly regulated inducible expression system for conditional gene knock-outs and dominant-negative genetics in Trypanosoma brucei, Molecular and Biochemical Parasitology, 99 (1999) 89-101.

46. M. Oberholzer, M.A. Lopez, K.S. Ralston, *et al.*, Chapter 2 - Approaches for Functional Analysis of Flagellar Proteins in African Trypanosomes, in: S.M. King, G.J. Pazour (Eds.) Methods in Cell Biology, Academic Press2009, pp. 21-57.

47. V.O. Nikolaev, M. Bünemann, L. Hein, *et al.*, Novel Single Chain cAMP Sensors for Receptor-induced Signal Propagation, Journal of Biological Chemistry, 279 (2004) 37215-37218.

48. M. Oberholzer, G. Langousis, H.T. Nguyen, *et al.*, Independent analysis of the flagellum surface and matrix proteomes provides insight into flagellum signaling in mammalian-infectious Trypanosoma brucei, Molecular & cellular proteomics : MCP, 10 (2011) M111.010538-M010111.010538.

49. K. Schlaeppi, J. Deflorin, T. Seebeck, The major component of the paraflagellar rod of Trypanosoma brucei is a helical protein that is encoded by two identical, tandemly linked genes, The Journal of cell biology, 109 (1989) 1695-1709.
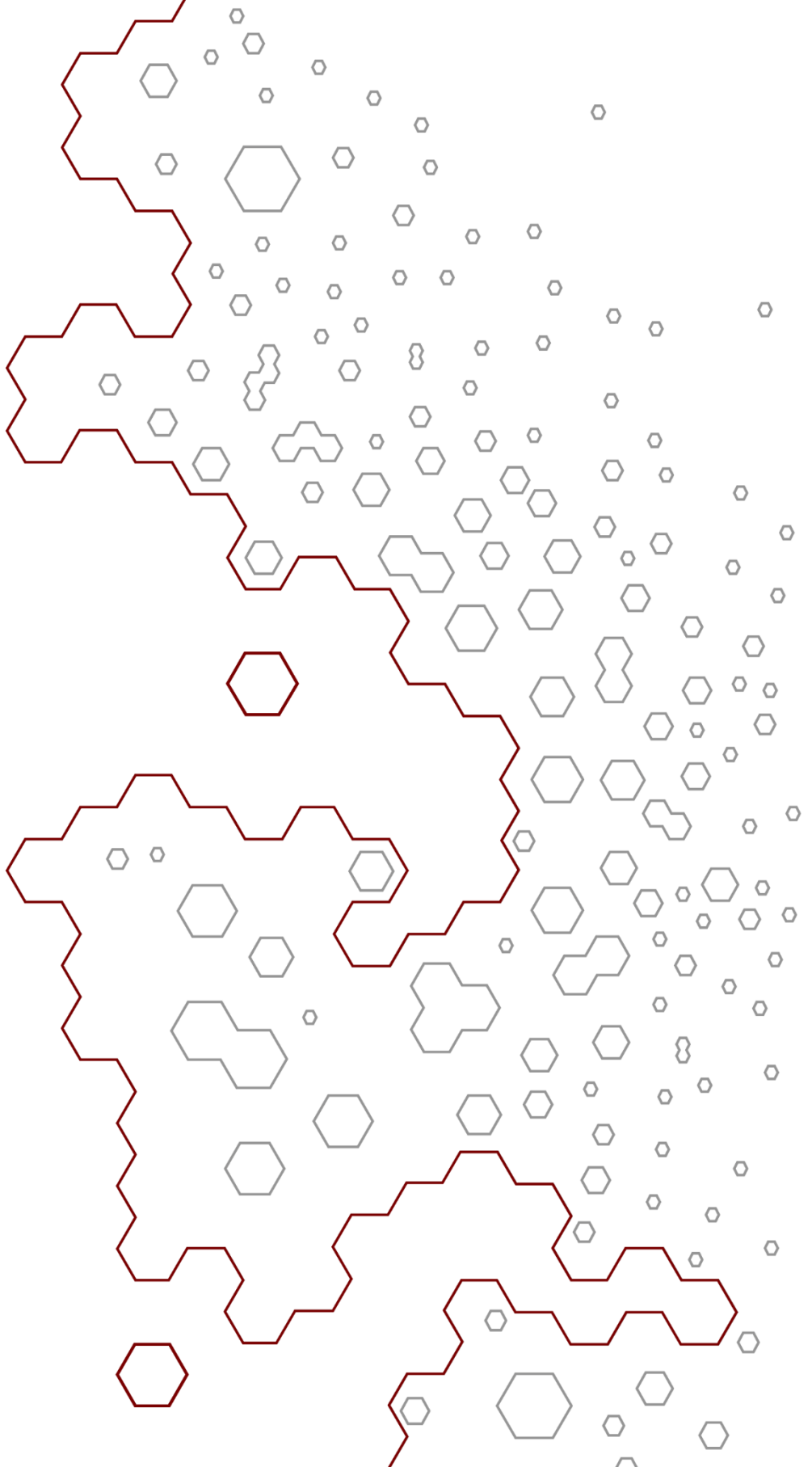
Chapter 6

Anti-parasitic activity of alkynamides and close analogues versus *Trypanosoma brucei*, *Trypanosoma cruzi*, *Leishmania infantum* and *Plasmodium falsiparum*

Erik de Heuvel, Geert Jan Sterk, Guy Caljon, Louis Maes, Iwan de Esch, Rob Leurs.

Abstract

Over the last decades the WHO has classified 19 diseases as neglected tropical diseases to raise awareness and shift the focus of drug development projects in order to boost the health of poorer communities. This approach has led to an increase in knowledge about these disease burdens and a large reduction in affected population. On the list of neglected tropical diseases are three diseases (human African trypanosomiasis, Chagas disease and leishmaniasis) which are caused by protozoan parasites. Recent development in drug discovery against human African trypanosomiasis led to the discovery of TbrPDEB1 inhibitors with good cellular activity. The large structural similarities between the parasite PDEs makes them interesting targets for target repurposing. An extended set of phenotypic active alkynamides and some close analogues was tested against four other protozoan parasites including *Trypanosoma brucei*, *Trypanosoma cruzi*, *Leishmania infantum* and *Plasmodium falsiparum*, the causative agents of human African trypanosomiasis, Chagas disease, leishmaniasis and malaria, respectively. Although the results obtained for *T. brucei* were not directly transferable to the other parasites, several interesting hits were identified for each individual parasite for further research.

6

1. Introduction

In 2003, the WHO shifted its focus to control the major killer diseases, e.g. HIV/AIDS, tuberculosis, and malaria towards the so-called Neglected Tropical diseases (NTDs) in an intensified effort to increase the health of poorer communities.[2] Nineteen diseases were classified as NTDs, see Box 1.[1, 2] These diseases are often found in resource poor communities who live in remote areas without direct access to health care.[2] Most of the NTD's are ancient diseases that have burdened the population for centuries, but are less visible in society due to several factors. Fear and stigma on community level can cause sufferers to conceal their condition, resulting in an inadequate documentation and registration of the disease occurrence. As a result, the impact of the disease is often unknown and is rarely given a high priority level on national level. The diseases are also often 'neglected' on international level because the diseases are mostly bound to geographical or environmental conditions and thereby not a direct threat for industrialized countries. These diseases are often given a low priority on the agenda of development agencies.[1] In collaboration with global partners the WHO was able to scale-up the screening and control programs and improve the access to medicine.[1]

Several of these NTDs can be clustered based on their similarity in causative agent, e.g. bacteria, trematode worms and protozoan parasites. Human African trypanosomiasis, Chagas disease and leishmaniasis form one of these clusters and are caused by protozoan parasites (*Trypanosoma brucei*, *Trypanosoma cruzi* and *Leishmania infantum* respectively). As described in the previous chapters, the *Trypanosoma brucei* parasite can be effectively killed by simultaneous inhibition of the phosphodiesterases TbrPDEB1 and TbrPDEB2 isoforms using decorated phthalazinone-based alkynamides. The success of this research and the similarity between the causative agents of Chagas disease and leishmaniasis provided the basis to extend the scope of these inhibitors towards *Trypanosoma cruzi* and *Leishmania infantum*. Moreover, as the causative agent of malaria is also a protozoan parasite (*Plasmodium spp*), *Plasmodium falicparum* was included in this extended scope as a first preliminary screening. The similarity between *Plasmodium* and *Trypanosoma* parasites have been of interest to accelerate drug development against both species.[3-5] Strategies to accelerate the development

include the repurposing of known FDA approved drugs against *Plasmodium falciparum* or the use of target similarity searches to find validated targets efficiently.[4-7]

Box 1: Neglected tropical diseases[1]

1. **Buruli ulcer** (Worldwide)
 - Bacterial infection
 - Rifampicin, clarithromycin
2. **Chagas disease** (Latin America)
 - Protozoan parasite infection
 - Benznidazole, nifurtimox
3. **Cysticercosis** (Asia, Africa, L.-America)
 - Intestinal tapeworm infection
 - Praziquantel
4. **Dengue** (Asia, Latin-America)
 - Mosquito-borne viral infection
 - No specific treatment
5. **Dracunculiasis** (Africa)
 - Guinea-worm infection
 - No treatment available
6. **Echinococcosis** (Asia, Europe, America)
 - Tapeworm infection
 - Surgery + albendazole
7. **Helminthiases** (Worldwide)
 - Round-, hook- or whipworm infection
 - Albendazole, mebendazole
8. **Leishmaniasis** (Asia, Africa, L.-America)
 - Protozoan parasite infection
 - Expensive medicines available (See 1.2)
9. **Leprosy** (Worldwide)
 - Bacterial infection
 - Rifampicin + clofazimine
10. **Lymphatic filariasis** (Worldwide)
 - Nematode infection
 - Albendazole, ivermectin, diethylcarbamazine citrate

11. **Mycetoma** (Worldwide)
 - Bacterial/Fungal infection
 - Antibacterial/Antifungal
12. **Onchocerciasis** (Africa, L.-America)
 - Filarial worm infection
 - Ivermectin
13. **Rabies** (Asia, Africa)
 - Viral zoonotic disease
 - Immunoglobulin
14. **Schistosomiasis** (Africa)
 - Trematode worm infection
 - Praziquantel
15. **Snakebite envenoming** (Worldwide)
 - Poisoning
 - Antivenom
16. **Trachoma** (Worldwide)
 - Bacterial infection
 - Azithromycin or surgical treatment
17. **Trematodiasis** (Africa)
 - Trematode worm infection
 - Triclabendazole, praziquantel
18. **Trypanosomiasis** (Africa)
 - Protozoan parasite infection
 - Multiple treatments available
19. **Yaws** (Worldwide)
 - Bacterial infection
 - Azithromycin, benzathine penicillin

1.1. Chagas disease

One of the diseases having large contribution to socio-economic problems in Latin-America is Chagas disease, caused by the protozoan parasite *Trypanosoma cruzi*.[8] The disease can be transmitted to human and over 150 different (domestic) animals via a bite of bloodsucking bugs from the Triatominae subfamily.[8] Although a large number of Triatominae bugs have been reported, *Triatoma infestans*, *Rhodnius prolixus* and *Triatoma dimidiate* have been by far the most important vectors for transmission.[8] However, non-vectorial mechanisms such as congenital transmission, sexual transmission and blood transfusion are also known.[9] It is estimated that 6 to 7 million people are infected with *T. cruzi* worldwide, with the highest occurrence in Southern America, and causing about 10000 deaths per year.[10, 11] The combination of global migration and the non-vectorial transmission has led to the spread of the disease outside of its biological boundaries.[11]

The clinical manifestation of Chagas disease consists of the acute phase and the chronic phase.[11] The acute phase can occur at any age and is often asymptomatic. Observed symptoms of the acute phase include fever, inflammation of the inoculation site and in case of a more severe acute phase myocarditis and meningoencephalitis.[11] Following the acute phase, which lasts about 2 months, the immune response of the host is not sufficient to clear the parasite, causing an immunological balance.[8, 12] The patient shows no visual signs of infection during this chronic phase, but most patients develop slow progressing cardiomyopathy, gastrointestinal or neurological disabilities.[8]

Only two drugs are currently on the market as first-line treatment, which are the nitroaromatic compounds benznidazole (**1**, Figure 1) and nifurtimox (**2**).[13-15] Both drugs require prolonged dosing regimen and have served as treatment against Chagas disease for almost 50 years, but the safety and efficacy profiles are far from ideal.[11, 16] Some of the side effects (e.g. digestive intolerance) result in early termination of the treatment, which is one of the factors for the increasing drug resistance.[17] Furthermore, the effectiveness of the drugs seems to decrease over time after the first infection, making early diagnosis and start of treatment essential.[11]

Despite the need for new efficacious chemotherapies, only a few new promising compounds are in development. A good overview of current drug development against Chagas disease has been provided by Sales Jr *et al*.[17]

Benznidazole (**1**)

Nifurtimox (**2**)

Figure 1: Structures of current marketed drugs against *T. cruzi* infections.

1.2. Leishmaniasis

Leishmaniasis is the second disease listed that is caused by protozoan parasites. *Leishmania Infantum* and *L. donovani* are the causative agent of visceral leishmaniasis, while all other *Leishmania* species cause cutaneous leishmaniasis. The disease is wide spread on all continents except Oceania and the transmission of the parasites to humans is facilitated by a bite of phlebotomine sand flies.[18-20] Leishmaniasis is reported by the WHO as one of the seven most important tropical diseases as it represents a serious world health problem with a broad spectrum of clinical manifestations and a potential fatal outcome. The disease is spread in about 89 countries and it is estimated that between 12 and 15 million people are infected, with about 1 million new infections every year.[18, 19] It is estimated that about 350 million people are at risk of infection.[18]

Despite the large number of infected people the disease has become one of the neglected tropical diseases, mainly caused by the relatively low fatality rate.[21] The clinical manifestation of the disease varies between parasite species, region and host factors (e.g. age, nutritional state).[22] Cutaneous leishmaniasis is characterized by local increase in temperature and swelling at the site of the bite. This will develop into a vesicle which opens to form a sharp edged ulcer that can last for months or even years.[20] Only extreme cases of cutaneous leishmaniasis are fatal and self-cure of the lesion is often observed, although resulting in a life-long scar.[21] Visceral leishmaniasis is manifested by lymphadenopathy, fever, night sweats, anorexia, and weight loss, which can progress rapidly in weeks or months. Furthermore, infected children typically present chronic diarrhea and growth retardation.[20] If the disease progresses without treatment it can lead to multisystem failure, superimposed infections and eventually death.[20]

The current standard treatment for leishmaniasis consists of a long regime of multiple injections with pentavalent antimonials meglumine antimoniate **3** (Figure 2) and sodium stibogluconate **4**.[22] However, a resistance against antimonials has arisen on the Indian subcontinent causing a 65% increase in treatment failure between 1980 and 1997.[20] Successes in drug development, including amphotericin B (**5**), miltefosine (**6**) and paromomycin (**7**), over the last decade resulted in a few new medications against leishmaniasis.[23] Due to different toxicity profiles, administration protocols, and limited availability of the drugs, first-line treatments can differ per region.[24] Despite the great efforts made the last decades, development of antileishmanials remain a challenge. Some are common challenges in drug discovery, such as lack of chemical diversity, while others are more disease specific, such as lack of validated targets.[24]

Meglumine antimoniate (**3**)   Sodium stibogluconate (**4**)   Amphotericin B (**5**)

miltefosine (**6**)   paromomycin (**7**)
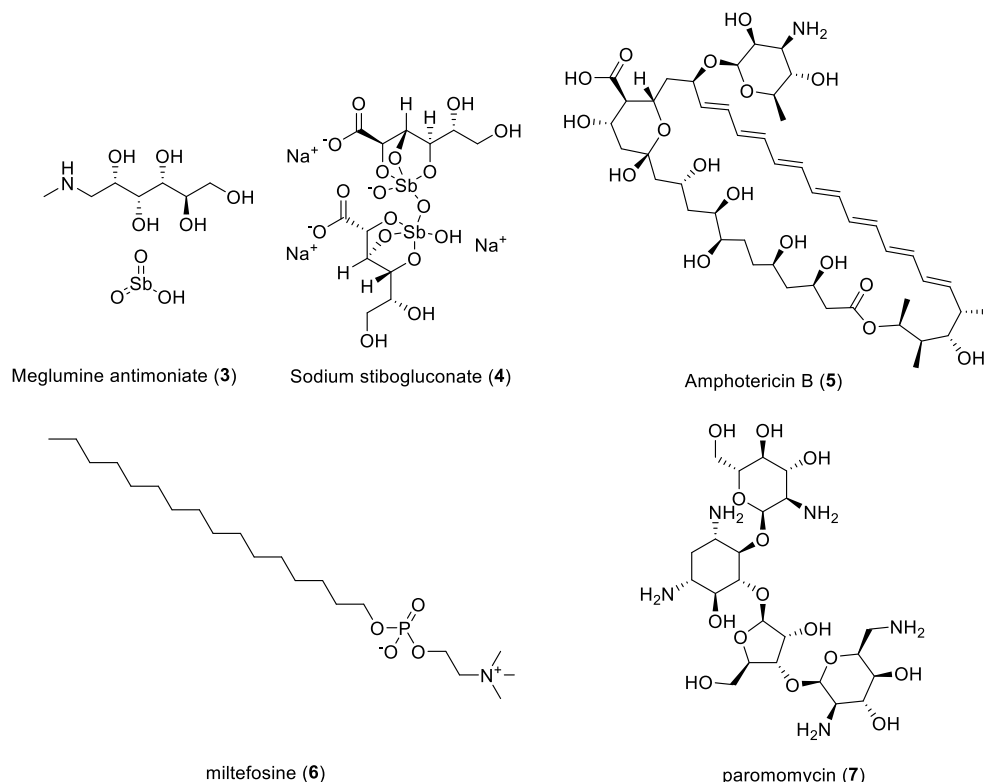
Figure 2: Structures of current marketed drugs against *L. infantum* infections.

1.3. Malaria

Another well-known protozoan parasite is the *Plasmodium falciparum*, the causative agent in 90% of the malaria cases.[5] Although malaria is not one of the 19 indicated neglected tropical diseases and has been investigated more extensively than NTDs, it remains one of the world's most important infectious diseases. With about 50% of the world population at risk of infection, the absence of an effective vaccine and increasing resistance of the parasite against current medications stresses the development for a new effective cure.[7, 25, 26] Resistance against the first effective drug against malaria, chloroquine, was reported 20 years after the discovery of the drug. The first cases of resistant strains against the current first in line treatment which are based on artemisinin were reported in 2008, 36 years after its discovery. [27, 28] The emerging drug resistance emphasizes the importance of having new drug leads in the pipeline for malaria.[7]

1.4. PDE target repurposing

The evolutionary similarity between *T. brucei*, *T. cruzi*, *L. inf.* and *P. fal.* parasites and the validated importance of phosphodiesterases in all parasites makes this enzyme an interesting candidate for target repurposing.[29-34] The crystal structures of *T. brucei*, *T. cruzi* and *L. inf.* PDEs show a high similarity between their active sites (Figure 3), all having an additional pocket (P-pocket) near the active site which is absent in hPDE4.[35] Therefore, the previously reported tetrahydrophthalazinone-based alkynamide series (**chapters 4** and **5**) which were designed to target this pocket could be a good starting point for such an endeavour.[36, 37] Although all alkynamides show some preference for the parasite PDE over its human paralogue, successful binding in the P-pocket was not observed in the crystal structures and the origin of the selectivity remains unknown.[37] Nevertheless, the alkynamide phthalazinone series showed submicromolar activity against *T. brucei* parasites via a PDE-mediated mode of action and showed low cytotoxicity human MRC-5 cells, making them interesting starting points for a broader phenotypic screening.[36, 37] Recently, the phenotypic activity against *T. cruzi* and *L. inf.* parasites have been reported by compounds with similar substructures, phenylpyrazolones, by Sijm *et al.*[14, 15, 29] increasing the potential for successful repurposing. Here, we report the synthesis and the phenotypic activity of an extended alkynamide phthalazinone series against *T. brucei*, *T. cruzi*, *L. inf.* and *P. fal.* parasites. In this extended series

the amide carbonyl is omitted or replaced by a bioisosteric oxetane. The results of this study are important for the development of new chemical entities for antiparasitic use.
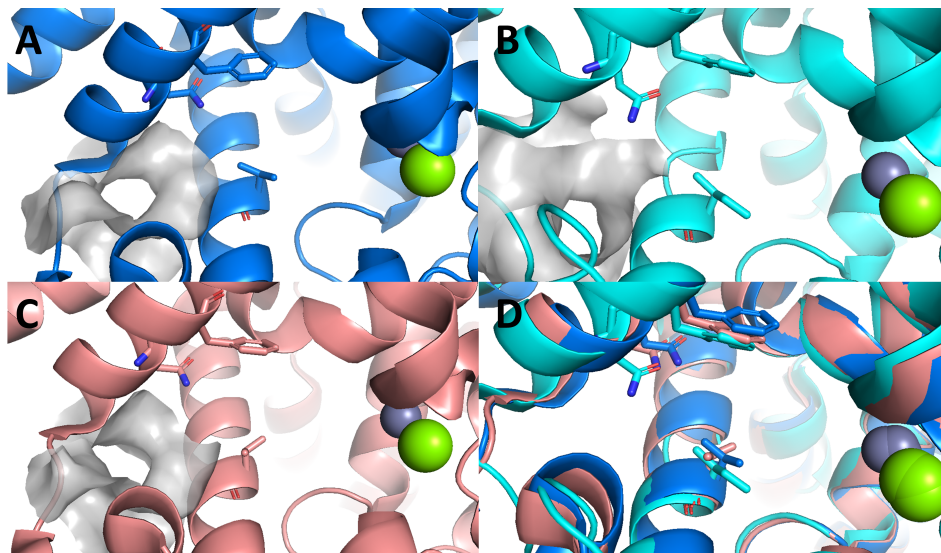
Figure 3: The highly similar active sites of TbrPDEB1 (A), TcrPDEC (B) and LmjPDEB (C). The parasitic pockets (P-pockets) in the crystal structures are indicated by the grey surface. D) An overlay of the different crystal structures.

2. Results and discussion

2.1. Chemistry

2.1.1. Alkynamides

All of the alkynamides were synthesized as reported in **Chapter 4** and **5**.[37]

2.1.2. Alkynamide isosteres

The alkynoxetanes were prepared using a comparable synthetic procedure (Scheme 1). Oxetane sulfinamide **8** was synthesized from oxetan-3-one and racemic *t*-butylsulfinamide using titanium isopropoxide. The alkyne functionality was introduced by nucleophilic addition of freshly prepared TMS-protected acetylene lithiate. TMS-protected alkynoxetane **9** was coupled to phthalazinone bromide **10**, which was synthesized as previously reported, using combined Sonogashira/Hiyama reaction conditions.[37] The sulfinamide bond was cleaved under acidic conditions to obtain primary oxetaneamine **12**, which was

subsequently used to synthesize sulfonamide **13**. Furthermore, sulfinamide **11** was alkylated using sodium hydride and an appropriate alkylbromide to obtain the sulfinamides **14a-c**, which were deprotected using methylsulfonic acid to obtain the respective alkynoxetanes in moderate yield.
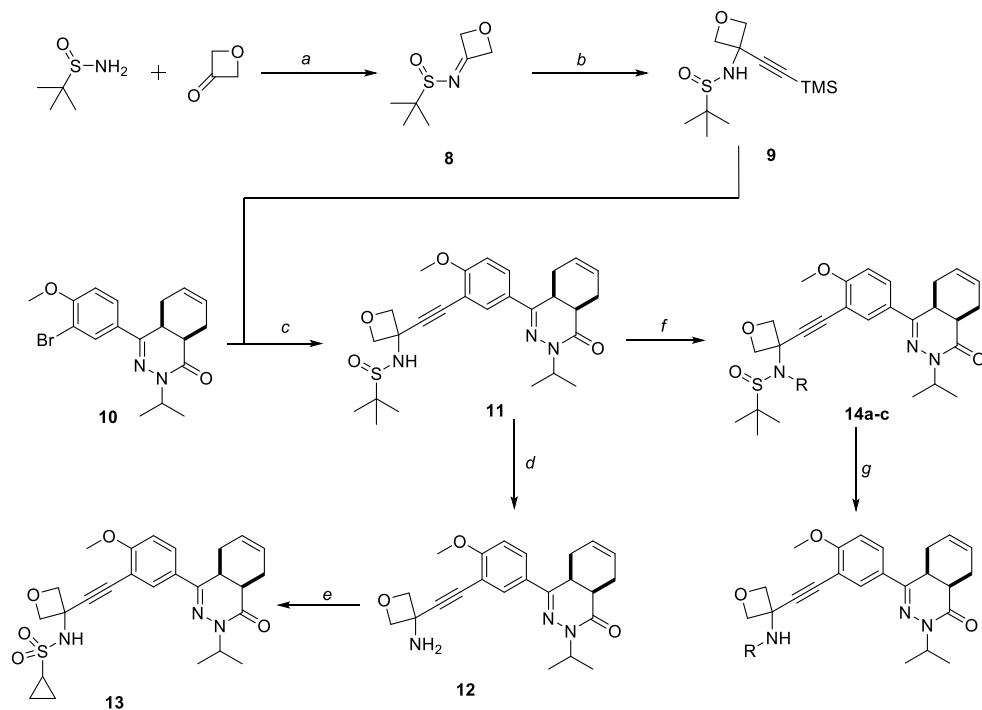
Scheme 1: Synthesis of modified alkynoxetane amines. *a*) Ti(OiPr)$_4$, DCM, reflux, 6 h, 56%; *b*) 1. TMS-acetylene, n-BuLi, THF, -78 °C, 30 min; 2. **8**, THF, -78 °C to rt, 76%; *c*) PdCl$_2$(dppf), CuI, CsF, DMF, 120 °C, 3 h, 56%; *d*) MsOH, EtOH, rt, overnight, 79%; *e*) Cyclopropanesulfonyl chloride, DCM, pyridine, rt, overnight, 69%; *f*) 1. NaH, DMF, rt, 10 min; 2. Corresponding bromide, rt, 10 h, 32-37%; *g*) MsOH, EtOH, rt, overnight, 61-76%;

Direct coupled alkyne aromatics were synthesized using a similar strategy as described above, starting from bromide **10,** in a Sonogashira reaction with TMS-acetylene (Scheme 2). The trimethylsilyl group was removed using lithium hydroxide to obtain alkyne **16** in good yield. The aromatic moieties were coupled in a second Sonogashira reaction with the corresponding bromide to obtain corresponding isosteres in moderate to good yields.

189
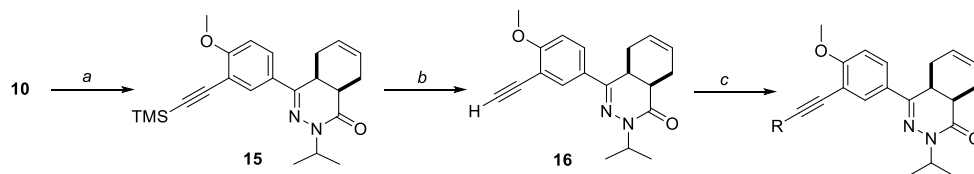
Scheme 2: Synthesis of diaryl alkynes. a) Ethynyltrimethylsilane, $PdCl_2(dppf)$, CuI, Et_3N, 80 °C, 3 h, 92%; b) KOH, MeOH, 50 °C, overnight, 95%; c) Corresponding bromide, $PdCl_2(PPh_3)_2$, CuI, Et_3N, THF, 80 °C, MW, 2 h, 20-35%;

2.2. Phenotypic screening

The antiparasitic activity of the alkyne phthalazinones was tested against *T. brucei*, *T. cruzi*, *L. infantum* and chloroquine resistant *P. falsiparum*-K1. The alkyne phthalazinones were divided into three separate classes: aliphatic alkynamides, aromatic alkynamides and alkynamide isosteres. The cellular assays were performed as reported elsewhere.[15, 29, 37, 38]

2.2.1. Aliphatic alkynamides

The previously reported set of aliphatic alkynamides (**Chapter 5**)[37] was extended with several short chained (**18**, **20**, **23** and **28**, Figure 4) and different (basic) cyclic moieties (**24**, **27**, **31** and **32**). The different tails increased the variety in size, polarity, basicity and flexibility, creating a set of compounds to probe the structure-activity relationship and the different physicochemical properties (Table 1) that might influence the P-pocket targeting.

The sixteen different aliphatic alkynamides were tested for their anti-proliferative activity against the various parasites (Table 1). Within this subclass only small differences were observed against *T. brucei* and *T. cruzi* parasites. With a few exceptions, most compounds displayed a pIC_{50} in the range of 5.0 – 5.2. For *T. brucei* the methylamine **18** and the ethylnitrile **29** showed a slightly lower inhibitory activity, while the racemic methylpyrrolidine (**24**) is the only compound with a slightly increased activity. The results for *T. cruzi* are very comparable to *T. brucei* with primary amide **17** and nitrile **29** as weakest inhibitors and again pyrrolidine **24** as most potent compound. However, compound **24** showed some increased cytotoxicity against MRC-5 cells, suggesting that the increased activity could be the result of an increased toxicity profile. The activities against *L. infantum* were generally about 0.5 log units higher when compared with *T. brucei* and *T. cruzi* and showed more variation between the compounds.
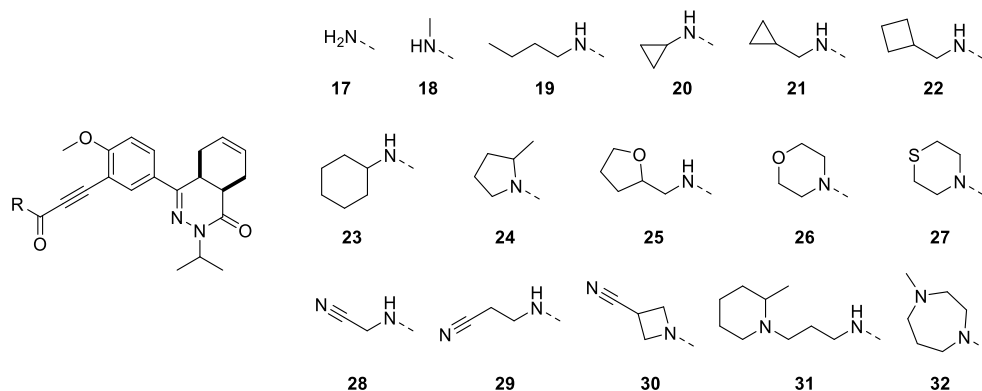
Figure 4: Structures of tested aliphatic alkynamides.

Table 1: Physicochemical properties and phenotypic activity of all alkynamides with aliphatic substituents against the protozoa and human MRC-5 cells.

#	NPD	cLogP	TPSA	pIC_{50}				pCC_{50}
				T. brucei	*T. cruzi*	*L. inf.*	*Pf-K1*	MRC-5
17	1170	2.4	85	5.2 ± 0.1	4.5 ± 0.1	5.0 ± 0.1	4.4 ± 0.1	4.5 ± 0.1
18	1172	2.6	71	4.7 ± 0.1	5.1 ± 0.1	5.2 ± 0.1	4.5 ± 0.1	4.4 ± 0.1
19	1024	3.9	71	5.1 ± 0.1	5.1 ± 0.1	5.6 ± 0.1	5.4 ± 0.1	<4.2
20	1017	3.1	71	5.1 ± 0.1	5.1 ± 0.1	5.6 ± 0.4	5.5 ± 0.3	4.5 ± 0.1
21	1038	3.4	71	5.1 ± 0.1	5.1 ± 0.1	5.6 ± 0.1	5.4 ± 0.2	<4.2
22	1042	3.8	71	5.2 ± 0.1	5.2 ± 0.2	5.7 ± 0.1	5.2 ± 0.3	<4.2
23	361	4.4	71	5.2 ± 0.1	5.4 ± 0.3	5.7 ± 0.1	6.1 ± 0.2	<4.2
24	1037	3.6	62	5.5 ± 0.1	5.7 ± 0.1	5.7 ± 0.1	5.5 ± 0.2	5.1 ± 0.1
25	1043	3.0	80	5.1 ± 0.1	4.9 ± 0.1	5.5 ± 0.1	5.2 ± 0.1	4.5 ± 0.1
26	1336	2.6	71	5.0 ± 0.1	5.1 ± 0.1	5.7 ± 0.1	5.4 ± 0.3	4.5 ± 0.1
27	1168	3.2	62	5.1 ± 0.1	5.1 ± 0.1	6.2 ± 0.1	5.3 ± 0.1	<4.2
28	1040	2.1	95	5.2 ± 0.1	5.1 ± 0.1	5.9 ± 0.3	5.3 ± 0.2	5.1 ± 0.1
29	1167	2.4	95	4.6 ± 0.1	4.5 ± 0.1	5.4 ± 0.2	4.7 ± 0.1	4.5 ± 0.1
30	1041	2.4	86	5.1 ± 0.1	5.1 ± 0.1	5.6 ± 0.1	5.5 ± 0.2	5.1 ± 0.1
31	1035	3.9	74	5.1 ± 0.1	5.1 ± 0.1	5.1 ± 0.1	5.5 ± 0.2	5.1 ± 0.1
32	1036	2.7	65	5.1 ± 0.1	5.1 ± 0.1	5.4 ± 0.1	5.5 ± 0.2	5.0 ± 0.1

In contrast to the other parasites, *L. infantum* is strongly inhibited by thiomorpholine **27** with a pIC_{50} of 6.2, which shows no sign of cytotoxicity against MRC-5 cells. Four other compounds (**19**, **21**-**23**) show a good activity against *L. inf.* parasites and do not display cytotoxicity, which all contain simple carbon chain tail

groups. The positive effect on activity of apolar tail groups in **19**, **21-23** and **27** against *L. inf*. and the lower cytotoxicity makes these interesting for further development. Overall the aliphatic alkynamides show a low cytotoxicity versus human MRC-5 cells with no pCC_{50} above 5.1.

The alkynamide series shows moderate potencies against malaria parasite *P. falsiparum*. The pIC_{50}s against *Pf-K1* varied between 4.4 and 6.1 and were the lowest for short chain alkynamides **17** and **18** and cyclohexane analogue **23** was the only aliphatic alkynamide to display a submicromolar activity. Most compounds with an interesting cytotoxicity profile ($pCC_{50} < 4.2$) are not active against multiple targets, with exception of cyclohexane **23** which showed a better activity against *L. inf*. and *Pf-K1*.

2.2.2. Aromatic alkynamides

Twenty (hetero)aromatic alkynamides (Figure 5) with various ring sizes and functional groups were screened against the four protozoa. As previously reported, alkynamides with aromatic substitutents show a generally higher inhibitory activity against *T. brucei* than the aliphatic alkynamides, with exception of triazole **51** (Table 2). Newly added aromatic alkynamides **46**, **48**, **49** and **50** are no exception to this rule and show a (slightly) higher activity than most aliphatic alkynamides. This trend is, however, not easily transferred to other parasites (Table 2).

The pIC_{50}-values against *T. cruzi* are very comparable between the aromatic alkynamides and the aliphatic alkynamides. Most activities of the alkynamides were in the pIC_{50}-range of 5.1 - 5.7, with a slight preference of the aromatic alkynamides for the higher end of this range. Imidazole **45** showed a remarkably high activity ($pIC_{50} > 6.6$) against *T. cruzi*, but this compound displayed high cytotoxicity against MRC-5 cells as well ($pCC_{50} > 6.6$). No clear structure-activity relationship is visible for *T. cruzi* amongst the alkynamides, but the alkynamides with higher cLogP or lower TPSA seem to give better results than their more polar analogues. In contrast to the observed effects against *T. brucei*, the activity of the aromatic alkynamides tend to have a slightly lower activity against *L. infantum* when compared to their aliphatic analogues. While the aliphatic substituents resulted in pIC_{50}-values between 5.0 and 6.2, the aromatic substituents result in pIC_{50}'s between <4.2 and 5.8. Interestingly, the most potent compound (**41**) against *T. brucei* ($pIC_{50} = 6.2$) showed no activity against *L. inf.* ($pIC_{50} < 4.2$), which is a remarkable difference since

pyridinyl **42** and **43** show moderate activities (*L. inf.* pIC_{50} = 5.8 and pIC_{50} = 5.6, respectively).
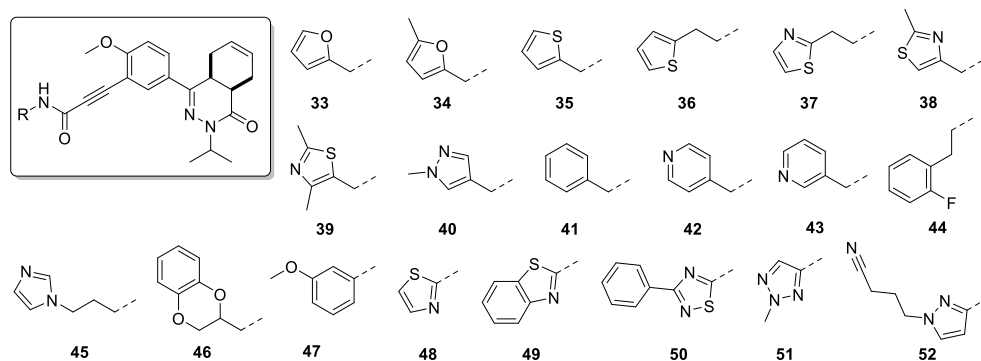
Figure 5: Overview of synthesized aromatic alkynamides.

Table 2: Phenotypical activities of all alkynamides with aromatic substituents.

#	NPD-	cLogP	TPSA	pIC_{50}				pCC_{50}
				T. brucei	*T. cruzi*	*L. inf.*	*Pf-K1*	MRC-5
33	1016	3.4	84	5.6 ± 0.1	5.2 ± 0.1	5.7 ± 0.1	5.7 ± 0.1	<4.2
34	1174	3.6	84	5.5 ± 0.3	5.5 ± 0.1	5.4 ± 0.2	4.9 ± 0.1	<4.2
35	1322	4.2	71	6.0 ± 0.4	5.7 ± 0.1	5.6 ± 0.1	5.6 ± 0.3	<4.2
36	1320	4.5	71	5.6 ± 0.1	5.7 ± 0.1	5.3 ± 0.3	6.0 ± 0.3	<4.2
37	1319	3.3	83	5.3 ± 0.2	5.3 ± 0.3	5.1 ± 0.1	5.8 ± 0.3	5.0 ± 0.1
38	1171	3.2	83	5.7 ± 0.1	5.1 ± 0.1	5.5 ± 0.1	5.0 ± 0.1	4.9 ± 0.1
39	3153	3.4	83	5.7 ± 0.1	5.1 ± 0.1	5.1 ± 0.1	4.9 ± 0.1	5.1 ± 0.1
40	1321	2.7	88	5.8 ± 0.3	5.1 ± 0.1	5.5 ± 0.2	5.3 ± 0.1	4.7 ± 0.1
41	1335	4.3	71	6.2 ± 0.1	5.3 ± 0.5	<4.2	5.6 ± 0.3	<4.2
42	1334	3.1	83	6.0 ± 0.4	5.1 ± 0.1	5.8 ± 0.9	<4.4	<4.2
43	1169	3.1	83	5.9 ± 0.1	5.2 ± 0.1	5.6 ± 0.1	4.7 ± 0.1	5.4 ± 0.2
44	1039	4.7	71	5.7 ± 0.1	5.7 ± 0.1	5.2 ± 0.2	5.6 ± 0.1	<4.2
45	1323	2.6	88	5.1 ± 0.1	>6.6	5.7 ± 0.1	5.4 ± 0.1	>6.6
46	1176	4.0	89	5.8 ± 0.1	5.6 ± 0.1	5.2 ± 0.4	5.0 ± 0.1	<4.2
47	1018	4.6	80	5.8 ± 0.1	5.7 ± 0.1	5.6 ± 0.1	5.5 ± 0.3	<4.2
48	1333	4.0	83	5.7 ± 0.1	5.7 ± 0.1	5.4 ± 0.4	5.3 ± 0.2	5.8 ± 0.1
49	1175	5.4	83	5.4 ± 0.5	5.8 ± 0.1	5.8 ± 0.1	5.1 ± 0.1	5.9 ± 0.1
50	1019	5.9	96	5.7 ± 0.1	5.7 ± 0.1	5.2 ± 0.1	4.8 ± 0.1	5.9 ± 0.1
51	3154	3.0	101	<4.2	4.3 ± 0.1	4.5 ± 0.1	<4.2	5.0 ± 0.1
52	3155	3.7	112	5.7 ± 0.1	5.6 ± 0.1	4.9 ± 0.1	5.1 ± 0.1	5.1 ± 0.1

6

The activities of aromatic alkynamides against *P. falciparum* was more divers than found with the aliphatic alkynamides, with large differences between structurally quite similar molecules. For instance, addition of the methyl on the furan group of **33** and **34** resulted in a decrease in activity of almost 1 log-unit (*Pf-K1* pIC_{50} = 5.7 *vs.* 4.9, respectively). Similarly, phenyl substitution towards a 3- or 4-pyridinyl in **41**, **42** and **43** led to loss in activity of 1 log-unit (*Pf-K1* pIC_{50} = 5.6 *vs.* <4.4 and 4.7, respectively). The origin for this variation could not be correlated to the change in physicochemical properties or cytotoxicity. The best activity against *P. falciparum* was observed for ethylthiophene **36** (*Pf-K1* pIC_{50} = 6.0), which does not show any cytotoxicity effect against MRC-5 cells. In general the alkynamide series has a good cytotoxicity profile, but several exceptions were found. Imidazole **45**, aminothiazoles **48** and **49** and aminothiadiazole **50** showed high cytotoxicity levels which were comparable to the activities obtained for the other parasites, indicating that the observed activity might be due to other off-target cytotoxicity effects.

Overall, several compounds showed promising activities against multiple parasites. Thiophene **35** and methoxyphenyl **47** are amongst the most active compounds for all four parasites and they show a good cytotoxicity profile. Similarly, benzyl analogue **41** and pyridyl analogue **42** both showed good potency against three of the four parasites (*T. brucei, T. cruzi* and *Pf-K1* for **41** and *T. brucei, T. cruzi* and *L. inf.* for **42**), while being inactive against one other parasite and human MRC-5 cells.

2.2.3. Alkynamide isosteres

Although most alkynamides do not show cytotoxicity effects the alkynamide group could be highlighted as a potential liability because of its Michael acceptor property. The alkynamides are exploited in medicinal chemistry as irreversible binder via a Michael reaction with cysteine or lysine residues.[39, 40] The Michael acceptor property was not an observed problem during synthesis of the alkynamides, but when **19** and **31** were mixed with 2-aminoethanethiol or glutathione in buffer under simple lab conditions fast consumption of the alkynamide was observed (unpublished results). To overcome this potential liability a small cluster of isosteres were synthesized having an oxetane amino group (**12**, **53**, **54**, **55** and **13**) or a (hetero)aromatic ring (**56**, **57** and **58**) to substitute the amide functionality (Figure 6). The oxetane functionality is well known as a carbonyl bioisostere and might increase solubility and metabolic stability.[41, 42] Methoxy

phenyl **56** and pyridine **58** both have a heteroatom positioned spatially similar to the carbonyl oxygen, but lacking the Michael acceptor properties.

Unfortunately, these modifications were mostly decreasing the activities of the alkyne phthalazinones (Table 3). All isosteres showed low phenotypical activity against *T. brucei* and *T. cruzi* parasites. In both assays cyclobutane **55** and 2-pyridinyl **58** showed the highest potency, but thit is comparable to the activity on MRC-5 cells. Surprisingly, the molecule with the weakest amide bioisostere motive (**57**) showed some potency against *L. infantum*. Pyrimidine **58** showed a slightly better toxicity profile (MRC-5 pCC_{50} = 4.9) and better activity against *L. infantum* (pIC_{50} = 6.0). The inhibitory activity of these bioisosteres against the malaria parasite was comparable to activity of the alkynamides.
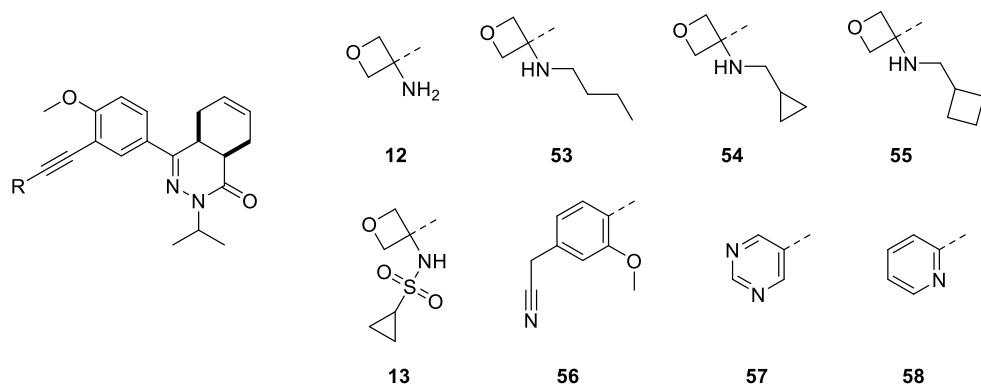
Figure 6: Overview of synthesized alkynamide isosteres.

Table 3: Phenotypical activities of all alkynoxetane and alkyne aromatics.

#	NPD-	cLogP	TPSA	pIC_{50}				pCC_{50}
				T. brucei	*T. cruzi*	*L. inf.*	*Pf-K1*	MRC-5
12	1328	2.4	77	<4.2	<4.3	4.4 ± 0.1	5.0 ± 0.2	<4.3
53	1329	4.1	63	4.6 ± 0.1	5.2 ± 0.1	<4.6	5.4 ± 0.2	5.2 ± 0.1
54	1331	3.6	63	4.5 ± 0.1	5.1 ± 0.1	5.3 ± 0.4	5.3 ± 0.1	5.3 ± 0.1
55	1332	4.0	63	4.9 ± 0.3	5.4 ± 0.4	4.9 ± 0.3	5.2 ± 0.2	5.3 ± 0.2
13	1330	2.4	97	4.5 ± 0.1	4.8 ± 0.4	4.5 ± 0.1	4.9 ± 0.1	<4.2
56	1026	4.7	75	4.7 ± 0.4	4.2 ± 0.1	<4.3	5.4 ± 0.2	<4.2
57	1025	3.2	68	4.5 ± 0.1	5.1 ± 0.1	6.0 ± 0.2	5.2 ± 0.1	4.9 ± 0.2
58	1020	4.3	55	5.3 ± 0.2	5.2 ± 0.1	5.4 ± 0.2	5.1 ± 0.3	5.0 ± 0.1

3. Conclusion

As shown, the trypanocidal activity that was observed for the alkyne phthalazinone class against *T. brucei* is transferable towards biologically closely related parasites. Most of the alkynamides showed interesting activity against the 4 protozoan parasites we used here. Unfortunately, the observed SAR for *T. brucei* parasites, a higher activity for aromatic alkynamides, was not found for the other parasites making the discovery of a single active molecule for all protozoan parasites unlikely. However, several molecules are identified amongst the alkyne phthalazinones as potential inhibitors against *T. cruzi*, *L. inf.* and *P. falsiparum*, which could function as starting points for the discovery of efficacious antiparasitic drugs.

4. Experimental

4.1. Chemistry

4.1.1. General

All reagents and solvents were obtained from commercial suppliers and were used as received. All reactions were magnetically stirred and carried out under an inert atmosphere. Reaction progress was monitored using thin-layer chromatography (TLC) and LC-MS analysis. LC-MS analysis was performed on a Shimadzu LC-20AD liquid chromatograph pump system, equipped with an Xbridge (C18) 5 μm column (50 mm, 4.6 mm), connected to a Shimadzu SPD-M20A diode array detector, and MS detection using a Shimadzu LC-MS-2010EV mass spectrometer. The LC-MS conditions were as follows: solvent A (water with 0.1% formic acid) and solvent B (MeCN with 0.1% formic acid), flow rate of 1.0 mL/min, start 5% B, linear gradient to 90% B in 4.5 min, then 1.5 min at 90% B, then linear gradient to 5% B in 0.5 min, then 1.5 min at 5% B; total run time of 8 min. Silica gel column chromatography was carried out with automatic purification systems using the indicated eluent. Reversed phase column purification was performed on Grace Davison iES system with C18 cartridges (60 Å, 40 μm) using the indicated eluent. Nuclear magnetic resonance (NMR) spectra were recorded as indicated on a Bruker Avance 500 (500 MHz for ^{1}H and 125.8 MHz for ^{13}C) instrument equipped with a Bruker CryoPlatform , or on a Bruker DMX300 (300 MHz for ^{1}H) or a Bruker Biospin (400 MHz for ^{1}H). Chemical shifts (δ in ppm) and coupling constants (*J* in Hz) are reported with residual solvent as internal standard (δ ^{1}H-NMR: CDCl$_3$ 7.26; DMSO-d_6 2.50; δ ^{13}C-NMR: CDCl$_3$ 77.16; DMSO-d_6 39.52). Abbreviations used for ^{1}H-NMR descriptions are as follows: s = singlet, d = doublet, t = triplet, q = quintet, hept = heptet dd = doublet of doublets, dt = doublet of triplets, tt = triplet of triplets, m = multiplet, app d = apparent doublet, br = broad signal. Exact mass measurements (HRMS) were performed on a Bruker micrOTOF-Q instrument with electrospray ionization (ESI): in positive ion mode and a capillary potential of 4,500 V. Microwave reactions were carried out in a Biotage Initiator$^+$ using sealed microwave vials. Systematic names for molecules were generated with ChemBioDraw Ultra 14.0.0.117 (PerkinElmer, Inc.). The reported yields refer to isolated pure products and are not optimized. The purity, reported as the LC peak area % at 254 nm, of all final compounds was ≥ 95% based on LC-MS. All compounds are isolated as a racemic mixture of *cis*-enantiomers.

4.1.2. Synthetic procedures

4.1.2.1. 2-Methyl-*N*-(oxetan-3-ylidene)propane-2-sulfinamide (**8**)

To a stirring suspension of 2-methylpropane-2-sulfinamide (20 g, 0.17 mol) and oxetan-3-one (9.6 mL, 0.15 mmol) in DCM (150 mL) was added titanium(IV) isopropoxide (66 mL, 225 mmol) and the slightly yellow solution was refluxed for 6 h. The reaction mixture was poured into sat. aq. NaHCO$_3$ (150 mL) and filtered over a pad of celite. The organic phase was separated and the aqueous phase was extracted using DCM (250 mL). The combined organic phases were dried over MgSO$_4$, filtered and concentrated to obtain a yellow oil. The compounds was purified using flash column chromatography (0-50% EtOAc/cyclohexane) to obtain the pure product as a yellow oil (14.8 g, 56%). ^{1}H NMR (500 MHz, CDCl$_3$) δ 5.83 − 5.75 (m, 1H), 5.75 − 5.57 (m, 1H), 5.52 − 5.41 (m, 2H), 1.26 (d, *J* = 1.7 Hz, 9H). ^{13}C

NMR (126 MHz, CDCl$_3$) δ 176.3, 86.2, 86.0, 58.1, 22.3. LC-MS (ESI): t_R = 3.08 min, area: >98%, *m/z* 176 [M + H]$^+$. HRMS (ESI) *m/z*: [M + H]$^+$ calcd. for C$_7$H$_{14}$NO$_2$S 176.0740, found 176.0748

4.1.2.2. 2-Methyl-*N*-(3-((trimethylsilyl)ethynyl)oxetan-3-yl)propane-2-sulfinamide (**9**)

A solution of ethynyltrimethylsilane (9.7 mL, 69 mmol) in dry THF (100 mL) was cooled to -78 °C and *n*-butyllithium in hexane (2.5 M, 25 mL, 63 mmol) was slowly added. The reaction mixture was stirred at -78 °C for 30 min prior to the addition of a solution of **8** (11 g, 57.1 mmol) in THF (20 mL). After 10 min the reaction mixture was allowed to warm to rt by removing the cooling bath. The thick suspension was quenched with sat. aq. NH$_4$Cl (250 mL) and extracted with EtOAc (3 × 200 mL). The combined organic phases were dried over MgSO$_4$, filtered and concentrated *in vacuo*. The crude product was purified using flash column chromatography (0-50% EtOAc/cyclohexane) to isolate the pure product as a slightly yellow oil that slowly crystallized over time (11.8 g, 76%). ^{1}H NMR (500 MHz, CDCl$_3$) δ 4.71 (dd, *J* = 6.5, 1.9 Hz, 2H), 4.66 – 4.46 (m, 2H), 4.18 (s, 1H), 1.06 (s, 9H), 0.00 (s, 9H). ^{13}C NMR (126 MHz, CDCl$_3$) δ 103.3, 92.5, 83.7, 83.3, 56.1, 53.9, 22.4, -0.3. LC-MS (ESI): t_R = 4.49 min, area: >98%, *m/z* 274 [M + H]$^+$. HRMS (ESI) *m/z*: [M + H]$^+$ calcd. for C$_{12}$H$_{24}$NO$_2$SSi 274.1292, found 274.1291

4.1.2.3. *N*-(3-((5-(*cis*-3-Isopropyl-4-oxo-3,4,4a,5,8,8a-hexahydrophthalazin-1-yl)-2-methoxyphenyl)ethynyl)oxetan-3-yl)-2-methylpropane-2-sulfinamide (**11**)

To a mixture of **10** (2.3 g, 6.1 mmol), CsF (2.3 g, 15 mmol), PdCl$_2$(dppf) (0.45 g, 0.61 mmol) and CuI (0.12 g, 0.61 mmol) in DMF (15 mL) was added **9** (2.5 g, 9.1 mmol). This mixture was heated to 120 °C by microwave irradiation and stirred for 4 h. The reaction mixture was poured into sat. aq. NH$_4$Cl (200 mL) and extracted with EtOAc (3 × 200 mL). The combined organic phases were washed with brine, dried over MgSO$_4$, filtered and concentrated to obtain a brown oil. The crude product was purified using flash column chromatography (50-100% EtOAc/cyclohexane) to obtain the pure product as a dark orange solid (1.6 g, 53%). ^{1}H NMR (500 MHz, CDCl$_3$) δ 7.91 – 7.79 (m, 2H), 6.93 (d, *J* = 8.5 Hz, 1H), 5.84 – 5.64 (m, 2H), 5.09 (d, *J* = 6.8 Hz, 2H), 5.05 (q, *J* = 6.7 Hz, 1H), 4.89 (t, *J* = 7.4 Hz, 2H), 4.10 (s, 1H), 3.93 (s, 3H), 3.30 (dt, *J* = 11.5, 5.7 Hz, 1H), 3.01 (dt, *J* = 18.1, 3.1 Hz, 1H), 2.74 (s, 1H), 2.28 – 2.12 (m, 2H), 2.05 – 1.97 (m, 1H), 1.34 (d, *J* = 6.6 Hz, 3H), 1.30 (s, 9H), 1.22 (d, *J* = 6.7 Hz, 3H). ^{13}C NMR (126 MHz, CDCl$_3$) δ 166.4, 161.2, 152.8, 131.1, 128.0, 127.7, 126.0, 123.9, 111.5, 110.8, 91.4, 84.1, 83.7, 83.5, 60.4, 56.4, 56.0, 54.5, 46.7, 34.7, 31.0, 23.0, 22.5, 22.3, 20.6, 20.2, 14.2. LC-MS (ESI): t_R = 4.78 min, area: >98%, *m/z* 498 [M + H]$^+$. HRMS (ESI) *m/z*: [M + H]$^+$ calcd. for C$_{27}$H$_{36}$N$_3$O$_4$S 498.2421, found 498.2419

4.1.2.4. *cis*-4-(3-((3-Aminooxetan-3-yl)ethynyl)-4-methoxyphenyl)-2-isopropyl-4a,5,8,8a-tetrahydrophthalazin-1(2*H*)-one (**12**)

To a solution of **11** (0.20 g, 0.40 mmol) in ethanol (4 mL) was added methanesulfonic acid (50 μL, 0.80 mmol) and was stirred at rt overnight. The reaction mixture was diluted with EtOAc (50 mL) and the organic phase was washed with sat. aq. NH$_4$Cl (50 mL) and brine (50 mL). The organic phase was dried over Na$_2$SO$_4$, filtered and concentrated to obtain the crude product as a yellow solid. The product was purified using flash column chromatography (20-100% EtOAc/cyclohexane + 0.1% Et$_3$N) to obtain the pure product as a white solid (125 mg, 79%). ^{1}H NMR (500 MHz, CDCl$_3$) δ 7.84 (s, 2H), 6.93 (d, *J* = 8.5 Hz, 1H), 5.84 – 5.65 (m, 2H), 5.11 – 5.00 (m, 3H), 4.64 (d, *J* = 6.0 Hz, 2H), 3.94 (s, 3H), 3.30 (dt, *J* = 11.5,

5.8 Hz, 1H), 3.07 – 2.96 (m, 1H), 2.74 (t, *J* = 6.0 Hz, 1H), 2.28 – 1.96 (m, 6H), 1.34 (d, *J* = 6.6 Hz, 3H), 1.22 (d, *J* = 6.7 Hz, 3H). ^{13}C NMR (126 MHz, CDCl$_3$) δ 166.4, 160.9, 152.8, 131.0, 127.7, 127.7, 126.0, 123.9, 111.8, 110.7, 94.4, 85.1, 80.4, 56.0, 50.7, 46.7, 34.7, 31.0, 23.0, 22.3, 20.6, 20.2. LC-MS (ESI): t_R = 3.69 min, area: >98%, *m/z* 377 [M − NH$_2^-$]$^+$ and 394 [M + H]$^+$. HRMS (ESI) *m/z*: [M + H]$^+$ calcd. for C$_{23}$H$_{28}$N$_3$O$_3$ 394.2125, found 394.2122

4.1.2.5. *N*-(3-((5-(*cis*-3-Isopropyl-4-oxo-3,4,4a,5,8,8a-hexahydrophthalazin-1-yl)-2-methoxyphenyl)ethynyl)oxetan-3-yl)cyclopropanesulfonamide (**13**)

To a solution of **12** (0.10 g, 0.25 mmol) in DCM (2 mL) was added pyridine (0.06 mL, 0.76 mmol) and cyclopropanesulfonyl chloride (0.05 mL, 0.51 mmol) and stirred at rt overnight. The reaction mixture was diluted with EtOAc (50 mL) and washed with sat. aq. NH$_4$Cl (50 mL) and brine (50 mL). The organic phase was dried over Na$_2$SO$_4$, filtered and concentrated to obtain the crude product as a yellow solid. The product was purified using flash column chromatography (0-80% EtOAc/cyclohexane) to obtain the product as a white solid (87 mg, 69%). ^{1}H NMR (500 MHz, CDCl$_3$) δ 7.87 (d, *J* = 2.1 Hz, 1H), 7.84 (dd, *J* = 8.8, 2.3 Hz, 1H), 6.94 (d, *J* = 8.7 Hz, 1H), 5.83 – 5.65 (m, 2H), 5.06 (p, *J* = 6.6 Hz, 1H), 5.00 (q, *J* = 6.5 Hz, 4H), 3.88 (s, 3H), 3.30 (dt, *J* = 11.5, 5.8 Hz, 1H), 3.12 – 2.97 (m, 2H), 2.75 (t, *J* = 6.0 Hz, 1H), 2.28 – 2.12 (m, 2H), 2.09 – 1.97 (m, 1H), 1.34 (d, *J* = 6.5 Hz, 3H), 1.32 – 1.25 (m, 2H), 1.22 (d, *J* = 6.7 Hz, 3H), 1.07 – 1.00 (m, 2H). ^{13}C NMR (126 MHz, CDCl$_3$) δ 166.4, 161.0, 152.6, 131.0, 128.1, 127.9, 126.1, 123.8, 111.3, 110.8, 91.5, 82.7, 82.7, 82.7, 55.9, 51.7, 46.7, 34.7, 31.7, 31.0, 23.0, 22.3, 20.6, 20.2, 6.5. LC-MS (ESI): t_R = 4.57 min, area: >98%, *m/z* 498 [M + H]$^+$. HRMS (ESI) *m/z*: [M + H]$^+$ calcd. for C$_{26}$H$_{32}$N$_3$O$_5$S 498.2057, found 498.2042

4.1.2.6. *N*-Butyl-*N*-(3-((5-(*cis*-3-isopropyl-4-oxo-3,4,4a,5,8,8a-hexahydrophthalazin-1-yl)-2-methoxyphenyl)ethynyl)oxetan-3-yl)-2-methylpropane-2-sulfinamide (**14a**)

To a solution of **11** (200 mg, 0.40 mmol) in DMF (1 mL) was added NaH (24 mg, 0.60 mmol) and stirred at rt for 10 min. 1-Bromobutane (0.08 mL, 0.80 mmol) was added and the reaction mixture was stirred for an additional 10 h. The reaction mixture was quenched with sat. aq. NH$_4$Cl (50 mL) and extracted with EtOAc (2 × 50 mL). The combined organic phases were washed with brine, dried over MgSO$_4$, filtered and concentrated to obtain a colourless oil. The product was purified using flash column chromatography (0-50% EtOAc/cyclohexane) to obtain the product as a white solid (70 mg, 32%). ^{1}H NMR (500 MHz, CDCl$_3$) δ 7.88 – 7.81 (m, 2H), 6.92 (d, *J* = 9.5 Hz, 1H), 5.83 – 5.65 (m, 2H), 5.10 (d, *J* = 6.3 Hz, 1H), 5.06 (p, *J* = 6.6 Hz, 1H), 4.97 (d, *J* = 5.6 Hz, 1H), 4.91 (d, *J* = 6.3 Hz, 1H), 4.79 (d, *J* = 5.5 Hz, 1H), 3.92 (s, 3H), 3.34 – 3.24 (m, 2H), 3.12 – 2.98 (m, 2H), 2.74 (t, *J* = 5.9 Hz, 1H), 2.27 – 2.13 (m, 2H), 2.08 – 1.96 (m, 1H), 1.52 – 1.45 (m, 2H), 1.43 – 1.33 (m, 6H), 1.31 (s, 9H), 1.23 (d, *J* = 6.7 Hz, 3H), 0.96 (t, *J* = 7.3 Hz, 3H). ^{13}C NMR (126 MHz, CDCl$_3$) δ 166.4, 161.5, 153.0, 131.0, 127.8, 127.6, 126.0, 124.0, 111.8, 110.8, 92.3, 83.3, 82.6, 81.9, 59.4, 58.7, 56.0, 46.7, 42.4, 34.7, 31.3, 30.9, 23.6, 23.0, 22.3, 20.8, 20.6, 20.2, 13.9. LC-MS (ESI): t_R = 5.68 min, area: 95%, *m/z* 554 [M + H]$^+$. HRMS (ESI) *m/z*: [M + H]$^+$ calcd. for C$_{31}$H$_{44}$N$_3$O$_4$S 554.3047, found 554.3035

4.1.2.7. *N*-(Cyclopropylmethyl)-*N*-(3-((5-(*cis*-3-isopropyl-4-oxo-3,4,4a,5,8,8a-hexahydrophthalazin-1-yl)-2-methoxyphenyl)ethynyl)oxetan-3-yl)-2-methylpropane-2-sulfinamide (**14b**)

To a solution of **11** (200 mg, 0.402 mmol) in DMF (1 mL) was added NaH (24 mg, 0.60 mmol) and stirred at rt for 10 min. (Bromomethyl)cyclopropane (0.08 mL, 0.80 mmol) was added and the reaction mixture was stirred for an additional 10 h. The reaction mixture was quenched with sat. aq. NH$_4$Cl (50 mL) and extracted with EtOAc (2 × 50 mL). The combined organic phases were washed with brine, dried over MgSO$_4$, filtered and concentrated to obtain a colourless oil. The product was purified using flash column chromatography (0-50% EtOAc/cyclohexane) to obtain the product as a white solid (81 mg, 37%). ^{1}H NMR (500 MHz, CDCl$_3$) δ 7.83 (dd, *J* = 7.9, 1.5 Hz, 2H), 6.94 – 6.87 (m, 1H), 5.84 – 5.65 (m, 2H), 5.15 (dd, *J* = 13.7, 6.1 Hz, 2H), 5.06 (hept, *J* = 6.6 Hz, 1H), 4.94 (d, *J* = 6.4 Hz, 1H), 4.84 (d, *J* = 5.7 Hz, 1H), 3.90 (s, 3H), 3.61 – 3.52 (m, 1H), 3.34 – 3.26 (m, 1H), 3.07 – 2.98 (m, 1H), 2.74 (t, *J* = 5.9 Hz, 1H), 2.63 (m, 1H), 2.28 – 2.13 (m, 2H), 2.08 – 1.96 (m, 1H), 1.38 – 1.29 (m, 12H), 1.23 (d, *J* = 6.6 Hz, 3H), 0.89 – 0.78 (m, 1H), 0.61 – 0.41 (m, 3H), 0.28 – 0.19 (m, 1H). ^{13}C NMR (126 MHz, CDCl$_3$) δ 166.5, 161.6, 152.9, 130.8, 127.8, 127.5, 126.0, 123.9, 111.8, 110.8, 92.2, 83.7, 83.1, 81.4, 58.9, 58.7, 55.9, 47.2, 46.7, 34.7, 30.9, 23.7, 23.0, 22.3, 20.6, 20.2, 9.4, 5.6, 3.1. LC-MS (ESI): *t*$_R$ = 5.56 min, area: >98%, *m/z* 552 [M + H]$^+$. HRMS (ESI) *m/z*: [M + H]$^+$ calcd. for C$_{31}$H$_{42}$N$_3$O$_4$S 552.2891, found 552.2879

4.1.2.8. *N*-(Cyclobutylmethyl)-*N*-(3-((5-(*cis*-3-isopropyl-4-oxo-3,4,4a,5,8,8a-hexahydrophthalazin-1-yl)-2-methoxyphenyl)ethynyl)oxetan-3-yl)-2-methylpropane-2-sulfinamide (**14c**)

To a solution of **11** (200 mg, 0.40 mmol) in DMF (1 mL) was added NaH (24 mg, 0.60 mmol) and stirred at rt for 10 min. (Bromomethyl)cyclobutane (0.09 mL, 0.80 mmol) was added and the reaction mixture was stirred for an additional 10 h. The reaction mixture was quenched with sat. aq. NH$_4$Cl (50 mL) and extracted with EtOAc (2x50 mL). The combined organic phases were washed with brine, dried over MgSO$_4$, filtered and concentrated to obtain a colourless oil. The product was purified using flash column chromatography (0-50% EtOAc/cyclohexane) to obtain the product as a white solid (82 mg, 36%). ^{1}H NMR (500 MHz, CDCl$_3$) δ 7.84 (d, *J* = 8.0 Hz, 2H), 6.95 – 6.88 (m, 1H), 5.84 – 5.65 (m, 2H), 5.11 – 5.01 (m, 2H), 4.89 (d, *J* = 6.3 Hz, 1H), 4.83 (d, *J* = 5.5 Hz, 1H), 4.73 (d, *J* = 5.5 Hz, 1H), 3.92 (s, 3H), 3.35 – 3.16 (m, 3H), 3.07 – 2.96 (m, 1H), 2.74 (t, *J* = 5.9 Hz, 1H), 2.33 (hept, *J* = 7.5 Hz, 1H), 2.28 – 2.19 (m, 1H), 2.18 – 1.96 (m, 4H), 1.96 – 1.72 (m, 4H), 1.37 – 1.29 (m, 12H), 1.22 (d, *J* = 6.7 Hz, 3H). ^{13}C NMR (126 MHz, CDCl$_3$) δ 166.4, 161.5, 153.0, 130.9, 127.7, 127.5, 125.9, 123.9, 111.8, 110.7, 91.9, 83.2, 82.9, 81.6, 58.8, 56.0, 48.0, 46.7, 34.7, 34.0, 30.9, 27.1, 26.3, 23.7, 23.0, 22.3, 20.5, 20.2, 18.0. LC-MS (ESI): *t*$_R$ = 5.83 min, area: 95%, *m/z* 566 [M + H]$^+$. HRMS (ESI) *m/z*: [M + H]$^+$ calcd. for C$_{32}$H$_{44}$N$_3$O$_4$S 566.3047, found 566.3032

4.1.2.9. *cis*-4-(3-((3-(Butylamino)oxetan-3-yl)ethynyl)-4-methoxyphenyl)-2-isopropyl-4a,5,8,8a-tetrahydrophthalazin-1(2*H*)-one (**53**)

To a solution of **14a** (50 mg, 0.09 mmol) in EtOH (1 mL) was added methanesulfonic acid (0.05 mL, 0.77 mmol) and the reaction was stirred at rt overnight. The reaction mixture was diluted with EtOAc (50 mL) and washed with sat. aq. NH$_4$Cl (50 mL) and brine (50 mL). The organic phase was dried over Na$_2$SO$_4$, filtered and concentrated to obtain the crude product as a yellow solid. The product was purified using flash column chromatography (0-80% EtOAc/cyclohexane + 0.1% Et$_3$N) to obtain the

product as a white solid (31 mg, 76%). ^{1}H NMR (500 MHz, CDCl$_3$) δ 7.84 (d, *J* = 2.3 Hz, 1H), 7.81 (dd, *J* = 8.7, 2.4 Hz, 1H), 6.93 (d, *J* = 8.7 Hz, 1H), 5.85 – 7.65 (m, 2H), 5.06 (hept, *J* = 6.7 Hz, 1H), 4.95 (d, *J* = 5.9 Hz, 2H), 4.63 (d, *J* = 5.9 Hz, 2H), 3.92 (s, 3H), 3.30 (dt, *J* = 11.5, 5.7 Hz, 1H), 3.07 – 2.97 (m, 1H), 2.80 (t, *J* = 7.2 Hz, 2H), 2.74 (t, *J* = 6.0 Hz, 1H), 2.27 – 2.12 (m, 2H), 2.09 – 1.97 (m, 1H), 1.56 (q, *J* = 7.4 Hz, 2H), 1.44 (q, *J* = 7.6 Hz, 2H), 1.34 (d, *J* = 6.6 Hz, 3H), 1.22 (d, *J* = 6.7 Hz, 3H), 0.96 (t, *J* = 7.3 Hz, 3H). ^{13}C NMR (126 MHz, CDCl$_3$) δ 166.4, 161.0, 152.8, 130.8, 127.6, 127.5, 126.0, 123.9, 112.1, 110.6, 93.2, 82.5, 81.5, 55.9, 55.0, 46.7, 44.1, 34.7, 32.3, 30.9, 23.0, 22.3, 20.5, 20.5, 20.1, 13.9. LC-MS (ESI): t_R = 4.01 min, area: >98%, *m/z* 450 [M + H]$^+$. HRMS (ESI) *m/z*: [M + H]$^+$ calcd. for C$_{27}$H$_{36}$N$_3$O$_3$ 450.2751, found 450.2742

4.1.2.10. *cis*-4-(3-((3-((Cyclopropylmethyl)amino)oxetan-3-yl)ethynyl)-4-methoxyphenyl)-2-isopropyl-4a,5,8,8a-tetrahydrophthalazin-1(2*H*)-one (**54**)

To a solution of **14b** (50 mg, 0.09 mmol) in EtOH (1 mL) was added methanesulfonic acid (0.05 mL, 0.77 mmol) and this mixture was stirred at rt overnight. The reaction mixture was diluted with EtOAc (50 mL) and washed with sat. aq. NH$_4$Cl (50 mL) and brine (50 mL). The organic phase was dried over Na$_2$SO$_4$, filtered and concentrated to obtain the crude product as a yellow solid. The product was purified using flash column chromatography (0-80% EtOAc/cyclohexane + 0.1% Et$_3$N) to obtain the product as a white solid (25 mg, 62%). ^{1}H NMR (500 MHz, CDCl$_3$) δ 7.89 – 7.74 (m, 2H), 6.92 (d, *J* = 8.6 Hz, 1H), 5.86 – 5.64 (m, 2H), 5.11 – 5.01 (m, *J* = 6.7 Hz, 1H), 4.96 (d, *J* = 6.0 Hz, 2H), 4.68 (d, *J* = 5.9 Hz, 2H), 3.92 (s, 3H), 3.30 (dt, *J* = 11.5, 5.7 Hz, 1H), 3.03 (dt, *J* = 17.7, 3.4 Hz, 1H), 2.75 (t, *J* = 6.0 Hz, 1H), 2.70 (d, *J* = 6.9 Hz, 2H), 2.28 – 2.14 (m, 2H), 2.09 – 1.98 (m, 1H), 1.35 (d, *J* = 6.5 Hz, 3H), 1.22 (d, *J* = 6.6 Hz, 3H), 1.04 (pd, *J* = 7.2, 3.5 Hz, 1H), 0.55 (t, *J* = 6.5 Hz, 2H), 0.24 (t, *J* = 4.9 Hz, 2H). ^{13}C NMR (126 MHz, CDCl$_3$) δ 166.4, 161.0, 152.8, 130.8, 127.6, 127.5, 126.0, 123.9, 112.0, 110.6, 93.0, 82.6, 81.8, 55.9, 54.8, 49.8, 46.7, 34.7, 30.9, 23.0, 22.3, 20.6, 20.2, 11.2, 3.6. LC-MS (ESI): t_R = 3.92 min, area: >98%, *m/z* 448 [M + H]$^+$. HRMS (ESI) *m/z*: [M + H]$^+$ calcd. for C$_{27}$H$_{34}$N$_3$O$_3$ 448.2595, found 448.2587

4.1.2.11. *cis*-4-(3-((3-((Cyclobutylmethyl)amino)oxetan-3-yl)ethynyl)-4-methoxyphenyl)-2-isopropyl-4a,5,8,8a-tetrahydrophthalazin-1(2*H*)-one (**55**)

To a solution of **14c** (50 mg, 0.09 mmol) in EtOH (1 mL) was added methanesulfonic acid (0.05 mL, 0.77 mmol) and this mixture was stirred at rt overnight. The reaction mixture was diluted with EtOAc (50 mL) and washed with sat. aq. NH$_4$Cl (50 mL) and brine (50 mL). The organic phase was dried over Na$_2$SO$_4$, filtered and concentrated to obtain the crude product as a yellow solid. The product was purified using flash column chromatography (0-80% EtOAc/cyclohexane + 0.1% Et$_3$N) to obtain the pure product as a white solid (28 mg, 69%). ^{1}H NMR (500 MHz, CDCl$_3$) δ 7.86 (d, *J* = 2.2 Hz, 1H), 7.81 (dd, *J* = 8.8, 2.3 Hz, 1H), 6.94 (d, *J* = 8.8 Hz, 1H), 5.85 – 5.65 (m, 2H), 5.06 (hept, *J* = 6.6 Hz, 1H), 4.95 (d, *J* = 5.9 Hz, 2H), 4.62 (d, *J* = 5.9 Hz, 2H), 3.93 (s, 3H), 3.30 (dt, *J* = 11.5, 5.7 Hz, 1H), 3.08 – 2.98 (m, 1H), 2.84 (d, *J* = 7.3 Hz, 2H), 2.75 (t, *J* = 6.0 Hz, 1H), 2.53 (hept, *J* = 7.6 Hz, 1H), 2.27 – 2.09 (m, 4H), 2.08 – 1.85 (m, 3H), 1.79 – 1.69 (m, 3H), 1.35 (d, *J* = 6.5 Hz, 3H), 1.23 (d, *J* = 6.7 Hz, 3H). ^{13}C NMR (126 MHz, CDCl$_3$) δ 166.4, 161.0, 152.8, 130.8, 127.6, 127.5, 126.0, 123.9, 112.1, 110.6, 93.2, 82.5, 81.6, 55.9, 54.9, 50.5, 46.7, 35.4, 34.7, 30.9, 26.3, 23.0, 22.3, 20.6, 20.2, 18.5. LC-MS (ESI): t_R = 4.07 min, area: >98%, *m/z* 462 [M + H]$^+$. HRMS (ESI) *m/z*: [M + H]$^+$ calcd. for C$_{28}$H$_{36}$N$_3$O$_3$ 462.2751, found 462.2743

4.1.2.12. *cis*-2-Isopropyl-4-(4-methoxy-3-((trimethylsilyl)ethynyl)phenyl)-4a,5,8,8a-tetrahydrophthalazin-1(2*H*)-one (**15**)

To a degassed solution of **10** (3.0 g, 8.0 mmol) in Et$_3$N (25 mL) was added ethynyltrimethylsilane (2.2 mL, 16 mmol), PdCl$_2$(dppf) (0.30 g, 0.40 mmol) and CuI (0.15 g, 0.80 mmol). This mixture was heated to 80 °C and stirred for 3 h. The reaction mixture was poured in sat. aq. NH$_4$Cl (250 mL) and extracted with EtOAc (2 × 250 mL). The combined organic layers were washed with brine (250 mL), dried over MgSO$_4$, filtered and concentrated *in vacuo*. The crude product was purified using flash column chromatography (0-25% EtOAc/Hept). The product was obtained as a fine light yellow solid (2.9 g, 92%). ^{1}H NMR (500 MHz, CDCl$_3$) δ 7.92 – 7.77 (m, 2H), 6.92 (d, *J* = 8.6 Hz, 1H), 5.85 – 5.63 (m, 2H), 5.05 (hept, *J* = 6.7 Hz, 1H), 3.94 (s, 3H), 3.30 (dt, *J* = 11.6, 5.8 Hz, 1H), 3.08 – 2.95 (m, 1H), 2.73 (t, *J* = 6.0 Hz, 1H), 2.29 – 2.12 (m, 2H), 2.09 – 1.94 (m, 1H), 1.34 (d, *J* = 6.6 Hz, 3H), 1.22 (d, *J* = 6.7 Hz, 3H), 0.30 (s, 9H). ^{13}C NMR (126 MHz, CDCl$_3$) δ 166.4, 161.4, 153.0, 131.5, 127.7, 127.6, 126.0, 124.0, 112.4, 110.8, 100.6, 99.2, 56.1, 46.7, 34.7, 30.9, 23.0, 22.3, 20.6, 20.2, 0.1. LC-MS (ESI): t_R = 5.93 min, area: >98%, *m/z* 395 [M + H]$^+$. HRMS (ESI) *m/z*: [M + H]$^+$ calcd. for C$_{23}$H$_{31}$N$_2$O$_2$Si 395.2149, found 395.2148.

4.1.2.13. *cis*-4-(3-Ethynyl-4-methoxyphenyl)-2-isopropyl-4a,5,8,8a-tetrahydrophthalazin-1(2*H*)-one (**16**)

To a suspension of **15** (2.9 g, 7.4 mmol) in MeOH (20 mL) was added KOH (0.83 g, 15 mmol) and the reaction mixture was stirred at 50 °C for 4 h. The reaction mixture was poured into aq. HCl (1 M, 100 mL) and the solids were filtered off to obtain the product as a light yellow solid (2.3g, 95%). ^{1}H NMR (500 MHz, CDCl$_3$) δ 7.90 (d, *J* = 2.4 Hz, 1H), 7.83 (dd, *J* = 8.8, 2.3 Hz, 1H), 6.93 (d, *J* = 8.8 Hz, 1H), 5.85 – 5.62 (m, 2H), 5.04 (hept, *J* = 6.7 Hz, 1H), 3.95 (s, 3H), 3.35 (s, 1H), 3.28 (dt, *J* = 11.5, 5.7 Hz, 1H), 3.05 – 2.95 (m, 1H), 2.73 (t, *J* = 6.0 Hz, 1H), 2.26 – 2.10 (m, 2H), 2.07 – 1.95 (m, 1H), 1.32 (d, *J* = 6.6 Hz, 3H), 1.20 (d, *J* = 6.7 Hz, 3H). ^{13}C NMR (126 MHz, CDCl$_3$) δ 166.4, 161.5, 152.7, 131.6, 127.9, 127.8, 126.0, 123.9, 111.5, 110.7, 81.6, 79.6, 56.1, 46.7, 34.7, 31.0, 23.0, 22.3, 20.6, 20.2. LC-MS (ESI): t_R = 4.88 min, area: >98%, *m/z* 323 [M + H]$^+$. HRMS (ESI) *m/z*: [M + H]$^+$ calcd. for C$_{20}$H$_{23}$N$_2$O$_2$ 323.1754, found 323.1759.

4.1.2.14. 2-(4-((5-(*cis*-3-Isopropyl-4-oxo-3,4,4a,5,8,8a-hexahydrophthalazin-1-yl)-2-methoxyphenyl)ethynyl)-3-methoxyphenyl)acetonitrile (**56**)

To a mixture of **16** (150 mg, 0.47 mmol) and 2-(4-bromo-3-methoxyphenyl)acetonitrile (126 mg, 0.68 mmol) in THF (2 mL) was added CuI (9.0 mg, 47 μmol), PdCl$_2$(PPh$_3$)$_2$ (32 mg, 47 μmol) and Et$_3$N (0.3 mL, 2.1 mmol). The reaction was heated to 80 °C in the microwave for 2 h. Reaction mixture was diluted with DCM (5 mL) and washed with aq. HCl (1 M, 5 mL) and separated by use of a phase separator. The organic phase was concentrated and the product was purified using flash column chromatography (EtOAc/Hept: 0-50%). The impure product was purified for a second time using reverse phase column chromatography (MeCN/H$_2$O: 5-95%) to obtain the product as a white solid (43 mg, 20%). ^{1}H NMR (500 MHz, DMSO-*d$_6$*) δ 7.96 – 7.87 (m, 2H), 7.46 (d, *J* = 2.4 Hz, 1H), 7.37 (dd, *J* = 8.6, 2.4 Hz, 1H), 7.18 (d, *J* = 8.6 Hz, 1H), 7.13 (d, *J* = 8.6 Hz, 1H), 5.76 – 5.58 (m, 2H), 4.89 (hept, *J* = 6.6 Hz, 1H), 3.99 (s, 2H), 3.91 (s, 3H), 3.86 (s, 3H), 3.48 (dt, *J* = 11.5, 5.8 Hz, 1H), 2.81 (t, *J* = 6.0 Hz, 1H), 2.78 – 2.69 (m, 1H), 2.24 – 2.06 (m, 2H), 1.82 (m, 1H), 1.25 (d, *J* = 6.6 Hz, 4H), 1.16 (d, *J* = 6.7 Hz, 3H). ^{13}C NMR

(126 MHz, DMSO-d_6) δ 166.5, 161.0, 159.4, 153.5, 133.1, 130.7, 128.6, 127.8, 126.4, 124.5, 123.7, 119.8, 112.4, 112.3, 112.1, 90.1, 56.5, 56.7, 46.2, 34.3, 30.3, 22.9, 22.4, 21.7, 20.9, 20.6. LC-MS (ESI): t_R = 5.17 min, area: 96%, *m/z* 468 [M + H]+. HRMS (ESI) *m/z*: [M + H]+ calcd. for $C_{29}H_{30}N_3O_3$ 468.2282, found 468.2271.

4.1.2.15. *cis*-2-Isopropyl-4-(4-methoxy-3-(pyrimidin-5-ylethynyl)phenyl)-4a,5,8,8a-tetrahydrophthalazin-1(2*H*)-one (**57**)

This compound was prepared from **16** (150 mg, 0.47 mmol) and 5-bromopyrimidine (89 mg, 0.56 mmol) as described for **57**. The title compound was obtained as a white solid (41 mg, 22%). ^{1}H NMR (500 MHz, DMSO-d_6) δ 9.21 (s, 1H), 9.02 (s, 2H), 8.02 (d, *J* = 2.4 Hz, 1H), 7.98 (dd, *J* = 8.8, 2.4 Hz, 1H), 7.23 (d, *J* = 8.9 Hz, 1H), 5.75 – 5.59 (m, 2H), 4.89 (hept, *J* = 6.6 Hz, 1H), 3.93 (s, 3H), 3.48 (dt, *J* = 11.6, 5.8 Hz, 1H), 2.82 (t, *J* = 6.0 Hz, 1H), 2.79 – 2.70 (m, 1H), 2.16 (m, 2H), 1.82 (m, 1H), 1.25 (d, *J* = 6.5 Hz, 3H), 1.15 (d, *J* = 6.7 Hz, 3H). ^{13}C NMR (126 MHz, DMSO-d_6) δ 166.5, 161.2, 159.1, 157.3, 153.3, 131.1, 129.5, 127.9, 126.3, 124.5, 119.5, 112.3, 110.9, 92.6, 87.1, 56.6, 46.2, 34.3, 30.3, 22.9, 22.4, 20.9, 20.6. LC-MS (ESI): t_R = 4.90 min, area: >98%, *m/z* 401 [M + H]+. HRMS (ESI) *m/z*: [M + H]+ calcd. for $C_{24}H_{25}N_4O_2$ 401.1972, found 401.1953.

4.1.2.16. *cis*-2-Isopropyl-4-(4-methoxy-3-(pyridin-2-ylethynyl)phenyl)-4a,5,8,8a-tetrahydrophthalazin-1(2*H*)-one (**58**)

This compound was prepared from **16** (150 mg, 0.47 mmol) and 2-bromopyridine (88 mg, 0.56 mmol) as described for **57**. The title compound was obtained as a white solid (65 mg, 35%). ^{1}H NMR (500 MHz, CDCl$_3$) δ 8.68 – 8.59 (m, 1H), 8.00 (d, *J* = 2.4 Hz, 1H), 7.88 (dd, *J* = 8.8, 2.3 Hz, 1H), 7.69 (d, *J* = 7.7 Hz, 1H), 7.59 (d, *J* = 7.9 Hz, 1H), 7.25 (m, 1H), 6.97 (d, *J* = 8.8 Hz, 1H), 5.73 (m, 2H), 5.05 (hept, *J* = 6.6 Hz, 1H), 3.97 (s, 3H), 3.30 (dt, *J* = 11.4, 5.7 Hz, 1H), 3.06 – 2.96 (m, 1H), 2.74 (t, *J* = 6.0 Hz, 1H), 2.26 – 1.96 (m, 3H), 1.34 (d, *J* = 6.6 Hz, 3H), 1.21 (d, *J* = 6.7 Hz, 3H). ^{13}C NMR (126 MHz, CDCl$_3$) δ 166.4, 161.3, 152.8, 150.1, 143.4, 136.1, 131.5, 128.1, 127.8, 127.2, 126.0, 123.9, 122.8, 111.7, 110.8, 92.9, 85.3, 56.1, 46.7, 34.7, 31.0, 23.0, 22.3, 20.6, 20.2. LC-MS (ESI): t_R = 4.95 min, area: >98%, *m/z* 400 [M + H]+. HRMS (ESI) *m/z*: [M + H]+ calcd. for $C_{25}H_{26}N_3O_2$ 400.2020, found 400.2021.

5. Author contributions

6

6. References.

1. WHO, Accelerating work to overcome the global impact of neglected tropical diseases – A roadmap for implementation, in: D.W.T. Crompton. (Ed.), 2012.
2. WHO, Intensified Control of the Neglected Diseases — Berlin, 10–12 December 2003, in: D.L.S.D.D. Daumerie (Ed.) Report of an international workshop, WHO, 2004, pp. 0-50.
3. L.C. Pollitt, P. MacGregor, K. Matthews*, et al.*, Malaria and trypanosome transmission: different parasites, same rules?, Trends Parasitol, 27 (2011) 197-203.
4. J.A. Engel, A.J. Jones, V.M. Avery*, et al.*, Profiling the anti-protozoal activity of anti-cancer HDAC inhibitors against Plasmodium and Trypanosoma parasites, International Journal for Parasitology: Drugs and Drug Resistance, 5 (2015) 117-126.
5. R.M. Mogire, H.M. Akala, R.W. Macharia*, et al.*, Target-similarity search using Plasmodium falciparum proteome identifies approved drugs with anti-malarial activity and their possible targets, PLOS ONE, 12 (2017) e0186364.
6. V. Jeffers, C. Yang, S. Huang*, et al.*, Bromodomains in Protozoan Parasites: Evolution, Function, and Opportunities for Drug Development, Microbiology and Molecular Biology Reviews, 81 (2017) e00047-00016.
7. N.M. Pazhayam, J. Chhibber-Goel, A. Sharma, New leads for drug repurposing against malaria, Drug Discovery Today, 24 (2019) 263-271.
8. A. Rassi, A. Rassi, J.A. Marin-Neto, Chagas disease, The Lancet, 375 (2010) 1388-1402.
9. C. Gomes, A.B. Almeida, A.C. Rosa*, et al.*, American trypanosomiasis and Chagas disease: Sexual transmission, International Journal of Infectious Diseases, 81 (2019) 81-84.
10. J. Gómez i Prat, P. Peremiquel-Trillas, I. Claveria Guiu*, et al.*, A Community-Based Intervention for the Detection of Chagas Disease in Barcelona, Spain, Journal of Community Health, 44 (2019) 704-711.
11. J.A. Pérez-Molina, I. Molina, Chagas disease, The Lancet, 391 (2018) 82-94.
12. E. Chatelain, Chagas Disease Drug Discovery: Toward a New Era, Journal of Biomolecular Screening, 20 (2014) 22-35.
13. J.A. Urbina, Recent Clinical Trials for the Etiological Treatment of Chronic Chagas Disease: Advances, Challenges and Perspectives, Journal of Eukaryotic Microbiology, 62 (2015) 149-156.
14. M. Sijm, J. Siciliano de Araújo, A. Ramos Llorca*, et al.*, Identification of Phenylpyrazolone Dimers as a New Class of Anti-Trypanosoma cruzi Agents, ChemMedChem, 14 (2019) 1662-1668.
15. M. Sijm, E. de Heuvel, A. Matheeussen*, et al.*, Identification of Phenylphthalazinones as a New Class of Leishmania infantum Inhibitors, ChemMedChem, n/a (2019).
16. J. Bermudez, C. Davies, A. Simonazzi*, et al.*, Current drug therapy and pharmaceutical challenges for Chagas disease, Acta Tropica, 156 (2016) 1-16.
17. P.A. Sales Junior, I. Molina, S.M. Fonseca Murta*, et al.*, Experimental and Clinical Treatment of Chagas Disease: A Review, The American Journal of Tropical Medicine and Hygiene, 97 (2017) 1289-1303.
18. D. Steverding, The history of leishmaniasis, Parasites & Vectors, 10 (2017) 82.
19. A. Hailu, D.A. Dagne, M. Boelaert, Leishmaniasis, in: J. Gyapong, B. Boatin (Eds.) Neglected Tropical Diseases - Sub-Saharan Africa, Springer International Publishing, Cham, 2016, pp. 87-112.
20. E. Torres-Guerrero, M.R. Quintanilla-Cedillo, J. Ruiz-Esmenjaud*, et al.*, Leishmaniasis: a review, F1000Res, 6 (2017) 750-750.
21. R. Reithinger, J.-C. Dujardin, H. Louzir*, et al.*, Cutaneous leishmaniasis, The Lancet Infectious Diseases, 7 (2007) 581-596.
22. H.W. Murray, J.D. Berman, C.R. Davies*, et al.*, Advances in leishmaniasis, The Lancet, 366 (2005) 1561-1577.
23. S.L. Croft, S. Sundar, A.H. Fairlamb, Drug Resistance in Leishmaniasis, Clinical Microbiology Reviews, 19 (2006) 111.
24. R. Balaña-Fouce, M.Y. Pérez Pertejo, B. Domínguez-Asenjo*, et al.*, Walking a tightrope: drug discovery in visceral leishmaniasis, Drug Discovery Today, 24 (2019) 1209-1216.
25. M.A. Phillips, D.E. Goldberg, Toward a chemical vaccine for malaria, Science, 362 (2018) 1112.
26. A. Pance, How elusive can a malaria vaccine be?, Nature Reviews Microbiology, 17 (2019) 129-129.
27. H. Noedl, Y. Se, K. Schaecher*, et al.*, Evidence of Artemisinin-Resistant Malaria in Western Cambodia, New England Journal of Medicine, 359 (2008) 2619-2620.
28. D.A. van Schalkwyk, C.J. Sutherland, Malaria resistance to non-artemisinin partner drugs: how to reACT, The Lancet Infectious Diseases, 15 (2015) 621-623.
29. M. Sijm, J. Siciliano de Araújo, S. Kunz*, et al.*, Phenyldihydropyrazolones as Novel Lead Compounds Against Trypanosoma cruzi, ACS Omega, 4 (2019) 6585-6596.

30. S. King-Keller, M. Li, A. Smith*, et al.*, Chemical Validation of Phosphodiesterase C as a Chemotherapeutic Target in Trypanosoma cruzi, the Etiological Agent of Chagas' Disease, Antimicrobial Agents and Chemotherapy, 54 (2010) 3738.

31. H. Wang, Z. Yan, J. Geng*, et al.*, Crystal structure of the Leishmania major phosphodiesterase LmjPDEB1 and insight into the design of the parasite-selective inhibitors, Mol Microbiol, 66 (2007) 1029-1038.

32. A. Johner, S. Kunz, M. Linder*, et al.*, Cyclic nucleotide specific phosphodiesterases of Leishmania major, BMC Microbiol, 6 (2006) 25-25.

33. V. Sebastián-Pérez, S. Hendrickx, J.C. Munday*, et al.*, Cyclic Nucleotide-Specific Phosphodiesterases as Potential Drug Targets for Anti-Leishmania Therapy, Antimicrobial Agents and Chemotherapy, 62 (2018) e00603-00618.

34. C. Flueck, L.G. Drought, A. Jones*, et al.*, Phosphodiesterase beta is the master regulator of cAMP signalling during malaria parasite invasion, PLOS Biology, 17 (2019) e3000154.

35. C. Jansen, H. Wang, A.J. Kooistra*, et al.*, Discovery of NovelTrypanosoma bruceiPhosphodiesterase B1 Inhibitors by Virtual Screening against the Unliganded TbrPDEB1 Crystal Structure, Journal of Medicinal Chemistry, 56 (2013) 2087-2096.

36. E. de Heuvel, A.K. Singh, E. Edink*, et al.*, Alkynamide phthalazinones as a new class of TbrPDEB1 inhibitors, Bioorganic & Medicinal Chemistry, 27 (2019) 3998-4012.

37. E. de Heuvel, A.K. Singh, P. Boronat*, et al.*, Alkynamide phthalazinones as a new class of TbrPDEB1 inhibitors (Part 2), Bioorganic & Medicinal Chemistry, 27 (2019) 4013-4029.

38. C. Courtens, M. Risseeuw, G. Caljon*, et al.*, Amino acid based prodrugs of a fosmidomycin surrogate as antimalarial and antitubercular agents, Bioorganic & Medicinal Chemistry, 27 (2019) 729-747.

39. C. Carmi, A. Lodola, S. Rivara*, et al.*, Epidermal Growth Factor Receptor Irreversible Inhibitors: Chemical Exploration of the Cysteine-Trap Portion, Mini-Reviews in Medicinal Chemistry, 11 (2011) 1019-1030.

40. S.R. Klutchko, H. Zhou, R.T. Winters*, et al.*, Tyrosine Kinase Inhibitors. 19. 6-Alkynamides of 4-Anilinoquinazolines and 4-Anilinopyrido[3,4-d]pyrimidines as Irreversible Inhibitors of the erbB Family of Tyrosine Kinase Receptors, Journal of Medicinal Chemistry, 49 (2006) 1475-1485.

41. G. Wuitschik, M. Rogers-Evans, K. Müller*, et al.*, Oxetanes as Promising Modules in Drug Discovery, Angewandte Chemie International Edition, 45 (2006) 7736-7739.

42. G. Wuitschik, M. Rogers-Evans, A. Buckl*, et al.*, Spirocyclic Oxetanes: Synthesis and Properties, Angewandte Chemie International Edition, 47 (2008) 4512-4515.

6
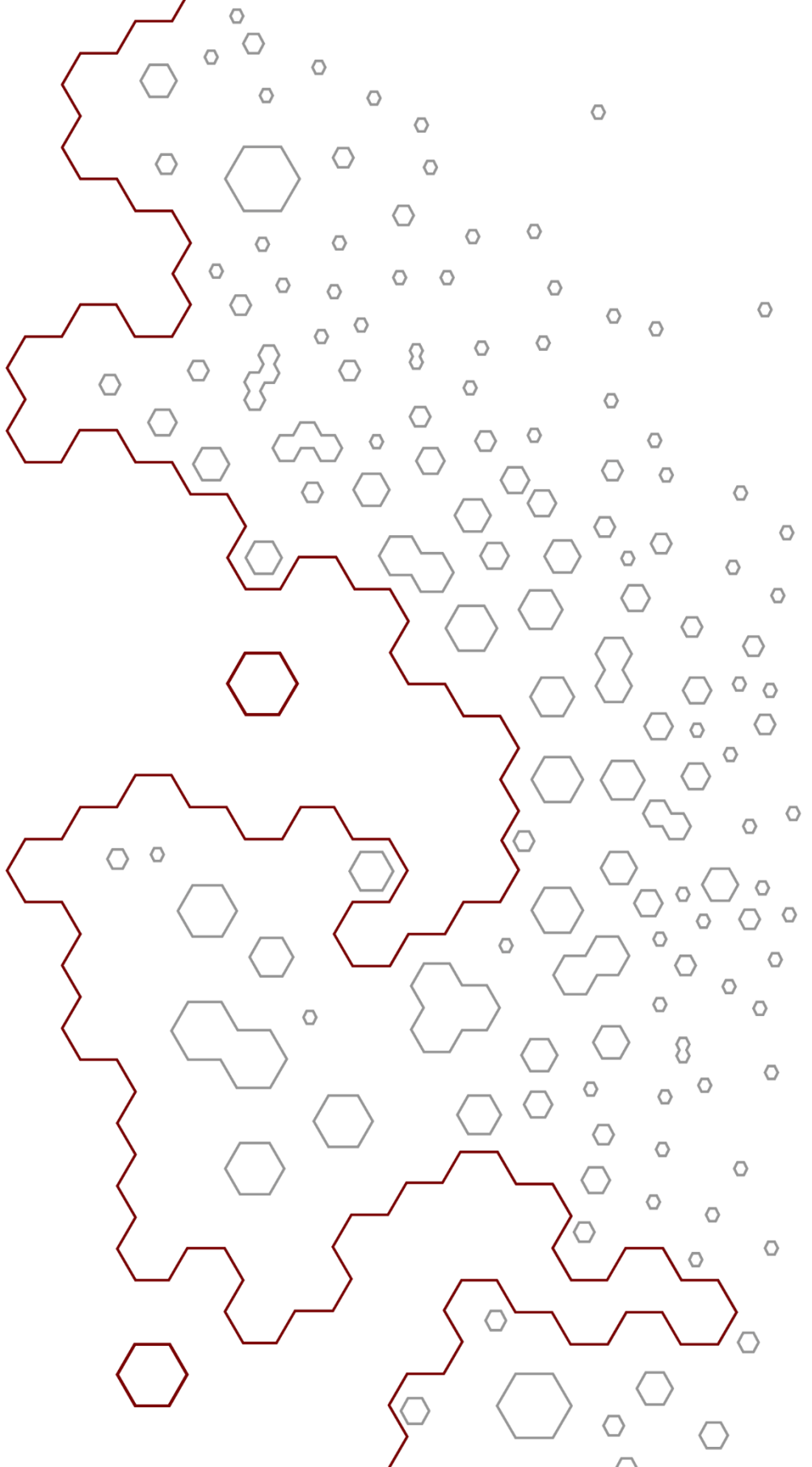
Chapter 7

Discussion and concluding remarks

1. General

The road map "*Accelerating work to overcome the global impact of neglected tropical diseases*" introduced by the WHO in 2012 specified global targets and milestones to prevent, control or even eradicate several listed neglected tropical diseases.[1] The renewed interest in these diseases has stimulated the discovery and development of new therapeutics. In the case of human African trypanosomiasis, this led to the approval of fexinidazole by the EMA as new treatment for *T. brucei gambiense* infections and the development of Acoziborole that is now in the last stages of clinical trials.[2-5] Both treatments show promising results and are significant improvements when compared with the infamous arsenic-containing drug Melarsoprol. However, since simple and efficient therapeutic options for human African trypanosomiasis are still limited, new leads for future medicine are still desired.

The research described in this thesis was focussed on the development such treatment by developing selective inhibitors of the parasite TbrPDEB1/2 enzyme via a repurposing methodology. Application of this method, in which inhibitors and clinical candidates that were developed for related human enzymes (e.g., hPDE4) are used to inhibit the pathogen's target. The development of a new drug is often less costly and less time consuming. By building on the medicinal chemistry and biochemistry knowledge of the previously explored human homologues, the repurposing approach can lead to an efficient and accelerated drug discovery program for the new (parasite) target.[6] The high structural similarity and identical cellular function of human hPDE4 and TbrPDEB1/2 seemed ideal for such effort. However, obtaining TbrPDEB1/2 selectivity over hPDE4 is deemed essential.[7, 8] Elucidation of the crystal structure of LmjPDEB1 in complex with IBMX provided the first insights in structural differences between human and parasite PDEs.[9] Close examination of the structure revealed the presence of an additional pocket near the active site of LmjPDEB1.[9] The design of homology models showed that this pocket is most likely also present in TbrPDEB1/2.[7, 10] It was hypothesized that the close proximity of the P-pocket to the active site might offer a valuable approach to obtain selectivity over the human homologue. [7, 9, 11, 12]

Our approach by iterative cycles of drug design led to the development of the first series of TbrPDEB1 inhibitors with a greatly improved selectivity index (**Chapter 2**). Close analysis of the crystal structures of NPD-001 in TbrPDEB1 revealed that the

ligand adopts a folded conformation (undergoing a hydrophobic collapse). It was hypothesized that selectivity over hPDE4 could be obtained by introduction of a rigid linker, pointing towards the P-pocket while properly positioning the known hPDE4 tetrahydrophthalazinone scaffold in the hydrophobic clamp of the enzyme (leading to a biphenyl phthalazinone series). As a first design idea, a phenyl linker was installed on the 3-position of the anisole in NPD-001. Although this modification directly led to an improved activity profile for TbrPDEB1 over hPDE4, it still affected the affinity for TbrPDEB1 and the antiparasitic activity against *T. brucei* parasites. A reduction in potency for TbrPDEB1 of a 25-fold and a 250-fold reduction in antiparasitic activity was observed for the best in class biphenyl phthalazinone. The hPDE4 activity was, luckily, reduced even more (1600-fold), resulting in an improved selectivity profile. Unfortunately, cellular cytotoxicity against MRC-5 cells was also increased. A first effort to compensate for this change in cytotoxicity profile by installing an ether functionality (**Chapter 3**) resulted in a reduction of cytotoxicity, but a complete loss of selectivity over hPDE4 and the moderate activity against *T. brucei* halted further research on this class of compounds. Efforts to further modify and optimize the linker and tail groups resulted in the alkynamide series of compounds that displayed some selectivity for TbrPDEB1 over hPDE4 and retained most of its activity in cellular assays (**Chapter 4 + 5**). The cytotoxicity profile was also improved when compared with the biphenyl series, but the activity in the biochemical assay was slightly reduced. As often observed in medicinal chemistry, changing one fragment of the molecule can benefit one property, but come with a negative effect on another important drug-like property. In this chapter I would like to focus on and discuss several of the observations and results of our research which could hopefully benefit future design of TbrPDEB1 inhibitors.

2.   Chemistry

Based on the synthetic approach, the structure of all compounds described in this thesis can be divided in 4 different fragments accessible for structural modifications, i.e. the tetrahydrophthalazinone core, the anisole, the linker and the tail group (Figure 1). The applied synthetic route allows introduction of different functionalities in the phthalazinone and anisole moiety in the first steps of the synthesis, while introduction of different structural features in the linker and tail group are applied in the later stages of the synthesis.
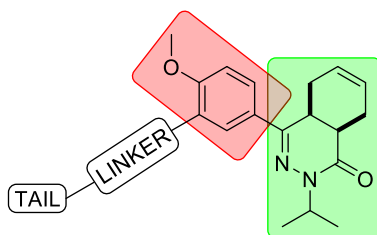
Figure 1: Schematic overview of the 4 different fragments of the compounds described in this thesis: Tetrahydrophthalazinone core (green), anisole (red), linker and the tail group.

2.1. The phthalazinone core and anisole moiety

All of the compounds reported in this thesis were synthesized with a tetrahydrophthalazinone core that was already investigated extensively in a series of hPDE4 inhibitors.[13-15] A series of tetrahydrophthalazinones was synthesized by Van de Mey *et al*. resulting in subnanomolar activities on hPDE4.[14] A similar activity was observed for the non-selective TbrPDEB1 inhibitor NPD-001, which was then used for further optimization. However, the tetrahydrophthalazinone does not have any apparent hydrogen bonding interaction with the proteins in the crystal structures of NPD-001 in complex with TbrPDEB1 or hPDE4, and therefor this scaffold seems not too essential for binding. Nonetheless, small modifications and variations on the phthalazinone core resulted in decreased activities for TbrPDEB1 and hPDE4.[8, 14] The spatial conformation of the tetrahydrophthalazinone seems to be essential for its activity, which is confirmed by 100-fold difference in binding affinity between the two optical isomers of **1** (Figure 2).

1a	1b
TbrPDEB1 pK_i = 5.4	TbrPDEB1 pK_i = 7.4
hPDE4B1 pK_i = 4.3	hPDE4B1 pK_i = 6.2
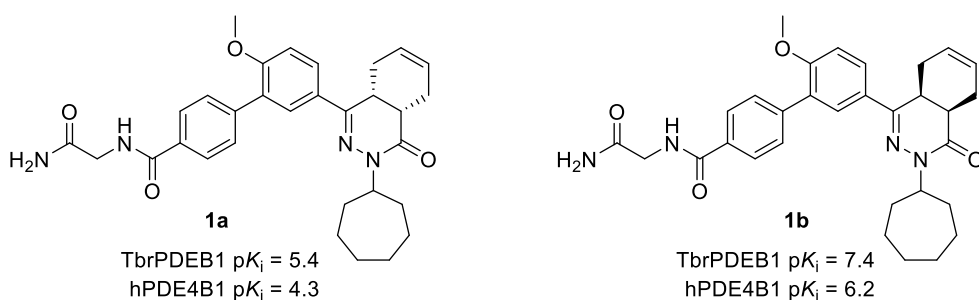
Figure 2: Inhibitory activity on TbrPDEB1 and hPDE4B1 of the two optical isomers of **1.**

The physicochemical properties of the phenylphthalazinone core are not optimal as a starting point. The core structure consists of several hydrophobic regions (e.g. cycloheptyl, cyclohexene, anisole) which combines to a scaffold with a relatively high cLogP for the unsubstituted core structure. This lipophilic bulk is not easily

compensated by installing hydrophilic groups on the linker and tail towards the P-pocket. The relatively high cLogP for most tetrahydrophthalazinones can facilitate the binding to the TbrPDEB1 protein, since it has a hydrophobic active site. However, this lipophilic character can lead to issues in a later stage of drug development caused by a higher chance of unfavorable metabolism and toxicity.[16, 17]

Replacing the cycloheptyl for an isopropyl substituent on the phthalazinone is a successful first step towards compounds with a lower cLogP. As shown with multiple compounds in the phenylamide and the alkynamide series, this simple modification to reduce the cLogP has no significant effect on the activity. Within the PDE4NPD program, modifications on the phthalazinone nitrogen atom with large substituents has been investigated by Salado et al., resulting in several compounds with good biochemical and cellular activities and a relatively low LogP.[18] It can be conceived that attachment of solubilizing groups is an interesting solution to lower the cLogP. Combination of results found by Salado et al. and our approach to obtain selectivity can potentially lead to better soluble and more selective TbrPDEB1 inhibitors. Although such a strategy will definitely lead to large molecules exceeding the threshold for molecular weight in Lipinski's rule of 5, improving the cLogP is often more important in drug development than limiting the molecular weight.[19]

Several new selective hPDE4 inhibitors containing a similar catechol moiety as our core scaffold have been discovered over the last few decades. A similar approach based on the linker that was present in NPD-001 was performed by Amata et al.[20] These authors combined the core structure of Cilomilast (**2**, Figure 3), a selective hPDE4 inhibitor that failed to reach the clinic, with the flexible phenyltetrazole tail of NPD-001.[20, 21] Although some improvement in activity for TbrPDEB1 was observed, selectivity over hPDE4 was not obtained. The chemical similarity between Cilomilast and our phenylphthalazinone suggests that our findings in obtaining selectivity might be transferable to this scaffold.

Cilomilast, **2**   GSK-256066, **3**   Apremilast, **4**
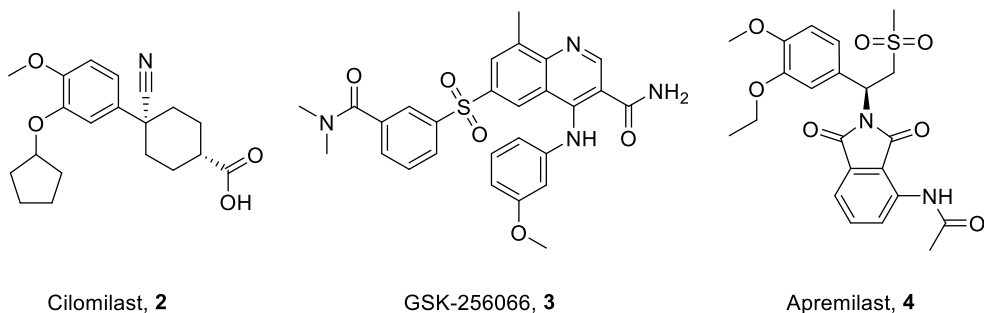
Figure 3: Structures of hPDE4 inhibitors.

The challenge in repurposing inhibitors for hPDE4 towards TbrPDEB1 is also demonstrated by Ochiana *et al.*[22] An extensive synthetic effort starting from hPDE4 inhibitor GSK-256066 (**3**) to find selective TbrPDEB1 inhibitors resulted in analogues with good biochemical and phenotypic potency. A docking exercise predicted successful P-pocket targeting, but selectivity was not observed for any of the measured analogues. Another recently discovered selective hPDE4 inhibitor that has similar structural features to NPD-001 and Cilomilast is Apremilast (**4**). This nanomolar inhibitor of hPDE4 was approved by the FDA in 2014 to treat adults with active psoriatic arthritis.[23-25] To date this scaffold has not been reported in literature for a similar repurposing study. However, unpublished results from our lab show that Apremilast has no significant inhibitory activity against the enzyme TbrPDEB1 ($pK_i < 5.0$) nor on *T. brucei* parasites ($pEC_{50} < 4.2$). This shows that selectivity can also be obtained by changing the core structure in the metal binding site, although, in this case, the selectivity is greatly in favour of hPDE4. The differences in the metal binding site between hPDE4 and TbrPDEB1 are small. Nevertheless computational methods could be used to screen for new substructures with the purpose of obtaining selectivity for TbrPDEB1.

2.2. Strategy of the linker variations

2.2.1. Phenyl linker

Several different linkers which had variations in length, shape and directionality of the tail group were investigated for efficient P-pocket targeting. The choice of a phenylamide led to a direct success in obtaining selectivity, but also a loss in cellular activity. From a medicinal chemistry point of view the choice of implementing a phenylamide as linker was a logical first choice. It is commonly stable under many different reaction conditions and synthetic methods to introduce phenyl moieties are robust and broadly applicable. Furthermore, building blocks with a variety of

functional groups on the phenyl ring are often cheap and readily available at commercial suppliers allowing fast and efficient modification and functionalization of the core scaffold. From a physicochemical perspective the phenylamide is a less optimal group for further optimization as it makes the overall tetrahydrophthalazinone structure even more flat and lipophilic, which is detrimental for the solubility in aqueous media. Furthermore, the flat and lipophilic character makes this class of compounds more prone to metabolism and toxic side effects.[16, 17] Unfortunately, small modifications on the phenyl ring immediately led to a decreased activity for TbrPDEB1. Common modifications to influence the ADME properties of a compounds, such as fluor atoms on the aromatic ring, were not allowed. These limitations in ring functionalization could hamper further development of this chemical class.

2.2.2. Alkynamide linker

Another linker that induced an improved selectivity index when compared to NPD-001 was the alkynamide. Similar to the phenyl linker, the triple bond offers a straight vector towards the P-pocket, but is smaller in size and length. As a result of this reduced length, the alkynamide series displays a new interaction with key residue Glu869 that forms a key interaction with the catechol group of the inhibitors. The co-crystal structures of the alkynamide series in TbrPDEB1 reveals that Glu869 forms a bidentate interaction with the ligands. Although this new interaction does not result in a notable improvement in binding affinity, it could be of interest for further design in the alkynamide series. In the biphenyl series, crystal structures show that the amide carbonyl is not involved in direct interactions with the protein (Figure 4), but mostly with the water network of the protein. The overall orientation of the amide carbonyl functionality in the biphenyl series shows greater variability when compared to the amide carbonyl of the alkynamide series. This additional interaction locks the amide of the alkynamide series in a position which seems suitable for direct P-pocket targeting.
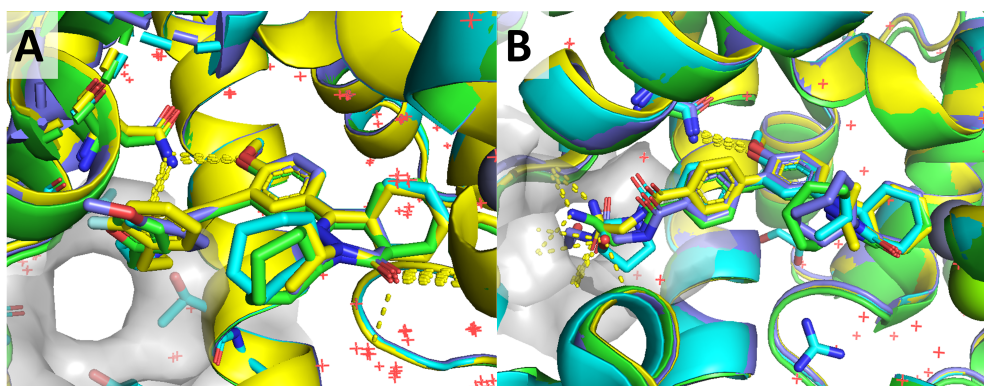
Figure 4: A) Overlay of the published alkynamide tetrahydrophthalazinones in TbrPDEB1 with a double interaction with Glu869, but no interactions in the P-pocket region. B) Overlay of all published biphenyl tetrahydrophthalazinones in TbrPDEB1 with interactions in the P-pocket region.

The crystal structures also show the difficulty of such endeavor, since none of the co-crystallized alkynamides was truly targeting the P-pocket region. The positioning of the tail-group towards the hydrophobic cycloheptane of the ligand, where the tail can also interact with lipophilic residues in the solvent exposed site of the receptor, was clearly favored over P-pocket occupation. This results in binding modes that are also seen for NPD-001. Functionalization of the remaining 'free' position of the amide nitrogen atom could be a possible solution to this, since it is positioned directly towards the P-pocket. Simple modification of the amide with small (methyl, ethyl, isopropyl) could give a good indication if such approach could be viable (Figure 5). Although some methylated amides were included in the design strategy, the current synthetic route was less successful for secondary amines and no double functionalized amides besides the reported cyclic structures could be obtained during the project described in this thesis.
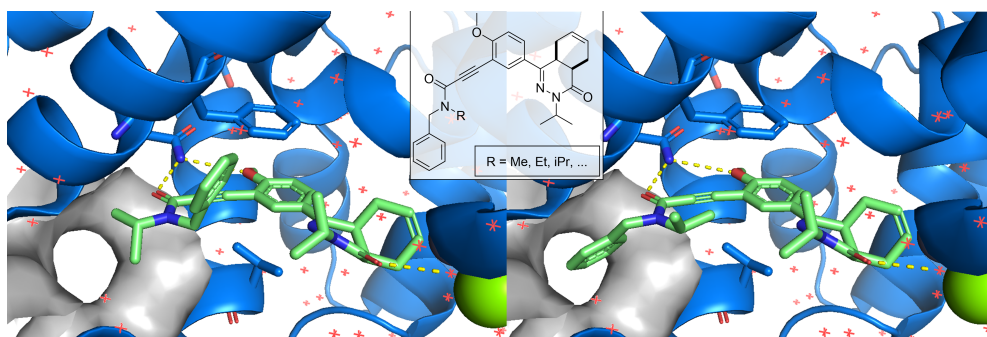
Figure 5: Structural representation of additional alkyl functionality on alkynamide nitrogen atom. The two rotamers of *iso*-propylated NPD-1335 are shown as example. Ligands were built in the protein site, no additional docking studies or other CADD studies were performed to generate this figure.

7

As briefly discussed in **Chapter 6**, the alkynamide functionality has potential shortcomings for further development. It can act as a Michael acceptor and this chemical reactivity can possibly lead to idiosyncratic adverse drug reactions.[26] The alkynamide has been successfully exploited for this purpose in several covalent inhibitor studies.[27-30] An LCMS-based incubation study of three alkynamides in PBS buffer with glutathione (unpublished data) shows that the alkynamide phthalazinone scaffold reacts slowly with glutathione in absence of glutathione transferase (<5% conversion after 24 h for all three tested compounds). Unfortunately, a first attempt to reduce the Michael accepting properties by installing an oxetane as carbonyl bio-isostere was shown unsuccessful as the resulting compounds showed reduced potency for TbrPDEB1 and a greatly reduced activity on *T. brucei*.

2.2.3. [1.1.1]-bicyclopentane linker

As shown in **Chapter 4** the directionality of the linker moiety is important for affinity towards TbrPDEB1. Most of the non-linear linkers gave a greatly reduced activity, making them less interesting for further research. So far only the *para*-substituted phenylamide and the alkynamide linkers give good potency. Both classes have their advantages and disadvantages, but none seems to excel as the better choice. The shorter, less lipophilic and more compact alkynamide seems more efficient in binding to key-residues in the active site. However, the lack of efficient P-pocket targeting seems detrimental for obtaining a good selectivity profile. Unfortunately, not many chemical structures show similarities in length, spatial filling and linearity with the *para*-substituted phenyl or alkyne functionalities. One structural moiety which is gaining interest in medicinal chemistry over the last decade is [1.1.1]-bicyclopentane. This structure has been proposed as phenyl bio-isostere with a positive effect on the solubility and physicochemical properties.[31-33] Incorporation of this linker might be the perfect cross over between the alkynamide and phenylamide classes (Figure 6A). The length between the bridgehead carbons is slightly longer than an alkyne, but shorter than two opposing phenyl carbons (Figure 6B),[34, 35] making it potentially long enough for efficient P-pocket targeting while being short enough to position the amide for an additional interaction with Glu869. The number of publications including synthetic pathways to include such moieties is slowly increasing,[36-39] but thus far it remains a synthetic challenge to

incorporate the [1.1.1]-bicyclopentane as linker in our tetrahydrophthalazinone series as initial efforts have failed so-far.
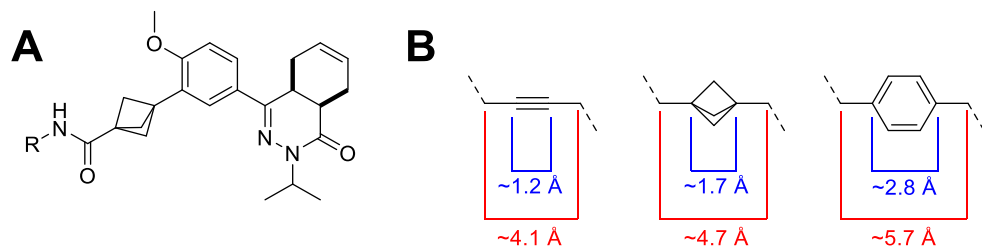
Figure 6: A) Structure of tetrahydrophthalazinone with bicyclo[1.1.1]-pentane as linker functionality. B) Overview of the different C-C distances of the alkyne, bicyclo[1.1.1]-pentane and phenyl group.

2.3. Tail group modifications

A variety of linkers and tail groups were used in all chemical classes, with the intention to probe binding to the P-pocket. The effect of a misdirected linker was immediately apparent and resulted in low potency for TbrPDEB1, but the effect of different tail groups was not directly visible. The largest variety of tail groups was tested in the alkynamide series, which resulted in a large number of molecules with comparable activities. Although a small preference for aromatic moieties was observed, most alkynamides displayed affinities around 1 μM. The similarity in binding pose of the molecules crystallized in TbrPDEB1 might explain the absence of a clear SAR for this class. Despite the seemingly good positioning of the alkynamide nitrogen in front of the P-pocket, none of the co-crystallized molecules address the P-pocket. The inability to address the P-pocket might be caused by the flexibility of the M-loop, which forms the P-pocket, preventing efficient binding of the ligands in the pocket caused by the variation in size. This effect was also observed in the molecular dynamics study performed on the phenyl glycinamide **8** (**Chapter 2**). The glycinamide tail showed good P-pocket targeting in the co-crystal structure with several interactions with the protein and water network, but in a MD study (unpublished data by Ton Blaazer) this conformation was altered with a conformation where the tail group was directing the solvent exposed site. This phenomenon could be the result of a possible large entropic penalty when the tail group is locked in the p-pocket. However, reduction of the flexibility of the tail group by cyclization to lock the compound in the correct conformation and thereby reducing the entropic penalty did not result in an increased affinity or selectivity. Unfortunately, computational efforts to predict successful chemical entities to target the P-pocket have not resulted in selective compounds. In both cases a static

P-pocket was used to reduce the needed computer power and accelerate the docking process. The actual flexibility of the P-pocket might impair the successfulness of finding tail groups via computational methods. Computational efforts to this end might benefit from including molecular dynamics to compensate for the flexibility of the P-pocket.

2.4. Selectivity towards TbrPDEB1

The flexibility of the P-pocket region makes it a very difficult cavity to target efficiently. As shown, obtaining selectivity over hPDE4 by targeting the P-pocket is possible. Although the affinity for TbrPDEB1 does not increase, these compounds have significantly reduced affinity for hPDE4, leading to an improved selectivity index. Modifications of the tail or linker group often resulted in a larger decrease in hPDE4 affinity rather than an increase in TbrPDEB1 affinity. Since the P-pocket region is the largest difference between the two PDEs it is tempting to solely focus on the P-pocket for activity. However, as observed in the biphenyl series, small gains in selectivity or activity can be obtained by modification on different parts of the molecule, such as the isopropyl or cycloheptyl substituents. Compared to NPD-001, the core structure has not changed while small changes could optimize the binding affinity for TbrPDEB1. Using the identified phenylamide and alkynamide selectivity handles, future research could focus on optimizing the binding of the phthalazinone core to selectively improve the affinity for TbrPDEB1.

The information obtained from the numerous crystal structures of the rigidified compounds in TbrPDEB1 and hPDE4 could be of great value for the design of new compounds. A new design strategy could start from the selectivity handles (anisole moiety with either alkynamide or phenylamide linker) as core structure (Figure 7), as incorporation of these moieties resulted in various compounds with a (slightly) positive selectivity index. Using a computational design approach or a fragment growing approach towards the metal-binding site in TbrPDEB1 could lead to new compound classes that are structurally different from the hPDE4 substructures and show a higher selectivity towards TbrPDEB1.
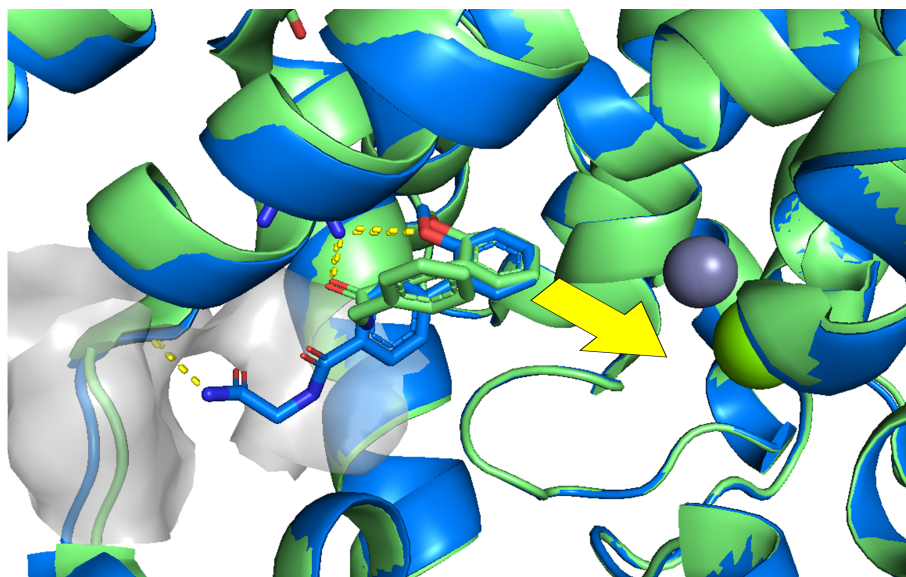
Figure 7: Possible design strategy based on the crystal structures of biphenyl or alkynamide selectivity handles. Crystal structure of alkynamide NPD-1335 in TbrPDEB1 (PDB: 6GXQ) shown in green and crystal structure of biphenylamide NPD-008 in TbrPDEB1 (PDB: 5G2B) shown in blue.

3.   Overall conclusion

The work described in this thesis shows the successful exploitation of the parasite specific P-pocket for obtaining TbrPDEB1 more selective inhibitors. Repurposing of a known hPDE4 inhibitor (NPD-001) was proven to be successful by implementing various selectivity handles. Two compound classes containing rigid linkers (phenylamide and alkynamide phthalazinones) were identified of which the compounds displayed some selectivity for TbrPDEB1 over hPDE4. Where selectivity observed in the phenylamide class is related to the successful targeting of the P-pocket, the origin of the selectivity observed by the alkynamide group was less apparent. Our results show that obtaining selectivity by addressing the P-pocket is possible and a viable route for obtaining selective TbrPDEB1 inhibitors, but at the same time the difficulty of targeting this flexible region was also shown. The obtained crystal structures will provide valuable insight for future efforts to find selective TbrPDEB1 inhibitors. The success and the applicability of repurposing hPDE4 inhibitors was also shown by extending the biological screening towards taxonomically related parasites (*T. cruzi* and *L. inf*., **Chapter 6**). The first steps in the search for selective PDE inhibitors with anti-parasitic activity were successful, but further development is still facing numerous challenges ahead.

7

4.   References

1. WHO, Accelerating work to overcome the global impact of neglected tropical diseases – A roadmap for implementation, in: D.W.T. Crompton. (Ed.), 2012.

2. A.K. Lindner, V. Lejon, F. Chappuis, *et al.*, New WHO guidelines for treatment of gambiense human African trypanosomiasis including fexinidazole: substantial changes for clinical practice, Lancet Infect Dis, 20 (2020) e38-e46.

3. DNDi Acoziborole, https://www.dndi.org/diseases-projects/portfolio/scyx-7158/; Accessed on 01-05-2018

4. E.D. Deeks, Fexinidazole: First Global Approval, Drugs, 79 (2019) 215-220.

5. E. Pelfrene, M. Harvey Allchurch, N. Ntamabyaliro, *et al.*, The European Medicines Agency's scientific opinion on oral fexinidazole for human African trypanosomiasis, PLOS Neglected Tropical Diseases, 13 (2019) e0007381.

6. M.P. Pollastri, R.K. Campbell, Target repurposing for neglected diseases, Future medicinal chemistry, 3 (2011) 1307-1315.

7. K.M. Orrling, C. Jansen, X.L. Vu, *et al.*, Catechol pyrazolinones as trypanocidals: fragment-based design, synthesis, and pharmacological evaluation of nanomolar inhibitors of trypanosomal phosphodiesterase B1, Journal of Medicinal Chemistry, 55 (2012) 8745-8756.

8. J. Veerman, T. van den Bergh, K.M. Orrling, *et al.*, Synthesis and evaluation of analogs of the phenylpyridazinone NPD-001 as potent trypanosomal TbrPDEB1 phosphodiesterase inhibitors and in vitro trypanocidals, Bioorganic & Medicinal Chemistry, 24 (2016) 1573-1581.

9. H. Wang, Z. Yan, J. Geng, *et al.*, Crystal structure of the Leishmania major phosphodiesterase LmjPDEB1 and insight into the design of the parasite-selective inhibitors, Mol Microbiol, 66 (2007) 1029-1038.

10. N.D. Bland, C. Wang, C. Tallman, *et al.*, Pharmacological validation of Trypanosoma brucei phosphodiesterases B1 and B2 as druggable targets for African sleeping sickness, J Med Chem, 54 (2011) 8188-8194.

11. C. Jansen, A.J. Kooistra, G.K. Kanev, *et al.*, PDEStrIAn: A Phosphodiesterase Structure and Ligand Interaction Annotated Database As a Tool for Structure-Based Drug Design, Journal of Medicinal Chemistry, 59 (2016) 7029-7065.

12. C. Jansen, H. Wang, A.J. Kooistra, *et al.*, Discovery of NovelTrypanosoma bruceiPhosphodiesterase B1 Inhibitors by Virtual Screening against the Unliganded TbrPDEB1 Crystal Structure, Journal of Medicinal Chemistry, 56 (2013) 2087-2096.

13. M. Van der Mey, A. Hatzelmann, I.J. Van der Laan, *et al.*, Novel Selective PDE4 Inhibitors. 1. Synthesis, Structure-Activity Relationships, and Molecular Modeling of 4-(3, 4-Dimethoxyphenyl)-2 H-phthalazin-1-ones and Analogues, Journal of Medicinal Chemistry, 44 (2001) 2511-2522.

14. M. Van der Mey, A. Hatzelmann, G.P.M. Van Klink, *et al.*, Novel Selective PDE4 Inhibitors. 2. Synthesis and structure-activity relationships of 4-aryl-substituted cis-tetra- and cis-hexahydrophthalazinones, Journal of Medicinal Chemistry, 44 (2001) 2523-2535.

15. N. Vila, P. Besada, T. Costas, *et al.*, Phthalazin-1(2H)-one as a remarkable scaffold in drug discovery, Eur J Med Chem, 97 (2015) 462-482.

16. F. Lovering, Escape from Flatland 2: complexity and promiscuity, MedChemComm, 4 (2013) 515-519.

17. F. Lovering, J. Bikker, C. Humblet, Escape from flatland: increasing saturation as an approach to improving clinical success, J Med Chem, 52 (2009) 6752-6756.

18. I.G. Salado, A.K. Singh, C. Moreno-Cinos, *et al.*, Lead Optimization of Phthalazinone Phosphodiesterase Inhibitors as Novel Antitrypanosomal Compounds, J Med Chem, 63 (2020) 3485-3507.

19. C.P. Tinworth, R.J. Young, Facts, Patterns, and Principles in Drug Discovery: Appraising the Rule of 5 with Measured Physicochemical Data, J Med Chem, (2020).

20. E. Amata, N.D. Bland, C.T. Hoyt, *et al.*, Repurposing human PDE4 inhibitors for neglected tropical diseases: Design, synthesis and evaluation of cilomilast analogues as Trypanosoma brucei PDEB1 inhibitors, Bioorganic & Medicinal Chemistry Letters, 24 (2014) 4084-4089.

21. D.W. Baeumer, P.I. Szelenyi, P.M. Kietzmann, Cilomilast, an orally active phosphodiesterase 4 inhibitor for the treatment of COPD, Expert Review of Clinical Immunology, 1 (2005) 27-36.

22. S.O. Ochiana, N.D. Bland, L. Settimo, *et al.*, Repurposing human PDE4 inhibitors for neglected tropical diseases. Evaluation of analogs of the human PDE4 inhibitor GSK-256066 as inhibitors of PDEB1 of Trypanosoma brucei, Chemical Biology & Drug Design, (2014).

23. L. Fala, Otezla (Apremilast), an Oral PDE-4 Inhibitor, Receives FDA Approval for the Treatment of Patients with Active Psoriatic Arthritis and Plaque Psoriasis, American Health & Drug Benefits, 8 (2015) 105-110.

24. H.-W. Man, P. Schafer, L.M. Wong, *et al.*, Discovery of (S)-N-{2-[1-(3-Ethoxy-4-methoxyphenyl)-2-methanesulfonylethyl]-1,3-dioxo-2,3-dihydro-1H-isoindol-4-yl}acetamide (Apremilast), a Potent and Orally

Active Phosphodiesterase 4 and Tumor Necrosis Factor-α Inhibitor, Journal of Medicinal Chemistry, 52 (2009) 1522-1524.

25. P.H. Schafer, A. Parton, L. Capone*, et al.*, Apremilast is a selective PDE4 inhibitor with regulatory effects on innate immunity, Cell Signal, 26 (2014) 2016-2029.

26. A.S. Kalgutkar, D.K. Dalvie, Drug discovery for a new generation of covalent drugs, Expert Opinion on Drug Discovery, 7 (2012) 561-581.

27. T. Barf, A. Kaptein, Irreversible protein kinase inhibitors: balancing the benefits and risks, J Med Chem, 55 (2012) 6243-6262.

28. C. Carmi, A. Lodola, S. Rivara*, et al.*, Epidermal growth factor receptor irreversible inhibitors: chemical exploration of the cysteine-trap portion, Mini Rev Med Chem, 11 (2011) 1019-1030.

29. S.R. Klutchko, H. Zhou, R.T. Winters*, et al.*, Tyrosine kinase inhibitors. 19. 6-Alkynamides of 4-anilinoquinazolines and 4-anilinopyrido[3,4-d]pyrimidines as irreversible inhibitors of the erbB family of tyrosine kinase receptors, J Med Chem, 49 (2006) 1475-1485.

30. T.T. Talele, Acetylene Group, Friend or Foe in Medicinal Chemistry, J Med Chem, (2020).

31. I.S. Makarov, C.E. Brocklehurst, K. Karaghiosoff*, et al.*, Synthesis of Bicyclo[1.1.1]pentane Bioisosteres of Internal Alkynes and para-Disubstituted Benzenes from [1.1.1]Propellane, Angew Chem Int Ed Engl, 56 (2017) 12774-12777.

32. G. Costantino, K. Maltoni, M. Marinozzi*, et al.*, Synthesis and biological evaluation of 2-(3'-(1H-tetrazol-5-yl) bicyclo[1.1.1]pent-1-yl)glycine (S-TBPG), a novel mGlu1 receptor antagonist, Bioorg Med Chem, 9 (2001) 221-227.

33. N.D. Measom, K.D. Down, D.J. Hirst*, et al.*, Investigation of a Bicyclo[1.1.1]pentane as a Phenyl Replacement within an LpPLA2 Inhibitor, ACS Med Chem Lett, 8 (2017) 43-48.

34. E. Kleinpeter, A. Frank, Quantification of the Push–Pull Effect in Substituted Alkynes. Evaluation of ±I/±M Substituent Effects in Terms of C≡C Bond Length Variation, The Journal of Physical Chemistry A, 113 (2009) 6774-6778.

35. J.M. Lopchuk, K. Fjelbye, Y. Kawamata*, et al.*, Strain-Release Heteroatom Functionalization: Development, Scope, and Stereospecificity, J Am Chem Soc, 139 (2017) 3209-3226.

36. K. Schwarzer, H. Zipse, K. Karaghiosoff*, et al.*, Highly Regioselective Addition of Allylic Zinc Halides and Various Zinc Enolates to [1.1.1]Propellane, Angew Chem Int Ed Engl, 59 (2020) 20235-20241.

37. D.F.J. Caputo, C. Arroniz, A.B. Durr*, et al.*, Synthesis and applications of highly functionalized 1-halo-3-substituted bicyclo[1.1.1]pentanes, Chem Sci, 9 (2018) 5295-5300.

38. J. Nugent, B.R. Shire, D.F.J. Caputo*, et al.*, Synthesis of All-Carbon Disubstituted Bicyclo[1.1.1]pentanes by Iron-Catalyzed Kumada Cross-Coupling, Angew Chem Int Ed Engl, 59 (2020) 11866-11870.

39. X. Zhang, R.T. Smith, C. Le*, et al.*, Copper-mediated synthesis of drug-like bicyclopentanes, Nature, 580 (2020) 220-226.

7

Appendix

223
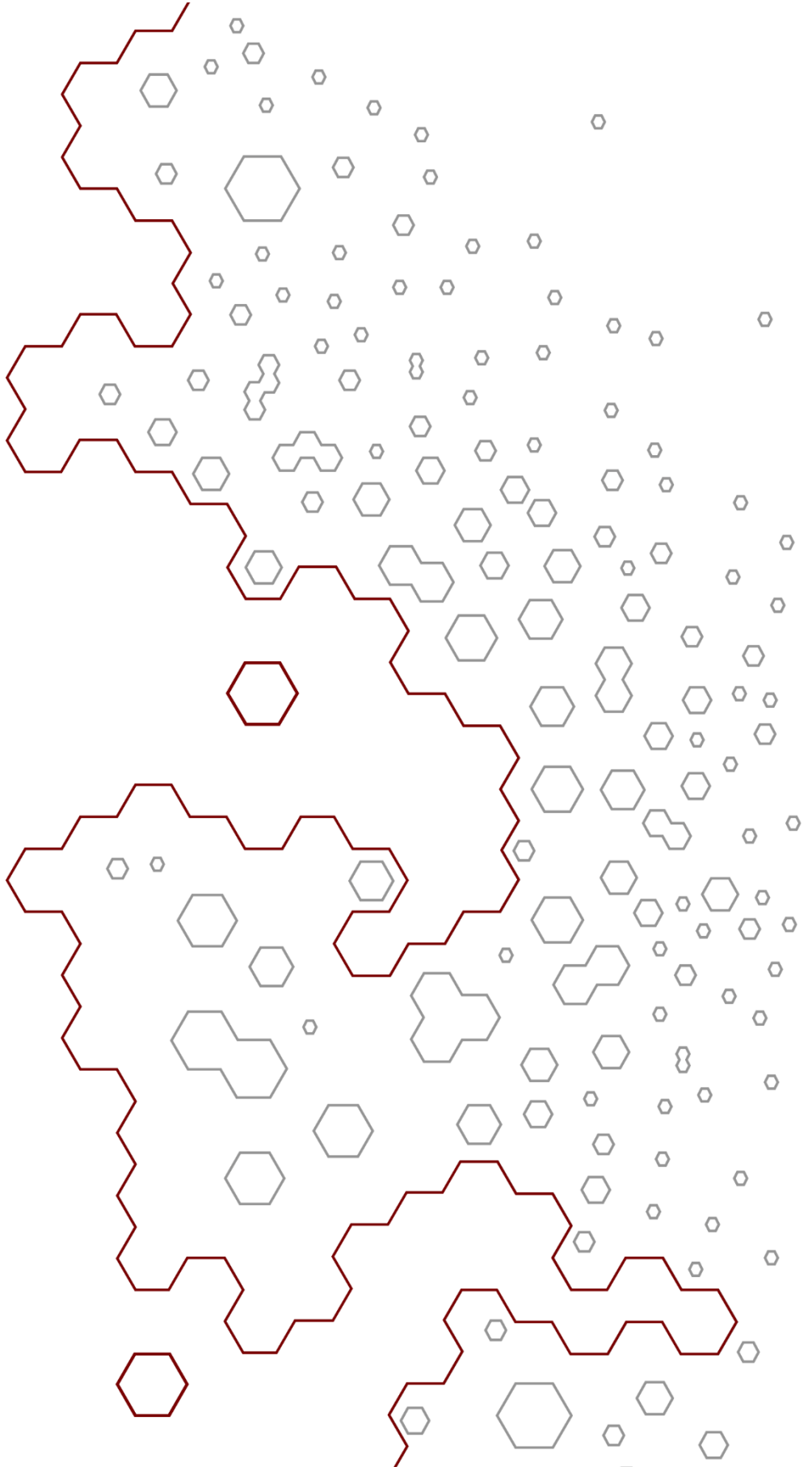
Nederlandse samenvatting

Over de afgelopen eeuwen heeft de 'moderne geneeskunde' (i.e. geneeskunde gebaseerd op wetenschappelijk onderzoek) grote ontwikkelingen doorgemaakt. De mensheid heeft de (moleculaire) basis van vele ziektes weten te ontrafelen en heeft daarnaast, met veel hulp van de natuur, ook methodes gevonden om deze ziektes te voorkomen, te remmen of te behandelen. Echter, ontwikkelingen in onder andere de pathologie hebben ervoor gezorgd dat het aantal geïdentificeerde ziektes verder is toegenomen en dat onderzoeksgeld en –tijd verdeeld moet worden over meer verschillende ziektes. Al deze ziektes verdienen aandacht, maar veel ziektes krijgen niet de aandacht die ze verdienen. Onderzoek naar nieuwe medicijnen is vaak gefocust op ziektes die voorkomen in westerse landen, omdat de ontwikkeling van een nieuw geneesmiddel veel geld kost en die ontwikkelingskosten terugverdiend moeten worden. Ziektes die endemisch zijn in armste landen van de wereld worden hierdoor in meer of mindere mate genegeerd door de farmaceutische industrie. Om meer aandacht te krijgen voor deze ziektes heeft de World Health Organization (WHO) een lijst opgesteld met 19 verschillende ziektes. Deze zogenoemde verwaarloosde ziektes (Engels: '*Neglected tropical diseases*' (NTDs)) hebben samen invloed op de gezondheid van ruim één miljard mensen wereldwijd. Een aantal van deze ziektes wordt veroorzaakt door parasitaire trypanosomen. Deze eencellige organismen veroorzaken onder andere de Afrikaanse slaapziekte (*Trypanosoma brucei*), de ziekte van Chagas (*Trypanosoma cruzi)* en Leishmania (*Leishmania major)*.

Samenwerking van verschillende organisaties en overheidsinstellingen op het gebied van screening en preventie heeft ervoor gezorgd dat het aantal besmettingen en sterftegevallen voor de Afrikaanse slaapziekte (Engels: *Human African Trypanosomiasis*) de afgelopen decennia drastisch is gedaald. Het aantal besmettingen kan echter weer toenemen als er minder aandacht is voor preventie, zoals dat eerder gebeurde in de jaren '90. Op dit moment zijn er maar een zeer beperkt aantal medicijnen beschikbaar voor een vergevorderd ziektestadium van de Afrikaanse slaapziekte en het meest gebruikte medicijn voor dit ziektestadium heeft in veel gevallen ernstige bijwerkingen. Door nieuw onderzoek is er de afgelopen jaren één nieuw medicijn (Fexinidazole) op de markt gekomen en is er op dit moment één kandidaatmedicijn in de late klinische studies (Acoziborole). Vanwege de kans op resistentie en verminderde werkzaamheid van Fexinidazole

ten opzichte van de huidige standaard (Nifurtimox-Eflornitine combinatie behandeling) blijft het wenselijk om nieuwe medicijnen te ontwikkelen.

Er bestaan binnen de farmacochemie verschillende methodes om stoffen met een bepaalde biologische activiteit te identificeren. Een van deze methodes is het zogenaamde herbestemmen van stoffen waarvan eerder al een andere biologische activiteit werd vastgesteld (Engels: *drug repurposing*). Het kan daarbij ook gaan om stoffen die biologische activiteit hebben in de mens, maar die vervolgens ook activiteit hebben op parasieten zoals *Trypanosoma brucei*. Ondanks ogenschijnlijk grote verschillen tussen dieren en parasieten zijn veel belangrijke enzym gekatalyseerde biologische processen hetzelfde, waardoor essentiële eiwitten structureel zeer vergelijkbaar kunnen zijn. Hierdoor kunnen medicijnen die voor de ene ziekte ontwikkeld zijn soms ook toegepast worden op andere ziektes die een zeer vergelijkbare biologische grondslag hebben. Door *drug repurposing* wordt het onderzoek significant versneld en kosten bespaard. Een zeer verwante methodologie genaamd *'scaffold repurposing'* is toegepast in het onderzoek beschreven in dit proefschrift. Deze techniek is gebaseerd op de modificatie van de kernstructuur (Engels: *scaffold*) van de bekende bioactieve stof ten behoeve van activiteit en selectiviteit voor het nieuwe doeleiwit. Het veranderen van de kernstructuur vergt meer synthetische inspanning, maar resulteert idealiter in een selectiever medicijn met minder bijwerkingen.

De fosfodiësterase (PDEs) enzymen is één van de eiwitklassen die gedurende de evolutie in veel organismen een vergelijkbare structuur en functionaliteit hebben behouden. De humane cel kent 11 families (hPDE1-11) die samen zorgen voor de regulering van de concentratie cyclisch AMP (cAMP) and cGMP in de cel. Zowel cAMP als cGMP spelen een belangrijke rol in verschillende cellulaire signaalcascades en zijn daardoor een belangrijke factor in verschillende biologische processen. De cruciale rol van de PDEs in regulering van deze zogenaamde secundaire boodschappers maakt deze klasse van eiwitten een interessant aanknopingspunt voor medicijnontwikkeling. De laatste decennia zijn verschillende humane PDEs remmers op de markt gekomen die als medicijn worden ingezet tegen uiteenlopende ziektes, bijvoorbeeld psoriasis, COPD, erectiestoornissen en hartfalen.

Er is al veel onderzoek gedaan naar de individuele humane PDEs en waaronder dus ook hPDE4. Humaan PDE4 is een eiwit dat in veel verschillende cellen en weefsels

tot expressie komt, bijvoorbeeld in leukocyten, endotheel-, spier- en hersencellen. Dit heeft geresulteerd in verschillende medicijnen die worden gebruikt in de behandeling van bijvoorbeeld COPD (Rolfumilast), psoriasis artritis (Apremilast) en constitutioneel eczeem (Crisaborole). Daarnaast verwacht men dat hPDE4-remmers ook een belangrijke rol kunnen gaan spelen in ziektes gerelateerd aan het centrale zenuwstelsel, zoals multiple sclerosis of depressie. Toch wordt remming van hPDE4 ook geassocieerd met vervelende bijwerkingen, waaronder misselijkheid en braken. Door het vele onderzoek dat naar PDE enzymen gedaan wordt is er een grote hoeveelheid data beschikbaar, zoals aminozuursequenties, bindingsactiviteiten en kristalstructuren die informatie geven over de moleculaire interacties tussen verschillende liganden en het eiwit.

TbrPDEB1/2 is een eiwit dat tot expressie wordt gebracht in de parasiet *Trypanosoma brucei* en wat betreft structuur en de binding van chemische stoffen (waaronder substraat en remmers) erg lijkt op hPDE4. In de parasiet speelt TbrPDEB een belangrijke rol in de regulering van cellulaire cAMP concentraties. Remming van het eiwit leidt tot verstoring van verschillende belangrijke cellulaire processen van de parasiet, waaronder celdeling. Het feit dat TbrPDEB veel lijkt op hPDE4 maakt het interessant om remmers voor het humane eiwit te gebruiken als startpunt voor de ontwikkeling van geoptimaliseerde en selectieve parasitaire PDE-remmers. In een eerder uitgevoerde 'high throughput screening' (HTS) is gebleken dat een klasse van hPDE4-remmers met een tetrahydrophthalazinone kernstructuur ook goede TbrPDEB1 remmers zijn. Verdere ontwikkeling van deze stoffen resulteerde in de identificatie van NPD-001, een molecuul met een hoge remmende activiteit op TbrPDEB1. De structuur van dit molecuul vormt het startpunt van het onderzoek beschreven in dit proefschrift. Helaas was de activiteit van NPD-001 op hPDE4 vele malen hoger dan de activiteit op TbrPDEB1 en deze selectiviteit voor het humane eiwit kan in het ontwikkelingsproces zorgen voor ongewenste bijwerkingen. Vergelijking van de kristalstructuren van beide eiwitten laat zien dat er in het bindingsdomein van TbrPDEB1 een extra holte beschikbaar is die specifiek voor de parasiet is. Deze unieke bindingsholte wordt daarom de P-pocket genoemd. Binding van een ligand in deze regio van het eiwit kan daardoor mogelijk resulteren in een verbeterde selectiviteit voor TbrPDEB1 over hPDE4.

Het onderzoek beschreven in dit proefschrift is gefocust op het verder ontwikkelen van deze tetrahydrophthalazinone klasse ten behoeve van de behandeling van de Afrikaanse slaapziekte. Het analyseren van de kristalstructuren van NPD-001

gebonden aan de parasitaire PDE en de humane PDE liet zien dat NPD-001 een zeer vergelijkbare conformatie aanneemt in beide eiwitten en dat de beoogde selectiviteit niet behaald kon worden met de flexibele staart (**Hoofdstuk 2**). Vervanging van de flexibele linker door een meer rigide fenylring resulteerde in de eerste klasse van TbrPDEB1 selectieve stoffen gevonden. Het decoreren van de fenylring met flexibele en hydrofiele groepen resulteerde in de meest actieve en selectieve stoffen. De kristalstructuren van een aantal van deze biphenyl tetrahydrophthalazinones in TbrPDEB1 laten zien dat deze klasse van stoffen inderdaad interactie heeft met de P-pocket en het is plausibel dat daardoor het selectiviteitsprofiel positief veranderd is. Het verbeteren van de selectiviteit van deze remmers gaat gepaard met een verlaging in cellulaire activiteit. Vermoedelijk zorgt het rigide en lipofiele karakter van de bifenyl klasse voor een verminderde oplosbaarheid en verlaagde cellulaire activiteit. In **Hoofdstuk 3** worden pogingen beschreven om deze klasse van stoffen verder te optimaliseren, waarbij met name het herstellen van de cellulaire activiteit centraal staat. De kristalstructuren van de bifenylserie vormde de basis voor een virtuele screening naar alternatieven voor een van de fenylringen. Met behulp van computer programma's werden bruikbare en commercieel verkrijgbare stoffen geëvalueerd en stoffen die goed passen in de eiwitmodellen werden geselecteerd voor synthese. Door een extra ether binding op te nemen in de structuur van deze remmers worden de fysicochemische eigenschappen verbeterd maar dit zorgde helaas niet voor een sterke verbetering van de cellulaire activiteit. Het onderzoek naar alternatieven voor de lipofiele fenylring werd daarom voortgezet in **Hoofdstuk 4**. Een variëteit aan (cyclische) alkyl en aromatische structuren werden onderzocht om de beste vector naar de P-pocket te vinden en zo het selectiviteitsprofiel te optimaliseren. De alkynamide klasse liet hierin veelbelovende biochemische en cellulaire resultaten zien. De kristalstructuur van het meest eenvoudige alkynamide (NPD-048) in TbrPDEB1 liet zien dat de verbinding in de richting van de P-pocket wijst, maar de structuur was niet lang genoeg om de P-pocket te bereiken. Omdat het terminale amide een goed uitgangspunt is voor verdere modificaties werd deze substructuur onder andere met behulp van computationele technieken verder onderzocht in **Hoofdstuk 5**. Op basis van commercieel verkrijgbare amines werd een virtuele set alkynamides verkregen. Dit cluster aan stoffen werd *in silico* vergeleken met de conformaties van twee stoffen uit de bifenylserie en de conformatie van NPD-048. Daarnaast werden een aantal nauw verwante analogen uit het eerste cluster alkynamides gesynthetiseerd voor verdere ontwikkeling van deze serie. Ondanks dat kristal

structuren van verschillende alkynamides in TbrPDEB1 lieten zien dat de alkynamide klasse niet in staat bleek te zijn om interacties met het eiwit aan te gaan in de P-pocket, lieten ze wel een lichte selectiviteit zien in het voordeel van TbrPDEB1 ten opzichte van hPDE4. Om te toetsen of de alkynamide klasse ook een veelbelovende rol kan gaan spelen voor medicijnontwikkeling tegen taxonomisch gerelateerde parasieten werden deze stoffen getest tegen *Trypanosoma cruzi, Leishmania major* en *Plasmodium falciparum* (**Hoofdstuk 6**). Omdat de alkynamide een Michael acceptor is (en daarom reactief en mogelijk toxisch kan zijn) werden er ook een aantal bioisosteren van de alkynamide getest. Een aantal alkyn tetrahydrophthalazinones lieten goede fenotypische activiteiten zien (*i.e.* verandering in de waarneembare kenmerken van de parasiet) en zijn daarom mogelijk interessante structuren voor verder onderzoek. Het is echter nog niet duidelijk of deze fenotypische activiteiten in de andere parasieten ook het resultaat zijn van PDE-remming en dit moet nog verder onderzocht worden.

Samenvattend laat dit proefschrift zien dat het mogelijk is om met verschillende rigide tetrahydrophthalazinones selectiviteit te behalen voor TbrPDEB1 over hPDE4. De beste selectiviteitsprofielen zijn behaald met de bifenyl klasse, maar de kleinere alkynamide klasse heeft ook potentie voor verdere ontwikkeling. Het onderzoek laat ook de complexiteit van de geneesmiddelenontwikkeling zien. Het implementeren van een meer rigide substructuur zorgde voor een verbeterd selectiviteitprofiel, maar resulteerde ook een gereduceerde cellulaire activiteit. Echter, met het behalen van selectiviteit door het adresseren van de P-pocket is een belangrijke stap gezet in het ontwikkelingstraject naar TbrPDEB selectieve inhibitoren. Verdere ontwikkeling van deze klasse van stoffen vergt nog tijd en aandacht. Zoals te lezen is in dit proefschrift zijn er veel verschillende vakgebieden betrokken bij het ontwikkelen van een nieuwe medicijn. De data beschreven in dit proefschrift werden gegenereerd door een samenwerkingsverband dat PDE4NPD heet. Gedurende de looptijd van dit project hebben collega's gezorgd voor kristalstructuren, biochemische en fenotypische resultaten en computationale expertise die het design- en daarop volgende synthesewerk geholpen hebben. Alles bij elkaar heeft deze bundeling van de individuele krachten geleid tot een beter inzicht in de binding van de liganden in zowel TbrPDE als hPDE4 en zullen de verkregen resultaten een belangrijke rol spelen in verdere ontwikkeling van de tetrahydrophthalazinones ten behoeve van verschillende parasitaire ziektes.

Dankwoord

I would like to start with a big thanks to **everyone** who helped me with exploring the wonderful world of (bio)chemistry and obtaining the results described in this thesis. Most of the work described here would not be possible without the help of others. Many thanks to everyone who helped me in the design of new molecules and those who generated the very valuable biological data. I'm grateful for all the help and support I got when Mother Nature did not want me to make the molecules I desired. Thanks for all the scientific discussions which helped me shaping my project. I've learned that a PhD is much, much more than 'just science'. Indeed, most of the time is spend with obviously enjoyable scientific activities like executing inefficient synthesis routes, endless purifications, cleaning glassware, tracking down missing starting materials, preparing LCMS solvents, preparing presentations, emptying waste bins, refilling the solvent cabinet or staring out of the window to watch the emergency helicopter land, but the real beauty is in the less common events. So besides the appreciation for all the help I got scientifically I would like to thank several people in special:

Rob, **Iwan**, **Marco**, bedankt voor de fantastische belevingen in Tahoe, USA. Als beginnende onderzoeker een appartement en skilift delen met de professoren was een unieke ervaring. Naast de wetenschappelijke discussies gedurende het congres en op de piste, heb ik ook zeker veel geleerd van het off-piste verdwalen en het trotseren van sneeuwstormen. Dit was een ervaring waar ik zeker nog lang met veel plezier op terug ga kijken.

Maikel, wat begon als werk gerelateerde non-verbale communicatie door een glazen wand (die ik wanhopig probeerde te blokkeren met nieuw vergaarde stadsplattegronden), draaide uiteindelijk uit op een redelijk efficiënte non-verbale communicatiestijl die in de stilteruimte van O|2 goed toepasbaar was om toch een beetje te kunnen ouwehoeren. Ik heb deze gemakkelijke en laagdrempelige manier van communiceren altijd erg prettig gevonden!

Ewald, bedankt voor alle steun en hulp tijdens het begin van m'n PhD-traject. De discussies en gesprekken over het consortium en het onderzoek in een obscure Dominicaanse bar in een duister straatje ergens in Madrid behoort tot een van de betere herinneringen van de afgelopen 4 jaar.

Geert Jan, bedankt voor de melding dat er een positie open stond bij de VU om het PDE-project voort te zetten. Zonder die informatie had ik hier mogelijk nooit gezeten en had ik de mooie momenten die het PhD-traject met zich mee heeft genomen afgelopen jaren niet kunnen beleven.

Andrea, als labmoeder was je van groot belang voor de orde op het lab, maar ook betrokken bij de organisatie van verschillende etentjes en activiteiten. Bedankt voor deze geslaagde borrels, kerstdiners en etentjes gedurende de afgelopen jaren.

Handsome (a.k.a. Hans), ik weet zeker dat zonder jouw hulp de vier MTB-weekendjes in Somme-Leuze en Zuid-Limburg op een totaal fiasco waren uitgedraaid. Jouw fantastische beheersing van de Franse taal voorkwam dat we zouden verhongeren in Somme-Leuze. Je geweldige ervaring in het verkennen van de omgeving (waarschijnlijk van je militaire achtergrond) bood een hoop gemak in Zuid-Limburg en zorgde ervoor dat ook die weekenden vlekkeloos verliepen.

Maarten, er zijn maar weinig mensen waar ik zo vaak een stedentrip mee heb gemaakt: Madrid, Hamburg, Parijs, Manchester, Sienna, Kent, Antwerpen en Cambridge. Het is moeilijk kiezen tussen de goede herinneringen aan deze stedentrips; Erbarmelijke omstandigheden tijdens de Summer school in Parijs proberen te vergeten met rode wijn uit pak in het park, op kosten van de baas kreeft eten in Manchester, Italiaanse wijnen drinken tijdens de lunchpauze op een idyllische locatie in Toscane, maar ook zeker de gehaaste jacht op stadsplattegronden en de meest exclusieve Pokémon. Bedankt voor al deze plezierige momenten.

Natuurlijk wil ik **Niels** bedanken voor het helpen bij het verkennen van de wondere wereld van de whisky's. De whisky woensdag, die regelmatig op dinsdag of donderdag viel, brak de week vaak doormidden met verhelderende discussies, slechte grappen en bood troost wanneer het nodig was.

Yang, thanks for all the non-scientific discussions (culture clashes) on the lab. I laughed a lot about our different visions and opinions on today's society and daily life. Furthermore, thanks for being so honest and direct when I did something stupid and you were clearly enjoying my 'suffering'. Although it was a bit annoying sometimes, it also delivered some great stories.

David, I have really good memories of the numerous festivals we went to. It was a good opportunity to vent and laugh about our frustrations on chemistry, colleagues

or anything else. I really appreciate your enthusiasm and commitment to be a part of every social event.

Marjolein, **Sebastiaan**, **Stephanie**, **Ton**, ik heb een aantal goede herinneringen aan de medewerkersvoorstellingen waar de focus lag op zo snel mogelijk eten te confisqueren en dan maar te zien of we nog zin hadden in een voorstelling. Met trots kijk ik terug op de overtuigende wijze waarop we het buffet geopend kregen, 2de en 3de rondes scoorden, extra drankjes wisten te bemachtigen en de volledige toetjesschaal hadden veroverd.

Sjors, **Dina**, **Mitchel**, **Yalda**, **Floran**, **Mikkel**, **Jeffrey**, **Amid**, thanks for all the joy you gave me while being your supervisor. I think supervising you gave an extra dimension to my PhD. Quotes like "I would do *anything* to get a 8.5.", "Oh.. I missed your ugly face." or "You are just a little… weird sometimes…" will not be forgotten any time soon.

Pap, **Mam**, bedankt voor het geven van de vrijheid en vertrouwen in de keuzes die ik maak. Ik mag me gelukkig prijzen dat ik altijd kan rekenen op jullie steun, ook al zijn sommige keuzes ietwat impulsief of onverwacht. De academische en chemische wereld is jullie wat vreemd, maar ik waardeer de interesse en verwoede pogingen om het te begrijpen enorm.

Zusjes, ik ben erg blij met onze natuurlijke vorm van rivaliteit die (vooral in m'n jongere jaren) het beste in me naar boven heeft gehaald. Ondanks dat meeste van onze gesprekken weinig serieus van aard zijn, zit er vaak toch wel een onderliggend puntje van kritiek of advies in. Ik hoop dat we dat we nog lang op deze manier rivalen van elkaar zijn.

Lotte, bedankt dat je al die jaren aan m'n zijde hebt gestaan en gesteund hebt wanneer nodig. Je hebt zeker ook een belangrijke bijdrage gehad in mijn keuze om dit promotieonderzoek te gaan doen. Ondanks dat ik zelf wat sceptisch was had jij alle vertrouwen dat ik dit aan kon.

Anja, **Dirk**, **Leoni**, **Luuk**, **Rob**, **Vincent**, bedankt voor alle avonden en weekenden dat het eigenlijk iets te laat is geworden. Ondanks dat het m'n productiviteit vaak niet ten goede kwam hecht ik hier heel veel waarde aan. De studententijd en de jaren erna hebben mij een heel ander persoon gemaakt en ik denk dat jullie daar een belangrijke bijdrage aan hebben geleverd.

Lieve **Jenny**, ondanks dat het lijkt dat door jou het hele afrondingsproces vertraging heeft opgelopen, denk ik dat je er netto vooral voor gezorgd had dat het wat sneller klaar was. Bedankt voor de (letterlijke) schop onder m'n reet die ik af en toe nodig had, maar ook voor de momenten dat je vond dat ik even niets hoefde te doen. Ook bedankt voor alle pogingen om mijn interesse in de (medicinale) chemie te begrijpen, ondanks dat de chemische kennis 'een beetje' weggezakt is. Echter, uit het feit dat je bij het horen van 'naamreactie' als een gekke Pavlov reactie "Grignard!" roept kan ik opmaken dat er nog hoop is voor de toekomst.

Jasmijn, onbewust en onbedoeld heb jij mij iets geleerd wat nog veel waardevoller is dan alle nieuwe kennis die ik vergaard heb gedurende mijn promotietraject. Mijn dank daarvoor valt niet in woorden te beschrijven.